

# **FLOWTHROUGH AND OVERTOPPED ROCKFILL DAMS**

**Bingjun Li**

**B.Eng. (Hohai), M.Eng. (NHRI), Reg. Engr. (China)**

**A Dissertation**

**Submitted to School of Graduate Studies**

**under the supervision of**

**Dr. Vinod K. Garga, P.Eng., F.EIC.**

**in partial fulfillment of the requirements for the degree of  
Doctor of Philosophy in Civil Engineering**

**Department of Civil Engineering**

**Faculty of Engineering**

**University of Ottawa**

**Ottawa, Canada K1N 6N5**

**The Doctor of Philosophy in Civil Engineering is a joint program between  
Carleton University and the University of Ottawa, which is administered  
by the Ottawa-Carleton Institute for Civil Engineering**

**©Bingjun Li, Ottawa, Canada, September 1995**



National Library  
of Canada

Bibliothèque nationale  
du Canada

Acquisitions and  
Bibliographic Services Branch

Direction des acquisitions et  
des services bibliographiques

395 Wellington Street  
Ottawa, Ontario  
K1A 0N4

395, rue Wellington  
Ottawa (Ontario)  
K1A 0N4

*Your file* *Votre référence*

*Our file* *Notre référence*

The author has granted an irrevocable non-exclusive licence allowing the National Library of Canada to reproduce, loan, distribute or sell copies of his/her thesis by any means and in any form or format, making this thesis available to interested persons.

L'auteur a accordé une licence irrévocable et non exclusive permettant à la Bibliothèque nationale du Canada de reproduire, prêter, distribuer ou vendre des copies de sa thèse de quelque manière et sous quelque forme que ce soit pour mettre des exemplaires de cette thèse à la disposition des personnes intéressées.

The author retains ownership of the copyright in his/her thesis. Neither the thesis nor substantial extracts from it may be printed or otherwise reproduced without his/her permission.

L'auteur conserve la propriété du droit d'auteur qui protège sa thèse. Ni la thèse ni des extraits substantiels de celle-ci ne doivent être imprimés ou autrement reproduits sans son autorisation.

ISBN 0-612-15734-2

**Canada**



UNIVERSITÉ D'OTTAWA  
UNIVERSITY OF OTTAWA

## Acknowledgements

This thesis is the result of a comprehensive study for a research project "Overtopping Flow in Rockfill Dams and Its Influence on Downstream Slope Instability" financially supported by Resources Canada (CANMET) under the supervision of Dr. Vinod K. Garga, P.Eng.. Dr. Garga's unflagging enthusiasm, continuing moral and practical support, persistent optimism, and wide practical experience have provided very strong influence on the author to continue the study in the direction of practical application. The friendship between the author and the Professor makes the discussion of all the results very efficient and this cooperation in the derivation of the new relationships and design methodology throughout the thesis was very successful. The author was fortunate in obtaining strong support from the Coastal Engineering Laboratory of National Research Council of Canada. Special thanks are extended to Dr. M. Davies. Without his contribution, the experimental work would have been impossible. His advice on the non-Darcy relationships, and finite element modelling were helpful for the author to conduct original and practical work. Many thanks are extended to Dr. B. Pratte, Director of the NRC Laboratory, for generously making available the excellent experimental facilities. His advice at the very beginning of the research was instrumental in changing the author's initial idea to conduct purely theoretical research. Dr. Andrew M. Cornnet designed the force panels and helped the author to set up the testing and be familiar with the GEDAP analysis system. The technical support of Mr. B. Aitkin made the experiments possible. The support of the computer network staff at the NRC allowed me to handle the network to make the computer analysis and simulation possible. Mr. J. Infante, a student at the Department of Civil Engineering also assisted the experiments at NRC and data analysis. The practical experience of overtopped rockfill dams, obtained when the author worked in China for five years with Mr. Qulie Hu, a senior engineer at Nanjing Hydraulic Research Institute, made the research on the practical design criteria and methodology possible. The author's experience on the extensive computer programming with Dr. Sam Wang at the Computational Center for Hydroscience and Engineering, the University of Mississippi, USA, helped him to write, debug, and test the finite element program efficiently. Finally none of this work would have been possible without the support of the author's family.

## **Abstract**

The emphasis of this thesis is on the derivation of original results or improvement to the available results in order to obtain a practical design methodology for overtopped rockfill dams. The work comprised of experiments in a large hydraulic flume, and extensive theoretical development of design aspects. A non-linear finite element analysis for non-Darcy flow in dams has also been formulated. The important contributions of the thesis are listed as follows:

### **I. Non-Darcy seepage flow**

(1) Development of a general relationship between the Reynolds number and the friction coefficient for seepage in rockfill;

(2) Development of a general relationship between the hydraulic gradient and the velocity of seepage flow in rockfill;

(3) Investigation of the difference between all the available formulae for non-Darcy flow by the computer simulation with wide range of porosity and size of rockfill. Comparisons between the simulated results of available formulae and the available prototype data have also been undertaken.

(4) Determination of the hydraulics mean radius of rockfill material by empirical relationship;

(5) Estimation of the seepage discharge through a rockfill dam without numerical modelling;

### **II. Numerical modelling of non-Darcy seepage flow**

(1) Development of a high-accuracy finite element method to model the non-Darcy seepage field within a flowthrough and overtopped rockfill dam;

### **III. Stability analysis and design methodology for flowthrough and overtopped rockfill dams**

(1) Development of a formula for the design of the external layer comprising of large-size particles at the downstream slope of a flowthrough and overtopped flow rockfill dam;

(2) Development of a formula for the design of mesh protection at the downstream slope of a flowthrough and overtopped rockfill dam;

(3) Development of a formula for the design of steel bars protected at the downstream slope of a flowthrough and overtopped rockfill dam;

(4) Development of a practical design methodology which applies to small flowthrough and overtopped rockfill dams;

### **IV. Behaviour of forces acting on the downstream slope**

(1) Investigation of the stochastic and statistical behaviour of the forces acting on the force panels installed at the downstream slope in a model flowthrough and overtopped rockfill dam;

### **V. Theoretical solution of 1-D seepage flow in overtopped rockfill**

(1) Development of a theoretical solution for the seepage flow at the transition zone in an overtopped rockfill dam.

# FLOWTHROUGH AND OVERTOPPED ROCKFILL DAMS

## CONTENTS

<i>Acknowledgements</i>	<i>i</i>
<i>Abstract</i>	<i>ii</i>
<i>Contents</i>	<i>iv</i>
<i>List of Tables</i>	<i>vii</i>
<i>List of Figures</i>	<i>xi</i>
<i>List of Photographs</i>	<i>xx</i>
Chapter 1 Introduction	1
1.1 Objectives of the Study	2
1.2 Scope of the Study	3
1.3 Outline of the Thesis	3
Chapter 2 Literature Review	6
2.1 Introduction	6
2.2 Expressions for non-Darcy Flow in Rockfill	7
2.3 Empirical and Theoretical Results on the Seepage Flow through Rockfill	15
2.4 Computation of Seepage Field within Rockfill Dams	20
2.5 Shear Stress and Seepage Force at the Downstream Slope	26
2.6 Slip Failure of A Flowthrough Rockfill Dam	31
2.7 Friction Head Loss During Overtopping Flow	34
2.8 Unravelling Failure of the Downstream Slope	37
2.9 Discussions and Conclusions	41

Chapter 3 Theoretical Solutions for the Seepage Flow in Overtopped Rockfill	55
3.1 Introduction	55
3.2 Turbulence Theory and Governing Equations	56
3.3 Boundary Conditions and Analytical Solutions	60
3.4 Computation of Seepage Discharge	65
3.5 Conclusions	69
 Chapter 4 Experimental Studies at NRC Hydraulics Laboratory	 72
4.1 Introduction	72
4.2 Model Description	72
4.3 Instrumentation and Data Acquisition	73
4.4 Behavior of the Forces Acting on the Rock Particles at the Downstream Slope	77
4.4.1 Stochastic Behavior	77
4.4.2 Average Behavior	78
4.5 Flow Pattern at the Downstream Slope of an Overtopped Rockfill Dam	80
4.6 Failure Condition of a Rockfill Dam	81
4.7 Conclusions	82
 Chapter 5 Non-Darcy Law in Rockfill	 145
5.1 Introduction	145
5.2 Derivation of General non-Darcy Law	147
5.3 Comparison between Different Formulae	154
5.4 Computer Simulation of $i \sim v$ Relationships	155
5.5 Computer Simulation of the Relationships between $Re$ and $f$	156
5.6 Parameters of Rockfill Material	157
5.7 Comparison between Power Law and Quadratic Law	160
5.8 Comparison with the Prototype Data	163

5.9	Determination of the Most Appropriate Formula in Design	167
5.10	Conclusions	173
<b>Chapter 6</b>	<b>Numerical Modelling of Flowthrough and Overtopped Rockfill Dams</b>	<b>195</b>
6.1	Introduction	195
6.2	Governing Equations and Boundary Conditions	196
6.3	Quadratic Quadrilateral Element	199
6.4	Variational Method	203
6.5	Formation of Element Matrix	205
6.6	Formation of Global Equations	207
6.7	Solution of FEM for non-Darcy Flow in Rockfill	210
6.8	Example Solution of the FEMND2D for Non-Darcy Flow in Rockfill	214
6.9	Conclusions	215
<b>Chapter 7</b>	<b>Derivation of New Formulae for Stability Analysis at the Downstream Slope of an Overtopped Rockfill Dam</b>	<b>225</b>
7.1	Introduction	225
7.2	Individual Particle at the Downstream Slope	225
7.3	Design of the Mesh at the Downstream Slope of an Overtopped Rockfill Dam	233
7.4	Design of Steel Bars in Rockfill Dams	236
7.5	Concluding Remarks	242
<b>Chapter 8</b>	<b>A Proposed Design Methodology for Flowthrough and Overtopped Rockfill Dams</b>	<b>247</b>
8.1	Introduction	247

8.2	Design Methodology for Flowthrough and Overtopped Rockfill Dams with or without Detailed Pore Pressure Distribution	247
8.2.1	Seepage Flow through the Dam	248
8.2.2	Overtopping Flow	249
8.2.3	Design of the Average Rock Size at the Downstream Slope	251
8.2.4	Design of Mesh at the Downstream Slope	253
8.2.5	Design of Anchor Bars in the Downstream Slope	254
8.2.6	Summary of Design Methodology	255
8.3	Summary	257
Chapter 9 Summary of Conclusions and Suggestions for Future Research		260
9.1	Conclusions	260
9.2	Suggestions for Future Research	262
Chapter 10 References		263
 Appendices:		
I.	Summary of Useful Results from Nanjing Hydraulic Research Institute (NHRI)	274
1.1	Introduction	274
1.2	Simulation Theory and Physical Model Design	274
1.3	Summary of Experimental Results from NHRI	277
1.4	Prototype Observation	281
1.5	Conclusions	282

II.	Examples for the Design of Flowthrough and Overtopped Rockfill Dams	289
II.1	Geometry of the Dam	289
II.2	Rockfill	290
II.3	Case 1: Design of the Rockfill Dam Protected by Large Particles only	290
II.4	Case2: Design of Steel Mesh Protection along the Downstream Slope	298
II.5	Discussion	303
III.	Case Studies	311
III.1	Xibeikou Concrete Faced Rockfill Dam	311
III.2	Hell Hole Dam	312
III.3	Pit 7 Afterbay Dam	315
III.4	Conclusions	318

Table	<u>List of Tables</u>	PAGE
Table 2-1	Previous research on non-Darcy flow	43
Table 2-2	Some prototype flowthrough rockfill dams/spillways	46
Table 3-1	Comparison of the discharge between computational models and measurement	71
Table 4-1	Test carried out at NRC (force measurement)	83
Table 4-2	Test carried out at NRC (stability)	85
Table 5-1	Relationship between hydraulic gradient $i$ and velocity $v$ from different Authors	175
Table 5-2	Simulation for $n=0.35$	176
Table 5-3	Simulation for $n=0.40$	176
Table 5-4	Simulation for $n=0.45$	177
Table 5-5	Simulation for $n=0.5$	177
Table 5-6	The coefficient in the relationship between $Re$ and $f$	178
Table 5-7	Coefficient in the power law (after Li and Hu, 1988)	179
Table 5-8	Comparison between simulations and the prototype data	179
Table 6-1	Location of sampling points and weighting factors for Gauss quadrature (after Allaire, 1985)	217

<b>Table</b>	<b><u>List of Tables</u></b>	<b>PAGE</b>
Table I -1	Determination of coefficients a and b	283
Table II-1	Water surface of overtopping of an overtopped rockfill dam	307
Table II-2	Stability analysis of the steel bars in the downstream slope	309
Table III-1	Water surface of overtopping flow at the downstream slope	322
Table III-2	Stability analysis of the downstream slope protected by mesh and rebars	324

Figure	<u>List of Figures</u>	PAGE
Figure 2-1 (a)	Nomenclature used for a flowthrough rockfill dam (after Hansen, 1992)	48
Figure 2-1 (b)	Illustration of a flowthrough and overtopped rockfill dam	49
Figure 2-1 (c)	Illustration of free fall zone in a flowthrough rockfill dam	49
Figure 2-2	Examples of friction factor versus Reynolds number plots for flow through porous media (after Hansen, 1992)	50
Figure 2-3	Examples of friction factor versus Reynolds number plots for flow through porous media (after Hansen, 1992)	51
Figure 2-4	Non -Darcy flow net for isotropic homogeneous porous media	52
Figure 2-5	Node Identification (after Curtis and Lawson, 1967)	52
Figure 2-6	Scheme for seepage - face definitions (after Hansen, 1992, p.152)	53
Figure 2-7	Schwmatic diagrams pertaining to the wedge method (after Hansen, 1992)	54
Figure 3-1	Definition sketch for flow over and through gravel bed (after Gupta et., 1985)	70
Figure 4 -1	Profile of the model in the wave basin of NRC Hydraulics Laboratory	88

Figure	<u>List of Figures</u>	PAGE
Figure 4-2	Models in the wave basin of NRC Hydraulics Lab.	88
Figure 4-3	Sketch of the downstream slope armour layer and force panels	89
Figure 4-4	Plan view of a force panel	89
Figure 4-5	Calibration of wave probe 1	90
Figure 4-6	Calibration of wave probe 2	91
Figure 4-7	Calibration of wave probe 3	92
Figure 4-8	Calibration of wave probe 4	93
Figure 4-9	Calibration of wave probe 5	94
Figure 4-10	Calibration of wave probe 6	95
Figure 4-11	Calibration of wave probe 7	96
Figure 4-12	Calibration of wave probe 8	97
Figure 4-13	Calibration of wave probe 9	98
Figure 4-14	Calibration of wave probe 10	99
Figure 4-15	Calibration of wave probe 11	100

Figure	<u>List of Figures</u>	PAGE
Figure 4-16	Calibration of wave probe 12	101
Figure 4-17	Calibration of velocity meter 1 in y direction (channel 13)	102
Figure 4-18	Calibration of velocity meter 1 in x direction (channel 14)	103
Figure 4-19	Calibration of velocity meter 2 in x direction (channel 15)	104
Figure 4-20	Calibration of velocity meter 2 in y direction (channel 16)	105
Figure 4-21	A time series record of the resultant force on the force panel	106
Figure 4-22	The power density function of the resultant force on the force panel	107
Figure 4-23	The probabilistic distribution of the resultant force on the force panel	108
Figure 4-24	The autocorrelation of the resultant force on the force panel	109
Figure 4-25	A time series record of the angle of the resultant force on the force panel	110
Figure 4-26	The power density function of the angle of the resultant force on the force panel	111

Figure	<u>List of Figures</u>	PAGE
Figure 4-27	The probabilistic distribution of the angle of the resultant force on the force panel	112
Figure 4-28	The autocorrelation function of the angle of the resultant force on the force panel	113
Figure 4-29	A time series record of the force in x direction on the force panel	114
Figure 4-30	The power density function of the force in x direction on the force panel	115
Figure 4-31	The probabilistic distribution of the force in x direction on the force panel	116
Figure 4-32	The autocorrelation of the force in x direction on the force panel	117
Figure 4-33	A time series record of the force in y direction on the force panel	118
Figure 4-34	The power density function of the force in y direction on the force panel	119
Figure 4-35	The probabilistic distribution of the force in y direction on the force panel	120

Figure	<u>List of Figures</u>	PAGE
Figure 4-36	The autocorrelation of the force in y direction on the force panel	121
Figure 4-37	A time series record of the momentum on the force panel	122
Figure 4-38	The power density function of the momentum on the force panel	123
Figure 4-39	The probabilistic distribution of the momentum on the force panel	124
Figure 4-40	The autocorrelation of the momentum on the force pane	125
Figure 4-41	Relationship between the resultant force R and the discharge Q (lower panel)	126
Figure 4-42	Relationship between the resultant force R and the discharge Q (upper panel)	126
Figure 4-43	Relationship between the angle of the resultant force $R_{xy}$ and the discharge Q (lower panel)	127
Figure 4-44	Relationship between the angle of the resultant force $R_{xy}$ and the discharge (upper panel)	127
Figure 4-45	Relationship between the resultant force R and the upstream water head H (lower panel)	128

Figure	<u>List of Figures</u>	PAGE
Figure 4-46	Relationship between the resultant force R and the upstream water head H (upper panel)	128
Figure 4-47	Relationship between the angle of the resultant force $R_{xy}$ and the upstream water head H (lower panel)	129
Figure 4-48	Relationship between the angle of the resultant force $R_{xy}$ and the upstream water head H (upper panel)	129
Figure 4-49	Profile of failed downstream slope (Pattern 1)	130
Figure 4-50	Profile of failed downstream slope (Pattern 2)	131
Figure 5 -1	Illustration of flow path in rockfill	180
Figure 5-2	New relationship between Re and f in terms of hydraulic mean radius	181
Figure 5-3	Relationship between Re and f in terms of $d_{50}$	181
Figure 5-4	Relationship between i and v for rockfill with $d_{50}=0.04m$ , $n=0.45$	182
Figure 5-5	Relationship between i and v for rockfill with $d_{50}=0.1m$ , $n=0.45$	182
Figure 5-6	Relationship between i and v for rockfill with $d_{50}=0.4m$ , $n=0.45$	183

Figure	<u>List of Figures</u>	PAGE
Figure 5-7	Relationship between $i$ and $v$ for rockfill with $d_{50}=1m$ , $n=0.45$	183
Figure 5-8	Relationship between $i$ and $v$ for rockfill with $d_{50}=2m$ , $n=0.45$	184
Figure 5-9	Relationship between $i$ and $v$ for rockfill with $d_{50}=0.65m$ , $n=0.45$	184
Figure 5 -10	Simulated relationship between $Re$ and $f$ (a)	185
Figure 5 -11	Simulated relationship between $Re$ and $f$ (b)	186
Figure 5 -12	Simulated relationship between $Re$ and $f$ (c)	187
Figure 5 -13	Simulated relationship between $Re$ and $f$ (d)	188
Figure 5 -14	Simulated relationship between $Re$ and $f$ (e)	189
Figure 5 -15	Simulated relationship between $Re$ and $f$ (f)	190
Figure 5 -16	Simulated relationship between $Re$ and $f$ (g)	191
Figure 5 -17	Simulated relationship between $Re$ and $f$ (h)	192
Figure 5-18	Relationship between diameter and hydraulic mean radius	193

Figure	<u>List of Figures</u>	PAGE
Figure 5-19	Definition of 1-D seepage flow in a dam	194
Figure 6-1	Boundary conditions	218
Figure 6-2	Element in global coordinates	219
Figure 6-3	Element in local coordinates	219
Figure 6-4	3x3-point Gauss quadrature integration	220
Figure 6-5	Selection of Darcy seepage coefficient for Non-Darcy seepage simulation	220
Figure 6-6	Flow chart of finite element method for free surface Darcy flow	221
Figure 6-7	Flow chart of finite element method for free surface non-Darcy flow	222
Figure 6-8	A simulation of finite element method	223
Figure 6-9	A simulation of a flow through dam with no cut-off wall	224
Figure 7-1	Forces acting on a particle at the downstream slope	244
Figure 7-2	Forces acting on a particle at the downstream slope protected with mesh	244

Figure	<u>List of Figures</u>	PAGE
Figure 7-3	Description of mesh	245
Figure 7-4	Diagram for the analysis of steel bars	245
Figure 7-5	Force diagram for the $i^{\text{th}}$ slice	246
Figure 7-6	Design of steel bars	246
Figure 8-1	Definition of an overtopped rockfill dam	259
Figure 8-2	Spatially varied flow at the downstream slope	259
Figure I-1	The configuration of physical models	284
Figure I-2	Value of $m$ and $\sigma$	285
Figure I-3	Definition of parameters in hydraulic jump	285
Figure I-4	A sample of pulsating pressure results	286
Figure II-1	An overtopped rockfill dam protected by large particles	305
Figure II-2	Apron of the overtopped rockfill dam protected by large particles	305
Figure II-3	An overtopped rockfill dam protected by steel mesh and steel bars	306
Figure II-4	Description of dividing the slices at the downstream slope	306

Figure	<u>List of Figures</u>	PAGE
Figure III-1	The downstream slope of the unfinished Xibeikou concrete rockfill dam	319
Figure III-2	Profile of Hell Hole dam	319
Figure III-3	Shape of the north at the Hell Hole dam	319
Figure III-4	Profile of Pit 7 Afterbay dam	320
Figure III-5	Simplified profile of Pit 7 Afterbay dam	320
Figure III-6	Description of dividing the slices at the downstream slope	321

Photograph	<u>List of photographs</u>	PAGE
Photograph 4-1	A view of the downstream slope of an overtopped rockfill dam	132
Photograph 4-2	A view of an overtopped rockfill dam in NRC Hydraulics Laboratory	132
Photograph 4-3	A view of the load cells at the left side of the model	133
Photograph 4-4	A close view of the load cells at the left side of the model	133
Photograph 4-5	A view of the load cells at the right side of the model	134
Photograph 4-6	A close view of the load cells at the right side of the model	134
Photograph 4-7	A view of the wave probe in the model	135
Photograph 4-8	A view of the velocity meters at the downstream slope	135
Photograph 4-9	A view of the pressure gauges used in the model	136
Photograph 4-10	Installation of the pressure gauges in the force panel	136
Photograph 4-11	A view of the hydraulic jump at the toe of an overtopped rockfill dam	137

Photograph	<u>List of photographs</u>	PAGE
Photograph 4-12	A view of the wave at the slope of an overtopped rockfill dam	137
Photograph 4-13	A view of the weak wave at the slope of an overtopped rockfill dam	138
Photograph 4-14	A view of the submerged downstream slope of an overtopped rockfill dam	138
Photograph 4-15	Flow over and through the downstream slope of an overtopped rockfill dam before initial failure	139
Photograph 4-16	Initial movement of individual particles at the downstream slope of an overtopped rockfill dam	140
Photograph 4-17	More rock particles move at the downstream slope	140
Photograph 4-18	The surface layer of particles near the toe at the downstream slope of an overtopped rockfill dam slid down	141
Photograph 4-19	More slides at the surface layer at the downstream slope of an overtopped rockfill dam caused rough water surface	142
Photograph 4-20	The total rock mass near the toe at the downstream slope of an overtopped rockfill dam slid down	142
Photograph 4-21	Rock particles at the upper part of the downstream slope of an overtopped rockfill dam slid down	143

Photograph	<u>List of photographs</u>	PAGE
Photograph 4-22	The second layer of particles at the downstream slope of an overtopped rockfill dam slid down	143
Photograph 4-23	The rock mass at the upper part of the downstream slope of an overtopped rockfill dam slid down	144
Photograph 4-24	The downstream slope of an overtopped rockfill dam slid at one side and flow concentrated on the same side	144
Photograph I-1	A downstream view of steep open channel flow	287
Photograph I-2	A side view of steep open channel flow	288

## Chapter 1 Introduction

Small-scale hydro schemes are generally located to serve small communities in relatively remote locations. In the Canadian context such works would very likely serve locations which experience severe winter conditions. The cost of traditional spillways including the overflow ("ogee" profile) type, the shaft (closed conduit) type, and the siphon spillway are often a major component of the total cost of civil works, particularly in remote northern environments (Hansen, 1992). As concluded by Hansen (1992), currently most small-scale hydro projects involve small concrete dams, spillways, and diversion structures which have three limitations:

(1) Concrete works require considerable site preparation before they can be constructed. A major cost is the excavation to a hard subsoil strata on which the structure can be found.

(2) Concrete structures require considerable engineering constructor skills and these are not readily available in many northern Canadian communities. Construction skills and equipment are usually "imported" to the area, thereby increasing construction costs.

(3) The durability of concrete in harsh winter conditions is poor, and periodic maintenance is required. This is especially true of small hydro schemes in remote locations where rigorous control of the quality of the concrete mix and of general workmanship is either lacking or non-existent.

Low-head rockfill dam requires very little site preparation and can be placed over many soil or rock conditions where the possibility of piping does not exist. The construction work can often be carried out by utilizing the resources available within many northern Canadian communities. Also, sound rockfill dam is highly resistant to freeze-thaw action. The rockfill dam is deformable and accommodates the imposed stresses and strains. In contrast to concrete, a rockfill structure is not prone to cracking (Hansen, 1992).

In high rockfill dams, the construction of diversion engineering structures may account for major costs of the civil works. With proper arrangement, engineering experience (Hu, Li, 1989a, b, c) indicated that it is safe to allow the flood to pass through and over the unfinished rockfill dam and the upstream and downstream cofferdams (usually also made up of rockfill). For high rockfill dams, it may take several years to complete the dam construction. Allowing the flood to pass an unfinished rockfill dam can greatly reduce the height of the cofferdams and the size of the diversion tunnels, and will be very economical in most cases. There is apparently no application of this kind of arrangement in Canada. This may be due to the difficulties that: (1) no experience exists in Canada; and (2) the lack of sound design theory.

## **1.1 Objectives of the Study**

The study deals essentially with the design of overtopped rockfill dams. However, overtopped rockfill conditions invariably also involve flowthrough the dam. Hence the study also includes a discussion of flowthrough conditions.

Literature search reveals that there are some difficulties with the design of a flowthrough and overtopped rockfill dam. Consequently, the objectives of this research are as followings:

- (1) The determination of the constants in the relationship of non-Darcy flow in practical design based on the size, the shape, and porosity of rockfill in the field.
- (2) Computer simulation of turbulent seepage field within an overtopped rockfill dam and a flowthrough rockfill dam.
- (3) Investigation of the characteristics of the forces acting on the rock particles at the downstream slope, and failure mechanisms.
- (4) Development of the governing equations and empirical relationships for both overflow and seepage flow, for the forces acting on the rock particles at the downstream slope, and for the downstream failure condition.
- (5) Derivation of formulae for the design of steel mesh and steel bars which are used to protect the downstream slope of an overtopped rockfill dam.

(6) Preparation of practical design guidelines and presentation of a design example for an overtopped rockfill dam.

## **1.2 Scope of the Study**

This study includes experimental investigations, theoretical studies and computer simulations.

Experimental studies were conducted on the following two aspects:

(1) Investigations in hydraulic flumes on the time-average and stochastic behaviors of the forces acting on the rock particles at the downstream slope of a rockfill dam which is subjected to both flowthrough and overtopping flow;

(2) Investigations in hydraulic flumes on the failure pattern of an overtopped rockfill dam protected with rockfill facing.

Theoretical studies were concentrated on a critical examination of the basic law for non-Darcy flow in rockfill, since this is a key problem for flowthrough and overtopped rockfill dams. Analytical solution of 1-D non-Darcy flow was obtained. Formulae for the stability of individual particle failure, the design of steel mesh at the downstream slope, and the design of steel bars inside the downstream slope, were derived.

For the purpose of stability analysis (including slope stability analysis and unraveled stability analysis) of a rockfill dam, the characteristics of two-dimensional non-Darcy flow are required. To solve this problem in the engineering design, a computational model was developed. The computational model studies include the development of a 2-dimensional finite element method model for non-Darcy flow within a rockfill dam.

## **1.3 Outline of the Thesis**

The thesis has been written in an attempt to produce the chapters as independent from each other as possible so that a practical engineer can address the specific issue of

interest to him/her. Apart from Chapters 1 and 2, original results have been presented in all the chapters.

In Chapter 1, an introduction to the study and the thesis has been presented.

In Chapter 2, a literature review for most issues related to the design of flowthrough and overtopped rockfill dams has been undertaken.

In Chapter 3, the derivation of the analytical solution of 1-D non-Darcy flow at the transition zone in rockfill dam overtopping is presented, and comparison with experimental results is provided.

In Chapter 4, experimental results from the work done at the NRC are summarized. The statistical and stochastic behaviour of the force acting on the force panels installed at the downstream slope of an overtopped rockfill dam, and the failure patterns of an overtopped rockfill dam are described.

In Chapter 5, the derivation of general non-Darcy law from a combination of the pipe theory and the characteristics of rockfill material, and relationships between the hydraulic gradient and the velocity within rockfill derived from the general law have been derived. Comparison between all the available formulae, computer simulation of these formulae, comparison with prototype data, and selection of the best formula in engineering design are fully described.

In Chapter 6, the finite element method is developed for 2-dimension non-Darcy free surface seepage flow with 8 nodes quadratic isoparametric elements. The steps of the derivation of the finite element method, the linearization method to solve the non-linear problem, the flow chart of the program, and examples are presented.

In Chapter 7, based on experimental observations and available experience of overtopped rockfill dams, expressions have been derived for the design of downstream slope which is protected by individual particles. The design of mesh along the downstream slope to protect the downstream slope, and the design of

steel bars in the rockfill dam to prevent the downstream slope instability are described.

In Chapter 8, a new design methodology has been proposed.

Finally Chapter 9 provides a summary of all the conclusions from each chapter. Suggested activities for further research in this field are also presented.

In Appendix 1, useful results from author's research at Nanjing Hydraulic Research Institute (cooperated with Mr. Hu, Qulie and worked with other scientific workers) have been summarized.

In Appendix 2, two examples of the design of flowthrough and overtopped rockfill dams in a real situation have been presented.

In Appendix 3, three practical case studies of flowthrough and overtopped rockfill dams have been presented. The observations have been compared with solutions presented in this thesis.

## Chapter 2 Literature Review

### 2.1 Introduction

It is important to have a complete picture about what has previously been presented in the literature in order to address the need for further research. Available results that are satisfactory can continue to be used in a practical design of a flowthrough or/and overtopped rockfill dam directly. Results that pose problems in design are studied in the present research.

In the design of a flowthrough and overtopped rockfill dam, several aspects are involved. Usually an impervious facing is built at the upstream slope. When water level is higher than the top of the upstream facing but lower than the crest of the dam, flowthrough conditions prevail (see Figure 2-1 (a)). When the reservoir water level is higher than the crest, both overtopping flow and flow through the rockfill dam occur (see Figure 2-1(b)). Hence consideration of flow through rockfill are of relevance to the design of an overtopped rockfill dam. It should be noted that the overtopping flow is significantly larger than the seepage flow. The latter, nevertheless, is important for the scope instability. The consideration of non-Darcy flow in rockfill is important. Table 2.1 shows a summary of publications on non-Darcy flow.

In order to estimate the seepage discharge through a rockfill dam, it is important to use a reliable non-Darcy equation, since the flow within a rockfill dam is usually turbulent seepage flow. The failure mechanisms of a flowthrough rockfill dam are usually the erosion (unravelling failure) of the downstream slope and the (massive) stability failure of this slope. The pore pressure distribution within both a flowthrough dam and an overtopped rockfill dam is therefore necessary for the stability analysis of the rockfill dam. The emergence point of the flow over the downstream slope of a flowthrough rockfill dam, the seepage force on the rockfill at or near the downstream slope, the water surface curve and the shear (friction) force at the downstream slope, are all

important parameters for the engineering design. A summary of the most important results from literature related to the above aspects is presented in this chapter.

Records from available prototype structures can be a practical way to examine the available expressions for non-Darcy flow and the failure pattern. Unfortunately there is not much such data available in the literature. Table 2-2 lists some available information on flowthrough and overtopped rockfill dams.

In the following text, it has been assumed that the reader is familiar with basic concepts of Darcy and non-Darcy seepage flow, and basic elements of dam design.

## 2.2 Expressions for non-Darcy flow in rockfill

In the design of a flowthrough or/and overtopped rockfill dam, the use of an expression for the non-Darcy flow within rockfill material is the most important. Hence numerous studies to derive non-Darcy flow equations have been carried by different authors. The following text presents a summary of the available related expressions in the literature.

### 2.2.1 Relationship between friction coefficient and Reynolds number

Ergun (1952) define the Reynolds number as:

$$R_{e\text{ergun}} = \frac{V d}{\nu} \frac{1}{1-n} \quad (2-1)$$

where  $V$  = the bulk velocity;

$d$  = representative diameter of the particles (generally  $d_{50}$ );

$n$  = porosity of the porous media;

$\nu$  = kinematic viscosity.

The friction coefficient is defined as:

$$f_{\text{ergun}} = \frac{idg}{V^2} \frac{n^3}{1-n} \quad (2-2)$$

where  $i$  = hydraulic gradient within rockfill;  $g = 9.8 \text{ m}^2/\text{s}$ .

The empirical result from Ergun (1952) is:

$$f_{\text{ergun}} = \frac{1}{R_{c\text{ergun}}} + 1.75 \quad (2-3)$$

The experimental results are shown in Fig.2-2(a). It is clearly seen in this figure how the Darcy flow differs from the non-Darcy flow.

Parkin (1963) defined the Reynolds number as:

$$R_{c\text{parkin}} = \frac{V_v m}{\nu} \quad (2-4)$$

and

$$f_{\text{parkin}} = \frac{2 g i m}{V_v^2} \quad (2-5)$$

where  $V_v$  = the void velocity;  $m$  = hydraulic mean radius (dimension: [L]). The data from Parkin (1963) is shown in Fig. 2-2(b).

It is noticed that Parkin's data is in the range of Reynolds number (as defined by Parkin (1963)) from 10 to 1,000, and not in the conventionally fully turbulent seepage range.

Arbhabhirama and Dinoy (1973) performed experiments for different sand and gravel (Fig.2-3(a)). The Reynolds number was defined as:

$$Re_{\text{arbhabhirama}} = \frac{V K^{1/2}}{\nu} \quad (2-6)$$

where  $K$  = intrinsic permeability associated with non-Darcy flow (dimension: [L]<sup>2</sup>).

Friction coefficient:

$$f_{\text{arbhabhirama}} = \frac{i K^{1/2}}{V^2} \quad (2-7)$$

The relationship between Reynolds number and the friction coefficient is:

$$f_{\text{arbhabhirama}} = \frac{1}{R_{c\text{arbhabhirama}}} + c \quad (2-8)$$

Where  $c$  is a constant, whose value for gravel is from 0.24 to 0.38, for sand is from 0.0584 to 0.0594, for the samples they used.

McCorquodale et al (1978) defined the modified Reynolds number as

$$Re_{\text{mccorquodale}} = \frac{m V n^{1/2}}{\nu} \quad (2-9)$$

and friction factor:

$$f_{\text{mccorquodale}} = \frac{i g n m^2}{\nu V} \quad (2-10)$$

They obtained the following relationship from their experimental results:

$$f_{\text{mccorquodale}} = 70 + 0.27 \left(1 + \frac{f_e}{f_o}\right) Re_{\text{mccorquodale}} \quad (2-11)$$

where

$f_e$  = effective Darcy-Weisbach friction factor for rock material;

$f_o$  = Darcy friction-Weisbah factor of a hydraulically smooth surface at the same Reynolds number (from a pipe-flow Moody diagram).

The experimental data from McCorquodale et al (1978) are shown in Fig. 2-3(b).

Stephenson (1979) defined the Reynolds number as:

$$Re_{\text{stephenson}} = \frac{V d}{n \nu} \quad (2-12)$$

and friction coefficient:

$$f_{\text{stephenson}} = \frac{i d g n^2}{V^2} \quad (2-13)$$

Stephenson (1979) obtained the following relationship from the data represented in Fig. 2-7(a):

$$f_{\text{stephenson}} = \frac{800}{Re_{\text{stephenson}}} + K_t \quad (2-14)$$

where  $K_t$  is the friction coefficient for fully developed turbulent seepage flow.

Stephenson (1979) recommended that:

$$K_t = \begin{cases} 1, & \text{for smooth polished marbles;} \\ 2, & \text{for semi - rounded stone;} \\ 4, & \text{for angular stone.} \end{cases} \quad (2-15)$$

Li and Hu (1988) found that Stephenson's relationship applied well to angular rockfill (representative diameter from 12mm to 44mm).

## 2.2.2 Quadratic law between $i$ and $V$

In 1901, Forchheimer (1901, 1930) suggested equations linking hydraulic gradient to the void velocity of the form:

$$i = r_v V_v + s_v V_v^2 \quad (2-16a)$$

$$i = rV + sV^2 \quad (2-16b)$$

where  $r$ ,  $s$ , and  $r_v$ ,  $s_v$  are constants which depend on the characteristics of particles.

Later he added another term  $tV^3$  to the right side of this equation, and suggested that:

$$i = r_{vt} V_v + s_{vt} V_v^2 + t_{vt} V_v^3 \quad (2-16c)$$

$$i = r_t V + s_t V^2 + tV^3 \quad (2-16d)$$

These two relationships were obtained purely from experimental results, in which the constants  $r_{vt}$ ,  $s_{vt}$ ,  $t_{vt}$ , and  $r_t$ ,  $s_t$ ,  $t_t$ , should be determined by experiments. Eq. 2-16s (b, c, d) were widely used by other authors later, while Eq. 2-16a is not common.

Polubarinova Kotchina (1952) added an unsteady term to Eq. (2-16):

$$i = rV_v + sV_v^2 + c \frac{\partial V_v}{\partial t} \quad (2-17a)$$

$$i = rV + sV^2 + c \frac{\partial V}{\partial t} \quad (2-17b)$$

From Ergun (1952) 's relationship between the defined friction coefficient (Eq. 2-1) and Reynolds number (Eq.2-2), i.e., Eq.2-3, the following relationship from the experimental results is obtained:

$$\frac{i d g n^3}{V^2 1-n} = 150 \frac{(1-n)v}{V d} + 1.75 \quad (2-18)$$

or

$$i = 150 \frac{(1-n)^2 v}{g n^3 d^2} V + 1.75 \frac{(1-n)}{d g n^3} V^2 \quad (2-19)$$

Ward (1964) obtained the following relationship:

$$i = \frac{\mu}{k} + \frac{0.55 \rho}{k^{1/2}} V^2 \quad (2-20)$$

where  $k$  = permeability of a porous medium.

Dinoy (1971) presented the following relationship:

$$i = \frac{v}{g k} V + \frac{100 k^{1/4}}{g d^{2/3} n^{3/4}} V^2 \quad (2-21)$$

In 1973, Nirandra (1973) obtained the experimental formula:

$$s = \frac{0.28}{d^{1.41}} \quad (2-22)$$

where  $s$  is defined in Eq. (2-16b). Nirandra (1973) found that the coefficient  $r$  is not clearly related to either the nominal particle diameter or porosity.

The relationship (Eq.2-11) from McCorquodale et al (1978) may be written as:

$$\frac{i g n m^2}{v V} = 70 + 0.27 \left(1 + \frac{f_c}{f_o}\right) \frac{m V n^{1/2}}{v} \quad (2-23)$$

or

$$i = \frac{70 v}{g n m^2} V + 0.27 \left(1 + \frac{f_c}{f_o}\right) \frac{n^{1/2}}{g n m} V^2 \quad (2-24)$$

McCorquodale's expression applies to rockfill material.

Ergun-Reichert ( see Fand & Thinakaran, 1990) proposed that:

$$i = 212 \frac{M \nu (1-n)^2}{g d^2 n^3} V + 1.57 \frac{M}{g d} \frac{(1-n)}{n^3} V^2 \quad (2-25)$$

where:

$$M = 1 + \frac{2}{3} \frac{d}{D(1-n)} \quad (2-26)$$

in which D = the diameter of permeameter. It is noticed that this relationship takes into consideration the wall effect of the permeameter. However Eq. (2-25) is valid for packed spheres only.

It should further be noted that the various relationships presented in the literature are only applicable in limited range of Reynolds number. It is therefore essential to provide a general expression applicable to the entire range of velocities including both Darcy and non-Darcy flow. This has been attempted in this thesis, and described in depth in Chapter 5.

### 2.2.3 Power law between i and V

The famous power relationship may have originated from Prony in 1804 as reported by Jaeger (1956) and also presented by Isbash (1931) as:

$$i = c_0 V_v^{c_1} \quad (2-27a)$$

or

$$i = c_0 V^{c_1} \quad (2-27b)$$

where  $c_0$  and  $c_1$  depend on the flow condition, the characteristics of the porous media and the fluid through the porous media. Equations 2-27 were obtained from the experimental results and also were proved by Isbash (1931) from dimensional analysis.

Escande (1953) presented the following relationship from purely experimental results in column tests:

$$V_v = \sqrt{B i} \quad (2-28)$$

where B is a constant whose value is from 80 to 290 cm<sup>2</sup> / sec<sup>2</sup> for particle with diameter of about 1.5 in.

Wilkins (1956) obtained a widely mentioned formula from column tests:

$$V_v = 5.3 m^{0.5} i^{0.54} \quad (2-29)$$

where  $V_v$  has the unit of m/sec, while the hydraulic mean radius  $m$  (taken to be  $d/10$  in this case, Parkin, 1991) has the unit of meter.

Slepicka (1961) presented a semi-empirical formula based on dimensional analysis:

$$V_v = \alpha \left(\frac{\mu}{\sigma_o}\right)^{f-1} K^f i^f \quad (2-30)$$

where  $\sigma_o$  = surface tension;

$\alpha$  = a constant;

$f$  = a constant;

$\mu$  = dynamic viscosity;

$K$  = hydraulic conductivity.

Parkin (1963) presented a similar formula for nominal 3/4 inch aggregates size:

$$i = 0.0351 V_v^{1.86} \quad (2-31)$$

where  $V_v$  has the unit of ft/sec.

Dudgeon (1968) used Eq. (2-26b) to evaluate the values of  $a$  and  $N$ , and concluded that  $n=1.79$  to  $1.87$ ,  $a=15.1$  to  $65.0$  for 0.75 in. river gravel;  $n=1.83$  to  $1.90$ ,  $a=8.3$  to  $23.7$  for 0.75 in. blue metal;  $n=1.80$  to  $1.83$ ,  $a=5.3$  to  $9.8$  for 16 mm marbles.

Basak (1977) reviewed non-linear seepage flow law and indicated that the value of 1.86 for  $N$  in Eq. (2-26) varies little, but that the coefficient  $a$  was dependent on the porous media.

Stephenson (1979) used the data available to present the following relationship for turbulent seepage flow:

$$i = \frac{K_t V^2}{g d n^2} \quad (2-32)$$

where  $K_t$  is a constant for specific porous media.

Li and Hu (1988) derived the following expression based on the available experimental data and Stephenson's relationship between the friction coefficient and the Reynolds number (1979):

$$i = \frac{a V^{2+b} \nu^{-b}}{d_{50} g n^{2+b}} \quad (2-33)$$

where  $d_{50}$  = average diameter of the particles (from 12mm to 44 mm in experiment). When Darcy seepage flow develops,  $b = -1$ . When fully turbulent seepage flow develops,  $b = 0$ . For rockfill with angular shape, the constant  $a$  is from 2.145 to 2.846, and the constant  $b$  from -0.507 to -0.774, when  $Re$  is from 10 to 3,300.

Martins (1990, 1991) presented the following expression for fully developed seepage flow:

$$V_v = \frac{C}{C_u^{0.26}} \sqrt{2gedi} \quad (2-34)$$

where  $C_u$  is the uniformity coefficient, and  $e$  the void ratio of rockfill. The constant  $C$  is 0.56 for angular particles, and 0.75 for rounded particles. For transition zone seepage flow, he defined another two variables and used his "Modified Moody diagram" to calculate the velocity (Martins, 1991). Unfortunately the data in his "modified Moody diagram" is only from limited experiments with particles with diameters 2.3mm, 6.0mm, and 11mm. It is not clear if these data apply to the prototype case with large particles.

It is noticed that all these expressions are similar in form. The differences are that different authors considered different parameters of the porous media, and conducted

experiments with different size, shape, and type of particles. Hence, each formula applies only to a certain range of Reynolds number. A relationship of non-Darcy flow based on a large amount of experimental data with wide range value of parameters for rockfill is very important for engineering design. This relationship should be able to predict the prototype non-Darcy seepage law based on some easily obtained parameters, e.g., diameter, shape, and porosity, similar to Eq. (2-33). More data are required to obtain the statistical constants  $a$ , and  $b$ . The shape factor should also be included in the improvement of such a formulation.

## **2.3 Empirical and theoretical results on the seepage flow through rockfill**

### **2.3.1 Research work on flow through a rockfill dam with an impervious upstream section**

In 1963, Parkin (1963) investigated the flowthrough rockfill dam with an internal cutoff wall inside the rockfill dam. Figure 2-1(a) shows the profile of the rockfill dam. There are two important control points in the design consideration, that is, the depth of water over the inlet spillway,  $h_c$ , and exit height of the seepage flow at the downstream slope,  $h_e$ .

The geometry of flow through a self-spillway rockfill dam will, in most cases, be fixed by two independent hydraulic control points. In the case of flowthrough seepage only, the control points are point of entry along the upstream slope and the exit point on the downstream slope. In the case of overtopping, there are no such control points.

Separating the two control points is a freefall zone at atmospheric pressure (Figure 2-1 (c)), wherein the hydraulic gradient equals 1, and wherein lateral dispersion and aeration takes place, as happens in the case of open channel flow over a weir. At high rates of discharge, the free zone may be eliminated, at which stage the control points are no longer independent (Parkin, 1991). However, the structure is then likely to be in

a precarious state with respect to stability, so that this is not normally a design consideration.

In the crest region, Wilkins (1956) estimated the crest depth by means of the critical depth formula, as normally applied to frictionless flow over weirs, modified only to allow for the volume of stones, that is:

$$y_c = \sqrt[3]{q^2 / gn^2} \quad (2-35)$$

Subsequent model studies (Sandie, 1961) have indicated that crest flow is characterized by the attainment of a terminal velocity, associated with a particular value of hydraulic gradient in the frictional environment. This gradient can be taken as 0.8 (rather less than the maximum of 1 in free -surface flow), in which case the associated value of  $h_c$  (assuming the hydraulic radius  $m = d/10$ ) can be compared with  $y_c$  from Eq. (2-35) in an analysis following Lawson, Trollope and Parkin (Parkin, 1991):

$$y_c^3 \approx h_c^2 d / 6 \quad (2-36)$$

It follows that the crest velocity will be less than that from a critical depth analysis for all depths of flow greater than  $d/6$ . It also follows that discharge will vary linearly with head over the crest, rather than head to the power 1.5, as confirmed experimentally by Sandie (1961).

Parkin (1963) found that the hydraulic gradient over the crest of an inbulit spillway was 0.82 for 3/4 inch crushed rock, and felt that this would also be a good first approximation for prototype. For a given porosity, the bulk velocity  $V$  can be determined by:

$$V = \frac{1}{n} \left( \frac{0.82}{c_0} \right)^{1/c_1} \quad (2-37)$$

Then the crest head  $h_c$  can be determined from:

$$Q = Vh_cL \quad (2-38)$$

where  $Q$  = desired flood capacity;

$L$  = width of the spillway;

$h_c$  = crest head ( the height of water above the impermeable element).

The value of  $a$  and  $N$  will depend on the characteristics of the material used and the fluid flow through the porous media. Parkin et al (1966) presented a nomogram to assist in estimating the value of  $a$  from porosity and the mean surface area per unit volume of the particles, but suggested that the values of  $a$  and  $N$  should be determined experimentally when approaching a design problem. The reason is that the value of  $N$  is much stable when the Reynolds number of the seepage is within a certain region, while the value of  $a$  may have a large range. Eq. (2-33) which is derived by Li and Hu (1988) takes consideration of this problem, and can be used to solved this problem. It is noticed that in Eq. (2-33), the two constants  $a$  and  $b$  have very narrow range of value, and the small difference is determined by the range of the Reynolds number.

Parkin (1963) concluded that if the tail water level is below the point of emergence on the seepage face, it had practically no effect on the height of the point of emergence, which was determined using the following formula:

$$h_e = \frac{q}{n} \left[ \frac{c_0}{\sin \theta} \right]^{(1/c_1)} \quad (2-39)$$

where  $q$  = unit width discharge,  $Q/L$ ;

$\theta$  = angle of downstream slope;

$c_0$  &  $c_1$  from Eq. (2-27a);

$h_e$  = exit height on downstream face, relative to the foundation.

It is noticed that in order to obtain Eq. (2-39), some assumptions was made by Parkin. The first is that the hydraulic gradient :

$$i = \sin \theta \quad (2-40-1)$$

The second is that the seepage velocities along the depth remains constant. Eq. (2-36) also applies to the case of rockfill dam without a cutoff wall inside the dam.

$$h_c \approx 1.1 \frac{q}{n V_v} = 1.1 \frac{q}{5.3 \text{ m}^{0.5} i^{0.54} n} = \frac{0.2075 q}{n \text{ m}^{0.5} i^{0.54}} \quad (2-40-2)$$

where  $m$  was taken to be  $10/d$ .

Parkin (1991) stated that this relationship gives predictions in close agreement with laboratory results by Sandie using models of 19mm aggregate and  $\theta$  value up to  $90^\circ$ .

Cohen de Lara (1956) examined the effect of tailwater on the quantity of flow through a model dam, and developed relationships for the discharge for trapezoidal sections and for rectangular sections, and used a limited range of particle sizes.

In 1979, Stephenson (1979) demonstrated that  $h_e$  is the depth of critical seepage flow if the downstream water level is lower than this depth. He used Eq. (2-35) as the expression for fully developed turbulent seepage flow.

Hansen (1992) obtained the following empirical relationship to calculate the average hydraulic gradient through the dam:

$$i_{\text{average}} = 0.8 \left( \frac{h}{H} \right)^{1.4} \left( \frac{B_u + B_c + 0.5 B_d}{H} \right)^{\frac{2}{3}} \quad (2-41)$$

### 2.3.2 Free surface line within the rockfill dam

Within a rockfill dam, the profile of the phreatic surface is usually of interest in the engineering design. Finite element methods or finite difference methods may be used to obtain this profile. However in many cases, proper simplified methods are accurate enough to estimate this surface. The results available in the literature are summarized below.

Wilkins (1956) derived a 1-dimension general equation for rockfill based on the assumption replacing the friction gradient in the general 1-dimension equation of open channel flow by the seepage gradient defined by his seepage formula (Eq. 2-29):

$$\frac{\delta h}{\delta l} = \frac{i_1 - \frac{v^{1.85}}{c_0^{1.85} c_1^{0.925}}}{1 - \frac{v^2}{gh}} \quad (2-42)$$

where  $c_0$  , and  $c_1$  are coefficients in the Eq. (2-27b).

Basak (1976) simply integrated a non-Darcy equation of the form from Eq. (2-16), applied Dupuit assumption while neglecting the kinetic energy of the flow. Basak obtained good agreement between the resulting equation and Volker's (1975) phreatic surface data, which were obtained from experimental studies on a rectangular embankment made up of small diameter angular gravel.

For rectangular section, Stephenson (1979) presented the following analytical solution which was also used by Hansen (1992):

$$(x_0 - x) \frac{3K_t}{d} = \left(\frac{y}{y_c}\right)^3 - 1 - \ln \frac{y}{y_0} \quad (2-43)$$

where  $x_0$  and  $y_0$  represent the coordinate of the initial point at the phreatic surface,  $y_c$  is the critical depth defined by the Eq. (2-35).  $x$  and  $y$  are the coordinates in the horizontal and vertical directions.

During this research it has been found that the Eq. (2-43) is not correct. The expression should be:

$$(x_0 - x) \frac{3K_t}{d} = \left(\frac{y}{y_c}\right)^3 - \left(\frac{y_0}{y_c}\right)^3 - 3 \ln \frac{y}{y_0} \quad (2-44)$$

It should be mentioned that this equation only applies to fully turbulent seepage flow in a rectangular section.

Jain et al (1988) presented the "variable gradient method". In this method, the computational procedure which is based on Wilkins' seepage formula proceeds in an upstream direction. It can also be used to generate a rough flow net consisting of a

series of straight lines. But Hansen (1992) argued that this method requires a priori knowledge of the upstream water level, which greatly reduces its usefulness.

For the purpose of engineering design,  $h_c$ ,  $h_e$  and the water surface curve within the rockfill dam should be determined. As an initial design, 1-dimensional empirical relationships may be used.  $h_c$  may be determined by Eqs. (2-37) and (2-38),  $h_e$  may be obtained by Eq. (2-39) (recommended by Parkin, 1963).  $h_c$  may be determined by Eq. (2-35). Eq. (2-44) may be used as the seepage surface curve. In the final design of a dam, computational modelling should be conducted to deal with the 2-dimensional problem.

## 2.4 Computation of the Seepage Field within Rockfill Dams

Pore pressure distribution within rockfill dam has been the subject of considerable study, because of two reasons: first of all, the pore pressure gradient at the downstream slope surface directly influences the stability of the rocks at the surface; secondly, pore pressure distribution is needed to perform any slope failure analysis. Basically there are three kinds of method available, that is, flow net sketching method, finite difference method, and finite element method.

### 2.4.1 Flow net sketching method (2-dimensional steady non-Darcy seepage flow)

For Darcy flow, Laplace equation applies. By sketching a flow net, the pore pressure distribution within a rockfill dam can be determined, then the velocity distribution and the discharge through rockfill dam can also be determined.

According to Wilkins (1956) and Parkins (1963) a non-Darcy flow net can be sketched using the following relationship:

$$l = b^N \quad (2-45)$$

where:

$l$  = mean distance between equipotential lines within a given mesh element;

b = mean distance between flow lines for a mesh element;  
 N = empirical exponent defined by Eq. (2-27).

From expression (2-45), it is noticed that for a given hydraulic gradient, the mean distance between flow lines is less than the mean distance between equipotential lines for any individual element in a non-Darcy flow net mesh. Decreasing the mean distance between flow lines relative to the mean distance between equipotential lines implies a greater number of flow paths. The large number of flow paths in a flow net is consistent with a greater total quantity of seepage for the semi-turbulent or turbulent nature of seepage flow. According to Parkin (1971), the element in a turbulent flow "change their geometry with increasing velocity while maintaining orthogonality" (Figure 2-4). This might make sketching the flow net difficult (Hansen, 1992).

#### 2.4.2 Finite difference method

Eq. (2-16) can be combined with the continuity equation to form the field equation of Lawson, Trollope, and Parkin(1962):

$$(\phi_{xx} + \phi_{yy})(\phi_x^2 + \phi_y^2) + (N-1)(\phi_x^2 \phi_{xx} + 2\phi_x \phi_y \phi_{xy} + \phi_y^2 \phi_{yy}) = 0 \quad (2-46)$$

where  $\phi$  is a scalar potential function with derivatives  $\phi_x$ ,  $\phi_y$ , in the Cartesian directions and  $N = 1/\alpha$ . This equation can be solved after the manner of Curtis and Lawson (1967). Curtis and Lawson (1967) used a 9-point finite difference as the basis for approximating the hydraulic gradients in various directions. Figure 2-5 shows the node identification for this method.

$$\phi_0 = \frac{1}{2(1+N)}(\phi_1 + \phi_5 + \phi_7 + \phi_3) + \frac{N-1}{2(N+1)} \frac{(\phi_1 + \phi_5)(\phi_1 - \phi_5)^2 + \frac{1}{2}(\phi_1 - \phi_5)(\phi_3 - \phi_7)(\phi_2 + \phi_6 - \phi_4 - \phi_8) + (\phi_3 + \phi_7)(\phi_3 - \phi_7)^2}{(\phi_1 - \phi_5)^2 + (\phi_3 - \phi_7)^2} \quad (2-47)$$

As concluded by Hansen (1992), three factors limit the wider applicability of the results of the study by Curtis and Lawson to the analysis of predominantly flowthrough rockfill dams. First, an unusual geometry for the embankment was used. The model embankment in this case was 25 cm high, 1.8m long, 1.2 m wide, and had vertical upstream and downstream faces. Secondly, flowthrough was only 5 to 10 percent of the total flow, making this more of a specialized overflow study. Thirdly, no phreatic surface existed within the model dam used. The pressure of the overflowing water was used as a boundary condition for the numerical solution of the partial differential equation.

In a brief discussion of Curtis and Lawson (1967), Kirkham (1968) argued that  $N$  does not have a fixed value for the entire flow field. This appears to be a debatable point (see also the closure to Curtis and Lawson, 1969). Kirkham (1967) presented an alternative equation to Eq. (2-47). However Volker (1969) considered Kirkham's method an "unwarranted refinement" of the method of Curtis and Lawson.

With the given phreatic surface within rockfill dam and the given water surface curve at the downstream slope, Hansen (1992) solved the seepage field within rockfill dam with and without facing by the method derived by Curtis and Lawson (1967), i.e. Eq. (2-47). Hansen used a commercially available electronic spreadsheet operating on a desktop microcomputer. From the simulation of two modelled rockfill dams in which the steady-state discharge through the dams did not follow, Hansen (1992) concluded that:

a). Applying finite difference expressions associated with Darcy's law for edge nodes provided a workable model for piezometric pressure head even though flow through the embankment was non-linear. Mean absolute derivations from observed piezometric heads were less than 10 percent (this is higher than the maximum absolute derivation 6% in Volker's finite element method , 1969). About 3100 nodes were used for each model and this high density of nodes was considered to be important for the success of the model (while in Volker's finite element method, the node number is about 100 to 500, and the difference of the result is within 2% when the node number is changed from 100 to 500).

b). The introduction of an impermeable upstream face on the dam necessitated a greater number of relaxations of the finite difference grid. It was found to be computationally intensive to model the piezometric heads in the size between the impermeable face and the base of the dam.

During this research, it has been noticed that the equation of Lawson, Trollope, and Parkin (1962) , Eq. (2-46) may be solved well for regular boundary (rectangular section) by the finite difference formula Eq. (2-47). For a trapezoidal rockfill dam without facing (this is not common in engineering), "high density of nodes" is the only way to make the model successful. If a facing is placed within a rockfill dam, it is more difficult to handle the finite difference method. The reasons may be: (a) the non-linear characteristics of the governing equation, which makes it difficult to obtain an accurate solution by the finite difference method proposed; (b) the irregular boundary behavior, which makes it difficult to handle the boundary conditions in finite difference method. These factors limit the use of finite difference method for non-Darcy flow.

### 2.4.3 Finite element method

The first work using finite element method (FEM) in turbulent seepage flow may be Fenton's research (1968). Fenton (1968) dealt with a finite element solution to Eq. (2-46) but allowed only for a horizontal impermeable base and did not attempt experimental correlation of the results.

Field equations for finite element method can be developed in a variety of ways from equations Eqs. (2-16) (quadratic law) and (2-27) (power law). Volker (1969) derived a series of equations for both laws.

For the quadratic law, Volker (1969) wrote the law in the following vector form:

$$\text{grad } h = (a + b |\nabla|) \nabla \quad (2-48)$$

Using the continuity condition, he derived the field equation governing seepage flow in a two-dimensional flow field:

$$\frac{\partial}{\partial x} \left\{ \left[ -\frac{a}{2b} + \sqrt{\left(\frac{a}{2b}\right)^2 + \frac{|h_s|}{b}} \right] \frac{(-h_x)}{|h_s|} \right\} + \frac{\partial}{\partial y} \left\{ \left[ -\frac{a}{2b} + \sqrt{\left(\frac{a}{2b}\right)^2 + \frac{|h_s|}{b}} \right] \frac{(-h_y)}{|h_s|} \right\} = 0 \quad (2-49)$$

where

$$-h_x = (a + b|V|)u \quad (2-50)$$

$$-h_y = (a + b|V|)v \quad (2-51)$$

and

$$|h_s| = (a + b|V|)|V| \quad (2-52)$$

in which  $u$  and  $v$  are the velocities in the direction of  $x$  and  $y$  respectively.

For the power law, Volker (1969) wrote it in the following vector form:

$$-h_s s = (c|V|^{m-1})V \quad (2-53)$$

The continuity relation gives:

$$\frac{\partial}{\partial x} \left[ \left( \frac{|h_s|}{c} \right)^{1/m} \frac{(-h_x)}{|h_s|} \right] + \frac{\partial}{\partial y} \left[ \left( \frac{|h_s|}{c} \right)^{1/m} \frac{(-h_y)}{|h_s|} \right] = 0 \quad (2-54)$$

where

$$-h_x = (c|V|^{m-1})u \quad (2-55)$$

$$-h_y = (c|V|^{m-1})v \quad (2-56)$$

Variational methods were used to build up the finite element equations using triangular elements.

McCorqudale (1970) simulated flow through a rectangular rockfill block without facing using triangular elements. Compliance of the double boundary condition on the free surface was accomplished by using the "membrane analogy", i.e. the free surface (which is a streamline) is positioned so that the pressure across it is zero. A trial free surface was chosen first and the finite element model was used to solve for the

pressure difference across the "membrane". On the basis of the computed pressure differences the surface ordinates were adjusted to decrease these differences (McCorqudale, 1970). The location of the outcrop point was determined by adjusting the seepage height until the upstream and downstream discharges were equal. McCorqudale (1970) undertook a few runs of tests and got the optimum value of the over-relaxation factor as 1.5.

McCorqudale (1970) concluded that:

- (1) In all the finite element solutions, the free surface elevation tended to be underestimated, except in the neighborhood of the outcrop point where there does not appear to be a significant trend in the estimates;
- (2) The FEM gave excellent predictions of discharge and good predictions of seepage height and fair predictions of piezometric levels;
- (3) The model is not very sensitive to the coefficient  $b$ .
- (4) The possible error in the numerical solution could result from the discretization of the flow regime and is influenced by the number of nodal points.

Parkin (1971) solved the non-Darcy seepage field of a uniform rockfill dam with the formula derived by Fenton (1968) with the variational principle. From the simulation, Parkin concluded that the turbulent flow net is seen to have a somewhat higher phreatic surface and a larger seepage face, which is associated with a higher discharge and with higher exit gradients, as depicted in the equipotential pattern; this would, if anything, tend to have an adverse effect on the stability of such slopes.

From the literature review, it can be concluded that:

- a. The FEM is advantageous when irregular boundaries exist (this is usually the case in engineering design, e.g. uniform or non-uniform rockfill dam with cut-off wall, non-uniform rockfill dam);
- b. The FEM has higher accuracy compared with finite difference method (FDM);
- c. In the FEM, a small number of nodes can achieve a good result, while in FDM, a high density of nodes (from the available records, at least 10 times the nodes used in FEM simulation) is required to make the simulation successful;
- d. The FEM is more suitable when a curved free surface exists, due to the difficulty in using FDM mesh to simulate the curved free surface correctly;

For non-Darcy flow, the flow-net sketching method would be very difficult. The only practical way is computer modelling. The available results show that FDM is useful only when the geometry is very simple, while FEM may be valid in almost all the engineering cases. FEM has been used in the present study.

Available results and experience have been used in the present study to make the model more efficient, more general, and easy to handle by an engineer. The seepage surface from Darcy law is quite close to that from non-Darcy flow. However, the discharge and the hydraulic gradient near the downstream slope calculated from non-Darcy flow model may be much higher than that from Darcy flow mode.

## **2.5 Shear Stress and Seepage Force at the Downstream Slope**

### **2.5.1 Shear stress in spatially varied flow**

For flowthrough rockfill dam, the total quantity of flow passing through the structure will be completely in overflow at the toe of the dam. Figure 2-6 shows the scheme for seepage-face definitions. Spatially varied flow occurs on the downstream slope face,

beginning at the point of flow emergence point. This category of flow occurs when discharge changes with the distance along a relatively short channel under steady-state conditions. Sharp and James (1963) presented the following equation describing this phenomenon:

$$\frac{dQ}{dx} = n \left[ \frac{\tan \theta}{a} \right]^N \quad (2-57)$$

where:

$dQ/dx$  = rate of discharge along downstream slope;

$\theta$  = angle of downstream slope;

$n$  = porosity;

$a$  and  $N$  are the coefficients from the exponential seepage law.

Sharp and James' result was based on several assumptions:

- a. A hydrostatic pressure distribution exists within the rock mass which is adjacent to the downstream slope (this approximation is not accurate);
- b. Only atmospheric pressure acts on the downstream slope;
- c. Exponential seepage law applies.

The well known equation for spatial varied open channel flow (lateral spillway channel) is (Chow, 1959):

$$\frac{dy}{dx} = \frac{S_0 - S_f - \frac{2\alpha Q q_s}{gA^2}}{1 - \frac{\alpha Q^2}{gA^2 D}} \quad (2-58)$$

where:

$x$  = coordinate in the direction of the slope;

$y$  = coordinate in the direction of the slope;

$dx/dy$  = rate of change of water surface elevation;

- $S_0$  = bed slope;
- $S_f$  = friction slope;
- $\alpha$  = velocity head correction coefficient;
- $Q$  = discharge of the flow;
- $q_x$  = rate of the change of discharge with distance (=  $dQ/dx$ );
- $A$  = vertical sectional area of flow;
- $D$  = hydraulic radius.

Sharp and James (1963) used this expression as the basics for their study on the spatial varied flow at the toe of flow through rockfill dam. It should be noticed that Eq. (2-81) is derived from the assumptions:

- a. The total pressure on a vertical section in the direction of flow is equal to the unit hydraulic static pressure at the centroid of the water area  $A$  multiplied by the area.
- b. The slope angle is small.
- c. The flow is unidirectional;
- d. The effect of air entrainment is neglected;
- e. The flow is constant;
- f. The lateral moment perpendicular to the direction of the flow is ignored.

Sharp and James (1963) presented the following expression for the steep slope case (the detailed procedure of derivation was shown by Hansen, 1992 with Chow's method):

$$\frac{d d}{d x} = \frac{\frac{S_0 - S_f}{\cos \theta} - \alpha \frac{2 q_x Q}{g A^2 \cos \theta}}{1 - \alpha \frac{Q^2}{A^2 D g \cos \theta}} \quad (2-59)$$

where  $d$  = water depth perpendicular to the downstream slope. All the assumptions except  $a$  and  $b$  of Chow (1959) also accompany this expression.

The friction slope,  $S_f$ , has the following relationship with the shear force:

$$\tau_o = \gamma_w R S_f \quad (2-60)$$

The main limitation in the expression by Sharp and James (1963) is that at or near the seepage exit point on the downstream slope, both the discharge and the momentum are small, and the direction of seepage is not perpendicular to the downstream slope. This implies that the assumption (f) mentioned on the previous page is incorrect. Indeed the momentum equation from this seepage is a major component of the momentum equation. Hence, the expression does not apply to the region at and near the seepage exit point on the downstream slope of a flowthrough rockfill dam.

### 2.5.2 Seepage force at the downstream slope

Seepage flow emerging from the downstream slope has a certain hydraulic gradient associated with it, and the destabilizing effect of this seepage must be considered in addition to that of overflow erosion (Hansen, 1992).

For Darcy flow in soils the "quick" condition, which occurs when intergranular contact forces becomes zero, is:

$$i_c = \frac{\rho_s - \rho_w}{\rho_w} \quad (2-61)$$

where:

$\rho_s$  = bulk density of the porous media;

$\rho_w$  = density of water.

For non-Darcy flow, it is not clear what the critical hydraulic gradient would be.

Wilkins (1956) stated that if the critical hydraulic gradient is unity and a factor of safety of 2 is used, then:

$$V_p = 16 m^{0.5} \quad (2-62)$$

where:

$m$  = hydraulic mean radius (inches);

$V_p$  = "piping velocity", inches/sec.

Hansen (1992) developed the empirical expression from experimental results:

$$\frac{\theta_{ff}}{\theta} = 1.41 \frac{h_e}{H} + 0.17 \quad (2-63)$$

where

$H$  = the total height of rockfill dam;

$\theta_{ff}$  = the angle between exit seepage line and horizontal line.

It should be noticed that the term  $h_e/H$  is not appropriate because  $\theta_{ff}$  should be related to both the upstream and downstream water levels.

Once the hydraulic gradient is known (by numerical method), the force per unit volume of material due to seepage flow can be estimated from:

$$\frac{F}{v} = \gamma_w i \quad (2-64)$$

where:

$F$  = seepage force;

$v$  = bulk volume;

$\gamma_w$  = unit weight of water;

$i$  = hydraulic gradient.

Craig (1987) and Hansen (1992) considered that the minimum bulk volume is given by:

$$v_{min} = e v_p + v_p \quad (2-65)$$

where:

$v_p$  = representative particle volume computed from average rock mass/rock density);

$v_{min}$  = minimum bulk volume which could contain a particle of volume  $v_p$ ;

$e$  = void ratio.

Seepage force per particle then may be calculated by:

$$F_{sp} = (e v_p + v_p) \gamma_w i \quad (2-66)$$

in which  $F_{sp}$  = seepage force per particle.

In this research seepage force distribution will be calculated based on the 2-dimensional non-Darcy finite element method and 1-dimensional overtopping finite difference method for the purpose of stability analysis.

## 2.6 Slip Failure of A Flowthrough Rockfill Dam

Wilkins (1956, 1963) and Parkin (1963) indicated that analyses based on an assumed slip surface are more applicable when downstream slope is anchored. Parkin (1991) concluded that in the absence of a stabilizing surface mesh, the primary mode of failure will in all cases be by the erosion of surface stones, in which case slip failures will not occur.

Many methods have been used in the design of rockfill dams, e.g., Bishop's Simplified Method, Spencer's Method, Janbu's Rigorous Method, Janbu's Simplified Method, Morgenstern-Price Method, and the Wedge Method.

As summarized by Hansen (1992), two methods have been reported in the stability analysis of the massive failure of downstream slope of a flowthrough rockfill dam, that is, Bishop's Simplified Method (for example, Craig, 1987), and the Wedge Method (described in Hansen, 1992). In both methods, the pore pressure plays an important role in the stability of the rockfill dam, due to the turbulence behavior of the flow through rockfill.

In engineering practice, there may be constraints as to the quantity and size of rock available at a given site. If it is concluded that some form of reinforcing mesh is necessary at a particular site, two questions should be solved in the stability analysis. First of all, what is the magnitude and direction of forces acting on the reinforcing mesh? Secondly, since the mesh must be anchored somewhere, how deeply into the body of the dam should the anchors extend? With regard to the first question, no references to actual measurements were found in the literature regarding the magnitude and direction of bursting forces on the reinforcing meshing a flowthrough rockfill dam. As to anchoring strategies, it is clear that anchor bars, to which the mesh is attached at intervals, must extend into the body of the dam to a location where the rocks will not be mobilized by excessive hydraulic gradients (Hansen, 1992).

From the development of Coulomb's expression for the active earth pressure against a retaining wall, Hansen (1992) derived the formula:

$$P_a = \frac{\sin(\rho - \phi + \xi)}{\sin(180 - \alpha - \rho + \phi + \delta)} F_B \quad (2-67)$$

where

$P_a$  = force against the fictitious wall, acting at angle  $\delta$  below the horizontal;

$\rho$  = angle of the rupture plane;

$\xi$  = angle of the net force  $F_B$ , measured above the vertical;

$\delta$  = angle of friction for the interaction between the media and the fictitious wall;

$\alpha$  = angle of the wall above the horizontal;

$F_B$  = the force per unit length of dam acting on the material between the rupture plane and the wall, which is a vector combination of the buoyant weight and the seepage force.

In Hansen's work,  $\alpha$  is always equal to  $90^\circ$ , i.e. the line separating the upper and lower wedges is always vertical, and  $\delta$  always equals to  $\phi$ , i.e. the angle of friction between the media and the fictitious wall is in fact simply that of the media itself (Figure 2-7). Under these two assumptions, Hansen (1992) obtained the final equation for the active pressure exerted by the upper wedge:

$$P_a = \frac{\sin(\rho - \phi + \xi)}{\cos(2\phi - \rho)} F_B \quad (2-68)$$

It is noted that  $F_B$  is the combination of seepage force and buoyant weight. The upstream extent of the lower wedge is found from the determination of the point at which frictional shear resistance ceases to exist at the base of the dam. The upstream extent of the upper wedge, which thrusts against the lower wedge, is determined by successive trials to find the critical angle of the rupture plane  $\rho$  which causes  $P_a$  to be a maximum. At the critical  $\rho$ , the force against the fictitious wall is a maximum. The value of the critical angle  $\rho$  is affected by the angle of the internal friction of the media and the 2-D configuration of the dam, as well as the pattern of pore pressures within the upper wedge. For any given  $\rho$ , the spatial variation of the pore pressure pattern within the upper wedge implies a certain overall seepage force within this wedge, and the variation of this overall seepage force with  $\rho$  cannot be described in simple analytical terms (Hansen, 1992). In general it will depend on the configuration of the dam (2-D shape), the location of the phreatic line, and the magnitude and proximity of all the boundary conditions.

In classical slope stability methods, minimum FOS (factor of safety) is searched by different trials. For any value of FOS less than unity or certain given design value, all the material above the assumed slip surface is considered unstable and will fail in the absence of restraint. In the wedge method, for a given  $\rho$ , the analysis provides a bursting pressure associated with the active pressure of the upper wedge against the lower wedge. The critical angle  $\rho$  of the interest is that angle which gives the largest active pressure of the upper wedge. Hansen (1992) measured the bursting forces with a typical designed equipment. The ratio of computational results over the measured values was from 1.0 to 2.1.

Slope stability analysis is an important feature of the design of a rockfill dam. It is noticed that the seepage force has an important contribution on the slope stability of a flowthrough rockfill dam. To obtain the seepage forces on the rock particles, finite element method simulation of the non-Darcy seepage field should be conducted. The

stability analysis with wedge method, or Bishop method, or other classical methods can then be conducted with the seepage field and force information obtained from the finite element method.

## 2.7 Friction Head Losses During Overtopping Flow

Determination of friction head losses is a classical problem in hydraulics. For rockfill, due to the high permeability and the uncertainty of the material, the determination of the head losses for flow over rockfill face is a very complex task.

The usual expression of relative roughness  $\varepsilon$ , for non-high relative roughness channel ( $\varepsilon \leq 0.05$ ):

$$\varepsilon = \frac{k'}{D} = \frac{k'}{4R} \quad (2-69)$$

in which

$k'$  = absolute roughness;

$D$  = the hydraulic diameter ( $D=4R$ );

$R$  = hydraulic radius.

If a channel is wide enough,  $R \approx h$ , where  $h$  is the depth of the flow over rockfill. Then Eq. (2-69) may be written as:

$$\varepsilon = \frac{D}{4h} \quad (2-70)$$

In rockfill hydraulics, the term  $D/h$  is usually used.

For flow over rockfill face, the relative roughness may be much higher than 0.05. Although we usually consider uniform flow for friction calculation for rockfill, the uniform flow in open channel will never happen in rockfill due to the uncertainty of the shape and roughness of rockfill surface. Since friction head losses expressions have been based on uniform flows, the non-availability of the general theory of friction head losses in rockfill hydraulics remains a problem in engineering design.

Friction head loss calculations are based on the Darcy-Weisbach equation:

$$i = f \frac{l}{D} \frac{U^2}{2g} \quad (2-71)$$

where

$l$  = the distance between the two cross sections when calculating  $i$ ;

$i$  = hydraulic gradient;

$f$  = friction factor;

$D = 4R$ ;

$U$  = the mean velocity;

$g$  = the gravity acceleration.

For turbulent flow,  $f$  is considered to depend only on relative roughness (this is argued by Li (1989), Zhou (1992)), and is given by the Karman-Prandtl equation:

$$\frac{1}{\sqrt{f}} = 2 \log \frac{3}{\varepsilon} \quad (2-72)$$

where  $\varepsilon$  is the relative roughness.

Bray (1979) obtained an expression for the friction coefficient from the analysis of the prototype data with Reynolds number from 200,000 to 20,000,000:

$$\frac{1}{\sqrt{f}} = 0.0519 \text{Re}^{0.294} \quad (2-73)$$

where  $f$  = friction coefficient in the Darcy-Weisbach equation.

From experiments (Reynolds number from 1,150 to 9,040, and the diameters of rockfill from 7.5 mm to 46.4 mm), Li (1989) indicated that for the flow over rockfill surface, the friction coefficient is not a constant but a function of the fluid field characteristics, especially the Reynolds number.

$$f = 42.267 \text{Re}^{-0.621} \quad (2-74)$$

When  $\varepsilon > 0.05$ , Martins (1991) recommended that the following two expressions may be used. The first expression is the Graf equation (1989):

$$\frac{1}{\sqrt{f}} = 2 \log \frac{1}{4\varepsilon} + 1.15 \quad (2-75)$$

The second expression is the Thompson-Chambell (1979) equation:

$$\frac{1}{\sqrt{f}} = 2(1 - 0.8\varepsilon) \log \frac{1.5}{\varepsilon} \quad (2-76)$$

However simulations during this research indicate that the above expressions lack adquant precision for the practical design of an ovetopped rockfill dam.

The Manning equation is written as (SI unit):

$$U = \frac{R^{2/3} S^{1/2}}{n} \quad (2-77)$$

where  $n$  = Manning coefficient which depends on the characteristics of the surface roughness alone. From Martins's (1991) result,  $n$  may be expressed as:

$$n = \frac{d^{1/6}}{20} \quad (2-78)$$

where  $d$  = the diameter of rockfill, which may be represented by the  $d_{50}$  or  $d_{90}$  size (in meter).

By Strickler equation:

$$n = 0.047 d_{50}^{1/6} \quad (2-79)$$

where  $d_{50}$  = median bed material size in m.

Maynord (1990) studied on the resistance of flow on riprap with diameter  $d_{50} = 0.055$  ft to 0.444 ft and the ratio of water depth to  $d_{50}$  larger that 5. With the data collected from others, he obtained the following relationships for the Strickler equation:

$$n = 0.0360 D_{90}^{1/6} \quad (2-80)$$

and

$$n = 0.0380 D_{50}^{1/6} \quad (2-81)$$

where  $D_{50}$  and  $D_{90}$  are in feet.

Very limited experimental data is available on the value of  $n$  near the exit face of a flowthrough rockfill dam. The only available but limited data is that presented by Sharp and James (1963). Hansen (1992) performed simulation for their data and concluded that the value of  $n$  at about 10% of the length of downstream slope from the seepage - exit point to the toe of the dam was taken as a relatively low value (about 0.015-0.017) and increased linearly along the seepage face to the toe, where the value of  $n$  was taken as that for fully turbulent flow. The value of  $n$  at the downstream toe calculated from Stricker equation is found to be higher than indicated in data presented by Sharp and James (1963).

Hansen's consideration (1992) about the linear variation of  $n$  along the downstream slope of an flowthrough and overtopped rockfill dam will also be used in the present study. Eq. (2-81) will be used in the design to predict the value of Manning coefficient  $n$  at the toe of the downstream slope.

## 2.8 Unraveling Failure of the Downstream Slope

Isbash (1935) investigated the construction of dams by dumping rounded stones into flowing rivers. He conducted a series of experiments that yield an expression indicating the critical transport velocity for displacing rounded stones as:

$$v = C \left[ 2g \left( \frac{\gamma_s - \gamma_w}{\gamma_w} \right) \right]^{1/2} D_{50}^{1/2} \quad (2-82)$$

where

$v$  = the velocity acting against the individual stones;

$D_{50}$  = average stone size;

$\gamma_s$  = the unit weight of the stone;

$C$  = a coefficient. For low turbulence,  $C=1.2$ .

A comprehensive investigation was also conducted by Olivier (1967) on the flow through and over rockfill dams. A series of laboratory experiments were performed to evaluate how rockfill could be safely overtopped by floods both during and after construction without risk of failure. Olivier carried out his experiments in 56cm wide and

152cm long flumes on slopes ranging from 8 to 45 %. Median stone sizes ranged from 1.3cm to 6cm for crushed granite and from 1.6cm to 2.6cm for pebbles and gravel.

Olivier observed two distinct stages during each test: threshold flow and collapse flow. Threshold flow was defined when incipient stone movement occurs. Collapse flow is the final stage where stone failure results. Olivier was the first to recognize that channelization occurred between the threshold and collapsing stages. Olivier empirically derived an expression for overtopping flow linking the design parameters of unit flow, slope, and median rock size for crushed or rough stones to threshold flow. The unit discharge at the stone movement is given by:

$$q_{cr} = 0.423 D_{50}^{3/2} \left[ \frac{\gamma_s - \gamma_w}{\gamma_w} \right]^{5/3} i^{-7/6} \quad (2-83)$$

where

$q_{cr}$  = the critical unit discharge at stone movement;

$i$  = the embankment gradient.

Hartung and Scheuerlein (1970) performed a series of overflow tests in a steep flume simulation steep open channels with natural roughness. The maximum unit discharge,  $q_{max}$ , that would resist stone movement can be expressed as:

$$q_{max} = T Y_m V_c \quad (2-84)$$

where

$$V_c = 1.2 \left[ 2g \left( \frac{\gamma_s - \gamma_w}{T \gamma_w} \right) \right]^{1/2} (d_s \cos \theta)^{1/2} \quad (2-85)$$

and

$$T = \frac{\gamma_w l}{\gamma_w} \quad (2-86)$$

or

$$T = 1 - 1.3 \sin \theta + 0.08 \frac{Y_m}{\zeta_m} \quad (2-87)$$

where

$y_m$  = the mean water depth;

$\zeta_m$  = the mean roughness height,  $\zeta_m \approx d_s/3$ ;

$d_s$  = the equivalent diameter of the stones (here it is equal to  $d_{50}$ );

- $\theta$  = the angle of the slope;
- $T$  = the aeration factor;
- $V_c$  = the critical velocity at which the stone begins to move;
- $\gamma_{wl}$  = the specific weight of the air-water mixture;
- $g$  = the acceleration of gravity.

Stephenson (1979) performed a stability analysis for the stones placed on the downstream face of a rockfill embankment subjected to overtopping. His analysis of the hydraulic reaction on the resisting stones related the stone size to the slope angle and flow rate. The equation that Stephenson derived to determine median stone size,  $d$ , for the threshold flow is expressed as:

$$d = \left[ \frac{q_{cr} (\tan \theta)^{7/6} n^{1/6}}{Cg^{1/2} [(1-n)(S-1) \cos \theta (\tan \phi - \tan \theta)]^{5/3}} \right]^{2/3} \quad (2-88)$$

where

- $q_{cr}$  = the threshold unit discharge;
- $n$  = the porosity of the rockfill;
- $S$  = the specific gravity of the stone;
- $\theta$  = the slope angle;
- $\phi$  = the angle of friction;
- $g$  = the gravitational acceleration;
- $C$  = the coefficient which is derived from Olivier (1967) and reported to be 0.22 for gravel and pebbles, and 0.27 for the crushed stone.

Knauss (1979) performed a comparison of the Olivier (1967) expression, (2-87), and the Hartung and Scheuerlein expression, (2-88), for the overtopping conditions. He determined that both equations were valid for crushed stone with angular shapes. However, Knauss (1979) recommended the Hartung and Scheuerlein equation (1970) for the design of overtopped rockfill dams with steep downstream slopes ranging from 20 to 67%.

Powledge and Dodge (1985) conducted a series of small-scale overtopping tests using riprap as embankment protection on the downstream face. Since the tests were to

evaluate embankment protection and not to provide riprap design criteria, the riprap fluidized and eroded the embankment. Powledge and Dodge determined that improperly designed riprap did not provide erosive protection to the embankment from overtopping flow.

Abt and Johnson (1991) conducted experiments for overtopping riprap protection with median stone sizes,  $D_{50}$ , from 2.58cm to 15.75cm. The tangent of the slope varied from 0.01 to 0.20. The proposed formula to estimate the minimum median stone size required to withstand a design overtopping unit discharge on an embankment with specific design slope is:

$$D_{50} = 5.23i^{0.43}q_f^{0.56} \quad (\text{in.}) \quad (2-89)$$

where

$q_f$  = the unit discharge at failure (cfs/ft);

$i$  = the gradient of the slope.

Eq. (2-89) may be rewritten as:

$$D_{50} = 0.503i^{0.43}q_f^{0.56} \quad (\text{m}) \quad (2-90)$$

The unit discharge  $q_f$  may be determined by:

$$q_f = c_f q \quad (2-91)$$

where

$c_f$  = concentration coefficient determined by the condition of overflow concentration. The following value is recommended by Abt (1987):

$$c_f = \begin{cases} 1.0, & \text{for overland sheet flow;} \\ 2.0, & \text{for a high probability of concentrated flow;} \\ 3.0, & \text{for a high probability of channelized flow.} \end{cases} \quad (2-92)$$

The depth of the protection layer is given by Abt's formula (Abt, 1988):

$$t_r = \max\{1.5D_{50}, D_{100}\} \quad (2-93)$$

Abt and Johnson (1991) also indicated that the rounded riprap appears to require oversizing of about 40% to provide a similar level of protection as angular riprap. But in rockfill dams, the shape of rock particles is usually not rounded.

## **2.9 Discussion and Conclusions**

Previous results from literature review that are satisfactory for use in the design of an overtopped rockfill dam are listed below:

- (1) Governing equation of spatially varied flow at the downstream slope of a flowthrough and overtopped rockfill dam and the solution procedure proposed by Chow;
- (2) The variation of Manning coefficient  $n$  along the downstream slope or the equations for friction coefficient of overtopping flow proposed by Hansen (1992);
- (3) The equation for the discharge of overtopping flow;
- (4) The wedge method for the stability analysis of a flowthrough rockfill dam;
- (5) Equations for unravelling failure of the downstream slope.

The literature review in this chapter also shows that in order to develop a proper design methodology, it is necessary to conduct research in the following areas:

- (1) The general relationship between the Reynolds number and the friction coefficient of the seepage in rockfill.
- (2) The general relationship between the hydraulic gradient and the velocity of seepage flow in rockfill.
- (3) The difference between all the available formulae for non-Darcy flow by the computer simulation with wide range of porosity and size of rockfill to show the behaviour of all the different formulae. Comparisons between the simulated results of available formulae and the available prototype data are also required to achieve at the best expression for design.
- (4) Determination of the hydraulic mean radius of rockfill material by empirical relationship;
- (5) Estimation of seepage discharge through a rockfill dam without numerical modelling.

- (6) High-accuracy finite element method to model the non-Darcy seepage field within a flowthrough and overtopped rockfill dam.
- (7) The failure patterns of a flowthrough and overtopped rockfill dam.
- (8) Formula for the design of large-size particles protected at the downstream slope of a flow-through (seepage flow) and overtopping flow rockfill dam.
- (9) Formula for the design of mesh protection at the downstream slope of a flowthrough and overtopped rockfill dam.
- (10) Formula for the design of steel bars protected at the downstream slope of a flowthrough and overtopped rockfill dam.
- (11) A practical design methodology which applies to small flowthrough and overtopped rockfill dams.

**Table 2-1 Previous research on non-Darcy flow**

Researcher	Description of work
Forchheimer 1901	Quadratic non-Darcy law based on experimental data
Isbash 1931	Power non-Darcy law based on experimental data and also dimension analysis
Weiss 1951	Documented construction and performance of rockfill spillways in Mexico
Escande 1953	Tests on rectangular model dams, 3.5 cm rock. Equation for the seepage coefficient assuming that the exponential constant is 2.
Cohen de Lara 1956	Tail water effects on the quantity of the seepage discharge and on the stability
Wilkins 1956	A widely accepted exponential expression based on experimental data using hydraulic mean radius. Non-Darcy flow net
Slepicka (1961)	Research on a new formula of exponential law based on dimensional analysis and semiempirically.
Sharp & James 1962	Detailed experiments & analysis of spatially varied flow
Wilkins 1963	Stability analysis using Bishop's method. Suggestion for reinforcement
Parkin 1963	A partial differential equation for non-Darcy flow. Flow zone of flow when inbuilt spillway present

**Table 2-1 Previous research on non-Darcy flow (continued)**

Researcher	Description of work
Dudgeon 1964,66	Column tests on 15 cm rock. wall effect
Curtis & Lawson 1967	Finite difference method for pore pressures
Olivier 1967	Overflow equation for threshold discharge for gradual slopes
Sarkaria 1968	Tests on reinforced model dam at Froude scale
Volker 1969	Concurrently developed FEM coding for computing pore pressure, free surface , and discharge
McCorquodale 1971	FEM coding for computing pore pressure and free surface
Parkin 1971	FEM for pore pressures and Bishop's method estimating the location of reinforcement
Arbhabhirama and Dinoy (1973)	Experiments on different sand and gravel
Basak (1977)	Analysis on constants of exponential law.
Stephenson 1978, 79	Dimensionless free water surfaces, textbook on rockfill in hydraulics
Gerodetti 1981	Model dam tests with full-height central impermeable core. Gabon's on downstream face found inadequate. Emergent important

**Table 2-1 Previous research on non-Darcy flow (continued)**

Researcher	Description of work
Jain et al 1988	Model tests to determine total head loss when no impermeable facing present. "variable gradient method" for computing phreatic surface and approximate flow net
Li and Hu 1988	General expression for the coefficients in power non-Darcy law. Simulation law for non-Darcy flow and overtopping flow
Hu and Li 1988	Experiments for flow net and the stability of a overtopped rockfill dam under construction in the flood period
Hu et al 1988	Design and prototype study on flow through and overtopping of a rockfill dam under construction
Hu and Li 1986-91	Experiments for the flow net of flowthrough rockfill dam and overtopped rockfill dam, and failure conditions.
Martins 1990	Packed column tests on a variety of material. Effect of gradation of the media.
Kells 1990-94	Flow through and over gabion weir, spatially varied flow.
Hansen, Garga, and Townsend, 1992	Shape factor of rocks, packed column tests, Finite difference method for non-Darcy seepage flow with given water surface, wedge method and Bishop method for stability analysis.

**Table 2-2 Some Prototype Flowthrough and Overtopped Rockfill Dams**

Name of Dam & Documentor	Descriptive Notes
San Ildefonso, Weiss (1951)	<p>Completed 1939 in Mexico.</p> <p>H=62m, <math>B_c = 5m</math>. Downstream slope 1V:4H.</p> <p>Rebar lattice + tie backs.</p> <p>Undamaged by 142 m<sup>3</sup>/s flood, but subsequently damaged by another flood after mesh removed.</p> <p>Present status unknown.</p>
Osceola, Barr & Rosene (1958)	<p>Completion date unknown; Iowa, USA.</p> <p>H = 3.6m, <math>B_c = 2.4m</math>, <math>L_c = 30.5m</math></p> <p>downstream slope 1V:5H; Concrete apron over the toe.</p> <p>Design discharge = 76.5 m<sup>3</sup>/s</p> <p>Present status unknown.</p>
Hellhole, Johnson (1971)	<p>Partly completed in 1964; California, USA.</p> <p>H = 67 m, <math>B_c = 18.3m</math></p> <p>Downstream slope: 1V:1.3H, no reinforcement.</p> <p>Failed by flow of about 56.6 m<sup>3</sup>/s</p> <p>Present status unknown.</p>
Cethana H. - E.C. (1969) Varty et al (1985)	<p>Completed 1971 in State of Tasmania, Australia.</p> <p>H = 110m, <math>B_c</math> small, <math>L_c = 215 m</math></p> <p>Downstream slope 1V:1.3H; gabion lattice + tiebacks.</p> <p>Damaged before completion, repaired.</p> <p>Subsequently undamaged by "massive" flood.</p>

**Table 2-2 Some Prototype Flowthrough Rockfill Dams/Spillways (continued)**

Name of Dam & Documentor	Descriptive Notes
Deyuxue Chen and Jin (1982)	<p>Place unknown</p> <p>H = 125m, <math>L_c = 479</math> m</p> <p>Downstream slope 1:1.3</p> <p>1964 failed before completion, water head over upstream facing about 41 m. discharge at initial failure at the toe due to seepage through about 540 m<sup>3</sup>/s. The hydraulic gradient at the initial seepage - through failure is 0.277. The dam failed progressively due to instability of the downstream slope</p>
Diexi Chen and Jin (1982)	<p>Mingjiang, China</p> <p>Dimension of the dam unknown</p> <p>Particles with diameter greater than 15 cm only accounted for 30% of the dam, particles with diameter smaller than 0.5 cm accounted for 40%. Seepage discharge is small.</p> <p>Failed due to overtopping.</p>
Dahaizi Chen and Jin (1982)	<p>Mingjiang, China</p> <p>particles with diameter greater than 1 m accounted for about 70%, and mainly placed at the low part of the dam, only a few small fragment placed at the top of the dam.</p> <p>worked well.</p>

Figure 2-1(a) Nomenclature used for a flowthrough rockfill dam (after Hansen, 1992)

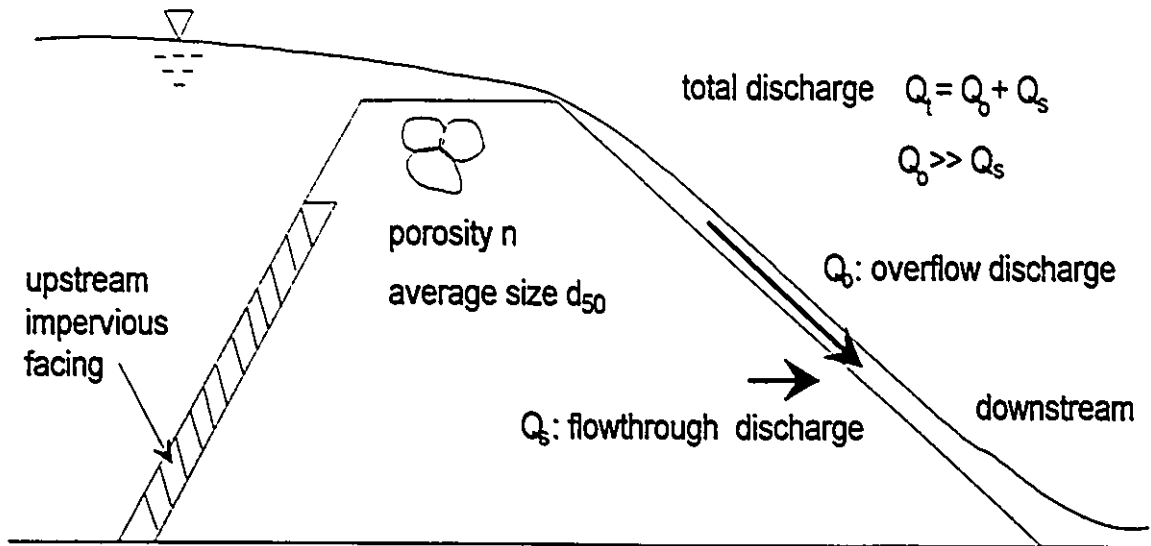


Figure 2-1 (b) Illustration of a flowthrough and overtopped rockfill dam

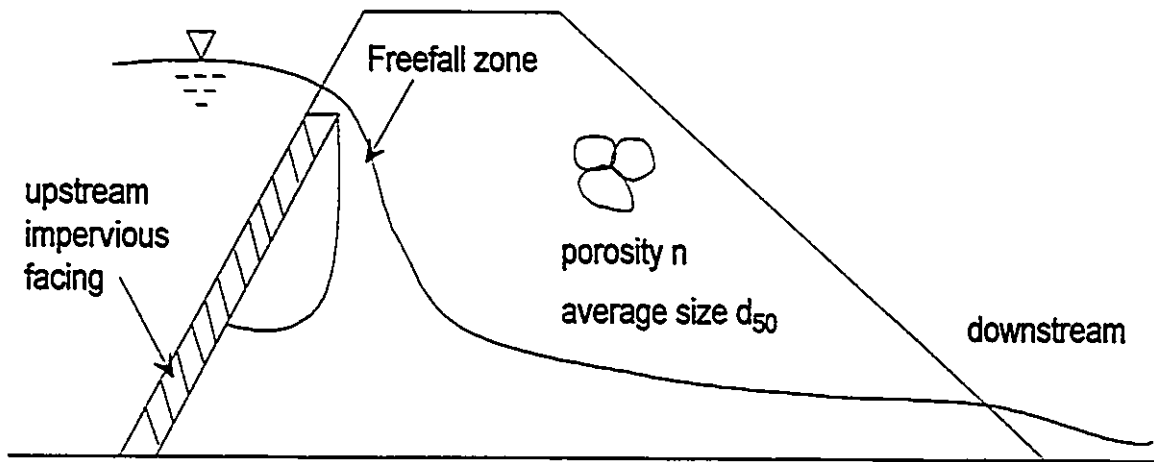
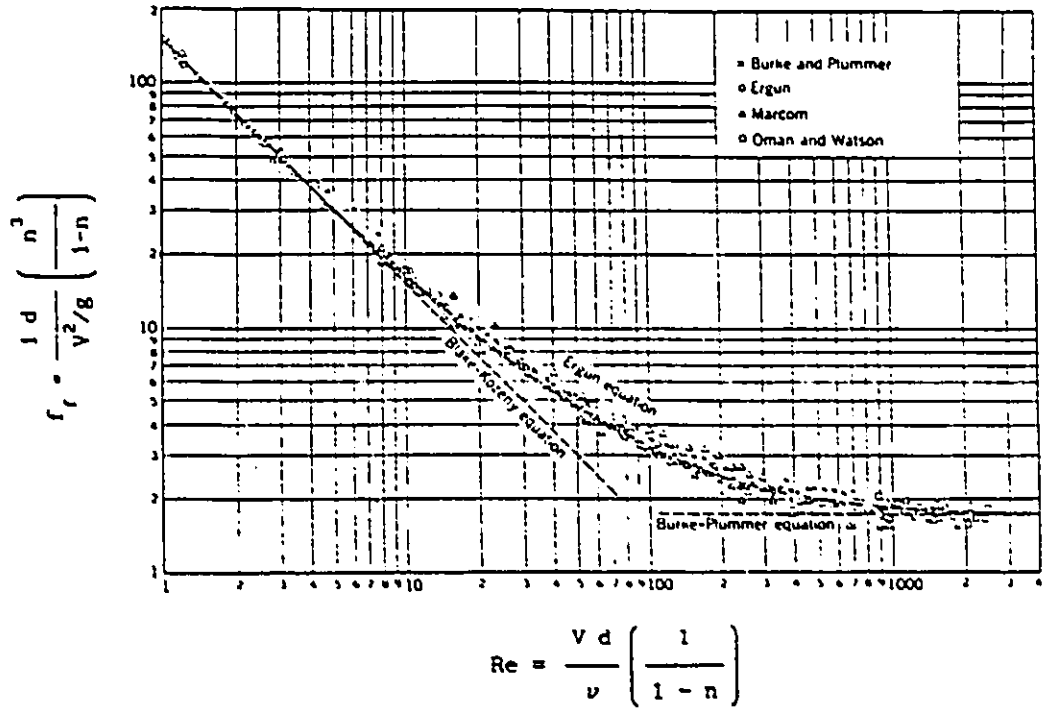
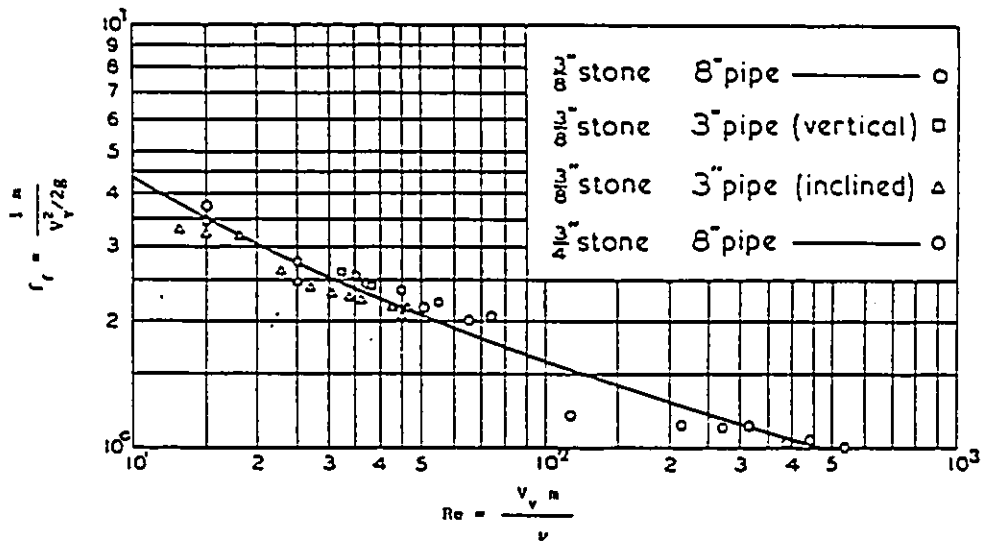


Figure 2-1 (c) Illustration of free fall zone in a flowthrough rockfill dam

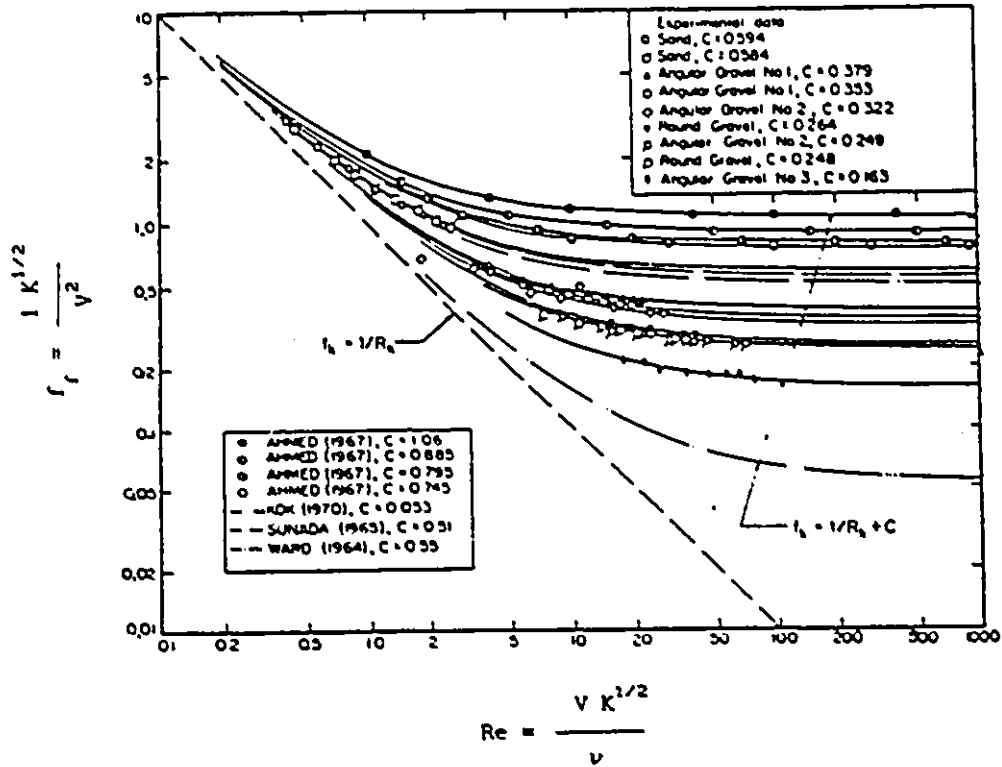


a) Ergun, 1952.

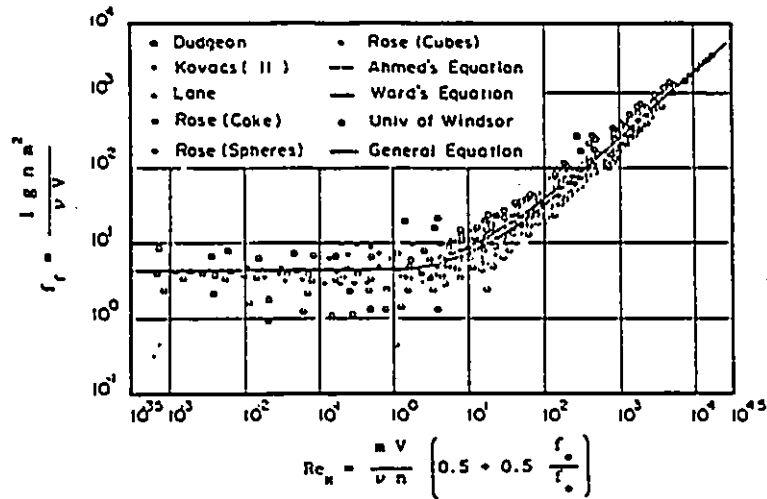


b) Parkin, 1963a.

Figure 2-2 Examples of friction factor versus Reynolds Number plots for flow through porous media (after Hansen, 1992)



a) Arbbhahirama and Dinoy, 1973.



b) McCorquodale et al, 1978.

Figure 2-3 Examples of friction factor versus Reynolds Number plots for flow through porous media (after Hansen, 1992)

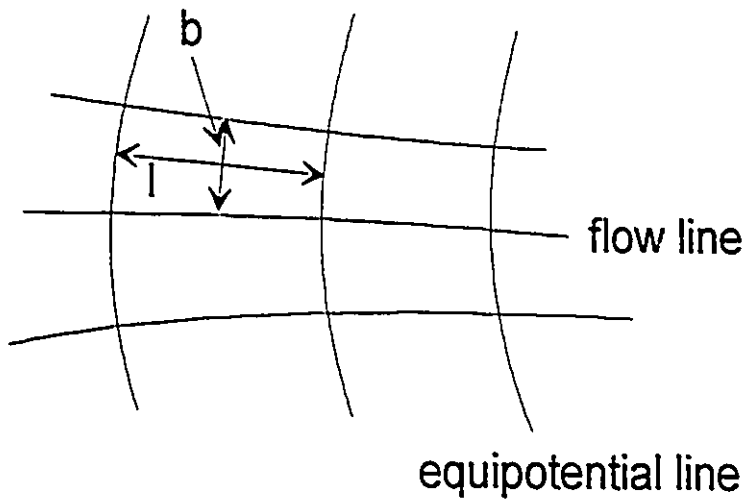


Figure 2-4, non -Darcy flow net for isotropic homogeneous porous media

	$(i-1, j-1)$	$(i, j-1)$	$(i+1, j-1)$
	4	3	2
	$(i-1, j)$	$(i, j)$	$(i+1, j)$
	5	0	1
	$(i-1, j+1)$	$(i, j+1)$	$(i+1, j+1)$
	6	7	8

Figure 2-5 Node Identification (after Curtis and Lawson, 1967)

AT ANY VERTICAL SECTION:  $Q_{TOTAL} = Q_{OVERFLOW} + Q_{SEEPAGE}$

AT SECTION  $h_e$ :  $Q_{TOTAL} = Q_{SEEPAGE}$

AT THE TOE:  $Q_{TOTAL} = Q_{OVERFLOW}$

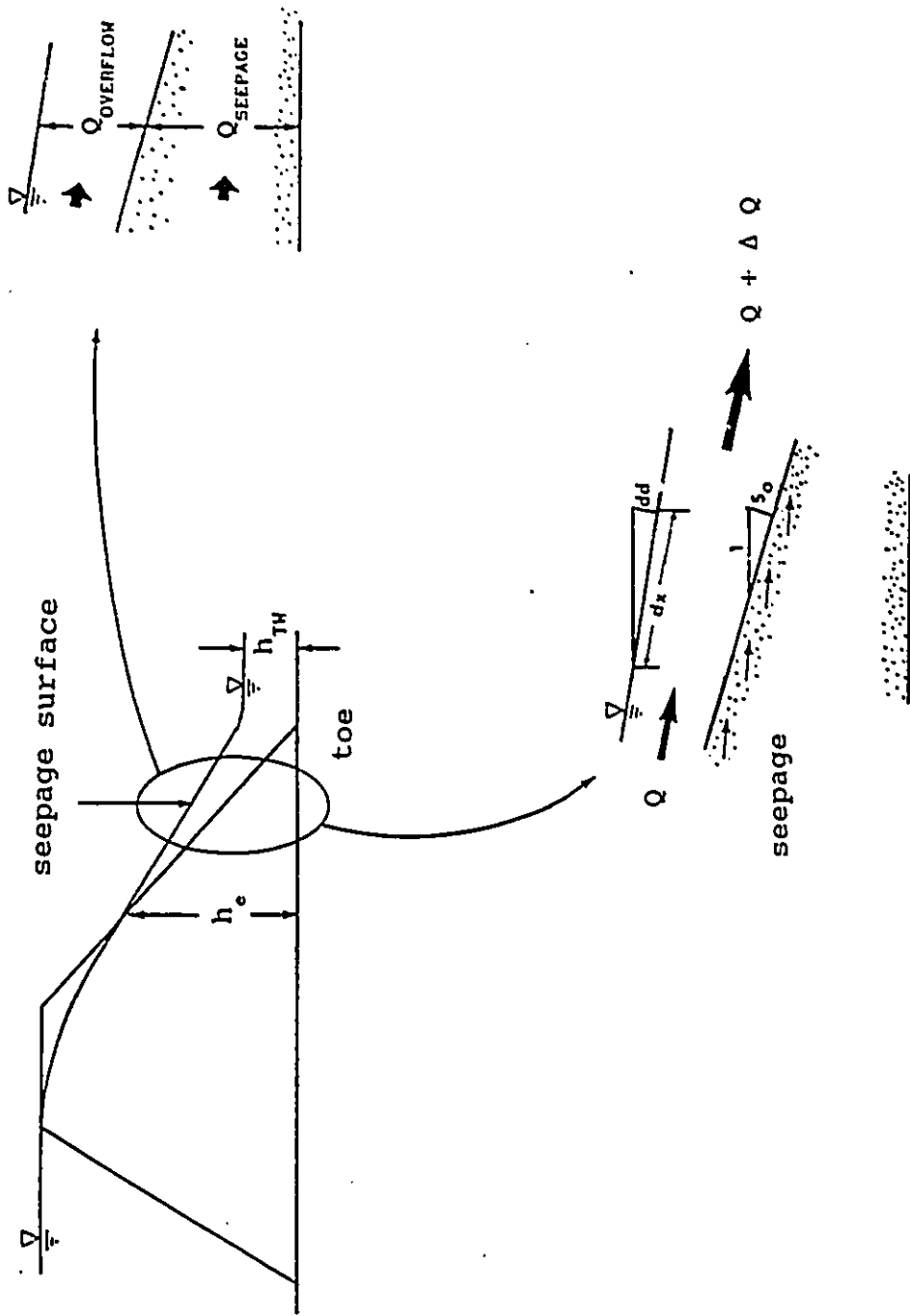
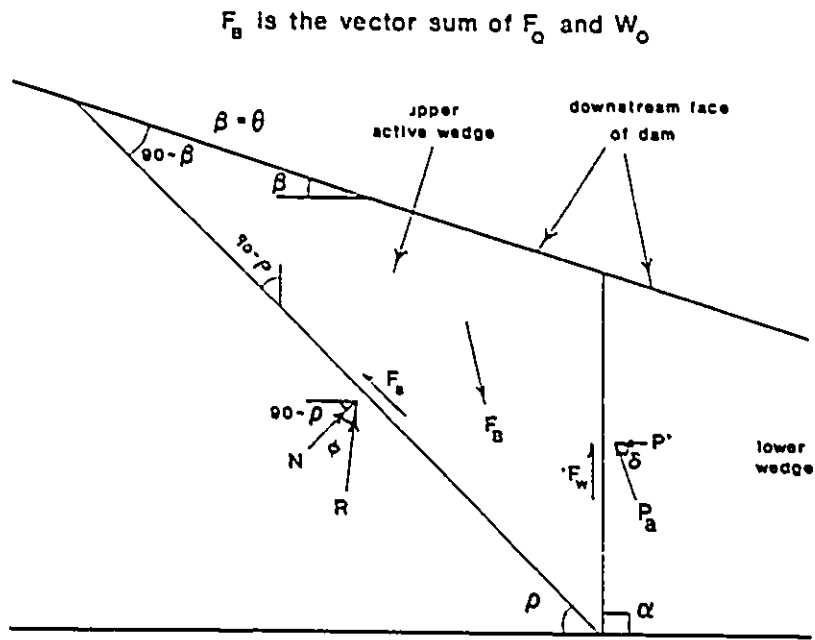
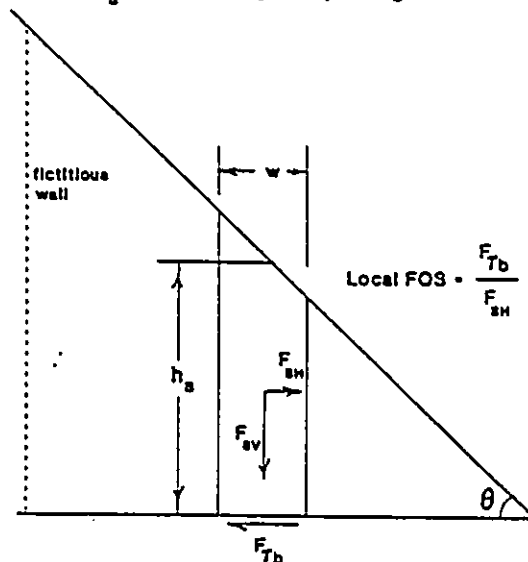


Figure 2-6 Scheme for seepage - face definitions (after Hansen, 1992, p.152)



Dimensions of vertical segment shown,  
 $h_s$  by  $w$ , are greatly exaggerated.



b) determination of local FOS at the base of a single vertical segment within the lower wedge.

Figure 2-7 Schematic diagrams pertaining to the wedge method (after Hansen, 1992)

## Chapter 3 Theoretical Solution for the Seepage Flow in Overtopped Rockfill

### 3.1 Introduction

For flow over rockfill dams with wide profile, and flow over permeable beds, the existence of turbulent overtopping open channel flow, seepage flow, and the potential movement of materials makes the overtopping phenomenon very complicated. Figure 3-1 shows a simplified section along the flow direction, where seepage flow occurs through the rockfill and an overflow occurs in the main channel above it. The domain of the open channel above the rockfill or gravel is defined as the main channel. The domain at the lower part of the rockfill or gravel bed where normal pressure seepage exists is called the normal pressure seepage zone or simply as the pressure seepage zone. The domain between the main channel flow and the normal pressure seepage zone is defined as the transition zone,  $t$ , in Fig. 3-1. Previous experimental and theoretical studies (Zagni, 1976, Gupta, et. al, 1985, Li, 1990) show that:

- (1) the hydraulic characteristics of general open channel flow dominate in the main channel, but the velocity at the bottom of open channel flow is not equal to zero, but a so called slip velocity  $V_0$ ;
- (2) at some distance below the normal surface of the rockfill or gravel bed, the normal pressure seepage flow occurs with a uniform velocity  $q_1$ ;
- (3) for flow above the normal surface of gravel bed, a logarithmic velocity profile fits well with the experimental data with some modifications;
- (4) the shear immediately above the gravel bed of overtopping flow is influenced by both overtopping flow and seepage flow conditions;

(5) between the top surface of rockfill boundary and the pressure seepage zone, there is a transition zone in which the fluid is not only acted upon by the seepage gradient, but also by shear stress acting at the main channel-transition zone interface.

The fluid shear stress in the permeable bed decreases very rapidly with the depth below the interface between overtopping flow and seepage flow, as a result of the transfer of momentum from the fluid to the particles. In order to obtain a complete velocity distribution profile with depth, it is important to define the depth of the transition zone and the velocity distribution in the transition zone for many practical problems related to overtopping flow in rockfill dams, and gravel river reaches.

Little information related to the velocity profile at the transition zone is available in the literature. This may be due to the difficulty in direct measurement of seepage velocities. Gupta, et. al (1985) derived two complex expressions for the depth of the transition seepage zone based on two assumptions.

This paper presents the analytical solutions based on the theory of turbulent fluid flow and non-Darcy seepage law in the transition zone. It is subsequently shown that the solutions derived in the present study lead to much simpler and practical expressions for the thickness of the transition zone.

### 3.2 Turbulent theory and governing equations

Considering the force balance of an element in the transition zone in Figure 3-1:

$$\frac{\tau(y+dy) - \tau(y)}{dy} dx dy + \frac{p(x) - p(x+dx)}{dx} - f_d dx dy = 0 \quad (3-1)$$

where

$f_d$  = drag force per unit volume;

$dx$  = the dimension in x direction of the element ;

$dy$  = the dimension in y direction of the element ;

$\tau(y)$  = shear stress at the bottom of the element;

$\tau(y)$  = shear stress at the bottom of the element;

$\tau(y+dy)$  = shear stress at the top of the element;

$p(x)$  = total pressure at the left side of the element;

$p(x+dx)$  = total pressure at the right side of the element.

From Taylor's series:

$$p(x + dx) = p(x) + \frac{\partial p}{\partial x} dx + 0(dx^2) \quad (3-2)$$

and

$$\tau(y + dy) = \tau(y) + \frac{\partial \tau}{\partial y} dy + 0(dy^2) \quad (3-3)$$

Ignoring the 2nd order terms in Eqs. (3-2) and (3-3), and substituting in Eq.(3-1),

$$\frac{\partial \tau}{\partial y} - \frac{\partial p}{\partial x} - f_d = 0 \quad (3-4)$$

Due to the momentum transfer from overtopping flow to the transition seepage zone, the flow in the transition zone is unlikely to be laminar (Gupta, et. al, 1985). The non-Darcy law may be represented by two expressions. The first is the power law :

$$q = k i^{1/N} \quad (3-5)$$

where  $q$  = seepage velocity (bulk) within the porous material;

$k$  = general seepage coefficient;  
 $i$  = gradient of the overtopping water surface;  
 $N$  = exponent of seepage law.

The second expression is from Ward's seepage relationship (Ward, 1964):

$$f_d = \frac{\mu}{k_p} q + \frac{c}{\sqrt{k_p}} \rho q^2 \quad (3-6)$$

where  $\mu$  = the dynamic viscosity of fluid;  
 $\rho$  = the density of fluid;  
 $k_p$  = non-Darcy seepage coefficient;  
 $c$  = dimensionless coefficient in Ward's relationship.

Eq. (3-6) was expressed by Zagni (1976) as:

$$-\frac{dp}{dx} = \frac{\mu}{k_p} q_1 + \frac{c}{\sqrt{k_p}} \rho q_1^2 \quad (3-7)$$

where  $q_1$  = the seepage velocity in the normal pressure seepage zone;  
 $dp/dx$  = the pressure gradient of the overtopping flow in main channel flow.

It can be shown that the term  $i$  in Eq. (3-5) has the following relationship:

$$i = -\frac{1}{\gamma} \frac{\partial p}{\partial x} \quad (3-8)$$

where  $\gamma$  is the unit weight of the fluid flow.

Substituting Eq. (3-8) in Eq. (3-5), and  $\frac{\partial \tau}{\partial x} = 0$  in Eq. (3-4) for unit volume:

$$f_d = \gamma \left(\frac{q}{k}\right)^N \quad (3-9)$$

In the normal pressure zone, the flow velocity may be obtained by the following expression:

$$-\frac{\partial p}{\partial x} = \gamma \left(\frac{q_1}{k}\right)^N \quad (3-10)$$

From the turbulent theory of fluid mechanics (Jin, 1989), turbulent shear stress is expressed as

$$\tau = \rho \nu_t \frac{\partial q}{\partial y} \quad (3-11)$$

where

$\tau$  = shear stress;

$\nu_t$  = kinematics eddy viscosity.

The Prandtl mixing length theory (Jin, 1989) gives the following relationship:

$$\nu_t = l_p^2 \left| \frac{\partial q}{\partial y} \right| \quad (3-12)$$

where  $l_p$  = Prandtl constant. From consideration of turbulent flow in a two-dimension boundary layer, the Prandtl mixing length may be expressed as (Jin, 1989):

$$l_p = \beta t \quad (3-12-1)$$

where

$\beta$  = constant of turbulent structure;

$t$  = the thickness of the transitional zone.

Considering that  $\frac{\partial q}{\partial y} > 0$ , Eq. (3-12) becomes:

$$v_x = \beta^2 t^2 \frac{\partial q}{\partial y} \quad (3-13)$$

From Eqs. (3-11) and (3-13),  $\tau$  may be expressed as

$$\tau = \rho \beta^2 t^2 \left( \frac{\partial q}{\partial y} \right)^2 \quad (3-14)$$

Substituting Eqs. (3-6), (3-7), and (3-14) in Eq. (3-4):

$$\rho \beta^2 t^2 \frac{\partial}{\partial y} \left( \frac{\partial q}{\partial y} \right)^2 = \frac{\mu}{k_p} (q - q_1) + \frac{c\rho}{\sqrt{k_p}} (q^2 - q_1^2) \quad (3-15)$$

Substituting Eqs. (3-9), (3-10), and (3-14) in Eq. (3-4):

$$\rho \beta^2 t^2 \frac{\partial}{\partial y} \left( \frac{\partial q}{\partial y} \right)^2 + \gamma \left( \frac{q_1}{k} \right)^N - \gamma \left( \frac{q}{k} \right)^N = 0 \quad (3-16)$$

Both Eq. (3-15) and Eq. (3-16) are the momentum equations for the transition seepage zone. Eq. (3-15) utilizes the Ward(1964) seepage relationship, while Eq. (3-16) is derived using Eq. (3-5) which is the well-known power law for non-Darcy flow..

### 3.3 Boundary conditions and analytical solutions

(1) The boundary conditions

At the surface of the rockfill,  $y=0$ , and the shear stress  $\tau_0$  may be expressed as:

$$\tau_0 = \rho \beta^2 t^2 \left( \frac{\partial q}{\partial y} \Big|_{y=0} \right)^2 \quad (3-17)$$

and the velocity is  $v_0$ , i.e.,

$$q|_{y=0} = v_0 \quad (3-18)$$

where

$v_0$  = the velocity at the top of the transition seepage zone, which may be determined by the velocity distribution of the main open channel flow;

$\tau_0$  = the shear stress at the top of the transition seepage zone, which may be calculated by the following equation:

$$\tau_0 = \rho u_*^2 \quad (3-19)$$

where

$u_*$  = shear velocity of the main channel flow.

At the bottom of the transition zone,  $y=t$ , the shear stress can be expressed as:

$$\tau|_{y=t} = \rho \beta^2 t^2 \left( \frac{\partial q}{\partial y} \Big|_{y=t} \right)^2 = 0 \quad (3-20)$$

and the velocity as:

$$q|_{y=t} = q \quad (3-21)$$

For gradually varied flow, experimental data by Hu and Li (1988) shown that the pressure gradient in y direction is negligible, i.e.,

$$\frac{\partial p}{\partial y} = 0 \quad (3-22-1)$$

and the seepage velocity gradient in x direction is negligible, i.e.,

$$\frac{\partial q}{\partial x} = 0 \quad (3-22-2)$$

So that,

$$\frac{\partial q}{\partial y} = \frac{dq}{dy} \quad (3-23-1)$$

and

$$\frac{\partial p}{\partial x} = \frac{dp}{dx} \quad (3-23-2)$$

## (2) Analytical solutions

Analytical solutions can now be derived for the depth  $t$  of the transition zones based on the power law for non-Darcy flow and the Ward expression.

Eq. (3-16) may be written as

$$\rho \beta^2 t^2 \frac{d}{dy} \left( \frac{dq}{dy} \right)^2 - \gamma \frac{q^N - q_1^N}{k^N} = 0 \quad (3-24)$$

Let

$$\frac{dq}{dy} = z \quad (3-25)$$

then

$$\frac{d}{dy} (z^2) = 2z \frac{dz}{dy} = 2z^2 \frac{dz}{dq} \quad (3-26)$$

So,

$$2\rho\beta^{-2}t^2z^2\frac{dz}{dq} = \gamma\frac{q^N - q_1^N}{k^N} \quad (3-27)$$

Integrating Eq. (3-27):

$$\frac{2}{3}\beta^{-2}t^2z^3 = \frac{q}{k^N}\left(\frac{q^{N+1}}{N+1} - q_1^Nq + D\right) \quad (3-28)$$

where  $D = \text{constant}$  which will be determined by the boundary conditions. By Eq. (3-20),

$$z\Big|_{y=x-t} = \frac{dq}{dy}\Big|_{y=x-t} = 0 \quad (3-29)$$

$D$  is derived as

$$D = q_1^{N+1} - \frac{q_1^{N+1}}{N+1} = \frac{N}{N+1}q_1^{N+1} \quad (3-30)$$

Substituting Eqs. (3-30) and (3-25) in Eq. (3-28):

$$\frac{2}{3}\beta^{-2}t^2\left(\frac{dq}{dy}\right)^3 = \frac{\gamma}{k^N}\left[\frac{q^{N+1} - q_1^{N+1}}{N+1} - q_1^N(q - q_1)\right] \quad (3-31)$$

Eq. (3-17) may be written as

$$\frac{\partial q}{\partial y}\Big|_{y=0} = \sqrt{\frac{\tau_0}{\rho\beta^{-2}t^2}} \quad (3-32)$$

Substituting Eqs. (3-18) and (3-32) in Eq. (3-31):

$$\begin{aligned} & \frac{2}{3} \beta^{-2} t^2 \left( \frac{\tau_0}{\rho \beta^{-2} t^2} \right)^{3/2} \\ & = \frac{g}{k^N} \left[ \frac{v_0^{N+1} - q_1^{N+1}}{N+1} - q_1^N (v_0 - q_1) \right] \end{aligned} \quad (3-33)$$

Substituting Eq. (3-19) in Eq. (3-33), the thickness of the transition zone based on power law Eq. (3-5) may be expressed as:

$$t = \frac{\frac{2 k^N u_*^3}{3 \beta g}}{\frac{v_0^{N+1} - q_1^{N+1}}{N+1} - q_1^N (v_0 - q_1)} \quad (3-34)$$

In order to derive the velocity distribution in the transition zone, Eq. (3-31) may be rewritten as:

$$\frac{dq}{dy} = \frac{\left[ \frac{q^{N+1} - q_1^{N+1}}{N+1} - q_1^N (q - q_1) \right]^{1/3}}{\left( \frac{2 \beta^{-2} t^2 k^N}{3 g} \right)^{1/3}} \quad (3-35)$$

Let

$$f_1(q) = \frac{\left( \frac{2 \beta^{-2} t^2 k^N}{3 g} \right)^{1/3}}{\left[ \frac{q^{N+1} - q_1^{N+1}}{N+1} - q_1^N (q - q_1) \right]^{1/3}} \quad (3-36)$$

From Eq. (3-35), by integration,

$$y = -t + \int_{q_1}^q f_1(q) dq \quad (3-37)$$

It is difficult to derive an explicit expression from Eq. (3-37). However a numerical solution is easily obtained by successively assuming various values of  $q$  between  $q_1$  and  $v_0$ , and calculating respective value of  $y$ .

Similarly, Eq. (3-15) which uses Ward expression for non-Darcy flow may be solved by applying the boundary conditions [Eqs. (3-17) to (3-21)], and the assumptions in Eqs. (3-22-1) to (3-23-2). The following solution is then obtained:

$$t = \frac{\frac{2}{3} \frac{v_0^3}{\beta}}{\left[ \frac{\mu}{k_p} \left( \frac{v_0^2 + q_1^2}{2} - q_1 v_0 \right) + \frac{c}{\sqrt{k_p}} \left( \frac{q^3 + 2q_1^3}{3} - q_1^2 q \right) \right]^{1/3}} \quad (3-38)$$

and

$$y = -t + \int_{q_1}^q f_2(q) dq \quad (3-39)$$

where

$$f_2(q) = \frac{\left( \frac{2}{3} \beta^{-2} t^2 \right)^{1/3}}{\left[ \frac{\mu}{k_p} \left( \frac{q^2 + q_1^2}{2} - q_1 q \right) + \frac{c}{\sqrt{k_p}} \left( \frac{q^3 + 2q_1^3}{3} - q_1^2 q \right) \right]^{1/3}} \quad (3-40)$$

### 3.4 Computation of seepage discharge

It may be observed from the above analyses that the thickness of the transition zone may be calculated from Eqs. (3-34) or Eq. (3-38), and the velocity profile in the transition zone may be obtained by Eq. (3-36) or Eq. (3-39). Computational results using Gupta et al (1988) experimental data indicates that the value of the constant  $\beta$  is about 0.0007.

In cases when the thickness  $t$  is very small in comparison with the total depth  $h$  of the rockfill or gravel bed, the total seepage flow may be evaluated by the following expression (Gupta et al, 1985):

$$Q_0 = [t(\frac{v_0 + q_1}{2}) + (h - t)q_1]B \quad (3-41)$$

$h$  = the thickness of the rockfill or gravel bed;

$Q_0$  = total seepage discharge;

$B$  = the width of the cross section for overtopping flow.

Eq. (3-41) assumes the velocity distribution in the transition zone is a straight line. This simplification is usually reasonable when gradually varied open channel flow occurs, since in practice, seepage discharge is usually much smaller than overtopping discharge.

Gupta et al (1985) also derived two complex expressions for the depth of transition zones. These expressions, referred to as, Model 1 and Model 2, were based on the following two assumptions respectively (Gupta, et. al, 1985):

$$v_t = B_0 h(v_0 - q_1) \quad (3-42)$$

and

$$v_t = B_0 h(q - q_1) \quad (3-43)$$

where  $B_0$  = a constant whose value was not mentioned in Gupta, et. al's paper.

Eq. (3-42) relates to a constant eddy viscosity if  $v_0$ ,  $h$ ,  $q_1$ , and  $B_0$  are constant. Eq. (3-43) assumes that the eddy viscosity is a linear function of the seepage velocity.

The expression for Gupta's model 1 is:

$$\begin{aligned}
& \ln \frac{\left[ \frac{q-q_1}{3v_o} + \frac{\sqrt{k_p}}{2ch} \left( \frac{vh}{k_p v_o} + \frac{2ch q_1}{\sqrt{k_p} v_o} \right) \right]^{1/2} - \frac{\sqrt{k_p}}{2ch} \left( \frac{vh}{k_p v_o} + \frac{2ch q_1}{\sqrt{k_p} v_o} \right)}{\left[ \frac{q-q_1}{3v_o} + \frac{\sqrt{k_p}}{2ch} \left( \frac{vh}{k_p v_o} + \frac{2ch q_1}{\sqrt{k_p} v_o} \right) \right]^{1/2} + \frac{\sqrt{k_p}}{2ch} \left( \frac{vh}{k_p v_o} + \frac{2ch q_1}{\sqrt{k_p} v_o} \right)} \\
& - \ln \frac{\left[ \frac{v_o-q_1}{3v_o} + \frac{\sqrt{k_p}}{2ch} \left( \frac{vh}{k_p v_o} + \frac{2ch q_1}{\sqrt{k_p} v_o} \right) \right]^{1/2} - \frac{\sqrt{k_p}}{2ch} \left( \frac{vh}{k_p v_o} + \frac{2ch q_1}{\sqrt{k_p} v_o} \right)}{\left[ \frac{v_o-q_1}{3v_o} + \frac{\sqrt{k_p}}{2ch} \left( \frac{vh}{k_p v_o} + \frac{2ch q_1}{\sqrt{k_p} v_o} \right) \right]^{1/2} + \frac{\sqrt{k_p}}{2ch} \left( \frac{vh}{k_p v_o} + \frac{2ch q_1}{\sqrt{k_p} v_o} \right)} \\
& = \frac{v_o}{v_o-q_1} \left( \frac{vh}{k_p v_o} + \frac{2ch q_1}{\sqrt{k_p} v_o} \right) \left[ \frac{2}{3} \left( \frac{v_o-q_1}{v_o} \right)^3 \left( \frac{vh}{k_p v_o} \right. \right. \\
& \left. \left. + \frac{2ch q_1}{\sqrt{k_p} v_o} \right) + \frac{\sqrt{k_p}}{2ch} \left( \frac{v_o-q_1}{v_o} \right)^4 \right] \frac{t}{h} \tag{3-44}
\end{aligned}$$

The expression for Gupta's model 2:

$$\begin{aligned}
& \ln \left\{ \frac{q-q_1}{3v_o} + \frac{\sqrt{k_p}}{3ch} \left( \frac{vh}{k_p v_o} + \frac{2ch q_1}{k_p v_o} \right) \right. \\
& \left. + \left[ \frac{\sqrt{k_p}}{3ch} \left( \frac{vh}{k_p v_o} + \frac{2ch q_1}{k_p v_o} \right) \frac{q-q_1}{v_o} + \frac{1}{4} \left( \frac{q-q_1}{v_o} \right)^2 \right]^{1/2} \right\} \\
& - \ln \left\{ \frac{v_o-q_1}{2v_o} + \frac{\sqrt{k_p}}{3ch} \left( \frac{vh}{k_p v_o} + \frac{2ch q_1}{k_p v_o} \right) \right. \\
& \left. + \left[ \frac{\sqrt{k_p}}{3ch} \left( \frac{vh}{k_p v_o} + \frac{2ch q_1}{k_p v_o} \right) \frac{v_o-q_1}{v_o} + \frac{1}{4} \left( \frac{v_o-q_1}{v_o} \right)^2 \right]^{1/2} \right\}
\end{aligned}$$

$$= \frac{2ch}{\sqrt{k_p}} \left[ \frac{2}{3} \left( \frac{v_0 - q_1}{v_*} \right)^3 \left( \frac{vh}{k_p v_*} + \frac{2ch}{\sqrt{k_p}} \frac{q_1}{v_*} \right) + \frac{\sqrt{k_p}}{2ch} \left( \frac{v_0 - q_1}{v_*} \right)^4 \right] \frac{t}{h}$$

(3-45)

It is noticed that the solutions provided by Eqs. (3-34) and (3-38) developed in this paper are simpler in form to those previously proposed.

The availability of experimental results obtained by Gupta et al. (1985) also provides an opportunity to compare the validity of the various expressions for the seepage flow. The absolute relative deviation may be defined as:

$$AA = \frac{1}{n} \sum_{i=1}^n \left| \frac{Q_{0si} - Q_{0mi}}{Q_{0mi}} \right| \times 100\% \quad (3-46)$$

where

AA = the absolute relative deviation;

$Q_{0si}$  = the seepage discharge simulated by the computational simulation ;

$Q_{0mi}$  = measured seepage discharge;

n = the number of total set of conditions.

Table 3-1 lists the simulations with Eq. (3-41), for all the cases in previously published experimental data by Gupta, et. al (1985). The simulation results from Gupta's two models are also presented in Table 3-1 for comparison. It is noticed that AA for Eq. (3-41) is 11.8%, and that for Gupta's model 1 and model 2 are 21.6% and 18.5% respectively. Eq. (3-36) could not be compared since necessary parameters were not provided in the Gupta et al (1985)'s published data.

The solutions presented above may be used to predict the seepage discharge for the cases of rockfill dam overtopping, flow in gravel bed, and overland flow.

### **3.5 Conclusions**

1. By combining the Prandtl mixing-length turbulent model with the general seepage law and the Ward's non-linear seepage equation, two analytical solutions are derived and presented.
2. In comparison to the other models, the solutions presented are simpler in form, and with a relative error of 12%.

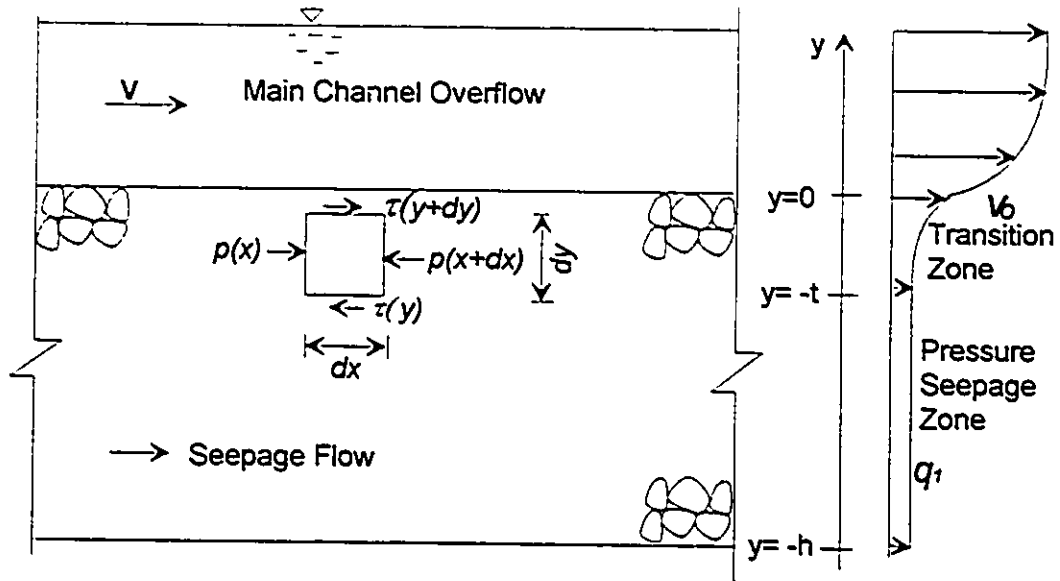


Figure 3-1, Definition sketch for flow over and through gravel bed (after Gupta et., 1985)

Table 3-1, Comparison of the Discharge Between Computational Models and Measurement \*\*

Run Number	I	Water Depth of overtopping (m)	Q <sub>0mi</sub> Gupta (cm <sup>3</sup> /s)	Q <sub>0si</sub> Gupta's model 1 (cm <sup>3</sup> /s)	Q <sub>0si</sub> Gupta's model 2 (cm <sup>3</sup> /s)	Q <sub>0si</sub> the new model (cm <sup>3</sup> /s)
1	2.367	3.54	43.0	40.0	36.0	45.4
2	2.367	3.85	46.0	39.0	36.1	45.9
3	1.842	2.93	41.0	31.0	30.5	36.0
4	2.167	4.45	48.0	41.0	36.0	43.7
5	2.733	4.87	55.0	46.0	44.0	53.3
6	2.542	5.22	48.0	51.0	38.0	50.9
7	2.050	5.36	47.0	42.0	35.0	43.3
8	2.342	5.95	52.0	42.0	39.0	48.9
9	2.400	6.64	54.0	40.0	46.0	50.9
10	2.983	7.14	65.0	50.0	46.0	60.8
11	0.991	10.38	34.0	13.0	18.0	30.2
12	0.458	11.63	28.0	10.0	9.0	19.0
13	2.875	5.84	46.0	48.0	44.0	57.0
14	3.592	3.59	62.0	53.0	52.0	60.2
15	3.633	4.74	49.0	54.0	52.0	66.5
16	3.217	5.82	63.0	49.0	48.0	62.2
17	3.209	7.78	84.0	91.0	90.0	65.3
18	3.383	3.70	55.0	50.0	48.0	68.5
19	3.392	5.32	56.0	51.0	50.0	64.0
20	3.333	7.96	62.0	51.0	50.5	67.5
21	3.584	6.10	63.0	56.0	50.0	68.2
22	3.325	6.91	65.0	51.0	53.0	65.7
23	4.917	2.62	65.0	68.0	50.0	56.8
24	4.475	3.56	72.0	64.0	67.0	69.1
25	4.000	4.79	70.0	60.0	62.0	70.9
26	4.092	6.31	69.0	63.0	58.0	76.0
27	3.817	8.21	75.0	61.0	59.0	75.8
28	7.585	3.55	62.0	99.0	59.0	96.7
29	7.657	4.45	104.0	107.0	57.0	104.2
30	7.383	5.30	113.0	99.0	95.0	107.6
31	6.908	6.47	135.0	113.0	93.3	110.2
32	11.642	3.56	101.0	136.0	92.4	127.2
33	10.458	4.55	136.0	129.0	85.3	127.6
34	9.475	6.09	136.0	145.0	128.3	131.2
35	13.542	2.77	157.0	145.0	119.0	130.9
36	12.192	3.54	155.0	136.0	108.0	130.7
37	12.667	4.26	185.0	141.0	142.0	141.0
38	12.408	5.08	228.0	140.0	133.0	146.6
39	12.092	5.61	159.0	139.0	137.0	148.6
40	12.066	6.28	172.0	140.0	134.0	153.7
41	11.941	7.17	185.0	139.0	135.0	159.2
AA				21.6%	18.5%	12.0%

\*\* The experiment data and the computational results of Gupta's model 1 and model 2 are from Gupta, et al.'s work (1985).

## **Chapel 4 Experimental Studies at NRC Hydraulics Laboratory**

### **4.1 Introduction**

Experimental studies were undertaken in the large hydraulic flume at the NRC Hydraulics Laboratory in Ottawa. The objective of these experiments was to investigate the following:

- (1) the average and stochastic behavior of the seepage and overtopping forces acting on the rock particles at the downstream face;
- (2) the failure mechanisms of rockfill dams.

The flume at the NRC Hydraulics Laboratory has a cross sectional area 60 x 100 cm (width x height), in which rockfill with diameter  $d_{50}$  of 3.0 cm was used. The porosity of the rockfill dam was 0.41.

### **4.2 Model Description**

The profile of the 2-dimensional physical model is shown in Figure 4-1. The dam configurations were tested in two modes. In the first mode, the intent was to measure the total force acting on the downstream face due to overtopping flow and seepage flow. These experiments are called stable models. In the second mode of testing, the rockfill embankments were taken to failure by increasing the discharge over and through the dam. These are called unstable models.

#### **(1) Stable Models**

The  $d_{50}$  particle size on the exposed downstream slope of the dam was 4 cm. Two force panels (which will be explained later) were installed at the face of the downstream slope. Steel mesh with a size of 110x60 cm (length x width) was used at the lower part of the downstream slope to keep it stable by affixing it to the side walls. Hence, all rock particles at the downstream slope were protected and were not erodible. A downstream gate, an upstream reservoir and pipe system to provide the flow to the

model were designed and constructed for the experiments. Photograph 4-1 shows the view of the downstream slope of the model.

The model dam is fully permeable since there is no impervious facing on either the upstream slope or the downstream slope. Overtopping and seepage flows occur simultaneously. The experiment were conducted in the following modes:

- a. Constant discharge: The downstream gate was controlled to different openings to generate all possible flow patterns. The water surface levels, forces acting on the force panel at the downstream slope, velocities, discharge, and pressure were recorded.
- b. Variable discharge: The downstream gate was kept open to keep steep open channel flow pattern at the downstream slope. Levels of discharge were controlled by the valve in the pipe connected to the upstream water tank. The data was recorded with the data collection system.

In the present study the behavior of the forces on the rock particles due to both the overflow and the seepage flow acting on the downstream slope of an overtopped rockfill dam was investigated. As present, there is apparently no sound theory to evaluate the combined forces due to overtopping and seepage flows acting on the blocks of rockfill material at the downstream slope. Table 4-1 listed all the tests carried out at the NRC Hydraulics Laboratory for the force measurement.

## (2) Unstable Models

Two kinds of models were tested in the experiments to study the failure mechanisms of rockfill dams with and without upstream impervious facing (Fig. 4-2).

## 4.3 Instrumentation and Data Acquisition

### (1) Force Panels

The force panels were made by A. M. Comett, a scientist at the Hydraulics Laboratory at NRC (Comett, 1995).

Two force panels made of aluminum "rock particles" with a diameter of 4 cm were installed on the downstream slope of a rockfill dam. In each force panel, 50 irregularly shaped, aluminum modeled rock particles were bonded together by spot-welds into a rigid, porous, rectangular mat of armour stones (Cornett, 1995). The modeled rock particles in each panel were randomly placed to closely approximate the packing and porosity of the loose granite armour. Each panel represents a rectangular patch of armour stones in a single layer with approximate overall dimensions 25 cm by 63 cm by 5 cm. Photograph 4-2 shows a photograph of the armour panels.

For each force panel, two load cells were located at the left side, and three at the right side (Photographs 4-3 and 4-4). The force panels were installed as part of the surface layer of armour at the downstream slope of a rockfill dam. Figure 4-3 shows the sketch of the downstream slope armour layer and force panels.

For each panel, the three load cells in the x direction (along the downstream slope, see Fig. 4-3) measure the force acting in this direction. The y component of the force is measured by two load cells in y direction (y direction is vertical to the downstream slope). The momentum in the xy plane due to overtopping and seepage flow can now be calculated. The load cells are connected to the data collection system linked to a VAX computer system. Figure 4-4 shows the plan view of a force panel.

Calibration of load cells was carried out in the NRC Hydraulics Laboratory. Every two weeks, a disk with known weight (2 kg) was placed on the force panels at different positions to check the load cells. The load cells feature a combined non-linearity and hysteresis of 0.06% (Cornett, 1995)

## (2) Wave probes

Twelve wave probes developed at the NRC were used in the experiment to record the water surface levels along the flume (Photograph 4-1). Each wave probes is made of 2 resistance wires. The water surface level was measured by the change of the resistance and hence the voltage. The wave probes feature an accuracy of  $\pm 1$  mm. Calibration was done regularly throughout the test by changing the elevation of the wave probes with respect to a fixed water surface. The calibration error was less than 0.6%. Figs. 4-5 to 4-16 show the calibration of the 12 wave probes. All the wave probes were connected to the data collection and computer system.

### (3) Velocity Meters

Two electronic-magnetic velocity meters made by NRC were used in the experiment to measure the velocity distribution at the downstream slope in the flow (Photograph 4-5). The Faraday principle of electromagnetic induction is used to measure the velocity of fluid flow. These instruments feature similar performance characteristics, including repeatability of 1% over a calibrated operating range up to 5 m/s. Calibration was done monthly by towing through still water at various speeds. It was noticed these velocity meters made by NRC have very stable behavior. Figs. 4-17 to 4-19 show the calibration results.

### (4) Pore Pressure Transducers (after Davies, 1992)

Small pressure transducers were used to measure the average and pulsating pressure beneath the force panel at selected locations. The pore pressure transducers use a miniature silicon bridge sensing mechanism, contained within a 3 mm diameter, 10 mm long titanium housing (Davies, 1992). The sensing element is covered with a porous ceramic disc which transmits soil loads to the housing so that only pore fluid pressures are measured by the silicon bridge (Davies, 1992). The transducers have a 7 kPa range (capable of withstanding a 70 kPa over-pressure) and are highly linear. Electrical connections to the transducer head are fully watertight and made through a 1.5 mm diameter cable through which the back of the silicon bridge is vented to atmospheric pressure. The pore pressure transducers used in the tests have a sensitivity of 4 mV per volt of excitation, per meter of water head. Using 10V excitation and an analog gain of 1000 applied prior to analog to digital (A/D) conversion of the signal results in a gauge sensitivity of 40 volts per meter of water head. A/D conversion is a 15-bit system over a range of  $\pm 10$  Volts which results in a bit resolution of 0.6 mV which corresponds, in hydraulic terms, to a bit resolution of 0.015 mm of water head. Transducer linearity represents an accuracy of 0.2% over the measurement range. This corresponds to a maximum likely measurement error due to gauge non-linearity of  $\pm 0.2$  mm on a 0.20 m amplitude pressure wave.

### (5) Discharge Meter

A discharge device (venturi type) installed in the inflow pipe was connected to a pressure gauge to measure the discharge with relative error of  $\pm 1\%$ . The calibration provided by NRC was:

$$Q = 223.34 \sqrt{\Delta H} \quad (4-1)$$

where

Q = total discharge through and over the dam, in l/sec;

$\Delta H$  = head of water measured, in m.

In the experiment,  $\Delta H$  was measured directly to determine Q by Eq. (4-1).

#### (6) Videocorder and Camera

A videocorder was installed over the rockfill dam, which can be easily handled by the operator to follow the tracks of the fast speed flow. A high-quality camera was used to record the flow patterns and the apparatus.

In the experiments, more than one thousand sets of data were recorded. Analyses were done as the experimental results were being obtained to ensure that the data was correct. Systematic analyses were carried out after experiments were concluded.

#### (7) Data Acquisition Software (Davies, 1992)

GEDAP is a general-purpose software system for the analysis and management of laboratory data, including real-time experimental control and data acquisition functions. It is a fully integrated, modular system tied together by a common data file structure. The system has many features, including:

i) a standard data file format so that any GEDAP program is able to process data generated by any other GEDAP program;

ii) a consistent user interface so that all programs are easy to use in either interactive or batch mode;

iii) a fully interactive graphics capability so that results can be conveniently examined at any stage of data synthesis of analysis process; and

iv) a mechanism whereby data can be automatically identified and labelled with correct engineering units whenever they are listed or plotted.

The data acquisition software package uses a concept of header files to store all the experiment setup and identification parameters to run each test. These disc files, known as GEDAP port files, contain descriptive test parameters, such as nominal wave conditions, wave type and model configuration. Also included are experiment setup parameters, such as transducer calibration constants, the number of points sampled per channel, the sampling rate and the gain factors to be applied to individual channels.

Demultiplexing was required to break up the multiplexed raw data files into individual channel data files that could be used directly by GEDAP analysis and plotting procedure files. The raw data, stored in millivolts, were converted to full-scale units using appropriate port file calibration coefficients.

## **4.4 Behaviour of the Force Acting on the Rock Particles at the Downstream Slope**

### **4.4.1 Stochastic Behavior**

As observed from the engineering experience and experiments, the movement of the rock particles at the downstream slope of a rockfill dam is a stochastic process and very difficult to predict. The turbulence of overtopping flow and seepage flow makes the forces acting on the rocks at the downstream slope very complicated. No data is available in the literature about the stochastic behavior of the forces acting on the rock particles at the downstream slope of a rockfill dam.

In this study, stochastic process of the forces acting on the force panels was measured. The GEDAP package of NRC Hydraulics Laboratory was used to analyze the data. Figures 4-20, to 4-39 is one set of data of the analysis.

Figs. 4-20 to 4-23 are the signal, the spectrum, the probability density distribution, and autocorrelation respectively for the total force,  $R$ . Figs. 4-24 to 4-27 are the signal, the spectrum, the probability density distribution, and autocorrelation respectively for the angle of the total force,  $R_{xy}$ . Analyses show that most energy is within the range between 0 and 10 Hz, the probability distribution is very close to Gauss distribution. This force has previously been accounted for the instability of overtopped rockfill dams (Hu and Li, 1989).

The results of pulsating pressures obtained at the Nanjing Hydraulic Research Institute are summarized in Appendix 2. The measurement of the pulsating force at the downstream slope of an overtopped rockfill dam indicated that pulsating energy is distributed in the frequency range of 0 ~ 10 Hz which is the same as that from the measurement of the forces on the force panels at NRC. The probability density curve of the pulsating pressure is close to the normal (Gauss) distribution. The pulsating pressure was found quite high due to turbulent seepage flow and the complicated boundary condition. In Chapters 7 and 8, the pulsating force will be considered in the stability analysis of the rock particles at the downstream slope of a flowthrough and overtopped rockfill dam.

The Gauss distribution of the total force is useful for the future study on the probabilistic analysis of the overtopped rockfill dam design.

Figs. 4-28 to 4-31 are the signal, the spectrum, the probability density distribution, and autocorrelation respectively for the force in x direction,  $F_x$ , (along the downstream slope, and bottom up, see Fig. 4-3). Figs. 4-32 to 4-35 are the signal, the spectrum, the probability density distribution, and autocorrelation respectively for the force in y direction,  $F_y$ , (vertical to the downstream slope, and out of the dam, see Fig. 4-3). Figs. 4-36 to 4-39 are the signal, the spectrum, the probability density distribution, and autocorrelation respectively for the momentum ( $M_z$ ). It is noticed that all the curves have similar characteristics of the total force.

#### 4.4.2 Average Behavior

In the design of a rockfill dam protected by a steel mesh, large rock particles, or concrete plate, the overtopping discharge is considered to be an important parameter for the prediction of failure. No data was available for the relationship between the

forces due to overtopping and seepage flow acting on the rocks at the downstream slope and the discharge, or the upstream water head of overtopping flow, in the literature prior to the experiments undertaken in this research.

In this series of experiments, the forces acting on the force panels, the water depth, and velocity were measured for each discharge. Analyses were conducted to reveal the relationships between the forces acting on the rock particles at the downstream slope and discharge, or water head when the downstream water level is very low and no hydraulic jump occurs at the downstream slope.

#### (1) Relationship between R and Q

Figs. (4-40) shows the relationship between the resultant force R on the lower force panel and the total discharge Q. It is clear that R increases with Q when Q is less than  $0.09 \text{ m}^3/\text{s}$  (width 0.6m); when Q is larger than  $0.09 \text{ m}^3/\text{s}$ , R varies insignificantly.

Figs. (4-41) shows the relationship between the resultant force R on the upper force panel and the total discharge Q. It is clear that R increases with Q when Q is less than  $0.06 \text{ m}^3/\text{s}$  (width 0.6m); when Q is larger than  $0.06 \text{ m}^3/\text{s}$ , R is almost constant.

#### (2) Relationship between $R_{xy}$ and Q

Figs. (4-42) shows the relationship between the resultant force angle  $R_{xy}$  on the lower force panel and the total discharge Q. It is clear that  $R_{xy}$  increases with Q in all ranges of the measurement.

Figs. (4-43) shows the relationship between the resultant force angle  $R_{xy}$  on the upper force panel and the total discharge Q. It is clear that  $R_{xy}$  decreases with Q.

#### (3) Relationship between R and H

The relationship between R and the upstream water head above the crest H is similar to that between R and Q. Figure 4-44 and Fig. 4-45 show that for both the lower panel and the upper panel, the increase of H, increases R. When H is large enough, R tends to a constant.

#### (4) Relationship between $R_{xy}$ and H

The relationship between  $R_{xy}$  and H is similar to that between  $R_{xy}$  and Q. Figure 4-47 and Fig. 4-48 show the trends for the lower panel and the upper panel respectively.

All the analyses conducted is on the behavior of the quantity and angle of the total force acting on the force panels. It is observed that for both panels, the quantity of the total force remains virtually a constant when the discharge of water head is not small, while the angle of the total force changes. This is the conclusion that can be obtained at this stage. As the direction and the quantity of seepage force and shear force on the force panels are not known, it is not possible to separate the two forces at this stage.

### **4.5 Flow Pattern at the Downstream Slope of an Overtopped Rockfill Dam**

It was found at the NHRI that there was no hydraulic jump at the downstream slope of an overtopped rockfill dam without upstream facing when the size of rock particles in the dam was large enough ( $>2.5$  cm). At the NRC Hydraulics Laboratory, this conclusion was verified. Photographs 4-11 to 4-14 show all the flow patterns of an overtopped rockfill dam in the large flume at the Laboratory. Photograph 4-11 shows a hydraulic jump at the downstream of the toe (not at the slope), when the downstream gate was fully open to make the downstream water level very shallow. With the increase of downstream water level (controlled by the downstream gate), the downstream water level met the downstream face (see Photograph 4-12). At this stage, the water surface became wavy, no hydraulic jump was found. With the increase of downstream water level, the surface wave becomes weak (see Photograph 4-13). When the downstream water level was high, there is no wave along the slope. Comprehensive experimental studies from NHRI show that the absence of a hydraulic jump can be attributed to the seepage flow out of the downstream face.

## 4.6 Failure Condition of a Rockfill Dam

A series of tests for the purpose of observing the failure mechanism were undertaken at the NRC Hydraulics Laboratory. Table 4-2 lists the detailed records of the experiments. The conclusions are:

- a. When the downstream water level is low, initial failure commences at the toe of the rockfill dam if the discharge increases gradually. The failure of the downstream slope occurs at the toe and progressively moves up-slope. Figure 4-48 shows the profile of the dam after the failure (pattern 1).
- b. When the downstream water level is low, initial failure may occur at the downstream slope near the crest if the discharge increases very rapidly. The failure proceeds very fast downstream. Fig. 4-49 shows the profile of the downstream slope of the dam after the failure (pattern 2). It is noticed that very fast speed of failure make the profile like a sine curve. A deep depression was caused by the fast slide.
- c. If a downstream pool level exists, the initial failure will occur at the slope where the downstream water surface meets the downstream slope.
- d. If the placement of rocks at the surface of the downstream is not even, rock particles may start to move at very low discharge where the unevenness is large.
- e. Anywhere along the downstream slope, local failure or movement of a few rock particles may cause flow concentration. The concentrated flow will accelerate the failure process of the downstream slope.
- f. The higher the downstream water level, the higher the stability of the downstream slope. The larger the discharge the less is the stability of the slope.

## **4.7 Conclusions**

1. For the first time, stochastic behavior of the forces acting on force panels is studied. It is found that the probability distribution of the resultant force, and the angle of the resultant force is very close to Gauss distribution, and most energy is within the range between 0 and 10 Hz.

2. For the first time, statistical behaviour of the forces acting on the force panels for overtopped rockfill dams has been studied. The resultant force increased with the discharge and also with water head very fast and reach at a constant value as indicated as both the upper and the lower force panels.

3. The initial failure of a uniform overtopped rockfill dam, unprotected or protected with large rock particles, is local and shallow. The position depends on the downstream water level.

Two basic possible failure patterns are found to depend on the rate of increase of the upstream water level. An overflow rockfill dam can be protected from failure during an extreme event if attention is paid to protecting the toe of the dam, and to controlling the rate of increase of the upstream water level.

Table 4-1 Test carried out at NRC (force measurement)

<u>Test</u>	<u>Date Performed</u>	<u>Main Purpose or Command</u>
		Q = discharge measured in discharge meter
Test1	Apr. 29, 93	Set up system for initial verification
Test2	Apr. 29, 93	Q=46.51 l/sec, undertake: force measurement, velocity measurement, and water depth measurements
Test3	May 4, 93	Q=0.132 m <sup>3</sup> /sec, undertake: force measurement, velocity measurement, and water depth measurements
Test4	May 7, 93	velocity meter not working, results not complete
Test5	May 10, 93	Q=0.001 ~ 0.164 m <sup>3</sup> /sec, study steep open channel flow, undertake: force measurement, velocity measurement, and water depth measurement
Test6	May 11, 93	Q=0.083 m <sup>3</sup> /sec, study different flow pattern, undertake: force measurement, velocity measurement, and water depth measurement (some wave gauges not working)

Table 4-1 Test carried out at NRC (force measurement) (continued)

<u>Test</u>	<u>Date Performed</u>	<u>Main Purpose or Command</u>
		Q = discharge measured in discharge meter
Test7	May 17, 93	Q=0.0834 m <sup>3</sup> /sec, study different flow pattern, undertake: force measurement, velocity measurement, and water depth measurement (some wave gauges not working, downstream water level influence the discharge)
Test8	May 18, 93	Q=0.0634 ~ 0.137 m <sup>3</sup> /sec, study steep open channel flow, undertake: force measurement, velocity measurement, and water depth measurement
Test9	May 26, 93	Q=0.0634 ~ 0.138 m <sup>3</sup> /sec, study steep open channel flow, undertake: force measurement, velocity measurement, water depth measurement

Table 4-2 Test carried out at NRC (Stability)

<u>Test</u>	<u>Date Performed</u>	<u>Main Purpose or Command</u>
		Q = discharge measured in discharge meter
Stab1	July 6, 93	<p>Toe of the dam was protected with steel mesh, discharge was increased slowly.</p> <p>Two layers of particles with average size of 4 cm were used to protect the downstream slope. Initially individual particles moved due to the overtopping flow (near the top of mesh), finally the top layer slid, and then lower layer also slid totally, <math>Q=0.21 \text{ m}^3/\text{sec}</math>.</p>
Stab2	July7, 93	<p>There is no steel mesh at the downstream slope. Initially individual particles at the toe of the downstream moved due to seepage flow;</p> <p>Two layers of particles with average size of 4 cm were used to protect the downstream slope. when <math>Q = 0.022 \text{ m}^3/\text{sec}</math>, due to steep open channel flow the rock particles at and near the toe slide totally; when <math>Q = 0.028 \text{ m}^3/\text{sec}</math>, 3 rock particles at the downstream slope near the crest slid; finally the downstream slope slid resembling like a progressive failure, layer by layer. The failure was originally due to the failure of the toe.</p>

Table 4-2 Test carried out at NRC (Stability) (continued)

<u>Test</u>	<u>Date Performed</u>	<u>Main Purpose or Command</u>
		Q = discharge measured in discharge meter
Stab3	July 8, 93	Upstream slope was impermeable, and there was no steel mesh at the downstream slope. Initially individual particles at the toe of the downstream moved due to the hydraulic jump. Two layers of particles with average size of 4 cm were used to protect the downstream slope. When $Q = 0.018 \text{ m}^3/\text{sec}$ , individual rock particles near the toe slid to and stop at the toe; when $Q = 0.022 \text{ m}^3/\text{sec}$ , more rock particles at the toe of the downstream slope near the crest slid; finally the downstream slope slid layer by layer. The failure was originally due to the failure of the toe.
Uniform1	July 9, 93	Upstream slope was impermeable, and there was no steel mesh at the downstream slope. Initially individual particles at the toe of the downstream moved due to the hydraulic jump. The dam was built of rockfill particles with average size of 3 cm including the downstream slope. During the test, the discharge was increased slowly. Particles at the toe failed first, then the rockfill near the toe. The failure increased progressively, very similar to that in Stab3. Fig. 4-48 shows the final profile of the dam after failure.

Table 4-2 Test carried out at NRC (Stability) (continued)

<u>Test</u>	<u>Date Performed</u>	<u>Main Purpose or Command</u>
		Q = discharge measured in discharge meter
Uniform2	July 10, 93	Upstream slope was impermeable, and there was no steel mesh at the downstream slope. Initially individual particles at the toe of the downstream moved due to the hydraulic jump. The dam was built of rockfill particles with average size of 3 cm including the downstream slope. During the test, the discharge was increased very fast to compare with the failure pattern in test Uniform1. It is interesting that the failure start from the position at downstream slope near the crest. With the very fast rise of upstream water level, the overtopping flow reached the crest while there was no seepage at that time. The failure proceeded very fast. The final shape of the profile of the dam was like a sine curve. The failure was very different from the pattern described in Uniform1. Fig. 4-49 shows the final profile of the dam after failure.

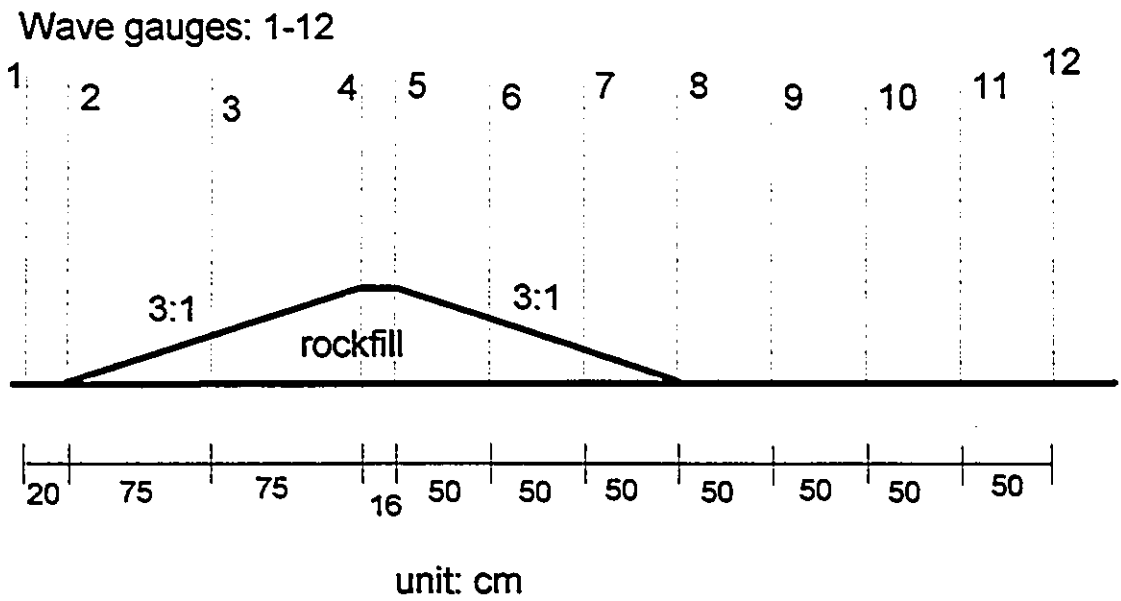
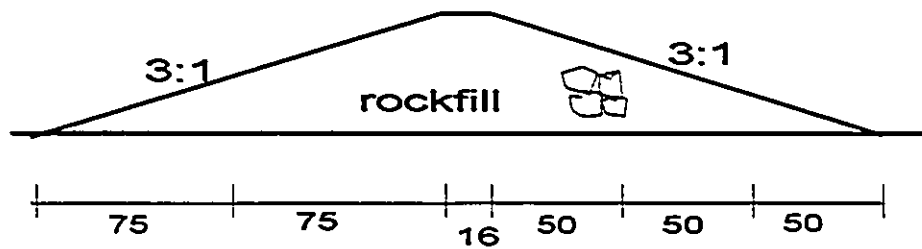
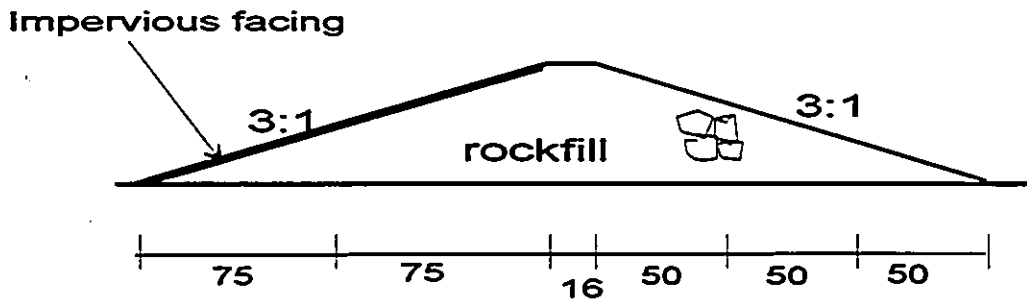


Figure 4 -1 Profile of the Model in the Wave Basin of NRC Hydraulics Laboratory



(1) Model 1 (no impermeable facing)



(2) Model 2 (upstream impervious facing)

Figure 4-2 Models in the wave basin of NRC Hydraulics Lab.

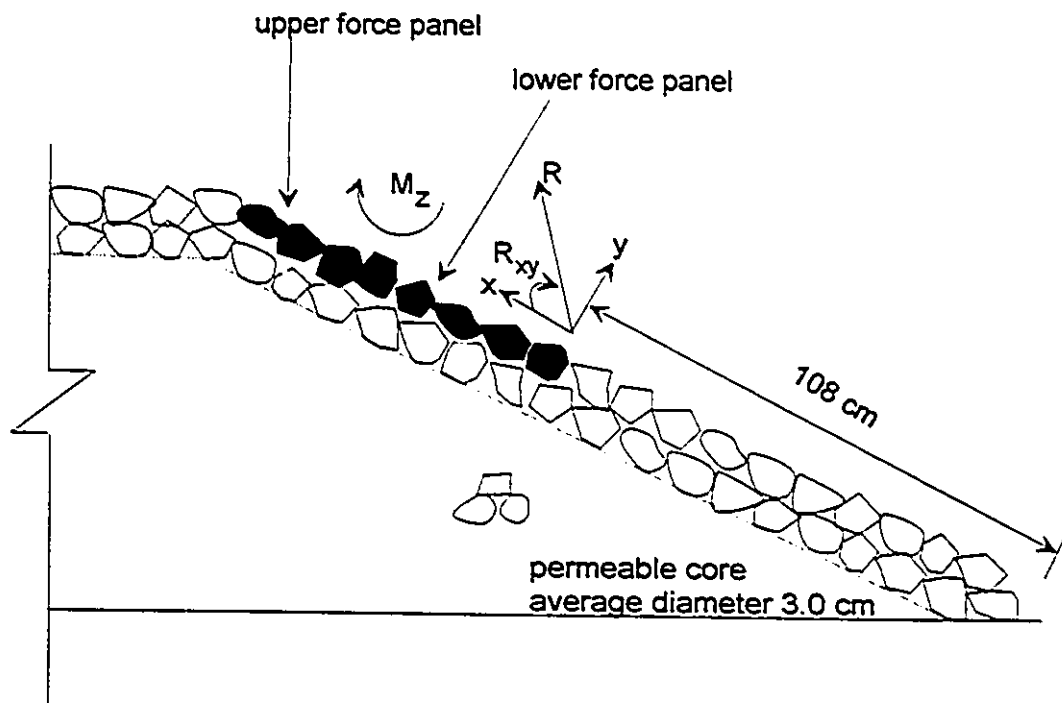


Figure 4-3 Sketch of the downstream slope armour layer and force panels

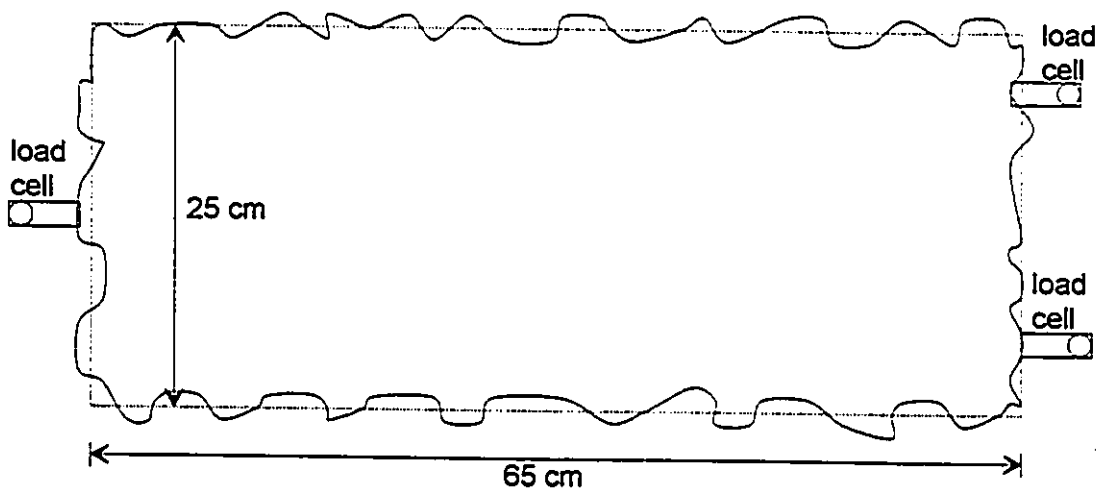


Figure 4-4 Plan view of a force panel

WAVE Probe 1

Point No.	Neff A/D Reading (volts)	Actual Value (m)	Cal Value (m)	Error (m)	
1	3.208	0.83700	0.83687	-0.00013387	
2	2.546	0.73700	0.73727	0.00026673	← Maximum Error
3	1.878	0.63700	0.63687	-0.00013280	

Maximum Error = 0.133% of Calibration Range.

Definition of Calibration Curve	
Polynomial Degree = 1 (Linear Fit)	
$Y = C_0 + C_1 \cdot V$	
where $Y(t)$	= WAVE Probe 1 (m),
$V(t)$	= sensor signal at Neff A/D converter (volts),
$C_0$	= 0.354402 m,
and $C_1$	= 0.150395 m/volt .

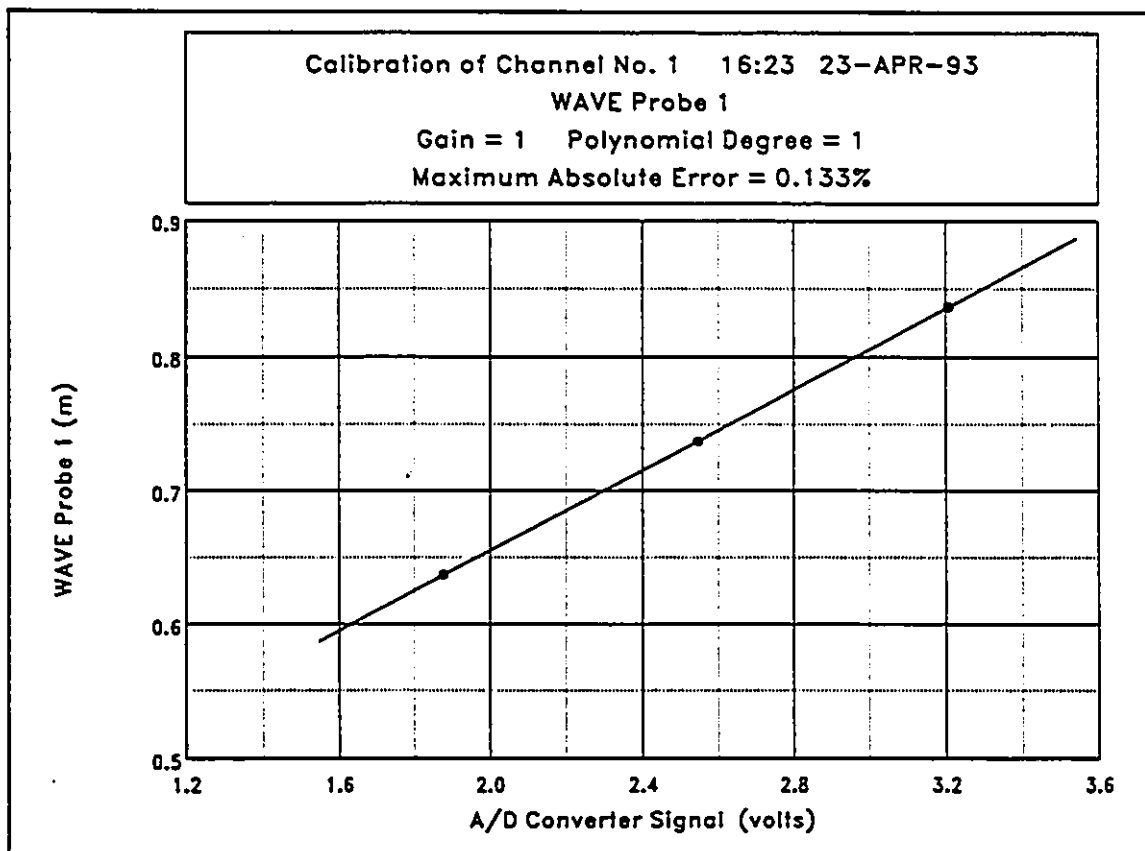


Figure 4-5 Calibration of wave probe 1

Wave Probe 2

Point No.	Neff A/D Reading (volts)	Actual Value (m)	Cal Value (m)	Error (m)	
1	3.311	0.83700	0.83690	-0.00009578	
2	2.615	0.73700	0.73719	0.00019109	← Maximum Error
3	1.915	0.63700	0.63690	-0.00009525	

Maximum Error = 0.0955% of Calibration Range.

Definition of Calibration Curve	
Polynomial Degree = 1 (Linear Fit)	
$Y = C_0 + C_1 \cdot V$	
where $Y(t)$	= Wave Probe 2 (m),
$V(t)$	= sensor signal at Neff A/D converter (volts),
$C_0$	= 0.362531 m,
and $C_1$	= 0.143278 m/volt .

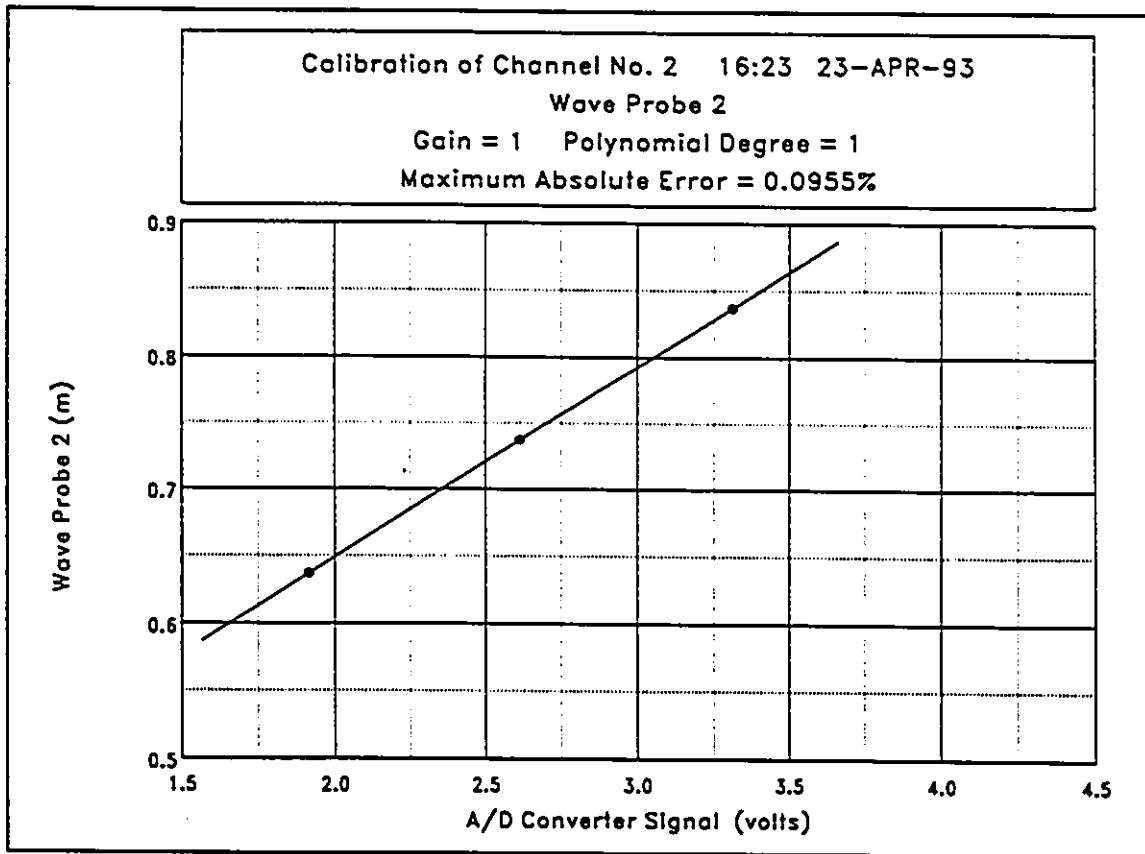


Figure 4-6 Calibration of wave probe 2

Wave Probe 3

Point No.	Neff A/D Reading (volts)	Actual Value (m)	Cal Value (m)	Error (m)	
1	3.161	0.83700	0.83698	-0.000016630	
2	2.471	0.73700	0.73703	0.000033379	← Maximum Error
3	1.780	0.63700	0.63698	-0.000016630	

Maximum Error = 0.0167% of Calibration Range.

Definition of Calibration Curve	
Polynomial Degree = 1 (Linear Fit)	
$Y = C_0 + C_1 \cdot V$	
where $Y(t)$	= Wave Probe 3 (m),
$V(t)$	= sensor signal at Neff A/D converter (volts),
$C_0$	= 0.379060 m,
and $C_1$	= 0.144870 m/volt .

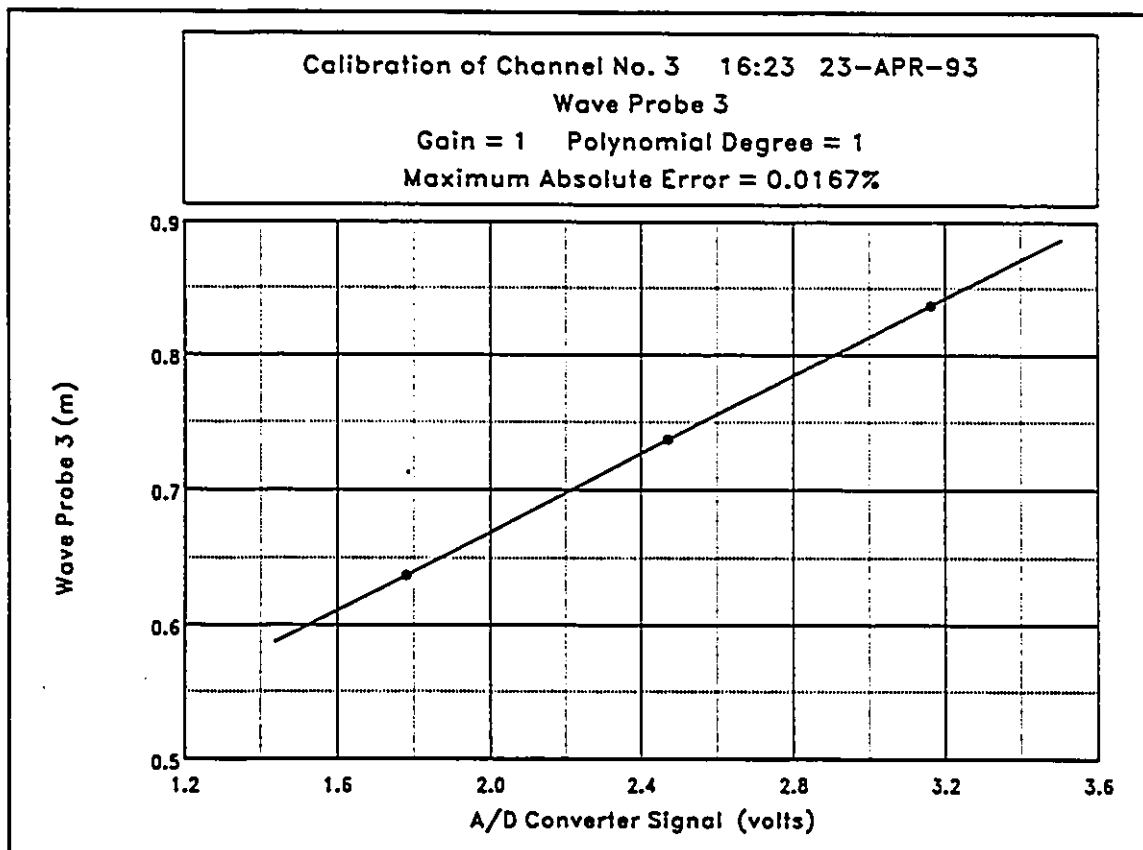


Figure 4-7 Calibration of wave probe 3

Wave Probe 4

Point No.	Neff A/D Reading (volts)	Actual Value (m)	Cal Value (m)	Error (m)	
1	0.714	0.53700	0.53724	0.00024211	
2	2.156	0.63700	0.63664	-0.00036216	← Maximum Error
3	5.065	0.83700	0.83712	0.00012004	

Maximum Error = -0.121% of Calibration Range.

<b>Definition of Calibration Curve</b>
Polynomial Degree = 1 (Linear Fit)
$Y = C_0 + C_1 \cdot V$
where $Y(t)$ = Wave Probe 4 (m),
$V(t)$ = sensor signal at Neff A/D converter (volts),
$C_0$ = 0.488003 m,
and $C_1$ = 0.0689267 m/volt .

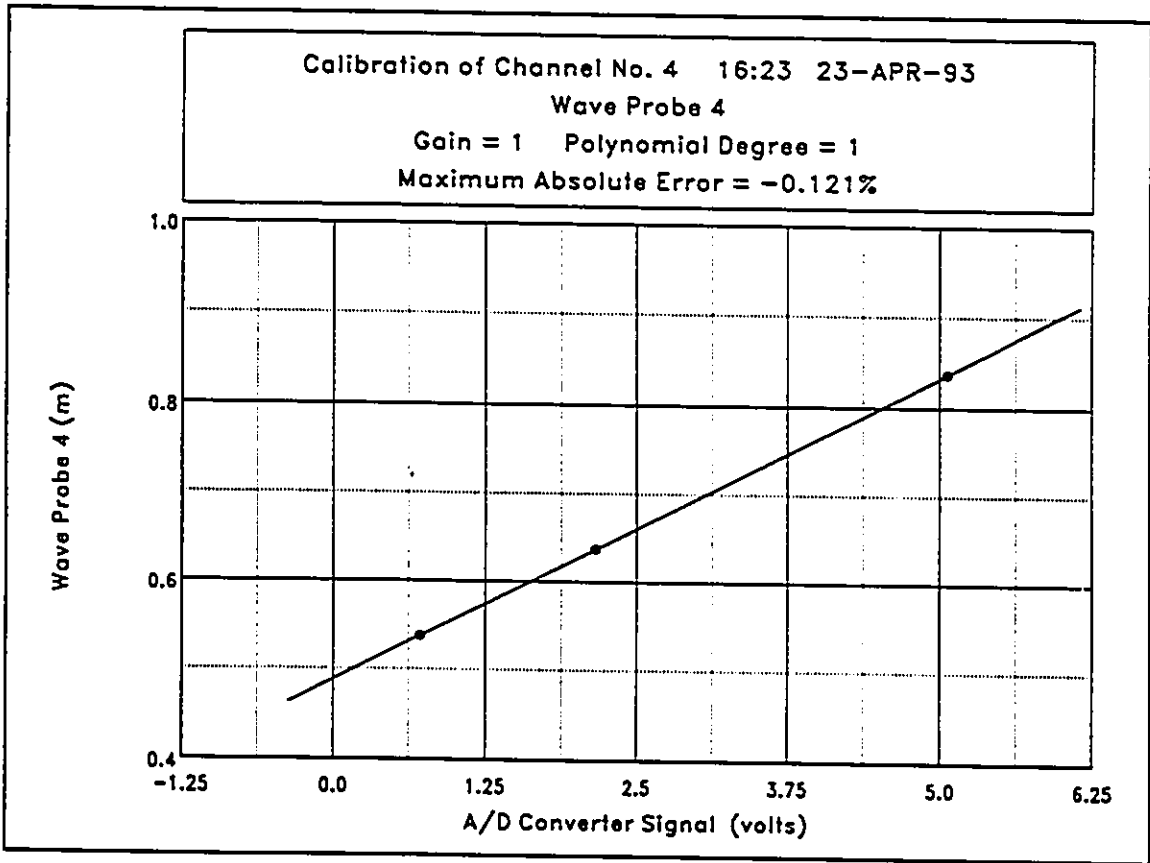


Figure 4-8 Calibration of wave probe 4

Wave Probe 5

Point No.	Neff A/D Reading (volts)	Actual Value (m)	Cal Value (m)	Error (m)	
1	0.370	0.53700	0.53802	0.0010189	
2	1.821	0.63700	0.63549	-0.0015104	← Maximum Error
3	4.827	0.83700	0.83749	0.0004916	

Maximum Error = -0.503% of Calibration Range.

<b>Definition of Calibration Curve</b>
Polynomial Degree = 1 (Linear Fit)
$Y = C_0 + C_1 \cdot V$
where $Y(t)$ = Wave Probe 5 (m),
$V(t)$ = sensor signal at Neff A/D converter (volts),
$C_0$ = 0.513133 m,
and $C_1$ = 0.0671999 m/volt .

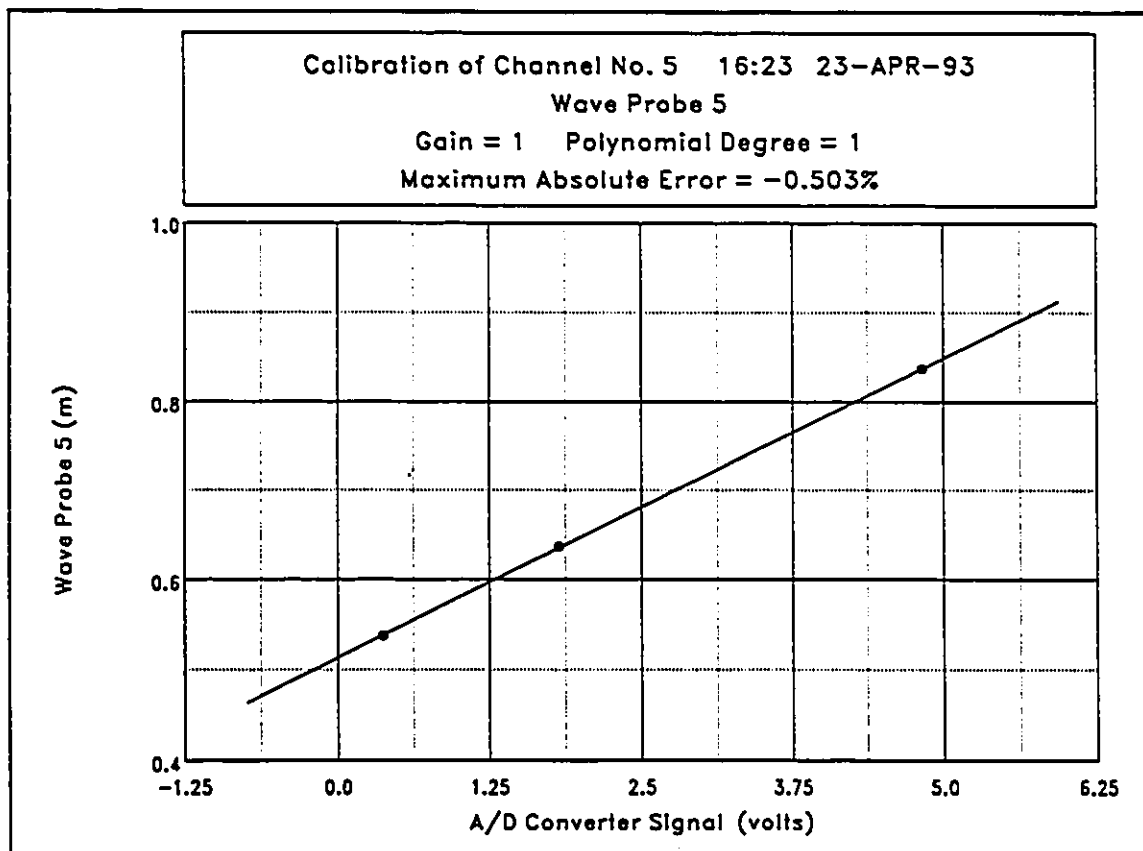


Figure 4-9 Calibration of wave probe 5

Wave Probe 6

Point No.	Neff A/D Reading (volts)	Actual Value (m)	Cal Value (m)	Error (m)	
1	3.241	0.83700	0.83725	0.00024605	
2	1.908	0.63700	0.63625	-0.00074679	← Maximum Error
3	1.253	0.53700	0.53750	0.00050074	

Maximum Error = -0.249% of Calibration Range.

Definition of Calibration Curve	
Polynomial Degree = 1 (Linear Fit)	
$Y = C_0 + C_1 \cdot V$	
where $Y(t)$	= Wave Probe 6 (m),
$V(t)$	= sensor signal at Neff A/D converter (volts),
$C_0$	= 0.348541 m,
and $C_1$	= 0.150790 m/volt .

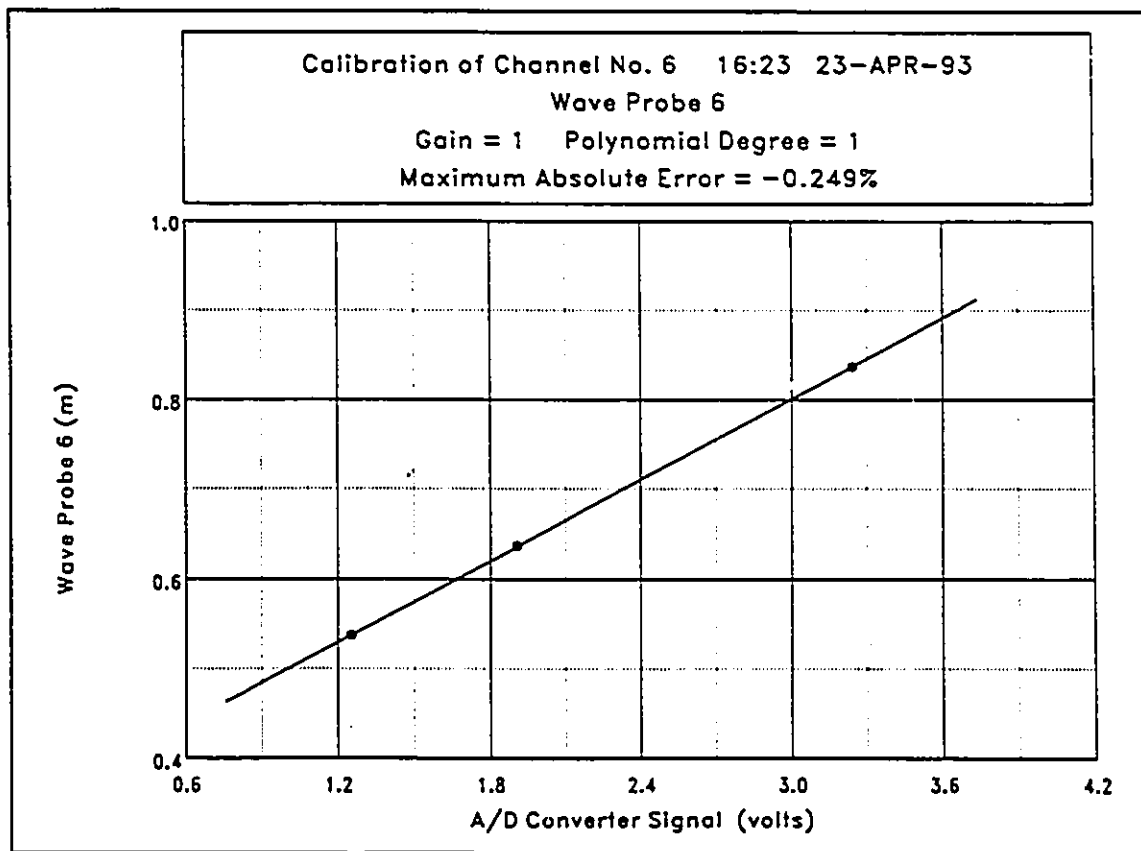


Figure 4-10 Calibration of wave probe6

Wave Probe 7

Point No.	Neff A/D Reading (volts)	Actual Value (m)	Cal Value (m)	Error (m)	
1	3.949	0.73700	0.73677	-0.00022668	← Maximum Error
2	3.302	0.63700	0.63745	0.00045043	
3	2.646	0.53700	0.53678	-0.00022364	

Maximum Error = 0.225% of Calibration Range.

Definition of Calibration Curve	
Polynomial Degree = 1 (Linear Fit)	
$Y = C_0 + C_1 \cdot V$	
where $Y(t)$	= Wave Probe 7 (m),
$V(t)$	= sensor signal at Neff A/D converter (volts),
$C_0$	= 0.130426 m,
and $C_1$	= 0.153544 m/volt .

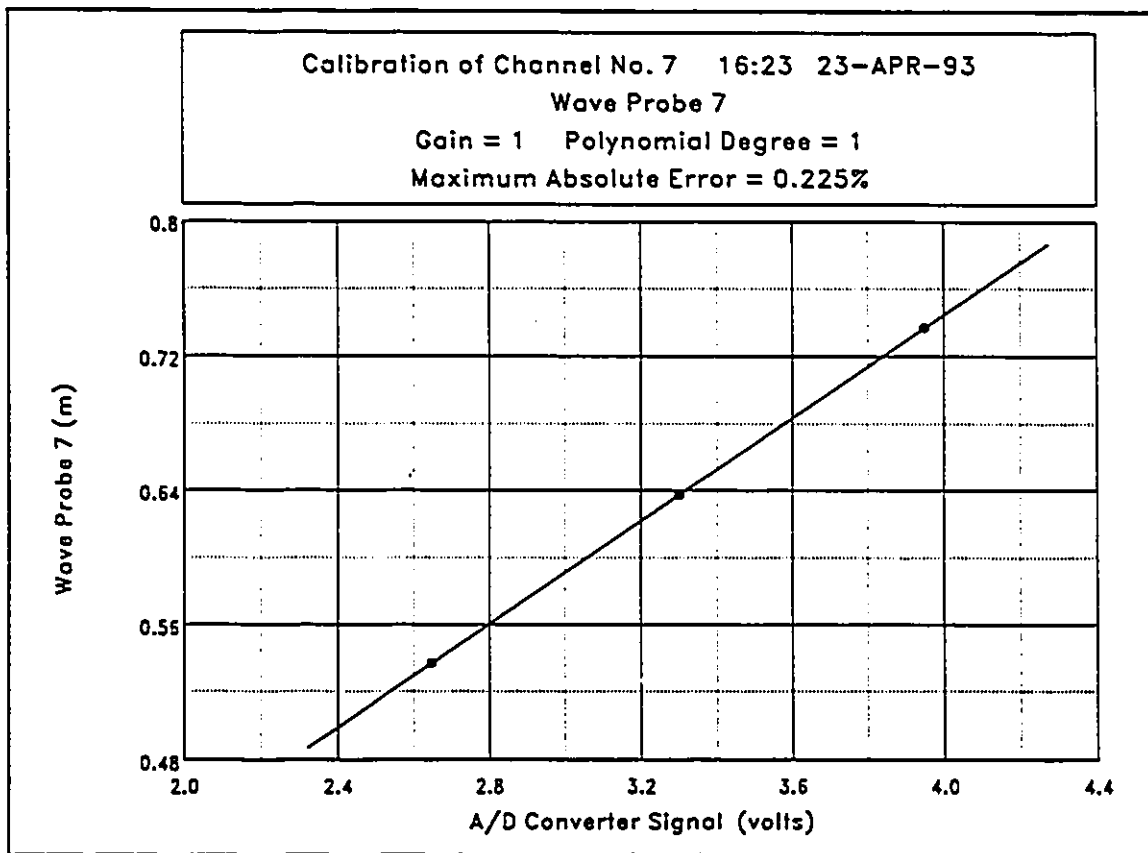


Figure 4-11 Calibration of wave probe 7

Wave Probe 8

Point No.	Neff A/D Reading (volts)	Actual Value (m)	Cal Value (m)	Error (m)	
1	8.749	0.63700	0.63670	-0.00030023	← Maximum Error
2	7.209	0.53700	0.53745	0.00044888	
3	4.096	0.33700	0.33685	-0.00014853	

Maximum Error = 0.150% of Calibration Range.

Definition of Calibration Curve	
Polynomial Degree = 1 (Linear Fit)	
$Y = C_0 + C_1 \cdot V$	
where $Y(t)$	= Wave Probe 8 (m),
$V(t)$	= sensor signal at Neff A/D converter (volts),
$C_0$	= 0.0729101 m,
and $C_1$	= 0.0644394 m/volt .

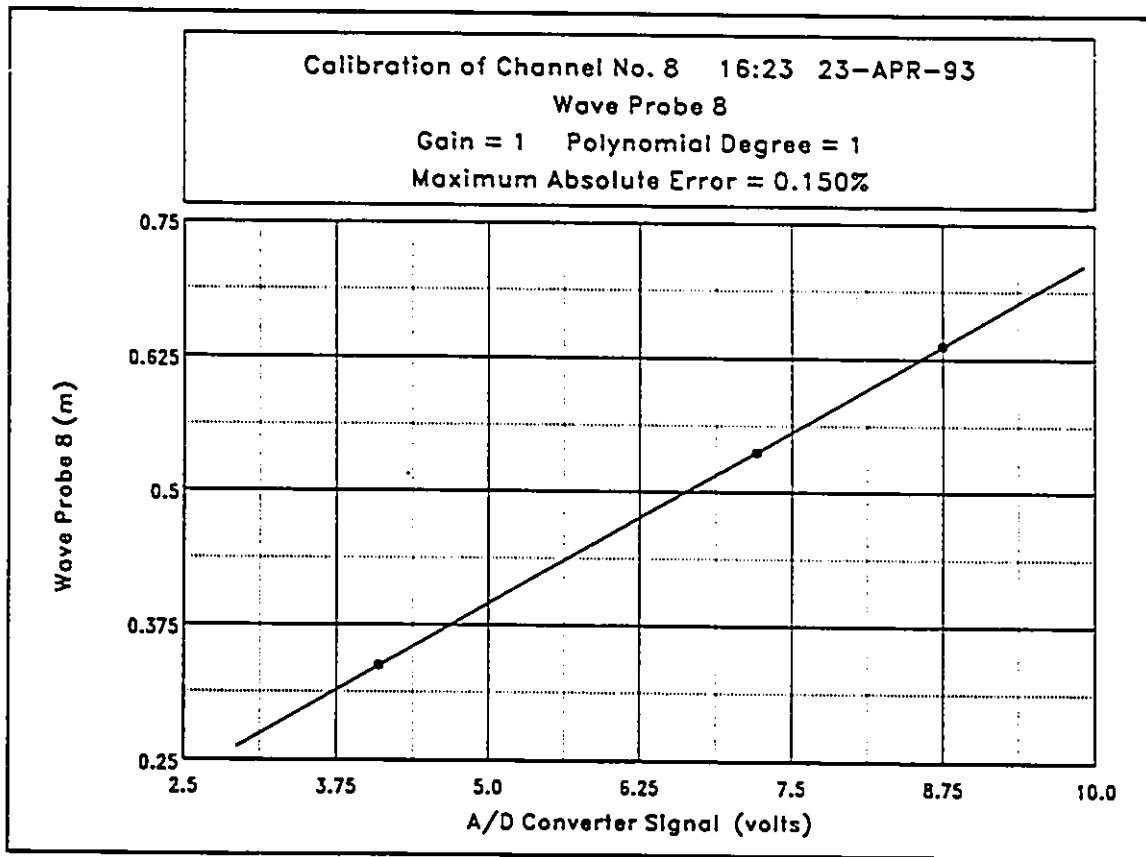


Figure 4-12 Calibration of wave probe 8

Wave Probe 9

Point No.	Neff A/D Reading (volts)	Actual Value (m)	Cal Value (m)	Error (m)	
1	9.375	0.73700	0.73691	-0.00008863	← Maximum Error
2	7.819	0.63700	0.63718	0.00017685	
3	6.254	0.53700	0.53691	-0.00008816	

Maximum Error = 0.0884% of Calibration Range.

Definition of Calibration Curve	
Polynomial Degree = 1 (Linear Fit)	
$Y = C_0 + C_1 \cdot V$	
where $Y(t)$	= Wave Probe 9 (m),
$V(t)$	= sensor signal at Neff A/D converter (volts),
$C_0$	= 0.136125 m,
and $C_1$	= 0.0640811 m/volt .

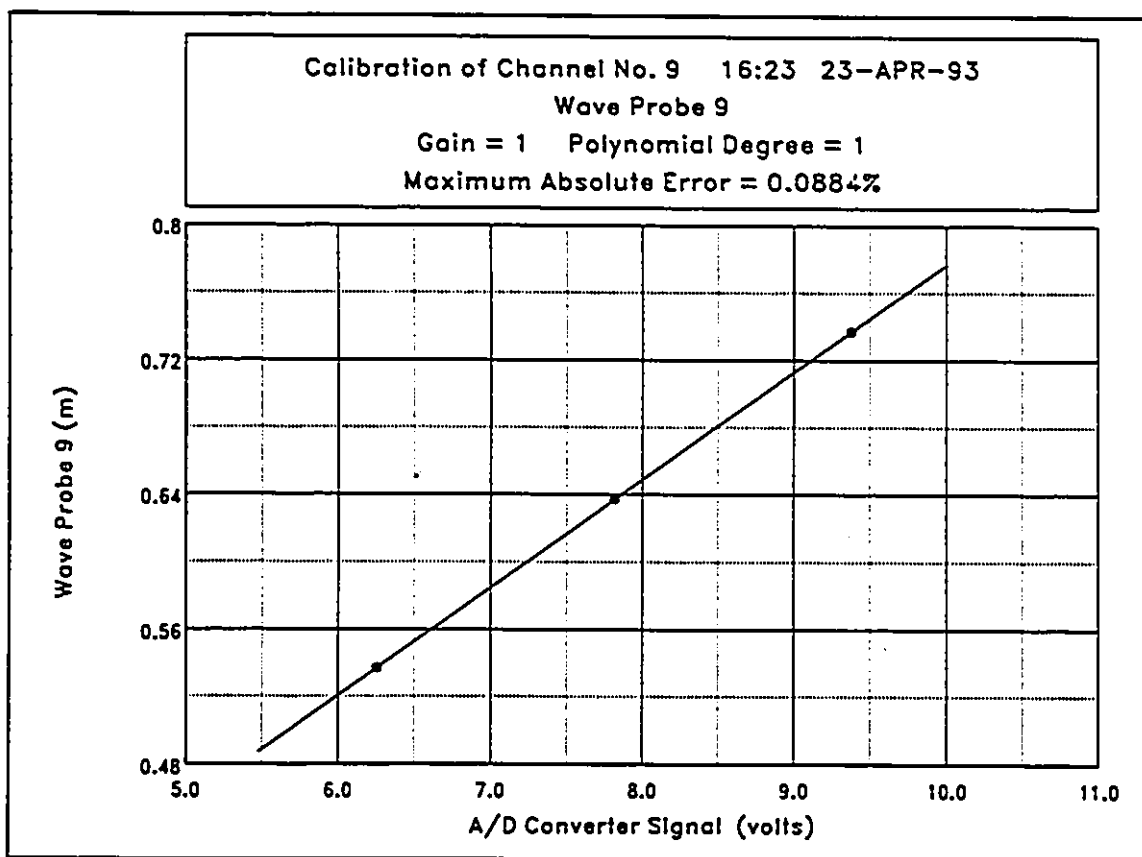


Figure 4-13 Calibration of wave probe 9

Wave Probe 10

Point No.	Neff A/D Reading (volts)	Actual Value (m)	Cal Value (m)	Error (m)	
1	4.590	0.73700	0.73694	-0.00005585	← Maximum Error
2	3.897	0.63700	0.63711	0.00011140	
3	3.202	0.53700	0.53694	-0.00005567	

Maximum Error = 0.0557% of Calibration Range.

Definition of Calibration Curve	
Polynomial Degree = 1 (Linear Fit)	
$Y = C_0 + C_1 \cdot V$	
where $Y(t)$	= Wave Probe 10 (m),
$V(t)$	= sensor signal at Neff A/D converter (volts),
$C_0$	= 0.0754553 m,
and $C_1$	= 0.144125 m/volt .

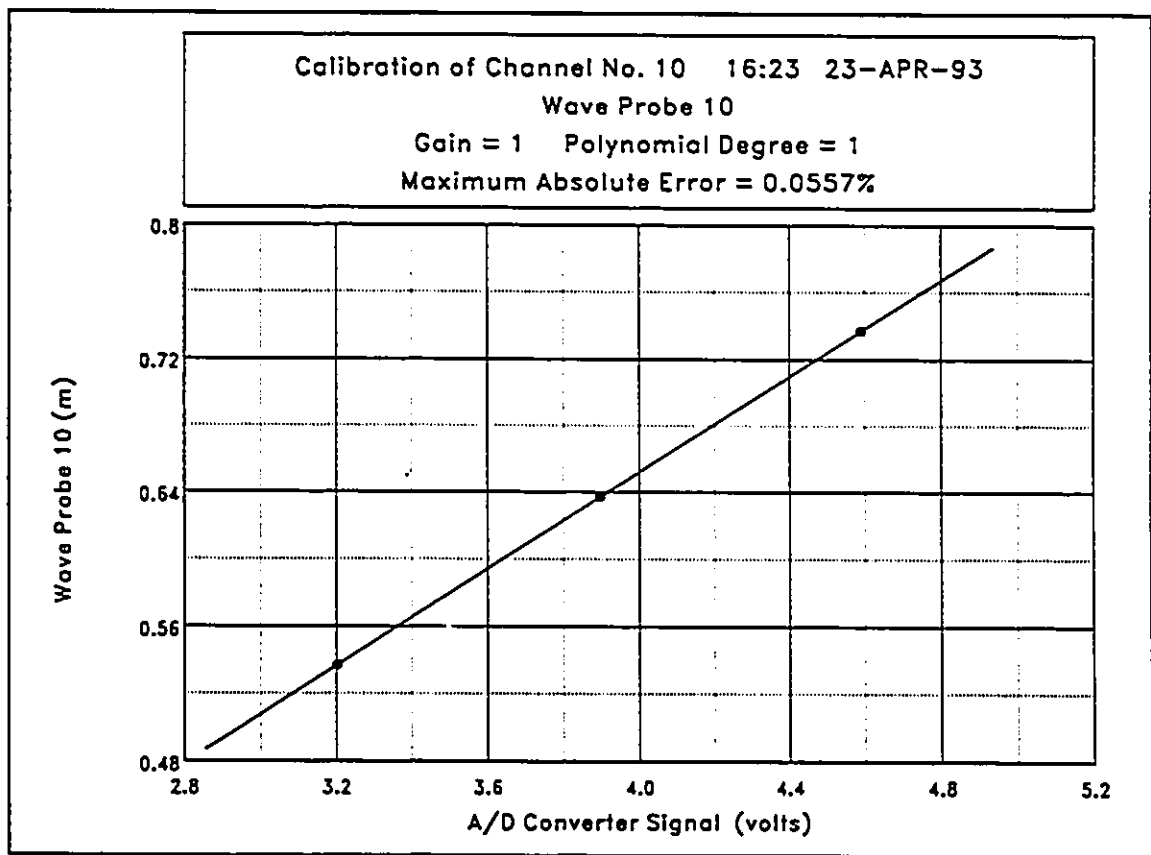


Figure 4-14 Calibration of wave probe 10

Wave Probe 11

Point No.	Neff A/D Reading (volts)	Actual Value (m)	Cal Value (m)	Error (m)	
1	6.074	0.43700	0.43650	-0.0004953	
2	7.690	0.53700	0.53801	0.0010059	← Maximum Error
3	9.258	0.63700	0.63649	-0.0005105	

Maximum Error = 0.503% of Calibration Range.

Definition of Calibration Curve	
Polynomial Degree = 1 (Linear Fit)	
$Y = C_0 + C_1 \cdot V$	
where $Y(t)$	= Wave Probe 11 (m),
$V(t)$	= sensor signal at Neff A/D converter (volts),
$C_0$	= 0.0549786 m,
and $C_1$	= 0.0628125 m/volt .

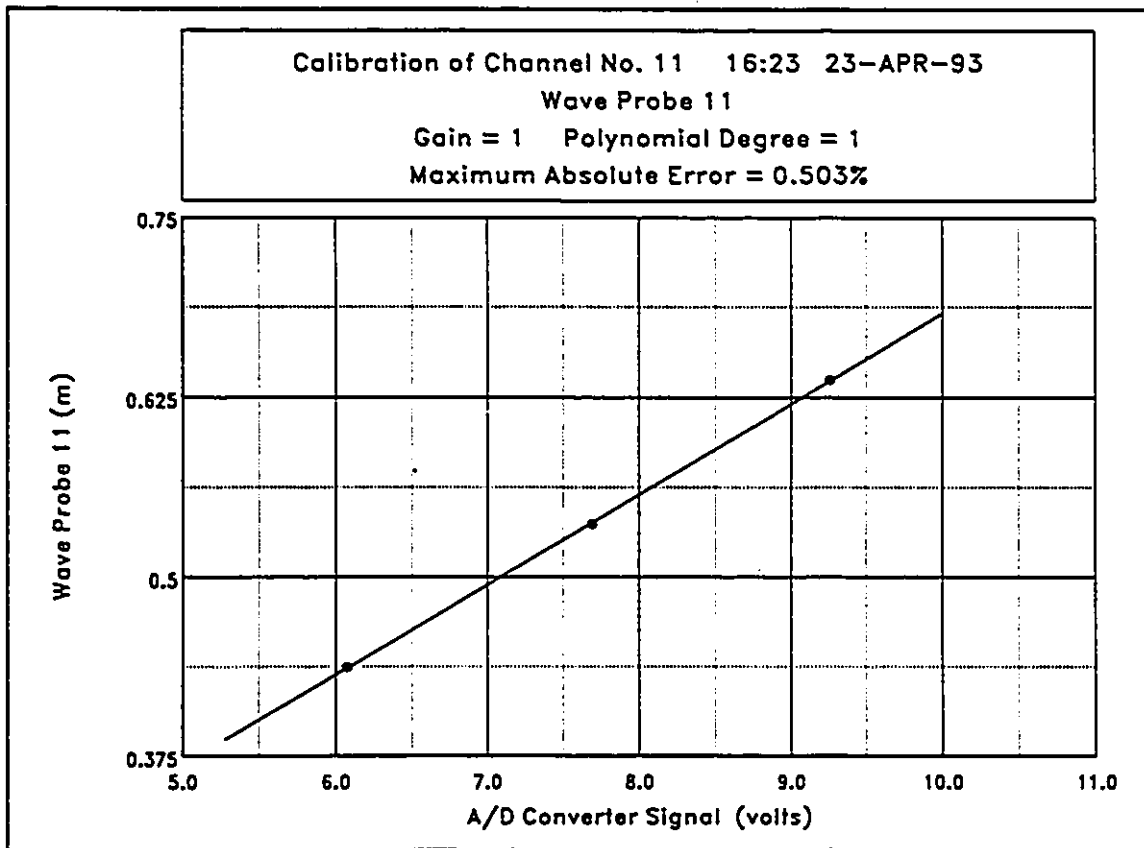


Figure 4-15 Calibration of wave probe 11

Wave Probe 12

Point No.	Neff A/D Reading (volts)	Actual Value (m)	Cal Value (m)	Error (m)	
1	7.871	0.63700	0.63697	-0.000031769	
2	4.700	0.43700	0.43710	0.000095099	← Maximum Error
3	3.111	0.33700	0.33694	-0.000063360	

Maximum Error = 0.0317% of Calibration Range.

Definition of Calibration Curve	
Polynomial Degree = 1 (Linear Fit)	
$Y = C_0 + C_1 \cdot V$	
where $Y(t)$	= Wave Probe 12 (m),
$V(t)$	= sensor signal at Neff A/D converter (volts),
$C_0$	= 0.140840 m,
and $C_1$	= 0.0630320 m/volt .

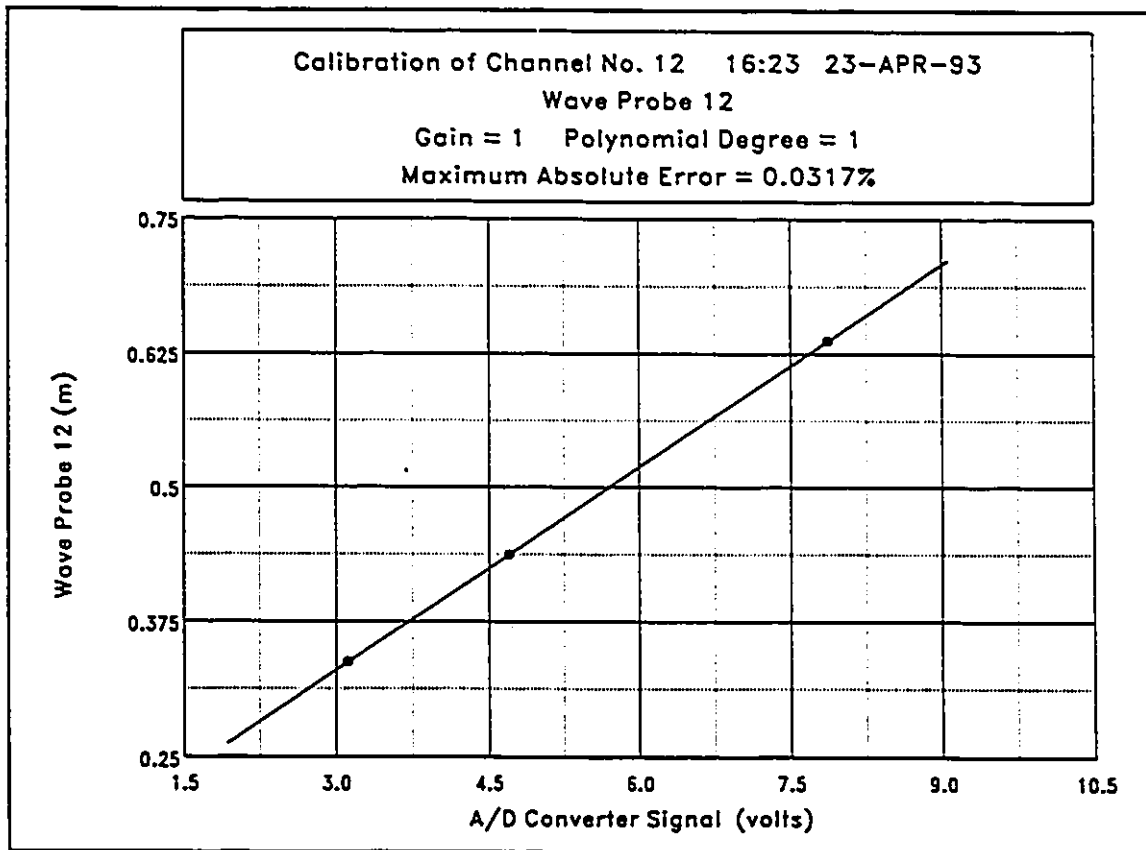


Figure 4-16 Calibration of wave probe 12

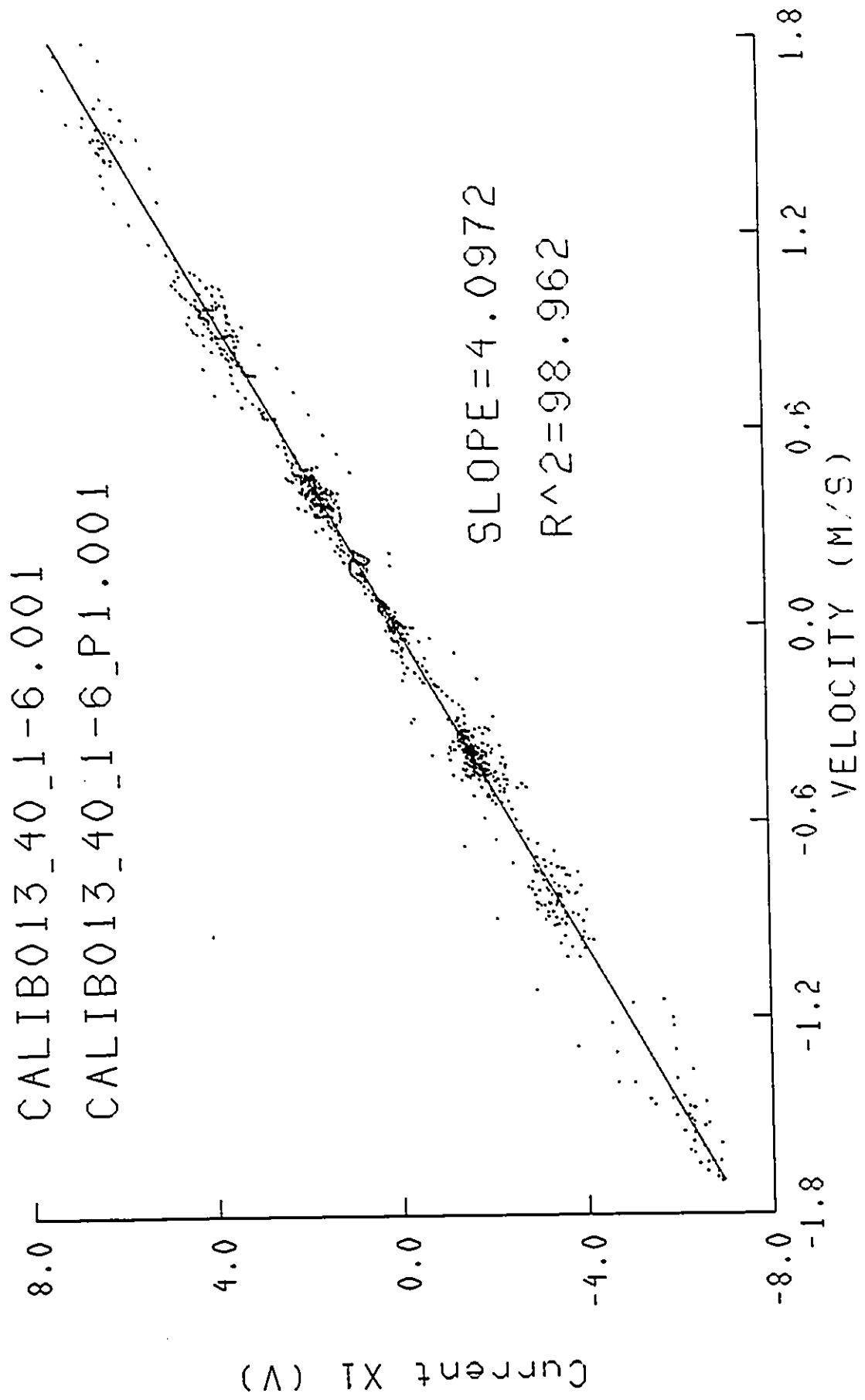


Figure 4-17 Calibration of velocity meter 1 in y direction (Channel 13)

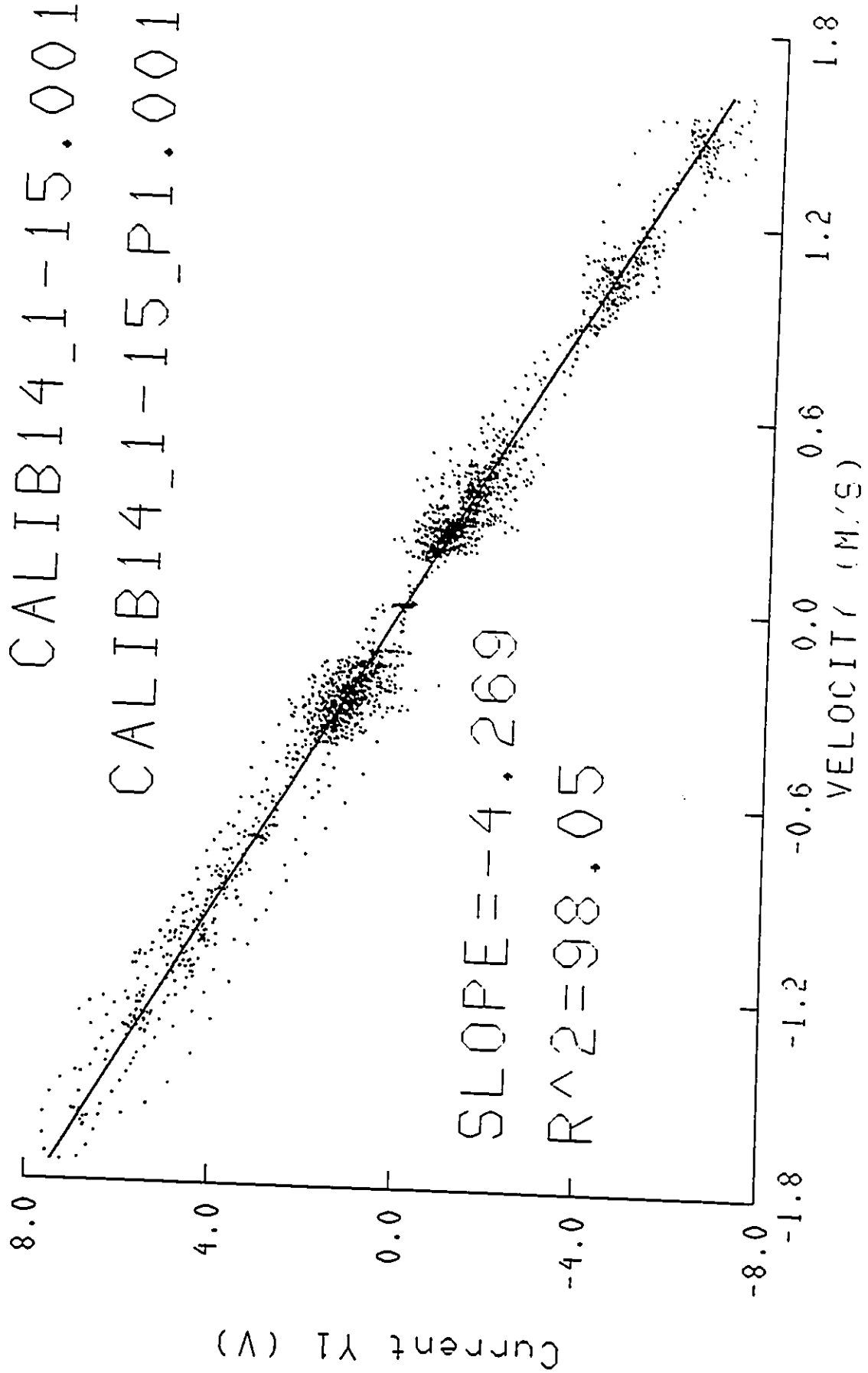


Figure 4-18 Calibration of velocity meter 1 in x direction (Channel 14)

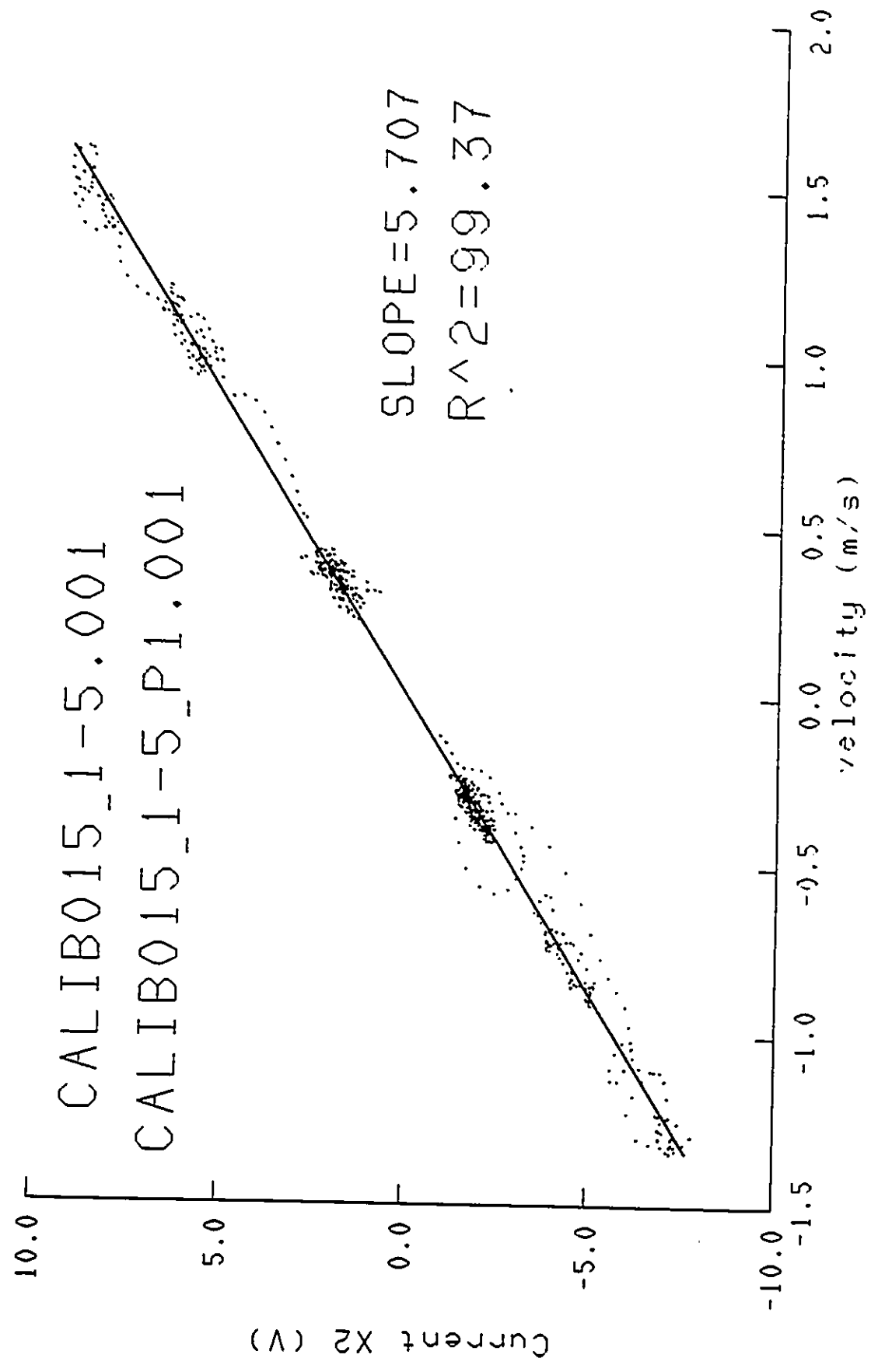


Figure 4-19 Calibration of velocity meter 2 in x direction (Channel 15)

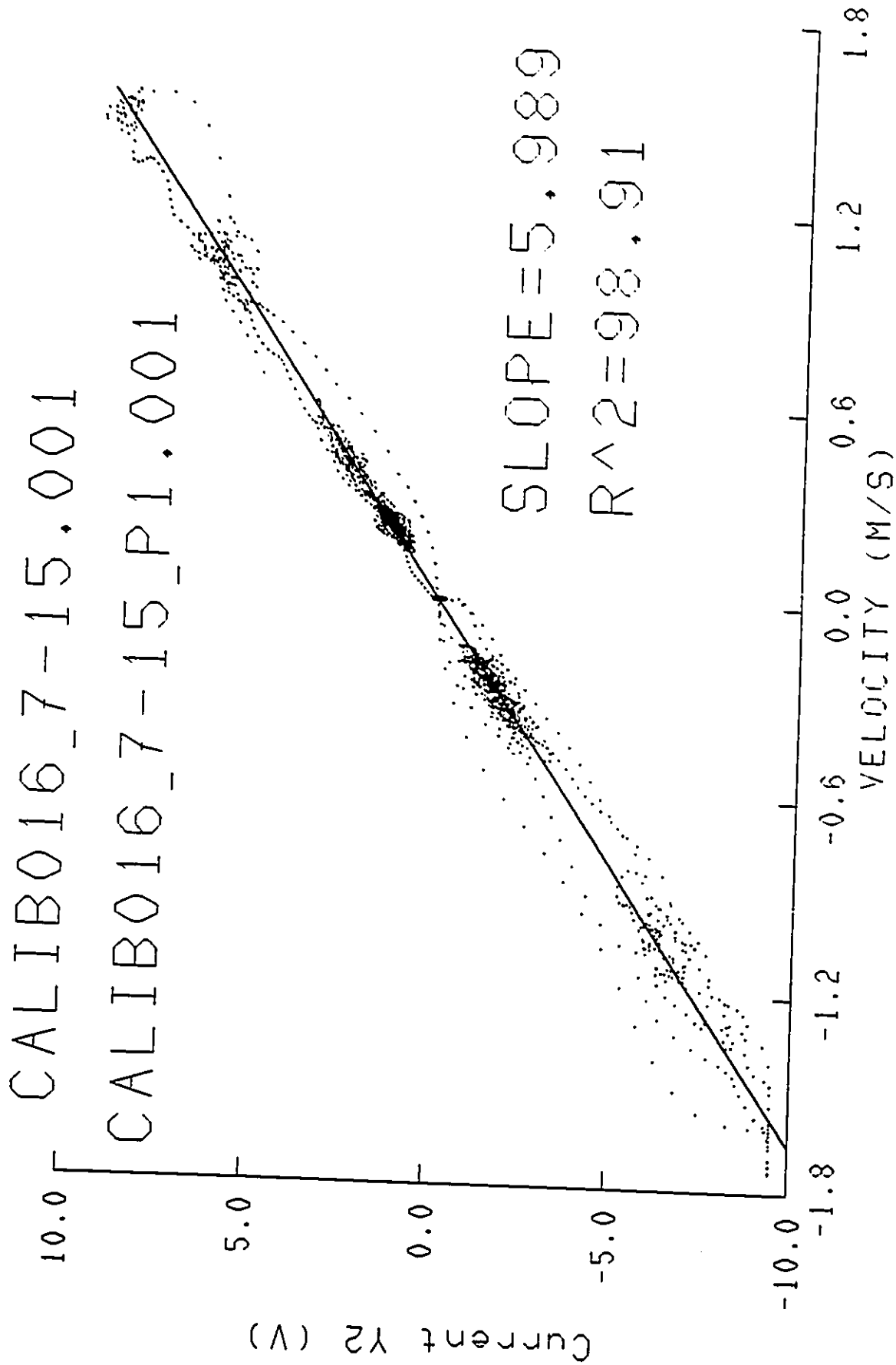


Figure 4-20 Calibration of velocity meter 2 in y direction (Channel 16)

cforce1-1\_r.045

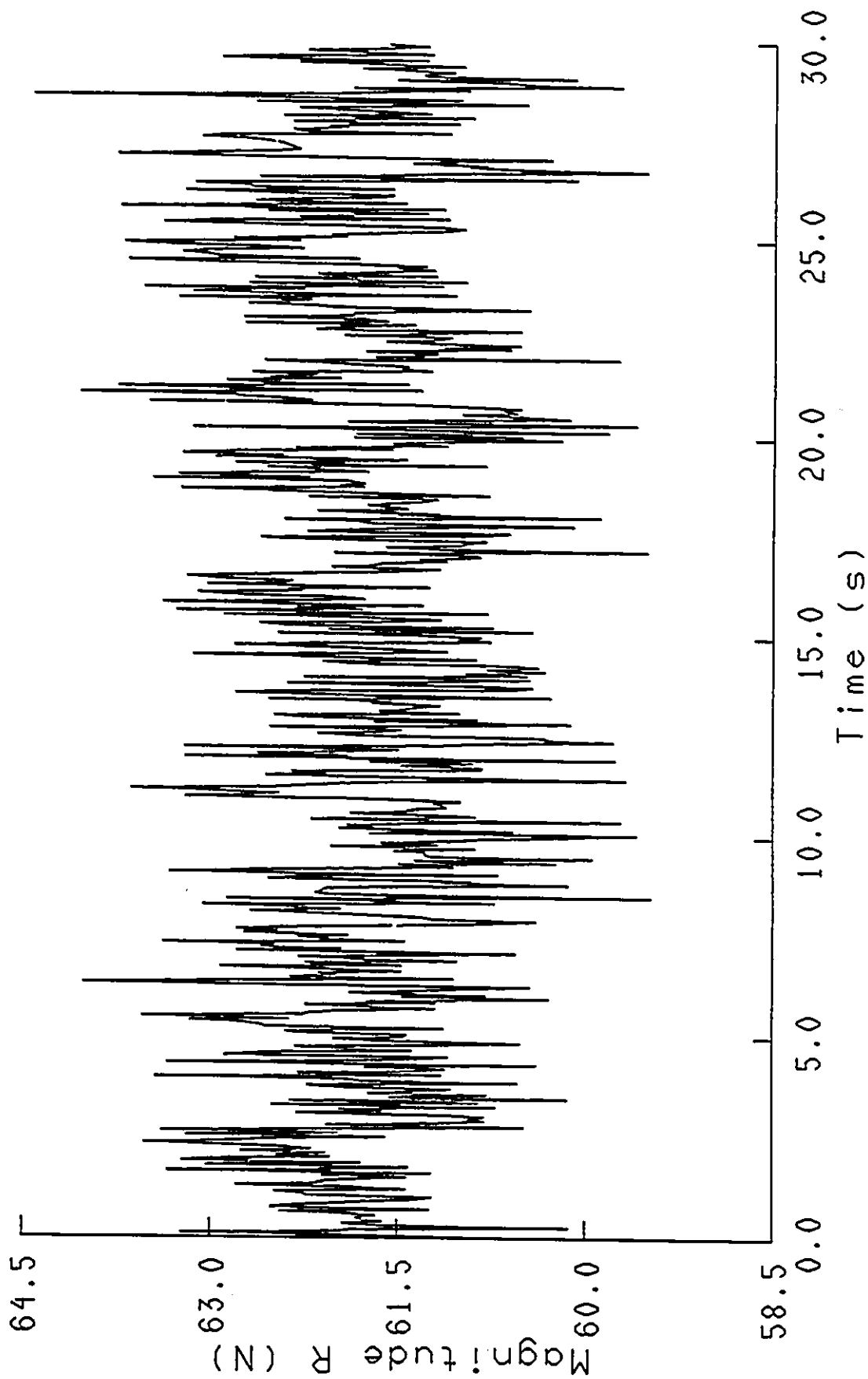


Figure 4-21 A time series record of the resultant force on the force panel

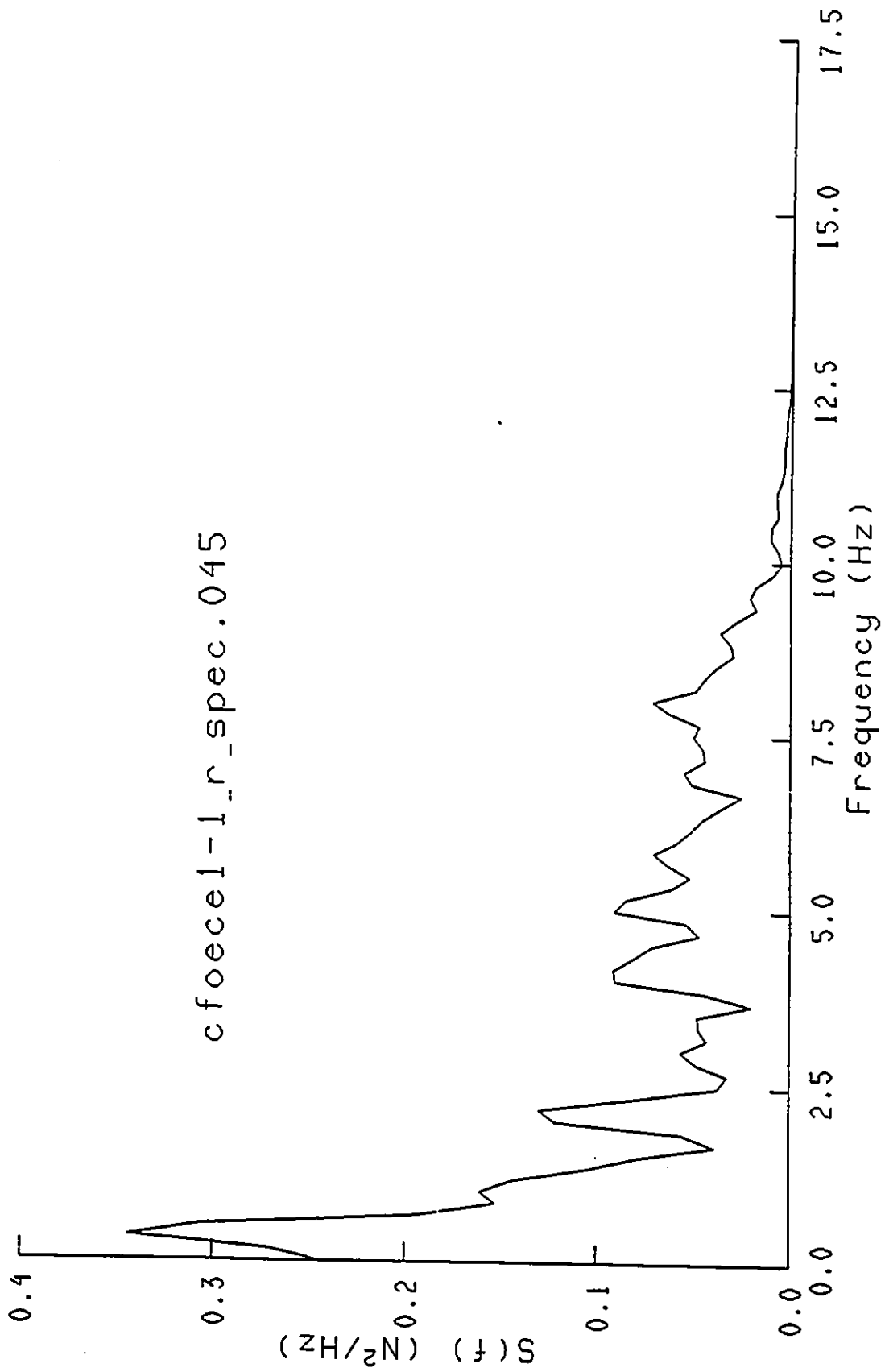


Figure 4-22 The power density function of the resultant force on the force panel

cforce1-1\_r.045

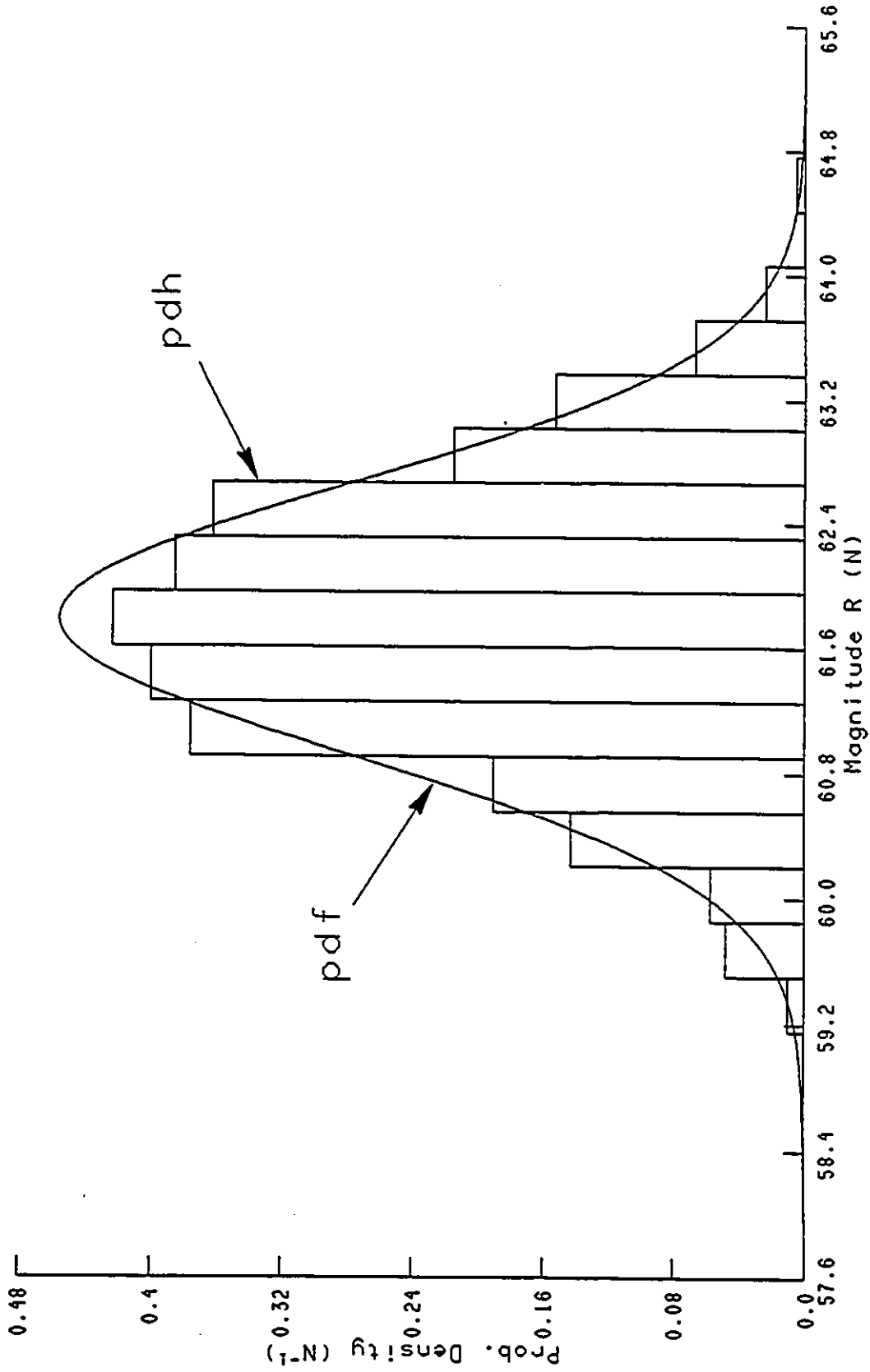


Figure 4-23 The probabilistic distribution of the resultant force on the force panel

cforce1-1\_r\_tr\_aco.045

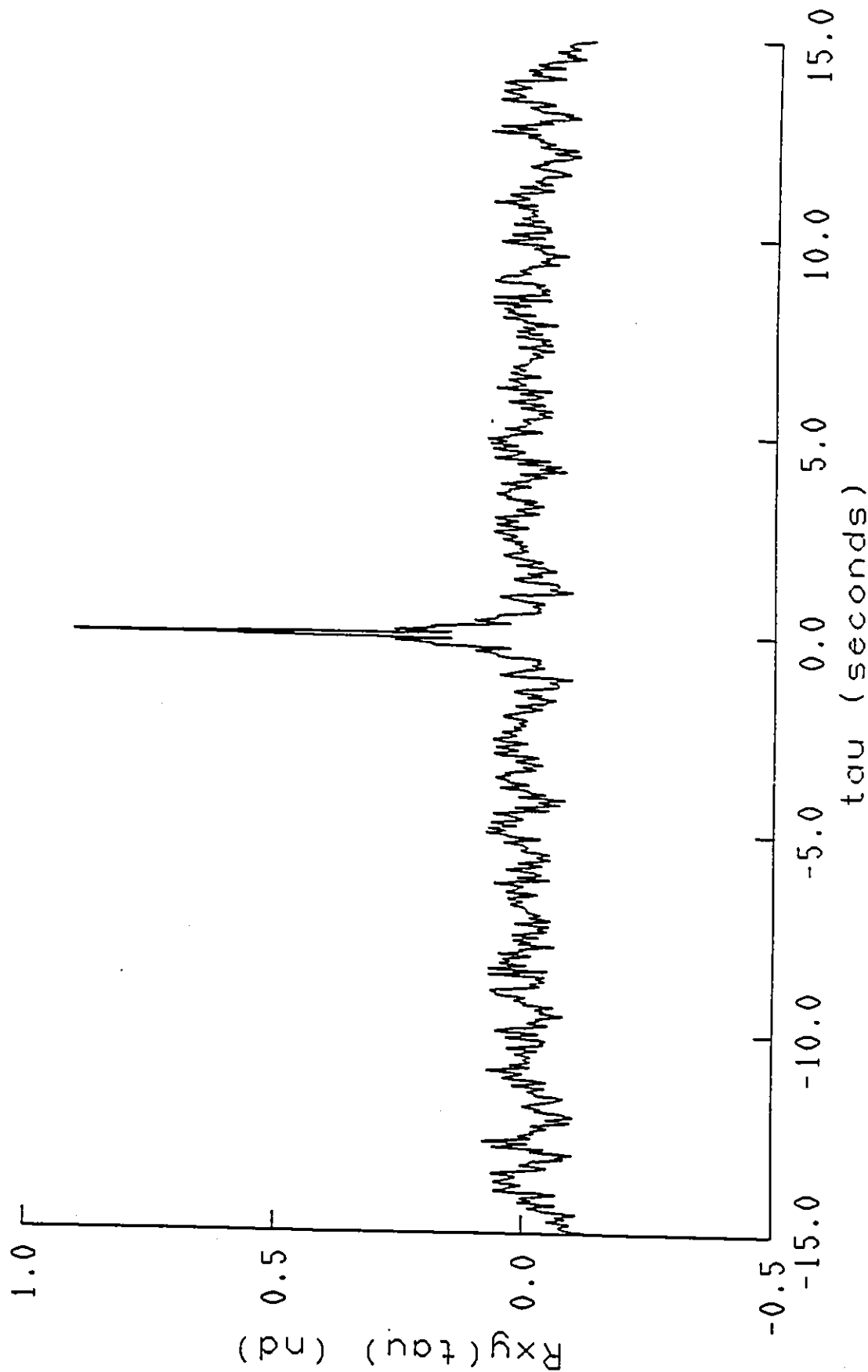


Figure 4-24 The autocorrelation of the resultant force on the force panel

, cforce1-1\_rxy.045

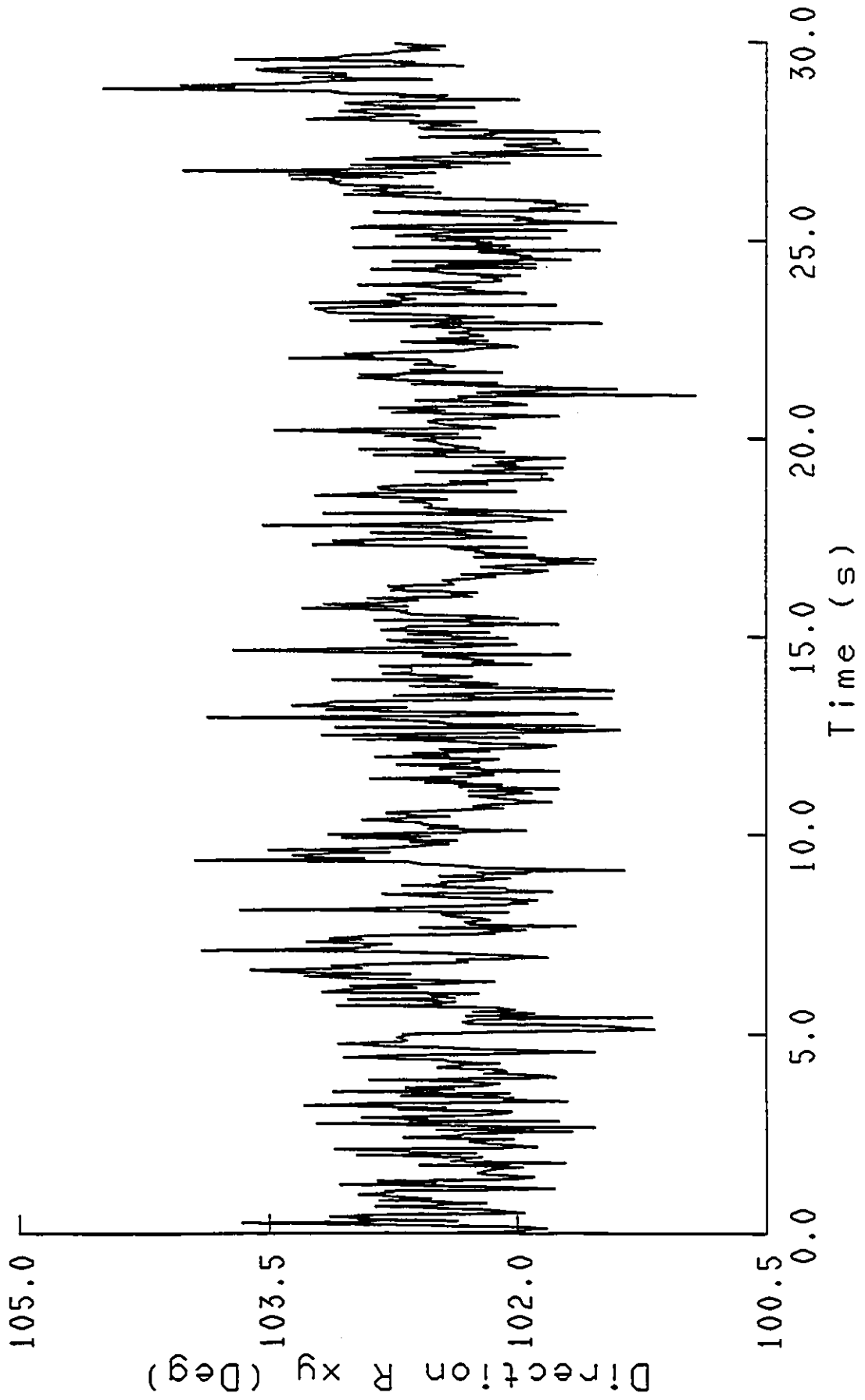


Figure 4-25 A time series record of the angle of the resultant force on the force panel

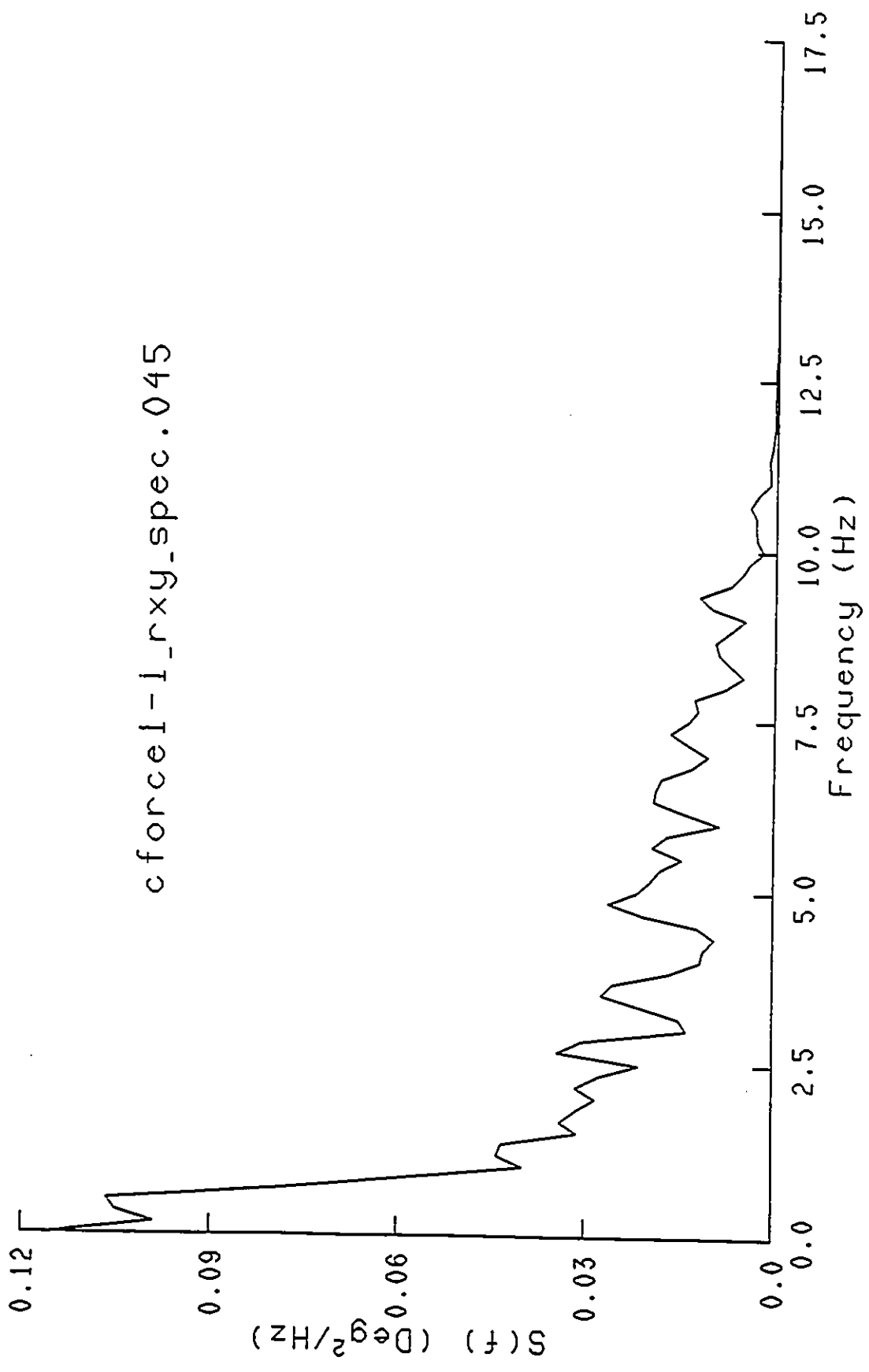


Figure 4-26 The power density function of the angle of the resultant force on the force panel

cforce1-1\_rxy.045

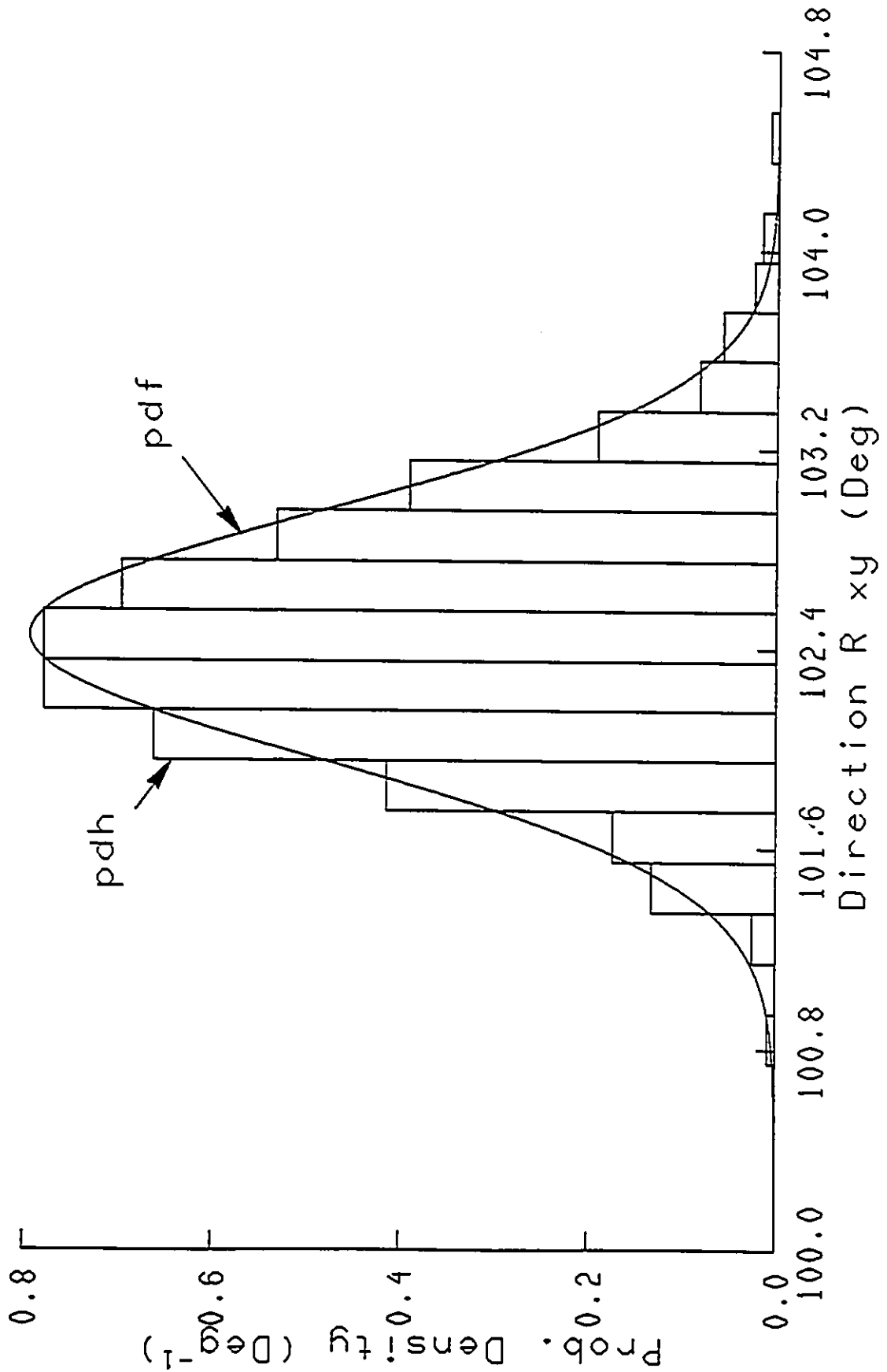


Figure 4-27 The probabilistic distribution of the angle of the resultant force on the force panel

cforce1-1\_rxy\_tr\_aco.045

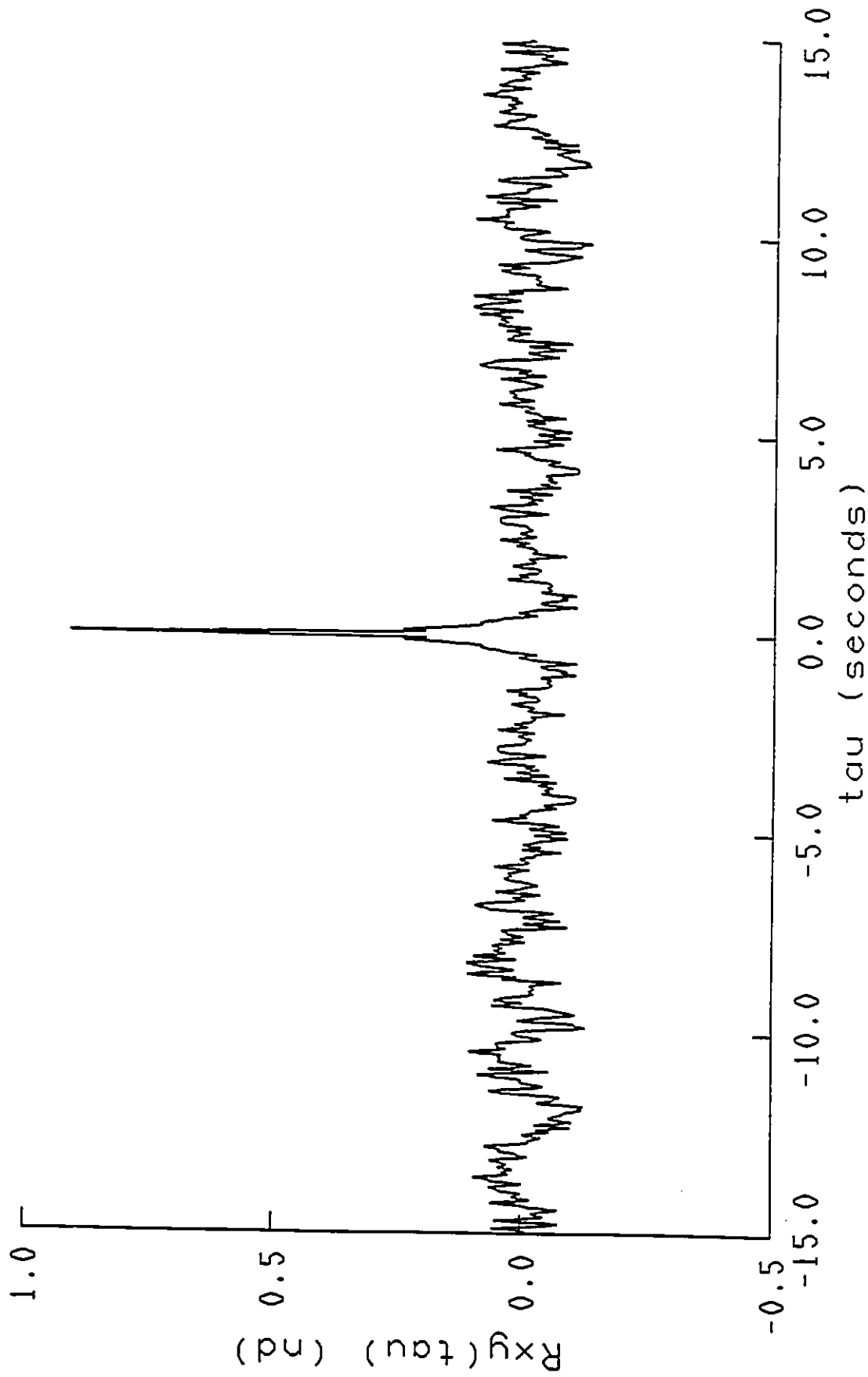


Figure 4-28 The autocorrelation function of the angle of the resultant force on the force panel

cforce1-1\_fx.045

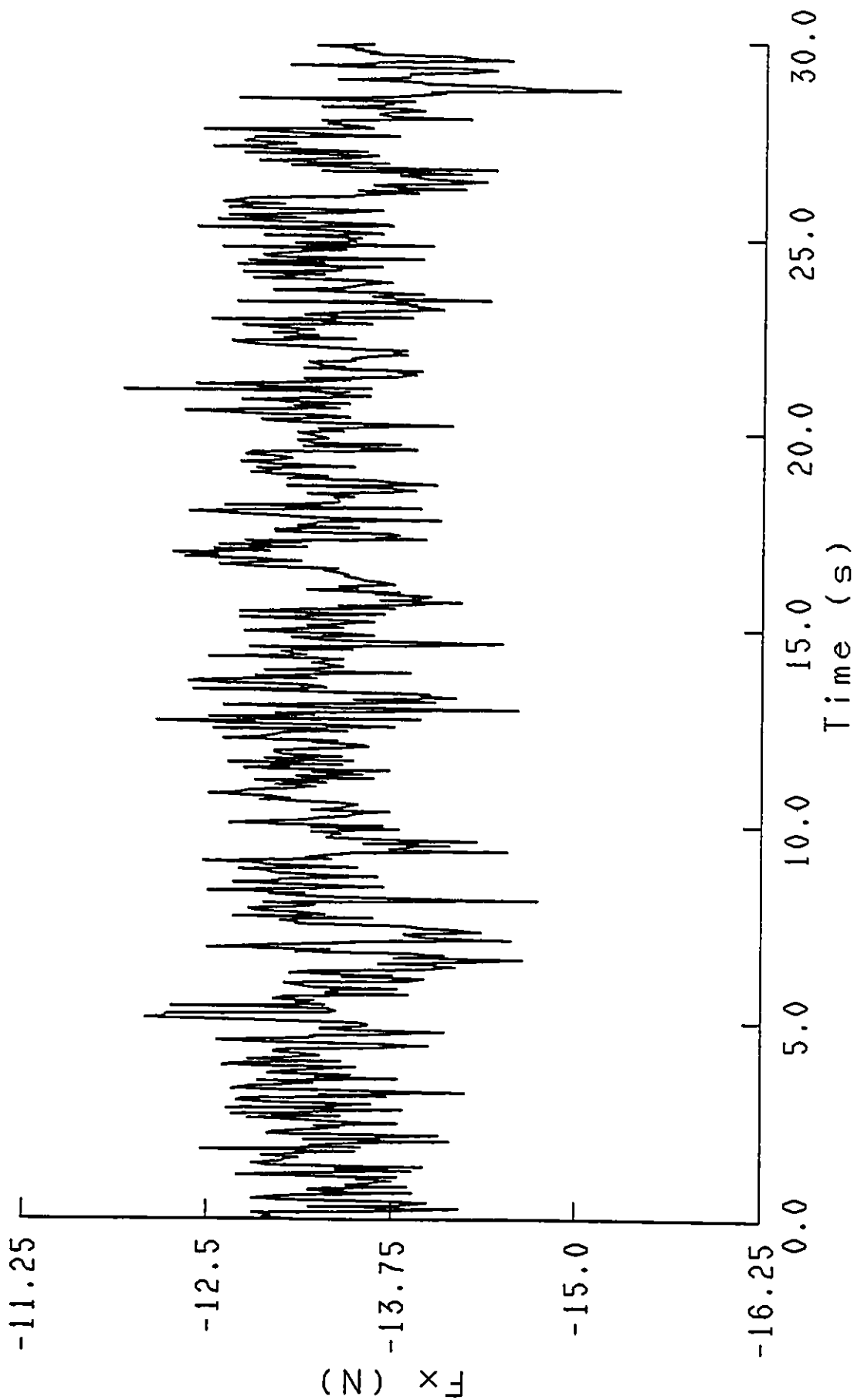


Figure 4-29 A time series record of the force in x direction on the force panel

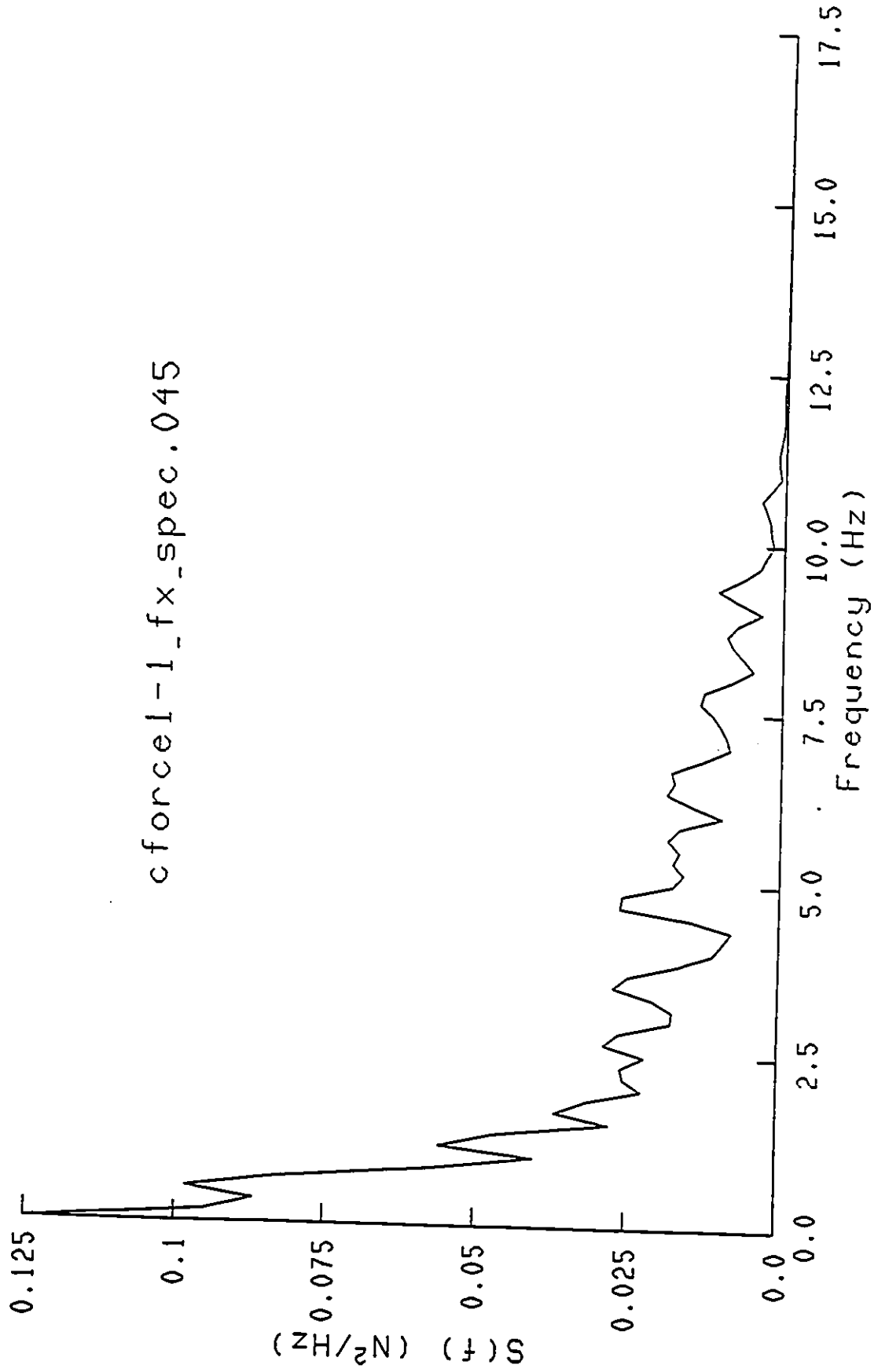


Figure 4-30 The power density function of the force in x direction on the force panel

cforce1-1\_fx.045

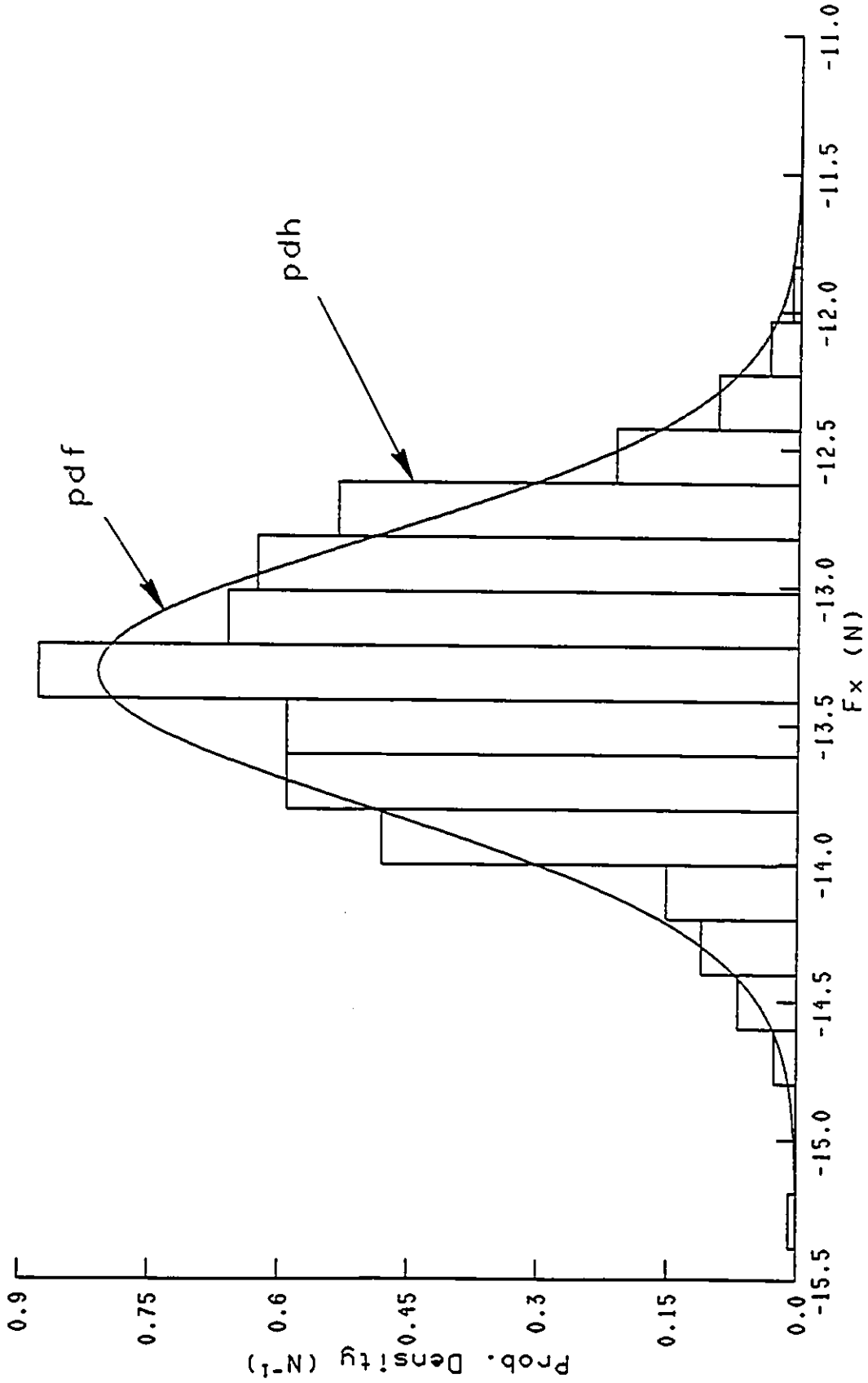


Figure 4-31 The probabilistic distribution of the force in x direction on the force panel

cforce1-1\_fx\_tr\_aco.045

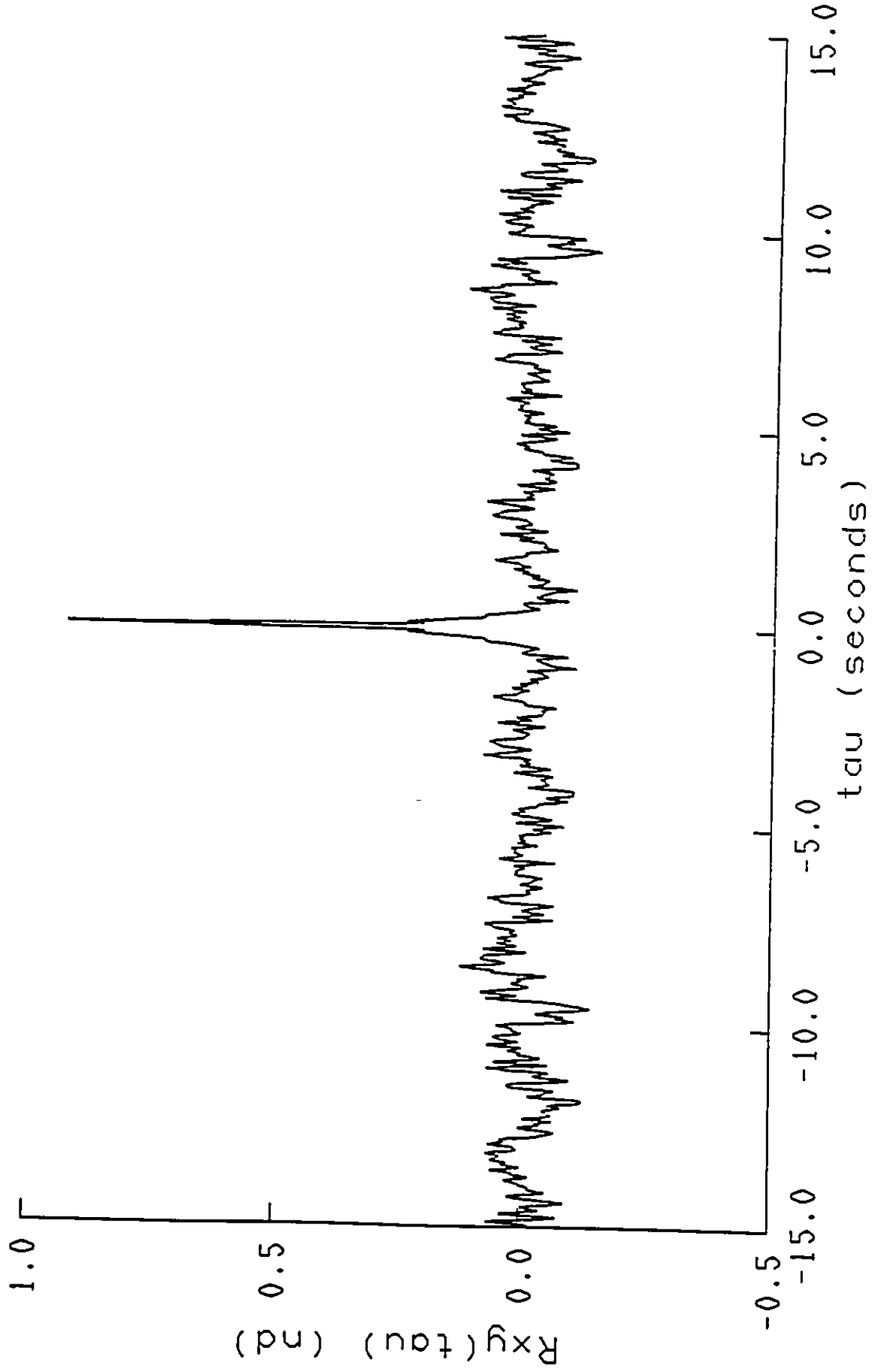


Figure 4-32 The autocorrelation of the force in x direction on the force panel

cforce1-1\_f.y.045

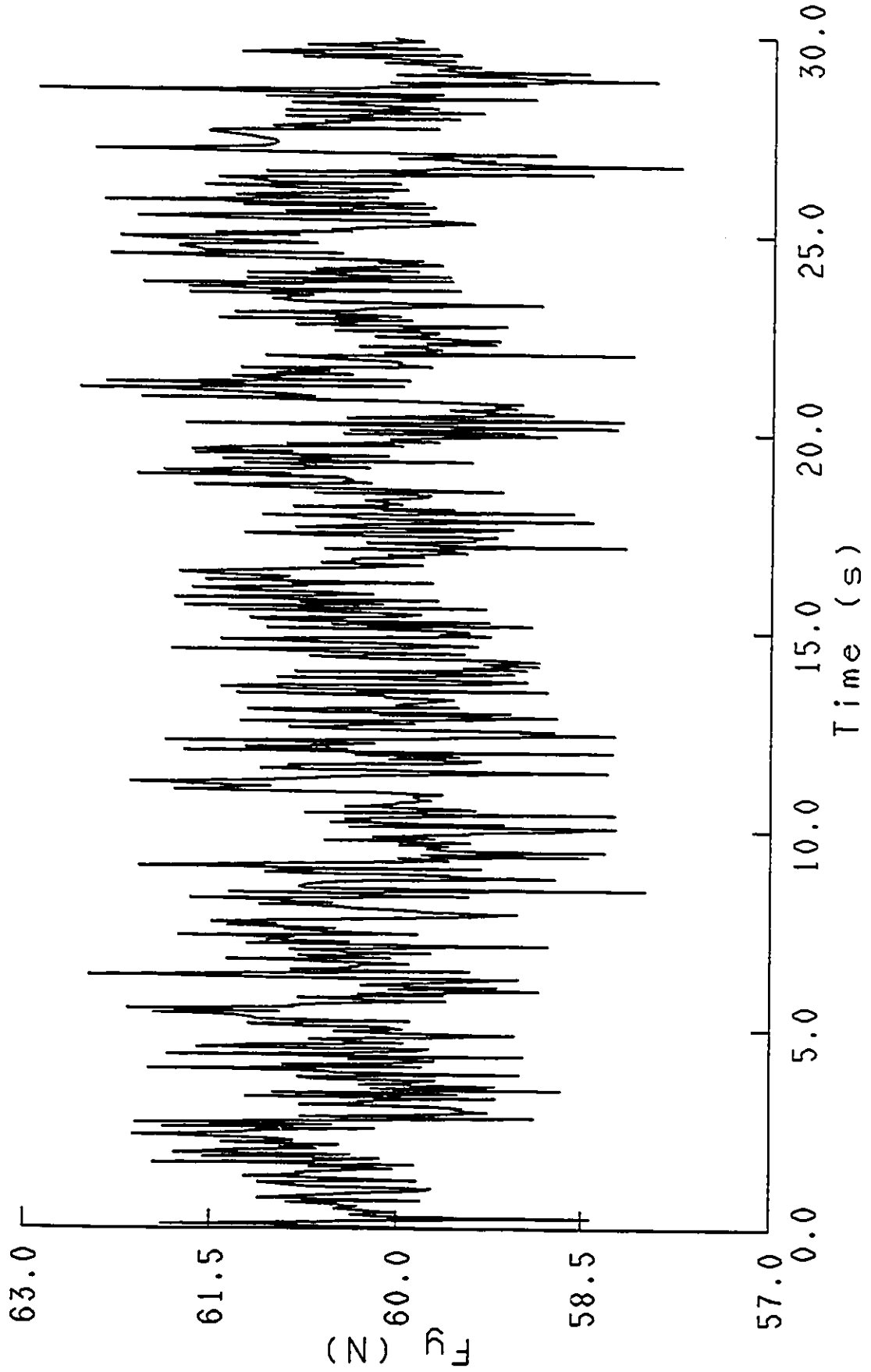


Figure 4-33 A time series record of the force in y direction on the force panel

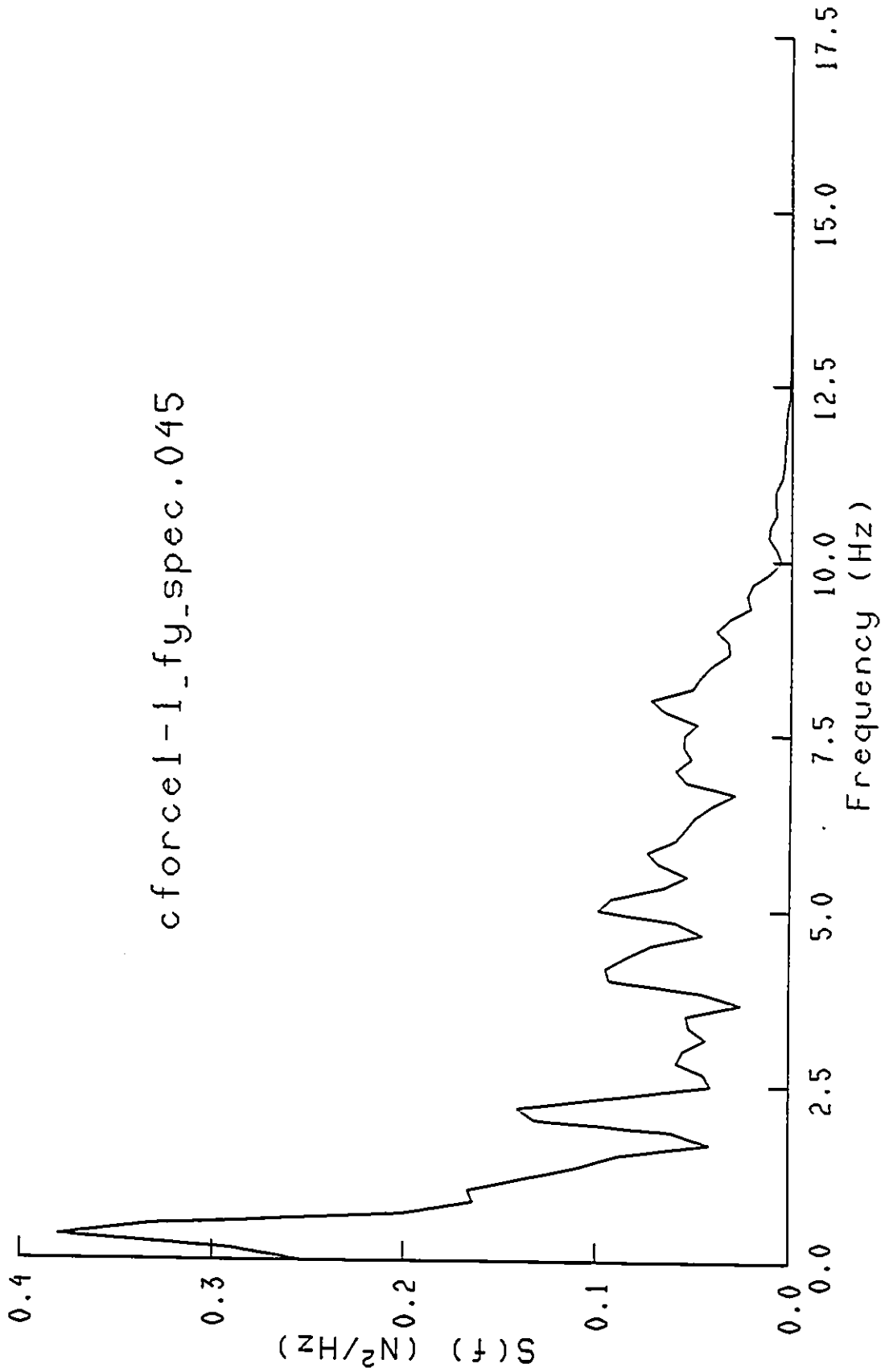


Figure 4-34 The power density function of the force in y direction on the force panel

cforce1-1\_fy.045

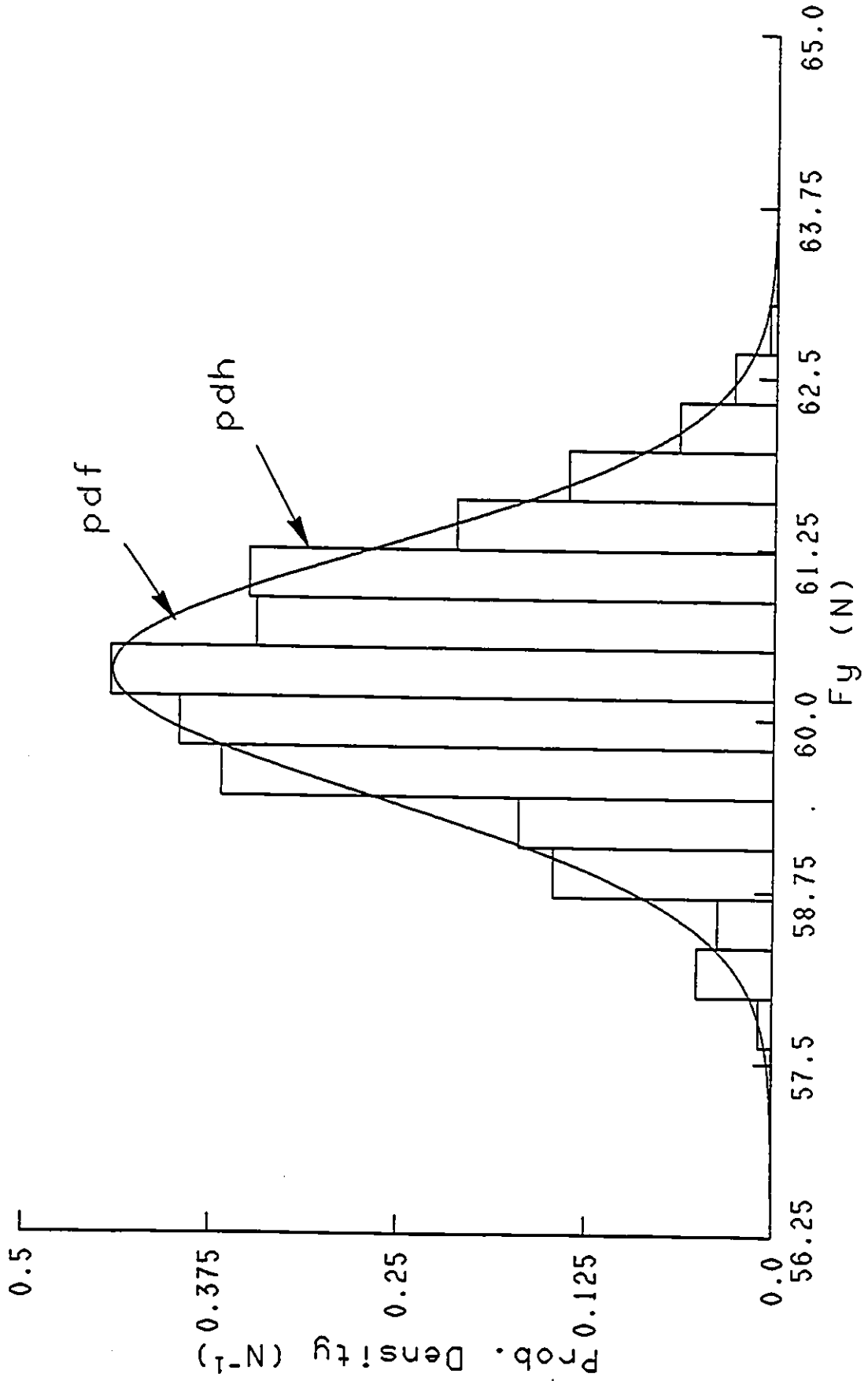


Figure 4-35 The probabilistic distribution of the force in y direction on the force panel

cforce1-1\_fy\_tr\_aco.045

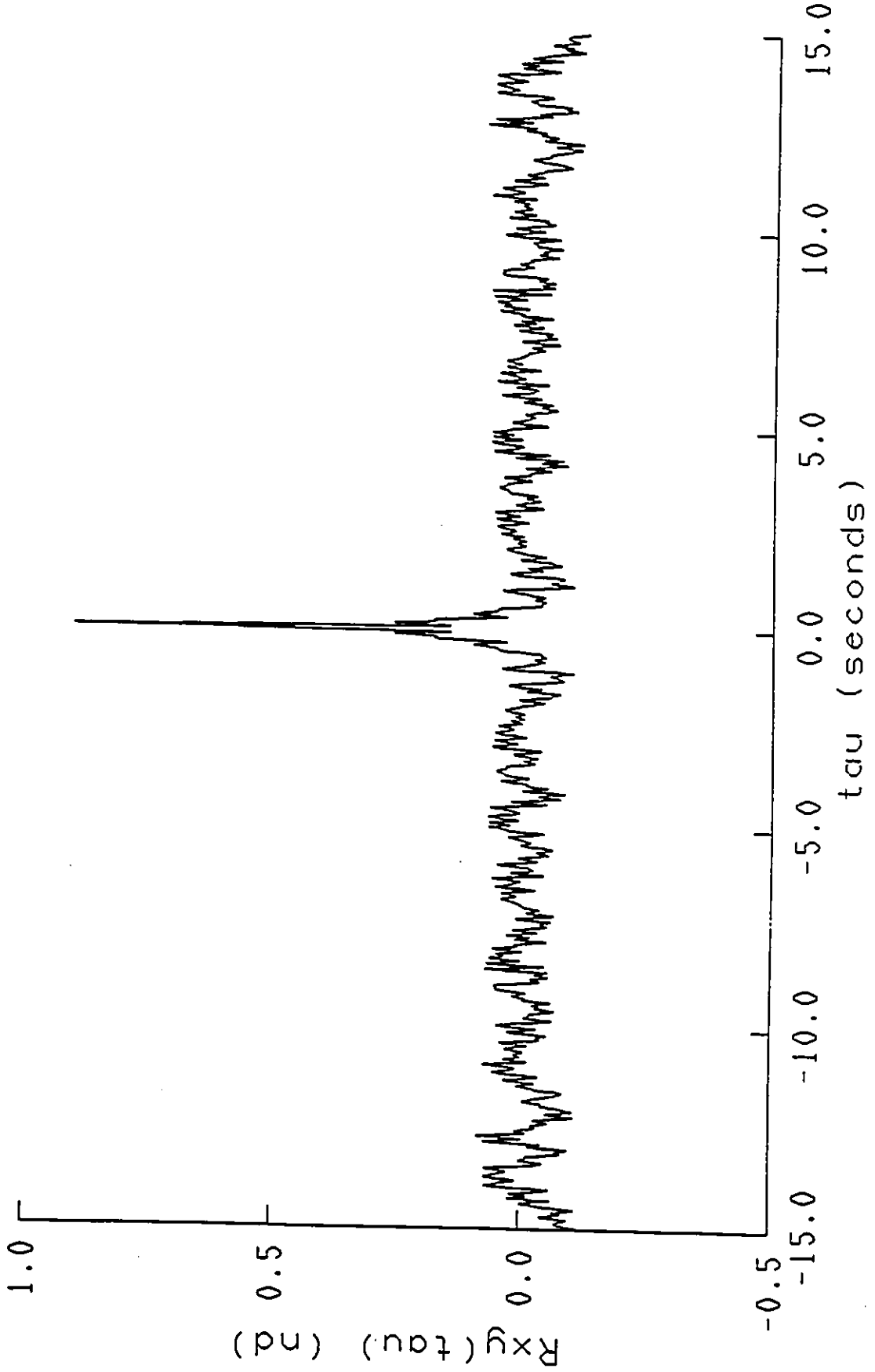


Figure 4-36 The autocorrelation of the force in y direction on the force panel

cforce1-1\_mz.045

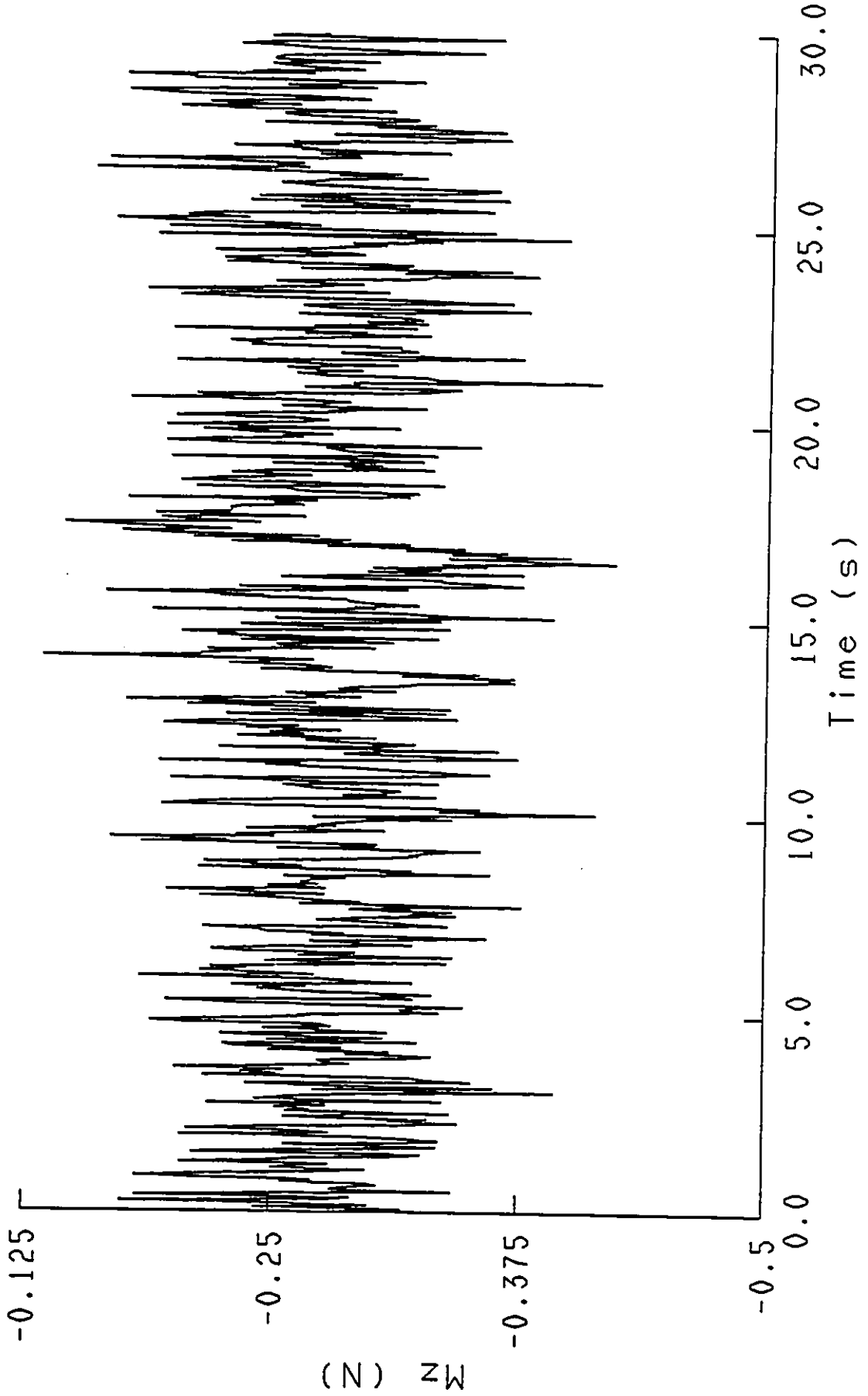


Figure 4-37 A time series record of the momentum on the force panel

cforce1-1\_mz\_spec.045

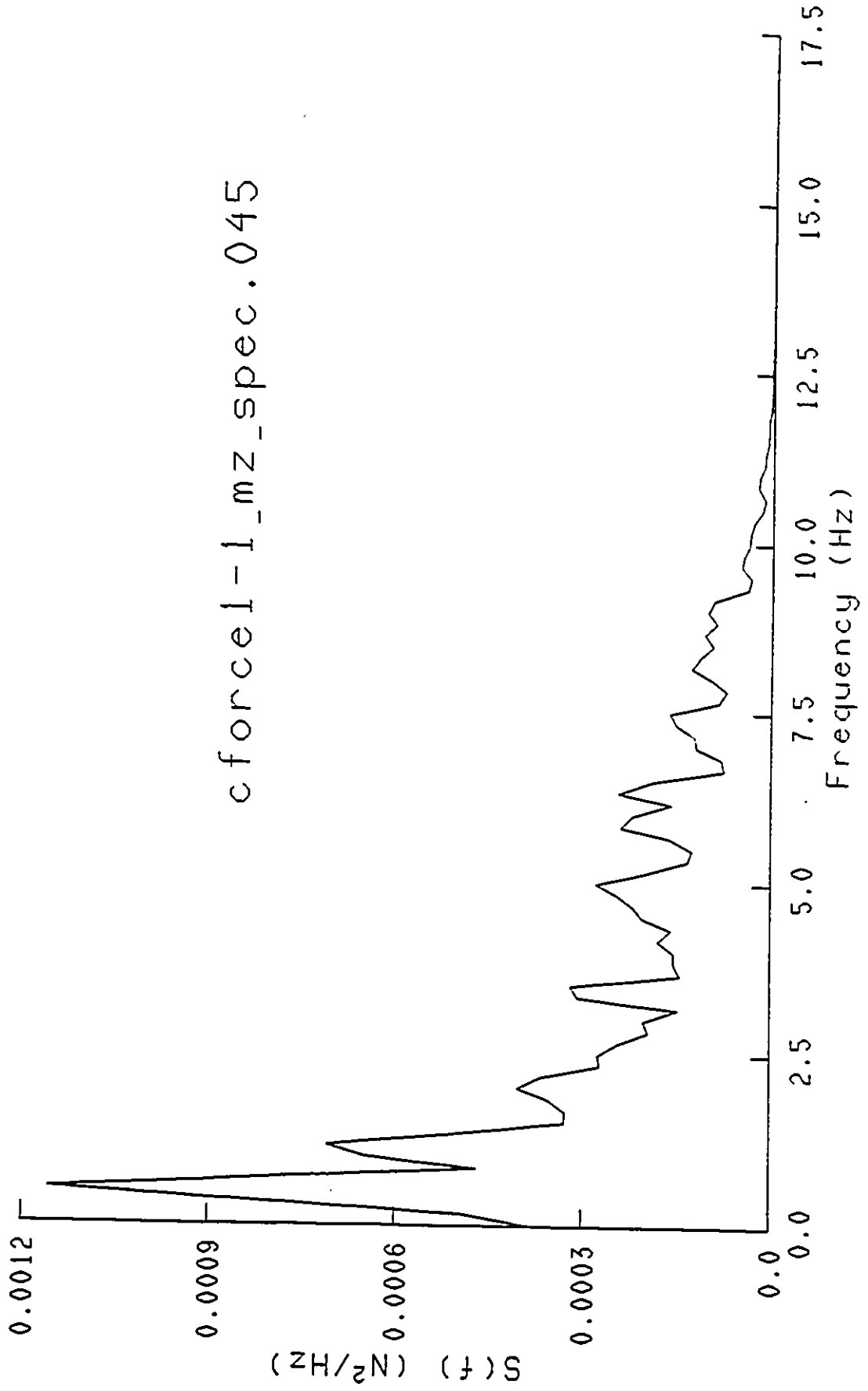


Figure 4-38 The power density function of the momentum on the force panel

cforce1-1\_mz.045

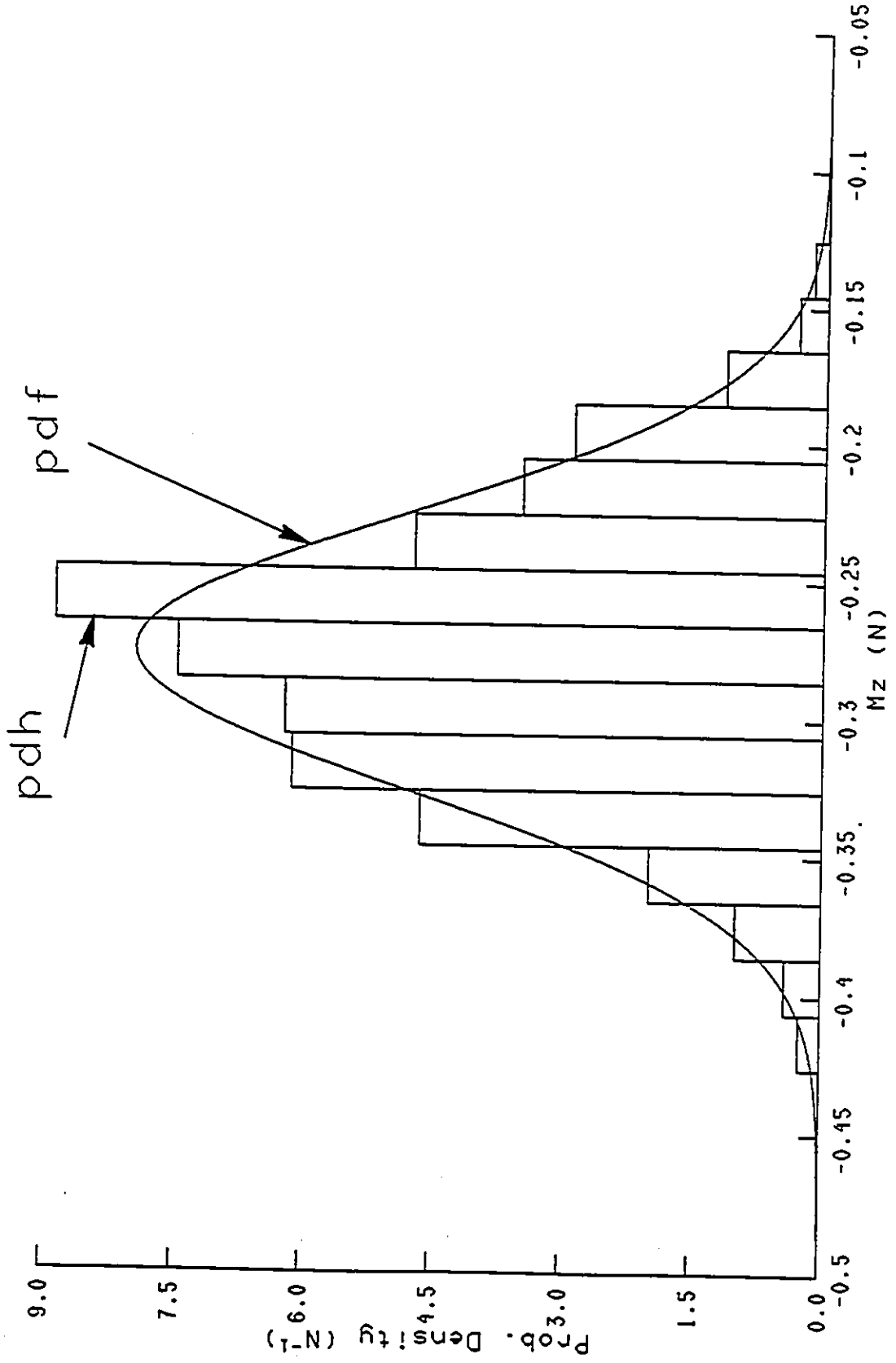


Figure 4-39 The probabilistic distribution of the momentum on the force panel

cforce1-1\_mz\_tr\_aco.045

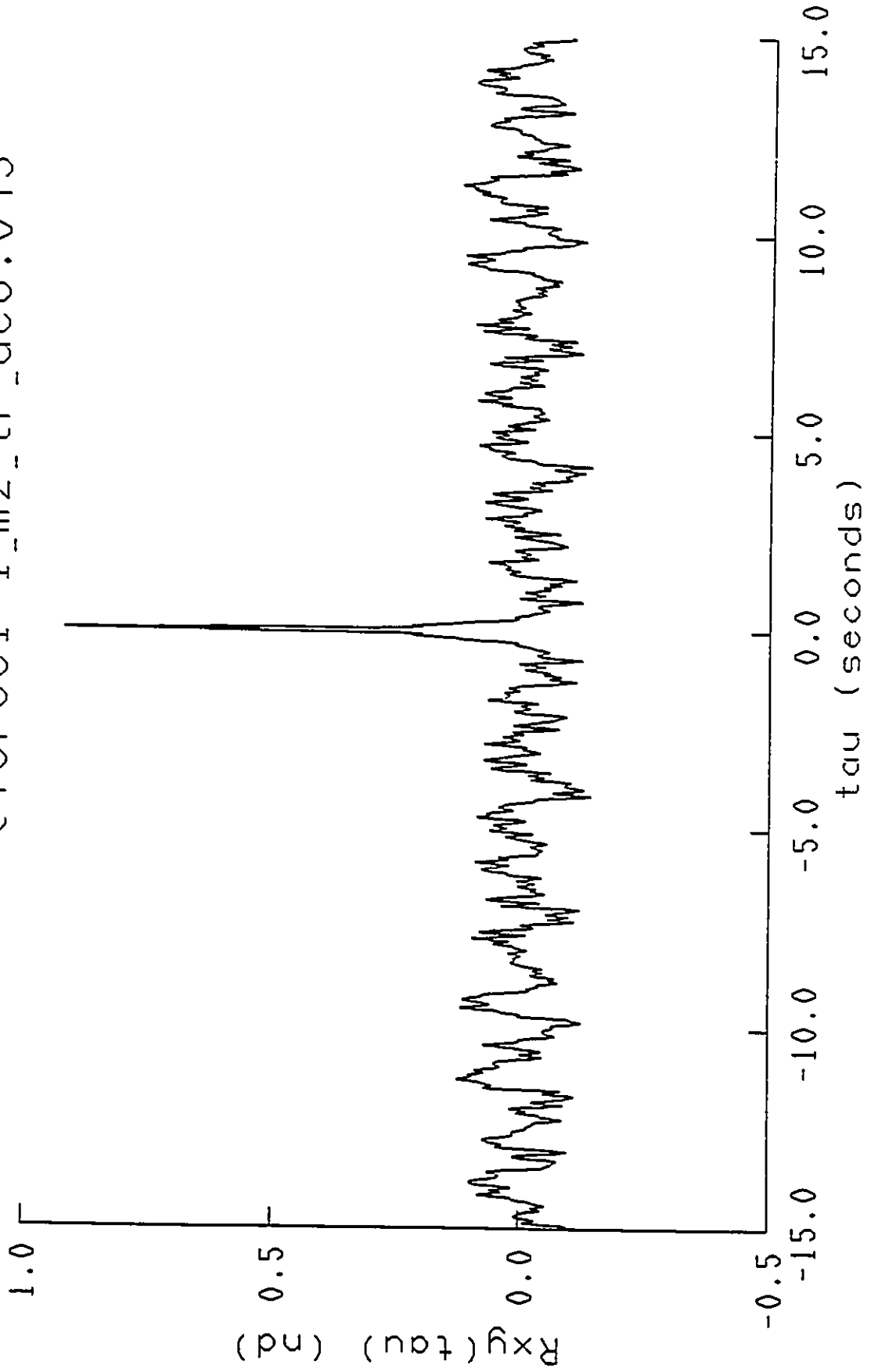


Figure 4-40 The autocorrelation of the momentum on the force pane

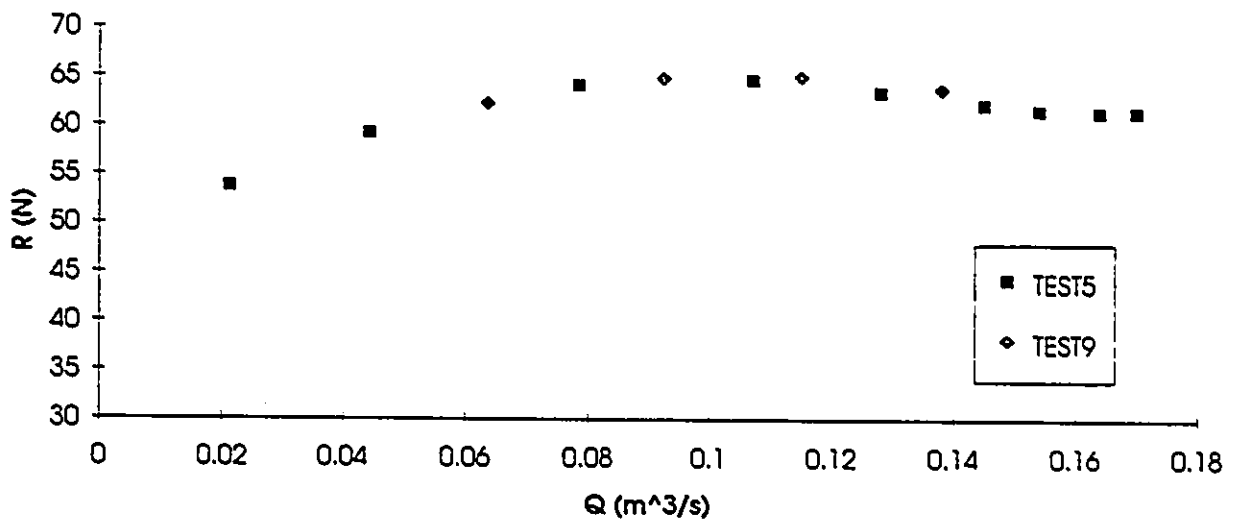


Figure 4-41 Relationship between the resultant force  $R$  and the discharge  $Q$   
(lower panel)

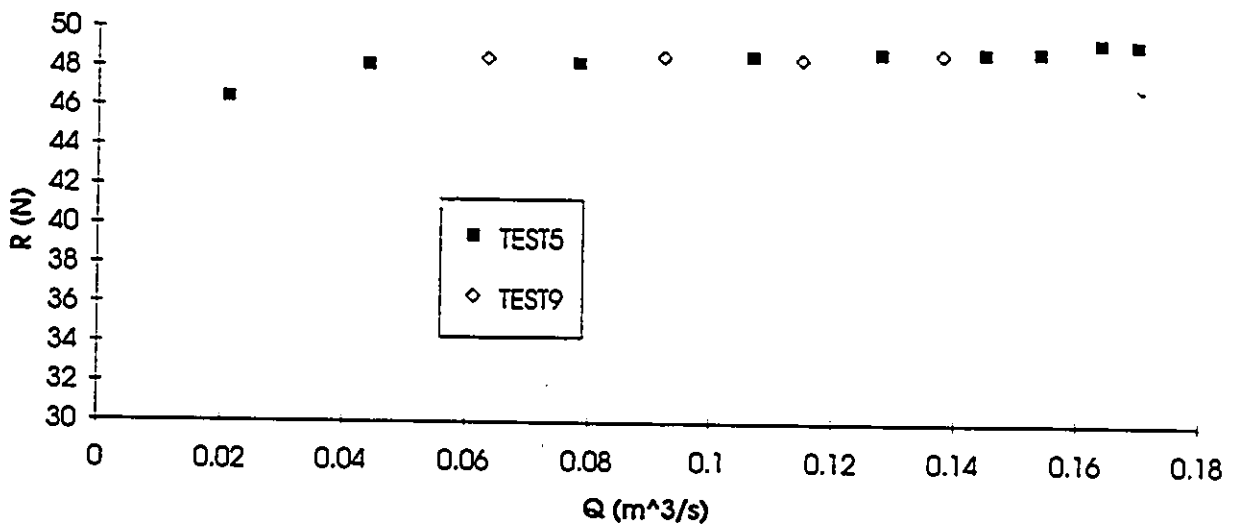


Figure 4-42 Relationship between the resultant force  $R$  and the discharge  $Q$   
(upper panel)

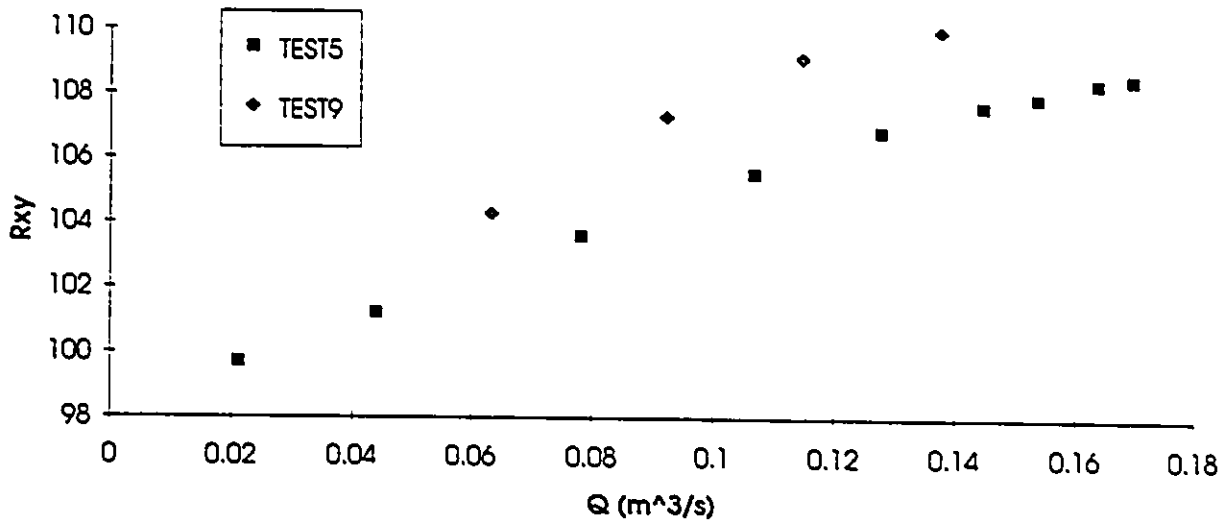


Figure 4-43 Relationship between the angle of the resultant force  $R_{xy}$  and the discharge  $Q$  (lower panel)

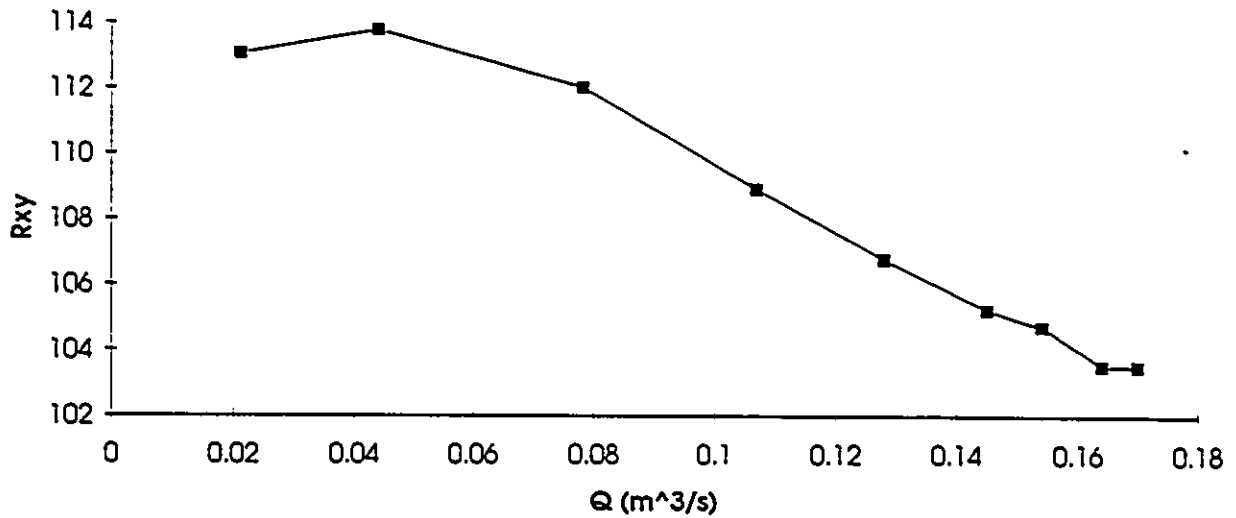


Figure 4-44 Relationship between the angle of the resultant force  $R_{xy}$  and the discharge  $Q$  (upper panel)

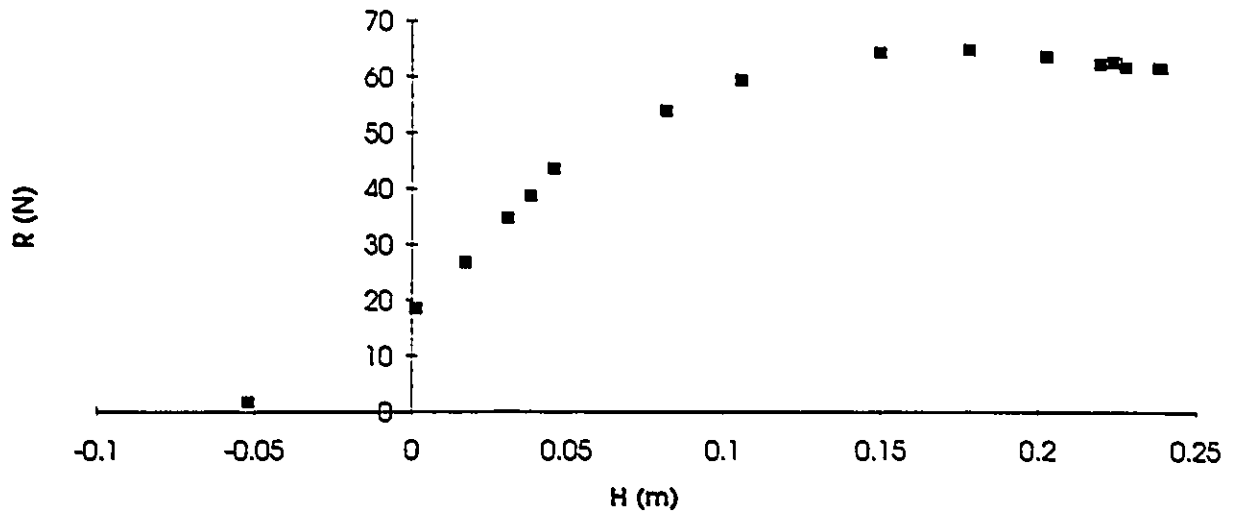


Figure 4-45 Relationship between the resultant force R and the upstream water head H  
(lower panel)

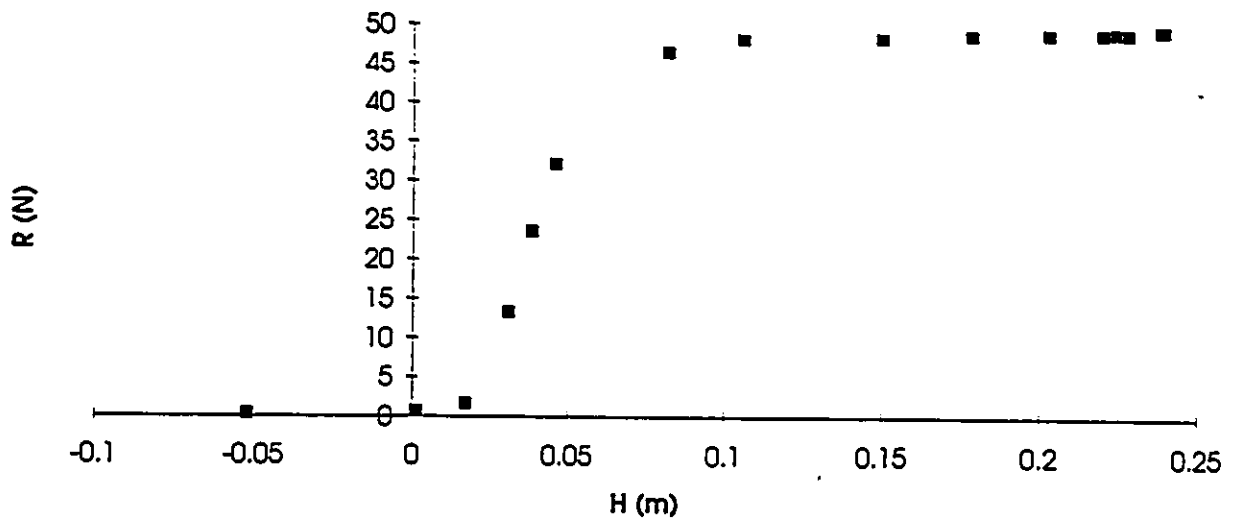


Figure 4-46 Relationship between the resultant force R and the upstream water head H  
(upper panel)

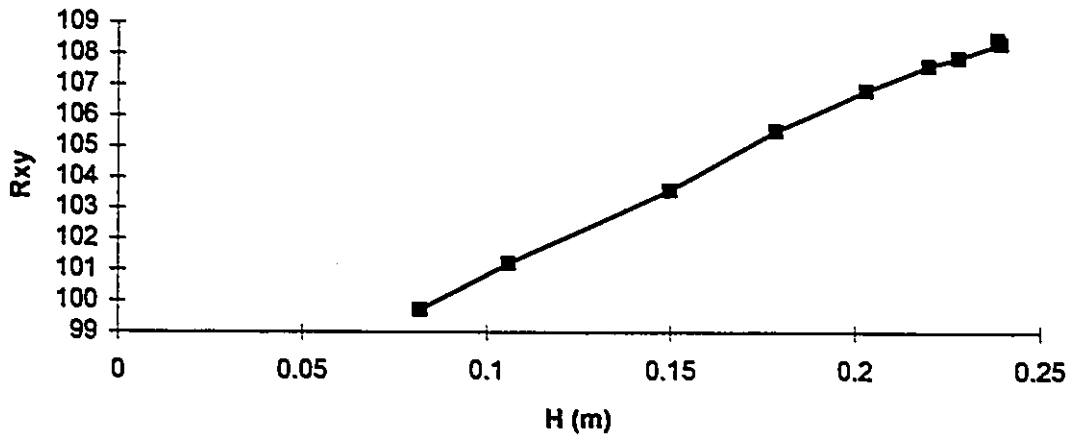


Figure 4-47 Relationship between the angle of the resultant force  $R_{xy}$  and the upstream water head  $H$  (lower panel)

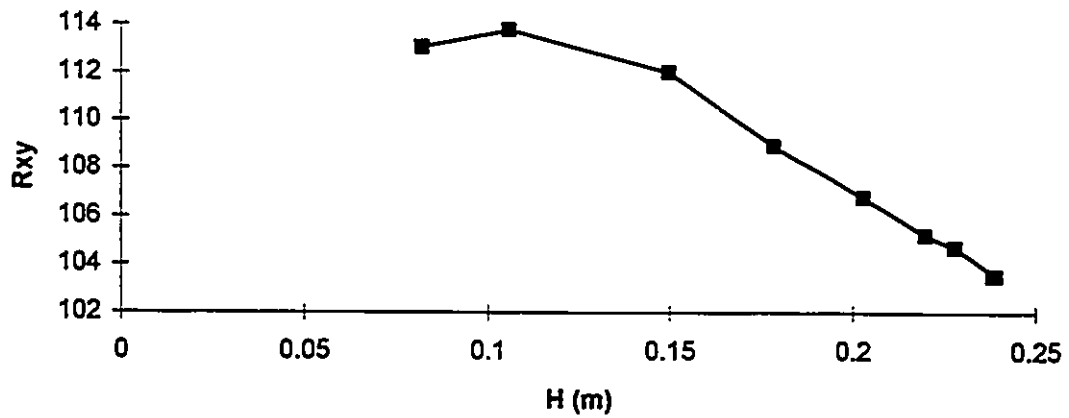


Figure 4-48 Relationship between the angle of the resultant force  $R_{xy}$  and the upstream water head  $H$  (upper panel)

Figure 4-49 Profile of a failed downstream slope (pattern 1)

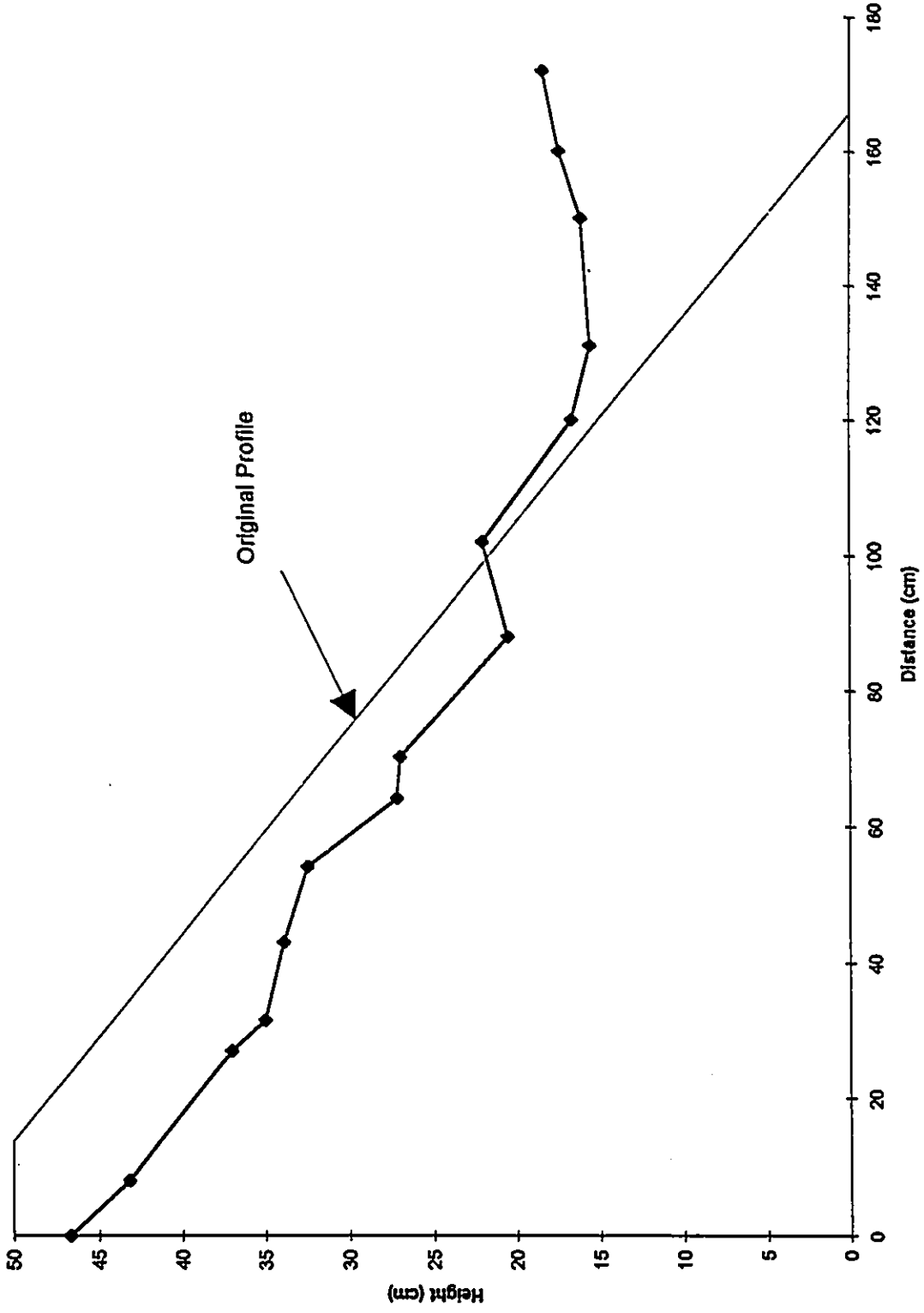
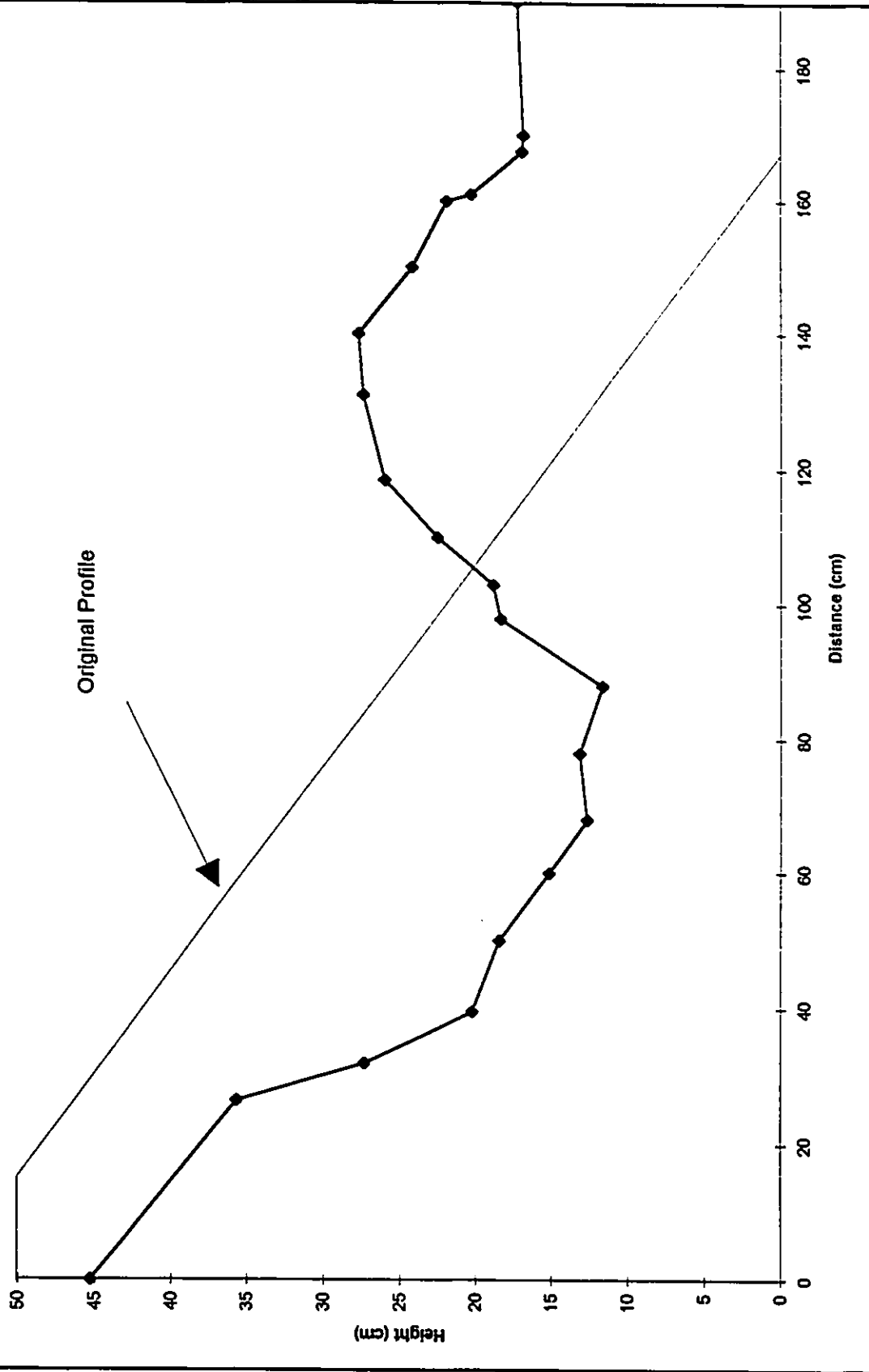
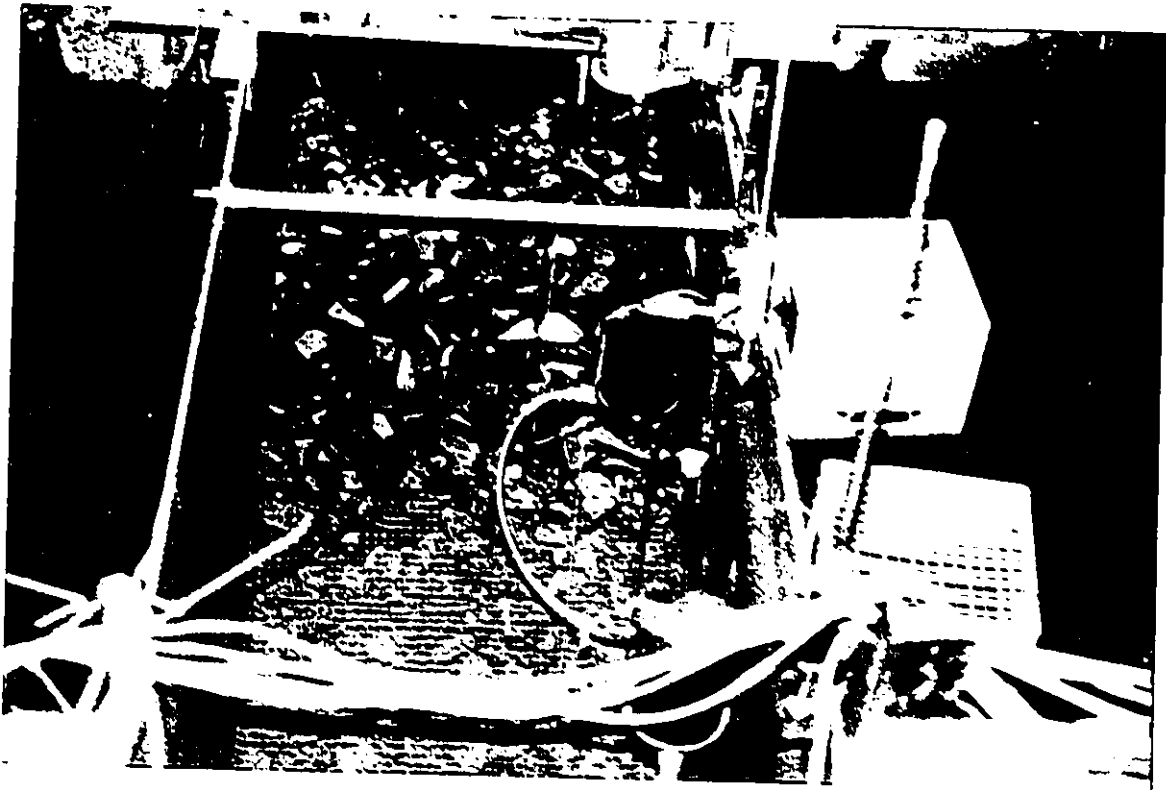


Figure 4-50 Profile of a failed downstream slope (pattern 2)

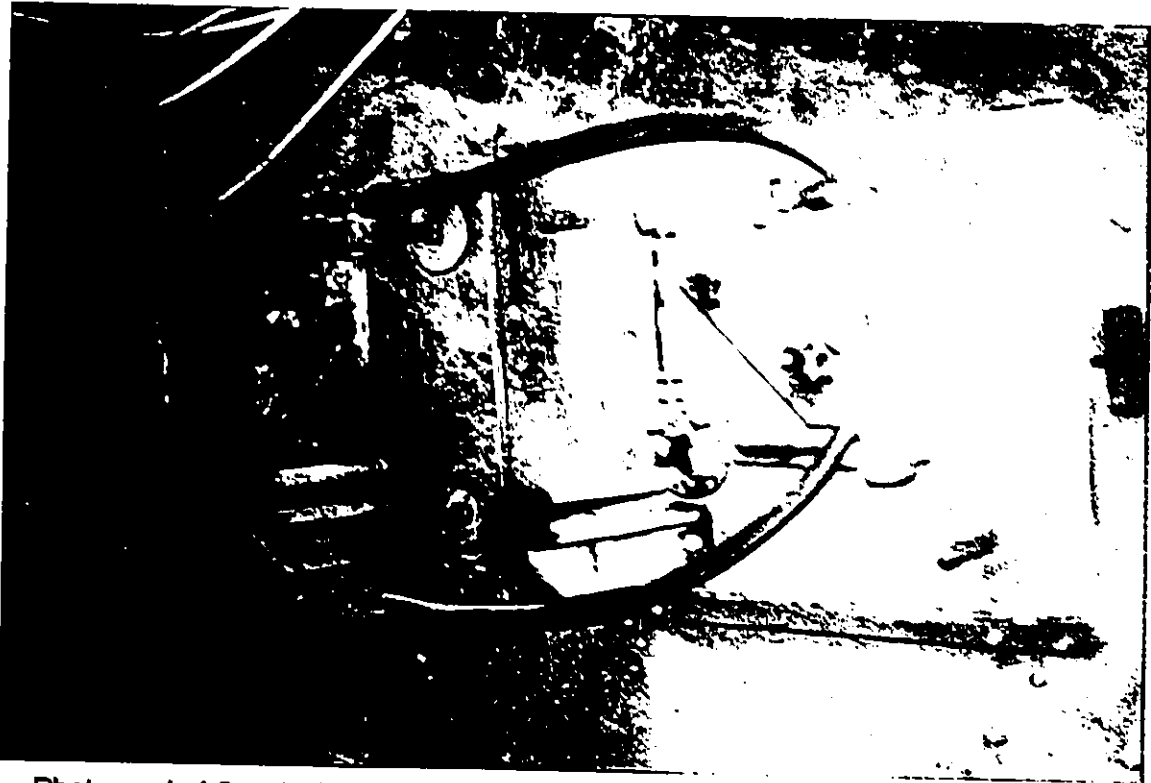




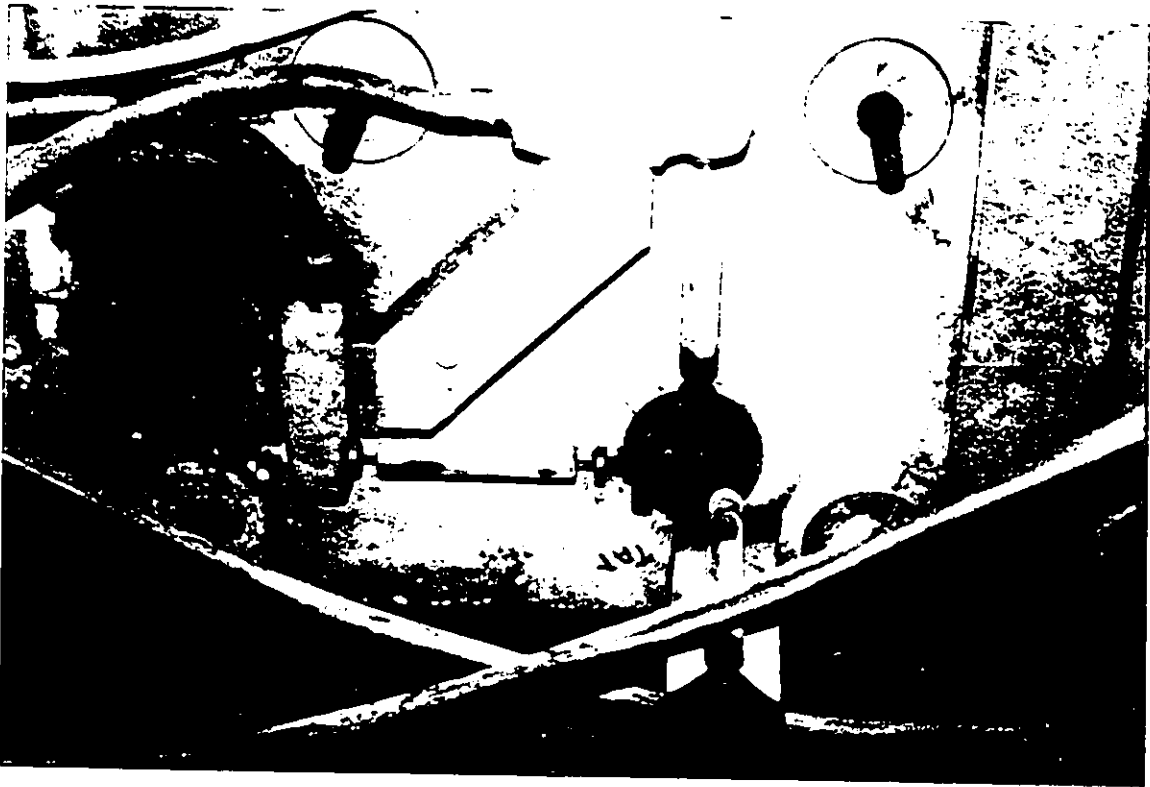
Photograph 4-1 A view of the downstream slope of an overtopped rockfill dam



Photograph 4-2 A view of an overtopped rockfil dam in NRC Hydraulics Laboratory



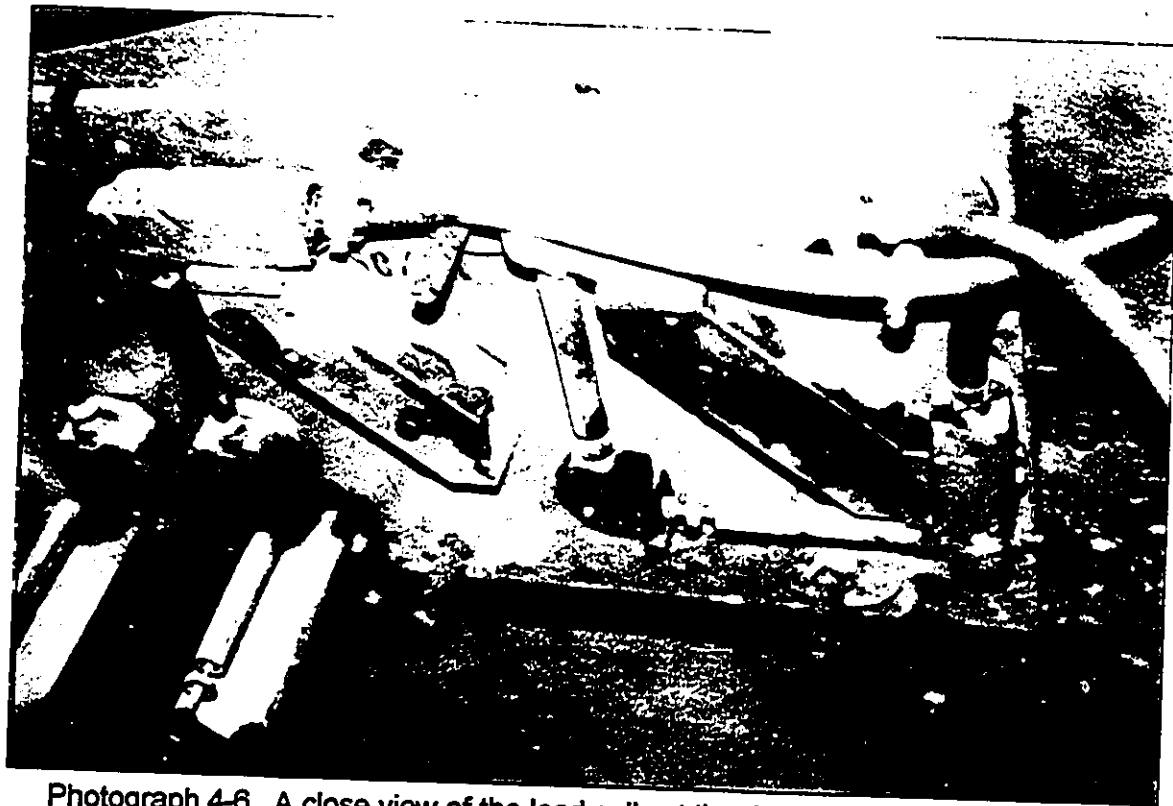
Photograph 4-3 A view of the load cells at the left side of the model



Photograph 4-4 A close view of the load cells at the left side of the model



Photograph 4-5 A view of the load cells at the right side of the model



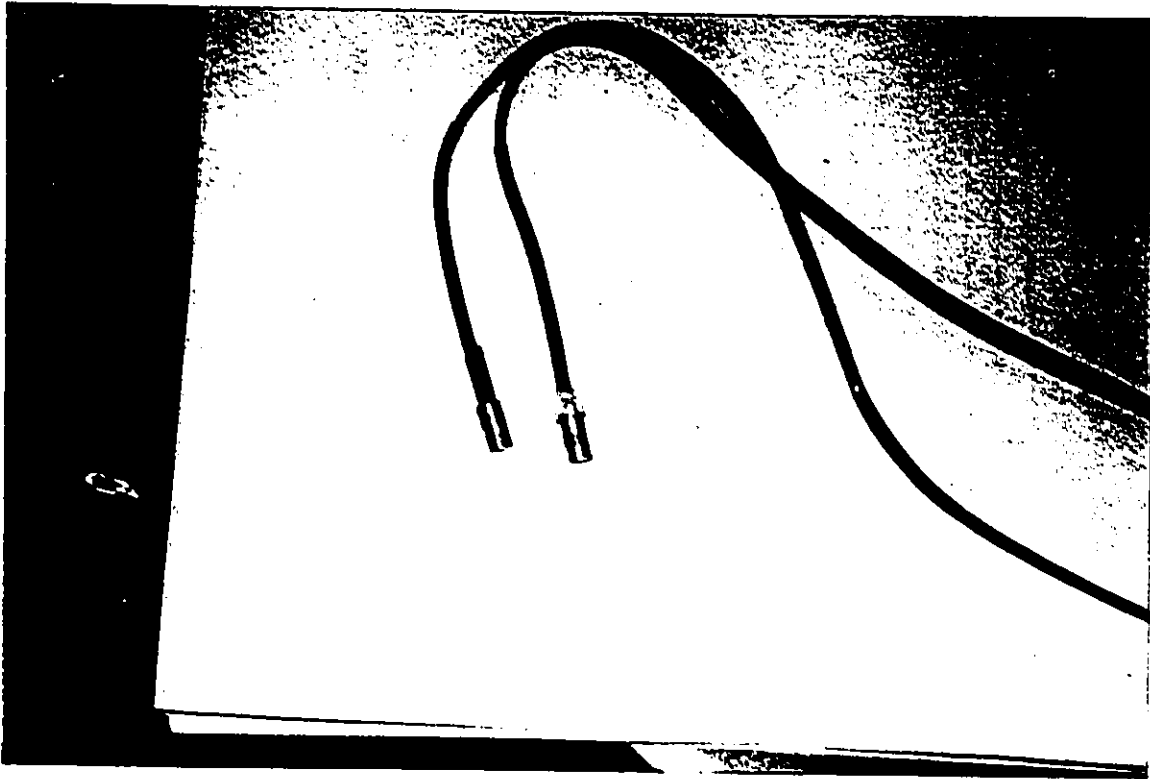
Photograph 4-6 A close view of the load cells at the right side of the model



Photograph 4-7 A view of the wave probe in the model



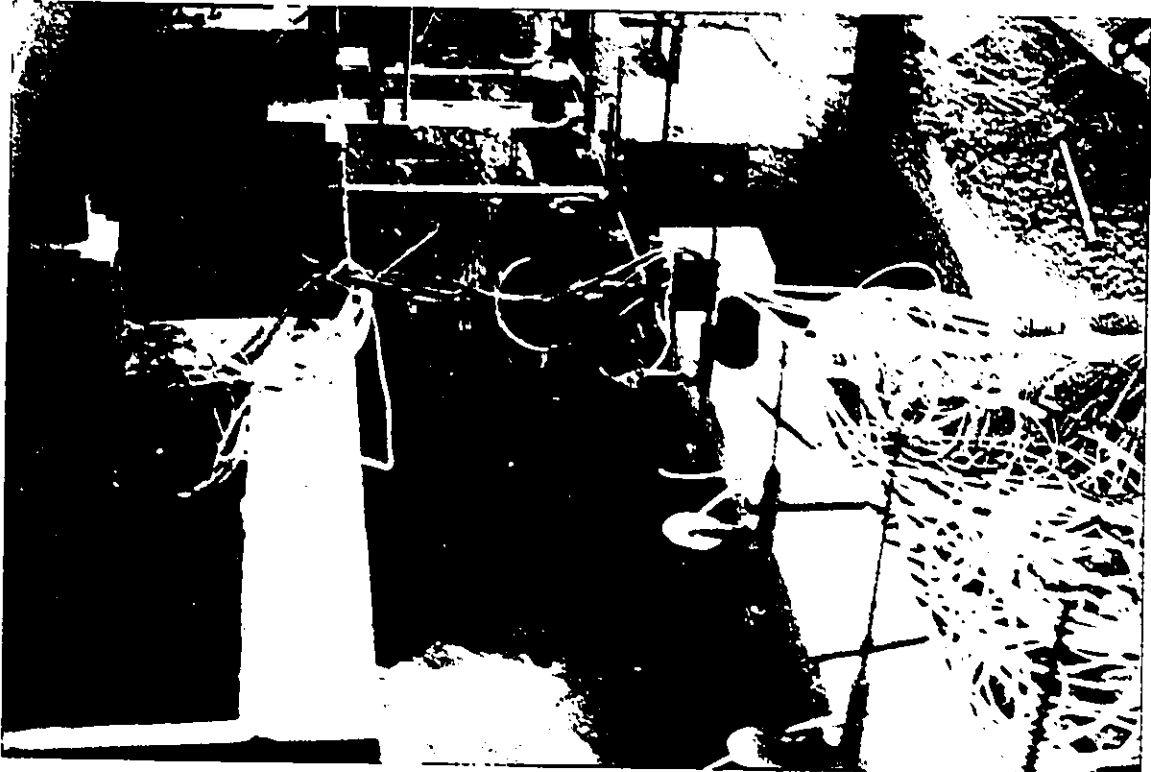
Photograph 4-8 A view of the velocity meters at the downstream slope



Photograph 4-9 A view of the pressure gauges used in the model



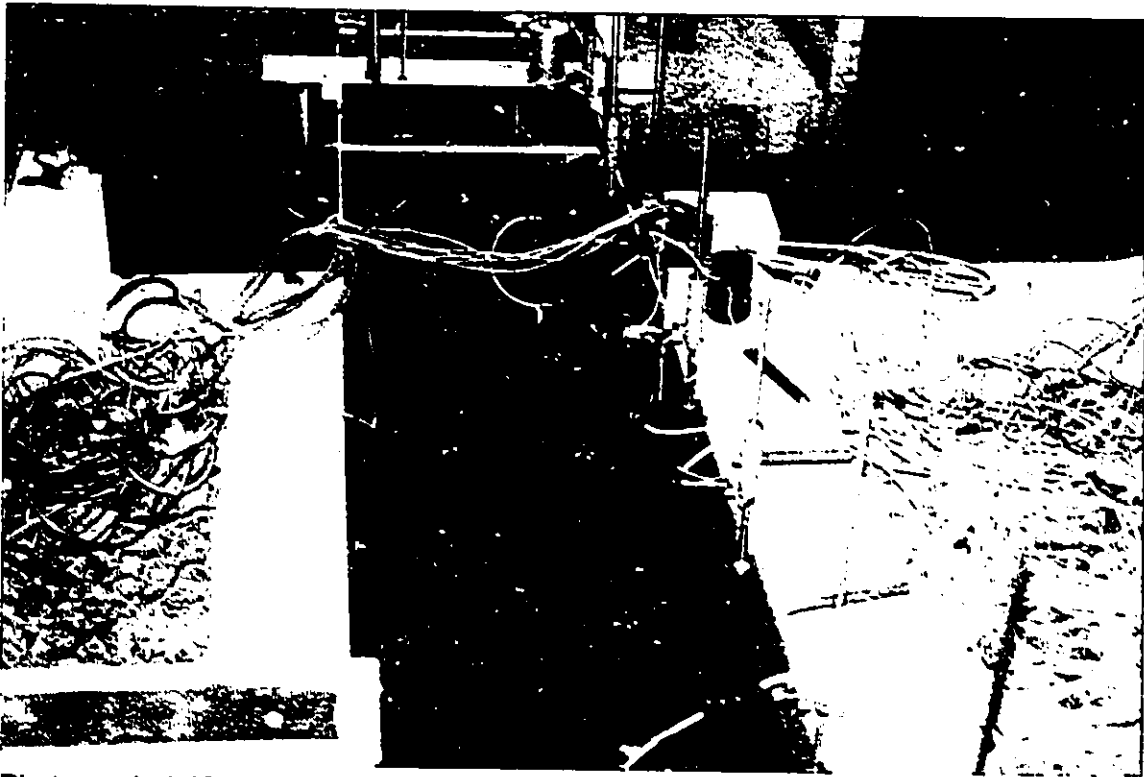
Photograph 4-10 Installation of the pressure gauges in the force panel



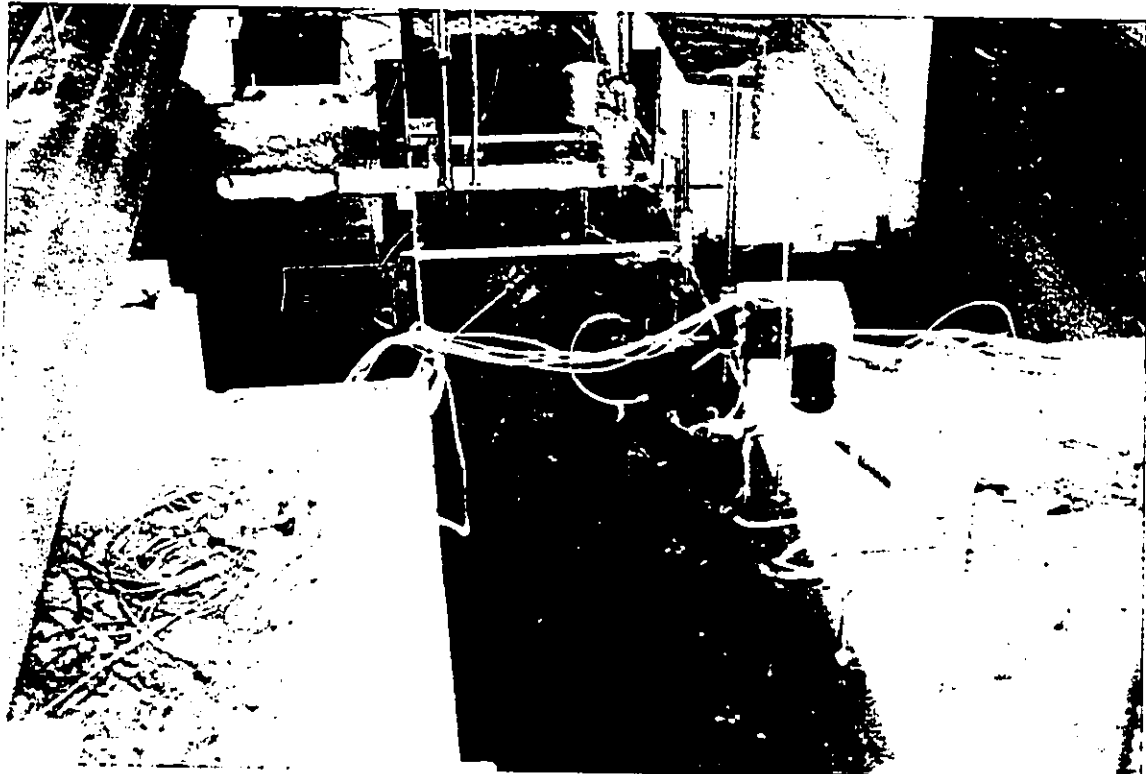
Photograph 4-11 A view of the jump at the toe of an overtopped rockfill dam



Photograph 4-12 A view of the wave at the slope of an overtopped rockfill dam



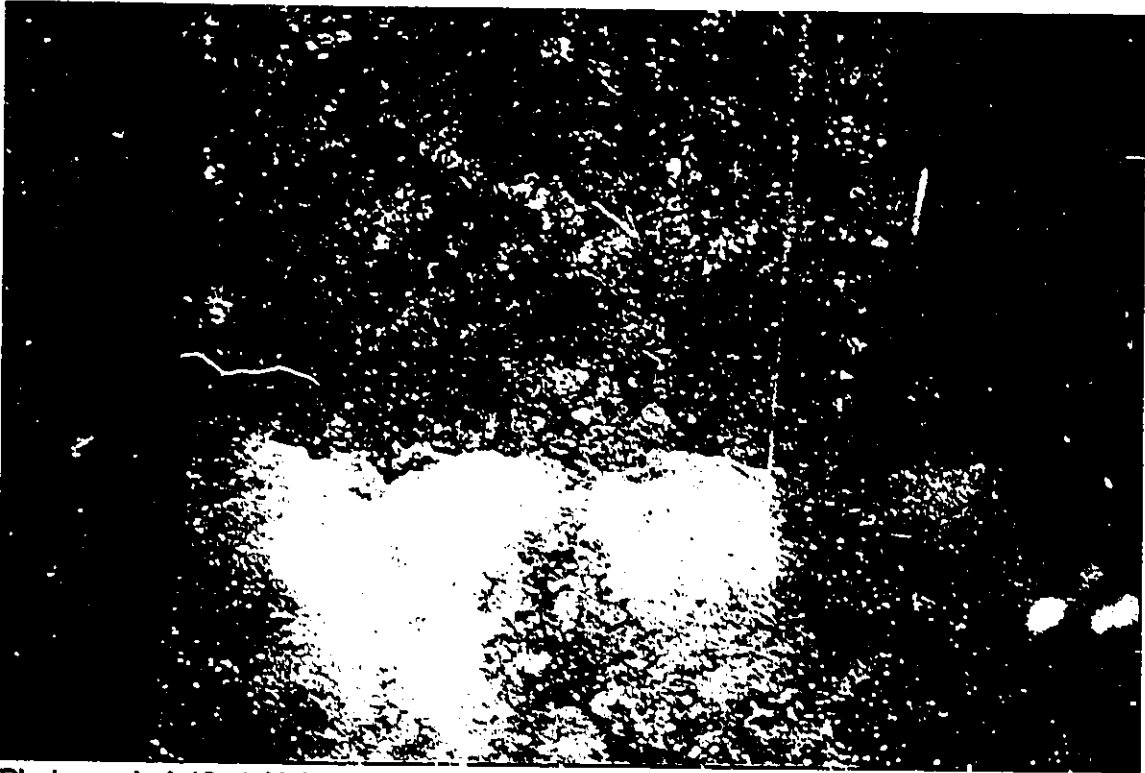
Photograph 4-13 A view of the weak wave at the slope of an overtopped rockfill dam



Photograph 4-14 A view of the submerged downstream slope of an overtopped rockfill dam



Photograph 4-15 Flow over and through the downstream slope of an overtopped rockfill dam before initial failure



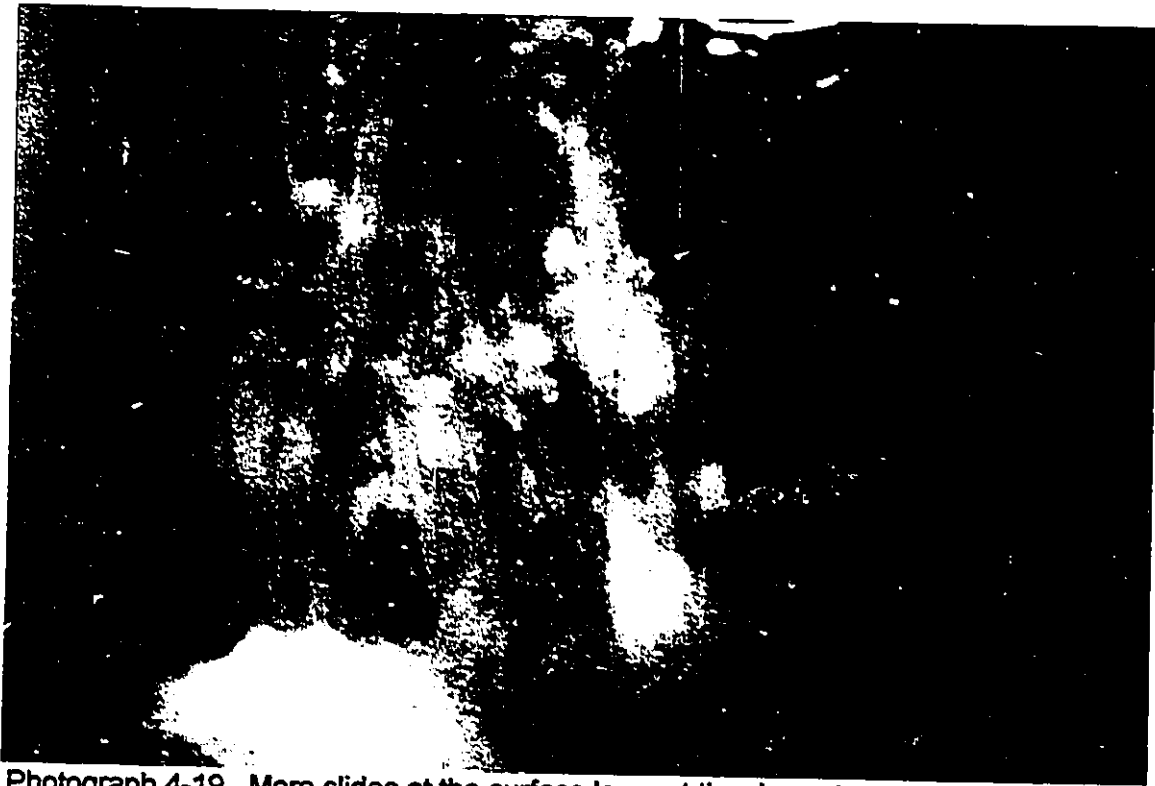
Photograph 4-16 Initial movement of individual particles at the downstream slope of an overtopped rockfill dam (the colour of the second layer of particles are yellow)



Photograph 4-17 More rock particles move at the downstream slope



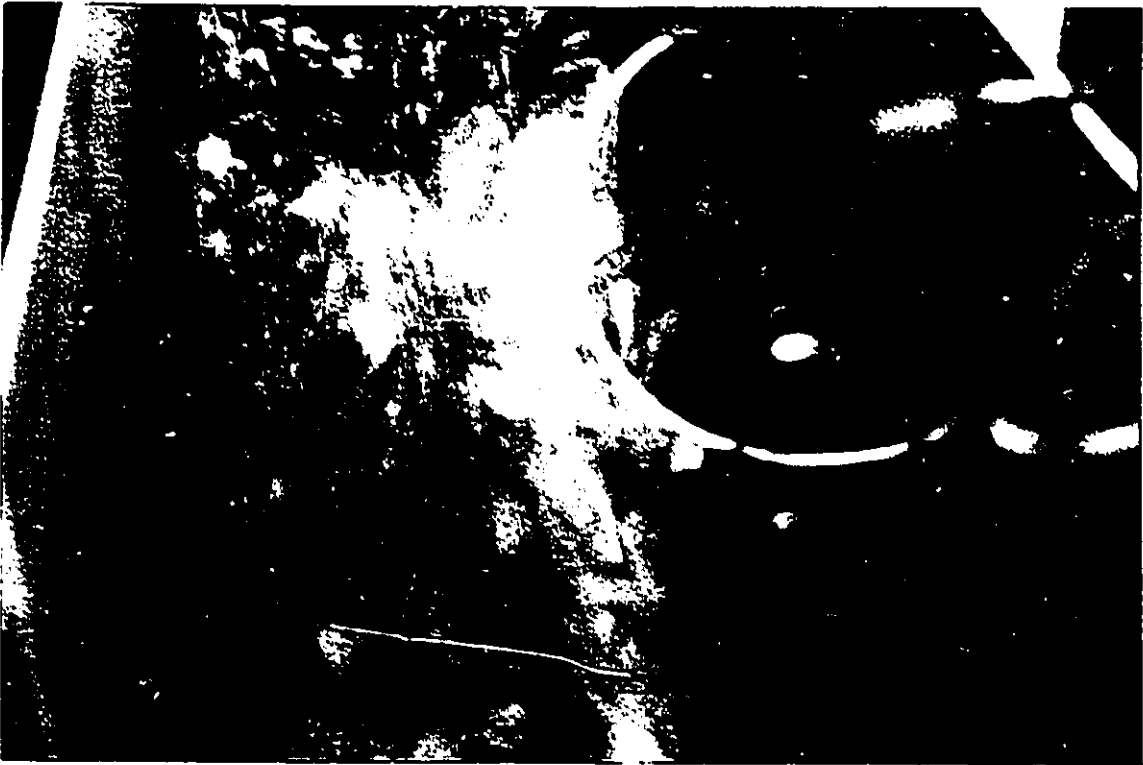
Photograph 4-18 The surface layer of particles near the toe at the downstream slope of an overtopped rockfill dam slid down



Photograph 4-19 More slides at the surface layer at the downstream slope of an overtopped rockfill dam caused rough water surface



Photograph 4-20 The total rock mass near the toe at the downstream slope of an overtopped rockfill dam slid down



Photograph 4-21 Rock particles at the upper part of the downstream slope of an overtopped rockfill dam slid down



Photograph 4-22 The second layer of particles at the downstream slope of an overtopped rockfill dam slid down



**Photograph 4-23** The rock mass at the upper part of the downstream slope of an overtopped rockfill dam slid down



**Photograph 4-24** The downstream slope of an overtopped rockfill dam slid at one side and flow concentrated on the same side

## Chapter 5 Non-Darcy Law in Rockfill

Based on pipe theory and Taylor's (1948) definition for mean hydraulics radius in rockfill material, theoretical relationships between friction coefficient and Reynolds number, and relationships between hydraulic gradient and bulk seepage velocity have been obtained. The new relationships between hydraulic gradient and this velocity are then compared to the various formulae for rockfill available in the literature, and by computer simulation. A comparison between the data from the flowthrough and ovetopped and the results obtained from available formulae will be presented. The chapter also finds guidelines for the selection of hydraulic mean radius for rockfill, and on the selection of the most appropriate theoretical expression for non-Darcy seepage flow.

### 5.1 Introduction

Rockfill has been widely used in dams, embankments, river reaches, riprap and breakwaters in coastal engineering. In flowthrough rockfill dams, the quantity of seepage flow is substantial when compared to that in a conventional earth dam. Also, in the former, the seepage forces on the rock particles are quite different from those acting in materials where Darcy law applies. The flow net for the flow in rockfill structures changes with Reynolds number. To determine the seepage discharge, seepage force, and flow net in a rockfill structure, it is important to use a reliable non-Darcy relationship, since the flow within a rockfill dam is usually turbulent. A knowledge of the relationship between the velocities and hydraulic gradients is essential for engineering design of flowthrough and overflow structures.

Two laws can describe the relationship between the hydraulic gradient and the bulk velocity for the non-Darcy seepage flow in rockfill (non-Darcy flow). One is the quadratic law which was suggested by Forchheimer (1901):

$$i = rV + sV^2 \quad (5-1)$$

where  $r$  and  $s$  are constants which depend on the characteristics of rockfill material,  $i$  is the hydraulic gradient, and  $V$  is the bulk velocity.

The other is the power relationship which may have originated from Prony in 1804 as reported by Jaeger (1956):

$$i = c_0 V^{c_1} \quad (5-2)$$

where  $c_0$  and  $c_1$  depend on the flow condition, the characteristics of the porous media and the fluid.

Both the quadratic and the power relationships are based on experimental results although researchers have provided some theoretical basis for them (Ven Gent, 1991). Presently both formulae are well accepted, and almost all studies on the basic law of the seepage flow in rockfill are concentrated on the determination of the coefficients  $r$  and  $s$ , or  $c_0$  and  $c_1$ .

In some formulae available in the literature (Ergun, 1952; Wilkins, 1956; McCorquodale, 1978; Stephenson, 1979; Li and Hu, 1988; Martins, 1990), the coefficients in the seepage law depend on the physical parameters of rockfill material only (e.g., the size of particles, the porosity, and the shape of particles). In other formulae (Slepicka, 1961; Ward, 1964), the coefficients can not be determined by these parameters alone and experimental determination of hydraulic conductivity is required. Since it is usually expensive to conduct prototype experiments, it is of practical interest to determine the necessary coefficients applicable to non-Darcy seepage flow in terms of the readily determined parameters of rockfill material. Various authors have considered different physical parameters of the porous media, and have conducted experiments with certain size, shape, and type of particles. It should be emphasized that each formula may apply only to a certain range of physical parameters. Therefore, a relationship for non-Darcy flow which is based on large amount of experimental data over a wide range of rockfill parameters (e.g., size, porosity) will be useful in engineering practice. Hence,

this chapter develops a general relationship for seepage flow in rockfill, and compares it with other presently commonly-used formulations.

In engineering design, it is important to determine the mean hydraulic radius  $R$  of rockfill material and the most appropriate formula to a specific problem. For the first aspect, some studies have been reported in the literature, e.g., Wilkins (1956), Leps (1973), Parkins (1991), and Garga (1992).

## 5.2 General Seepage Law

The relationship between hydraulic gradient and bulk velocity may be obtained from the friction law, that is, from the relationship between friction coefficient and Reynolds number.

(1) A new relationship based on the theory of pipe flow

The flow in the pores of rock particles can be regarded as being essentially similar to flow in a pipe network, but with more complicated configuration (Fig. 5 - 1). This analogy provides a convenient tool to analyze flow through rockfill material.

The hydraulic mean radius is a measure of the diameter of an average pore within a porous media. Taylor (1948) defined the hydraulic mean radius,  $R$ , as:

$$R = \frac{V_v}{S_A} \quad (5-3)$$

where:

$v_v$  = volume of voids within a control volume containing rockfill;

$S_A$  = surface area of voids with total volume  $v_v$ .

The value of  $R$  can also be calculated from:

$$R = \frac{V_b n}{A_{MS} M_R} \quad (5-4)$$

or

$$R = \frac{e}{A_{VS}} \quad (5-5)$$

where:  $V_b$  = control volume (bulk volume), containing porous media;  $n$  = porosity;  $e$  = void ratio;  $A_{MS}$  = mass-specific surface area, i.e. the surface area per unit rock mass;  $A_{VS}$  = volume-specific surface area, i.e. the surface area per unit volume of rock;  $M_R$  = mass of rock.

The mass-specific and volume - specific surface areas are related by:

$$A_{VS} = \rho A_{MS} \quad (5-6)$$

where  $\rho$  is the density of rock.

For a porous medium made up of perfect spheres (Taylor, 1948):

$$A_{VS} = \frac{\pi d^2}{\frac{1}{6} \pi d^3} = \frac{6}{d} \quad (5-7)$$

Hence:

$$R = \frac{e d}{6} \quad (5-8)$$

The sphere is the geometric shape which has the least surface area per unit volume. Highly angular rocks with many sharp and jutting edges are relatively inefficient with respect to surface area per unit volume and will have higher values of  $A_{VS}$ . Note that equation (5-5) does not apply to porous media made up of plate-like rock particles because a significant amount of particle area is lost in inter-particle contact. When the amount of interparticle contact is large, the assumption that the surface area of the voids is equal to the surface area of the rocks is not valid. Such special cases are not considered in this study.

The volume-specific surface area may be expressed by

$$A_{VS} = \frac{J}{d} \quad (5-9)$$

where  $J$  is a constant. For spheres,  $J=6$ . The value of  $J$  represents the degree of surface area efficiency of the particle. The shape factor, which also indicates relative surface area efficiency,  $r_E$ , can be stated as (Hansen, 1992):

$$r_E = \frac{J_{\text{ROCK}}}{J_{\text{SPHERE}}} = \frac{J_{\text{ROCK}}}{6} \quad (5-10)$$

So that:

$$A_{\text{VS}} = \frac{6r_E}{d} \quad (5-11)$$

and:

$$R = \frac{e d}{6 r_E} \quad (5-12)$$

where:

R = hydraulic radius;

e = void ratio;

d = diameter of a rock particle;

$r_E$  = shape factor.

From hydraulics of pipe flow, the head loss is given by:

$$h_f = f \frac{L V_p^2}{4R 2g} \quad (5-13)$$

where

$h_f$  = head loss of energy over a distance L along the pipe;

f = friction coefficient in pipe flow;

$V_p$  = average velocity of the pipe flow;

R = hydraulic radius;

L = a distance in the pipe along the flow direction;

g = gravity acceleration.

Rearranging Eq. (5-13):

$$f = \frac{h_f 8gR}{L V_p^2} \quad (5-14)$$

Define the hydraulic gradient i as:

$$i = \frac{h_f}{L} \quad (5-15)$$

In seepage flow,  $V_p$  is the void velocity in the porous media which can be defined as:

$$V_p = \frac{V}{n} \quad (5-16)$$

where:

$n$  = porosity of the porous media;

$V$  = bulk velocity in porous media.

Substituting Eqs. (5-12), (5-15), and (5-16) in Eq. (5-14):

$$f = \frac{8 g i R n^2}{V^2} = \frac{4 c i d g n^2}{3 r_E V^2} \quad (5-17)$$

Reynolds number  $R_e$  can be defined as:

$$R_e = \frac{V_p R}{\nu} = \frac{V R}{\nu n} \quad (5-18)$$

where  $\nu$  = the kinematic viscosity of fluid.

It is noted that

$$e = \frac{n}{1-n} \quad (5-19)$$

Substituting Eqs. (5-12), (5-16), and (5-19) in (5-18):

$$R_e = \frac{e V d}{6 \nu n r_E} = \frac{V d}{6 \nu (1-n) r_E} \quad (5-20)$$

Substituting Eq. (5-19) in (5-17):

$$f = \frac{4 i d g n^3}{3 r_E V^2 (1-n)} \quad (5-21)$$

In this study, the data from the University of Ottawa and Nanjing Hydraulic Research Institute has been used to derive the relationship between  $R_e$  and  $f$  defined by Eqs. (5-20) and (5-21). Figure 5-2 shows the results calculated from the test data from 300 mm diameter column tests on rockfill materials obtained at the University of Ottawa

(Hansen, 1992). In these experiments, the mean particle diameter varied between 1.6 cm to 4 cm.

(a) Relationship in quadratic form

The data in Fig. 5 - 2 may be expressed as:

$$f = \frac{98}{Re} + 3 \quad (5-22)$$

In general, the curve has the following form:

$$f = \frac{a}{Re} + b \quad (5-23)$$

Here, from the data available, a=98, b=3. The fitted curve is shown in Fig. 5 - 2.

From Eqs. (5-17), (5-18), and (5-23):

$$i = \frac{a v}{8 g R^2 n} V + \frac{b}{8 g R n^2} V^2 \quad (5-24)$$

From Eqs. (5-20), (5-21), and (5-23):

$$i = \frac{4.5 a v r_E^2 (1-n)^2}{d^2 g n^3} V + \frac{0.75 b r_E (1-n)}{d g n^3} V^2 \quad (5-25)$$

Equations (5-24) and (5-25) produce a general relationship in quadratic form which is applicable to all ranges of seepage flow. These equations have been derived based on sound theoretical considerations. The use of these general expressions in practice requires a database in order that the coefficients a and b may be evaluated.

If the values of a=98, b=3 are inserted in Eqs. (5-24), and (5-25), the following relationships may be derived respectively:

$$i = \frac{12 v}{R^2 g n} V + \frac{0.38}{R g n^2} V^2 \quad (5-26)$$

and

$$i = \frac{441 \nu r_E^2 (1-n)^2}{d^2 g n^3} V + \frac{2.3 r_E (1-n)}{d g n^3} V^2 \quad (5-27)$$

(b) Relationship in power form

The fitted curve in power form is:

$$f = 8.75 \text{Re}^{-0.17} \quad (5-28)$$

The general power form is:

$$f = C \text{Re}^N \quad (5-29)$$

Hence  $C=8.75$ ,  $N=0.17$ .

If only the fully turbulent flow is of interest ( $\text{Re} \geq 200$ ),  $N=0$ , and  $C=3.15$ , friction coefficient  $f$  is independent of Reynolds number and:

$$f = 3.15 \quad (5-30)$$

From (5-17), (5-18), and (5-29):

$$i = \frac{C}{8gR^{1+N} n^{2+N} \nu^N} V^{2+N} \quad (5-31)$$

From Eqs. (5-20), (5-21), (5-29), it is derived:

$$i = \frac{3C (1-n)^{1+N} r_E^{1+N}}{4 (6\nu)^N d^{1+N} g n^3} V^{2+N} \quad (5-32)$$

Equations (5-31) and (5-32) produce a general relationship in power form which are applicable to all ranges of seepage flow. Again a database is required to evaluate the parameters  $C$  and  $N$  for use of these expressions in practice.

Substituting the values of  $C=8.75$ , and  $N=0.17$  in Eqs. (5-31) and (5-32):

$$i = \frac{1.1 \nu^{0.17} V^{1.83}}{gR^{1.17} n^{1.83}} \quad (5-33)$$

$$i = \frac{8.9 \nu^{0.17} (1-n)^{1.17} r_E^{1.17}}{d^{1.17} g n^3} V^{1.83} \quad (5-34)$$

For fully turbulent flow,  $Re \geq 200$ ,  $N=0$ ,  $C=3.15$ . The relationship between bulk velocity  $V$  and hydraulic gradient  $i$  is obtained from Eq. (5-32):

$$i = \frac{CV^2}{8gRn^2} \quad (5-35)$$

Substituting  $C=3.15$  in Eq. (5-35):

$$i = \frac{0.4V^2}{gRn^2} \quad (5-36)$$

## (2) Relationship based on Stephenson's definition

Stephenson(1979) has used considerable compiled data in his definition of friction coefficient and Reynolds number. This compilation can further be enhanced by adding the data from Hu and Li (1988), and from the University of Ottawa (Hansen, Garga, and Townsend, 1992) to produce Fig. 5 - 3, covering a wide range of values of  $Re$ . It should be noted that Stephenson's compilation includes data by Dudgeon (1966), Leps (1973), Volker(1969), Cedergren(1977), and Stephenson (1978).

Stephenson expressed the Reynolds number:

$$Re_{stephenson} = \frac{V d}{n \nu} \quad (5-37)$$

and the friction coefficient:

$$f_{stephenson} = \frac{i d g n^2}{V^2} \quad (5-38)$$

Stephenson (1979) original relationship from the data for angular rock particles is given by:

$$f_{stephenson} = \frac{800}{Re_{stephenson}} + 4 \quad (5-39)$$

Hence a regression analysis of more complete data shown in Fig. 5 - 3 provides the following expression:

$$f_{\text{stephenson}} = \frac{1298}{\text{Re}_{\text{stephenson}}} + 3.84 \quad (5-40)$$

The curves describing Eqs. (5-39) and (5-40) are shown in Figure 5 -3. It is noticed that the curve for Eq. (5-40) lies close to the experimental data. It may further be noted that, when  $\text{Re}_{\text{stephenson}}$  is larger than 2000, the seepage flow is fully turbulent. This is in contrast to the results shown in Fig. 5 - 2, where fully turbulent flow develops at  $\text{Re} \approx 200$ .

A general expression for  $i$  can now be obtained from Eqs. (5-37), (5-38), and (5-40):

$$i = \frac{1300 \nu}{d^2 g n} V + \frac{3.84}{d g n^2} V^2 \quad (5-41)$$

Stephenson (1979) omitted the first term in Eq. (5-39) in his derivation of an expression for the hydraulic gradient  $i$ . However, an expression for  $i$  which covers the entire range of seepage flow can be obtained from Eqs. (5-37), (5-38), and (5-39):

$$i = \frac{800 \nu}{d^2 g n} V + \frac{4}{d g n^2} V^2 \quad (5-42)$$

Note that in Eq. (5-41) and Eq. (5-42), if the velocity term  $V$  is small, then the second term becomes negligible and these equations now represents Darcy flow; if the velocity term is large, the second term dominates and the equation now represents turbulent flow. Eq. (5-42) has been identified as the "modified Stephenson" expression in subsequent discussion.

### 5.3 Comparison between different formulae

A discussion of the differences between different formulations presented in the literature is now necessary. To facilitate comprehension, the following terminology has

been used in subsequent discussion. Eq. (5-41) is defined as "general" implying that it is based on larger experimental data base than compiled by Stephenson(1979). The term "quadratic" and "turbulent", are used for Eqs. 26 and 36 respectively which have been formulated in this study on the concept of pipe flow. The relationships proposed by different authors are identified by their names (Table 5-1).

A comparison shows that:

(1) the formula proposed by Gent (1991) Eq. (5-47), and Ergun (5-1952) Eq. (5-43) are typical cases of "quadratic law" Eq. (5-25) when the shape factor  $r_E$  is a constant.

(2) the "general" Eq. (5-41), and "modified Stephenson" are typical cases of "quadratic law" Eq. (5-26) when the mean hydraulics radius  $R$  is related to the diameter of rockfill particles  $d$ , typically when  $R$  is proportional to  $d$ . If  $R=0.1d$ , Eq. (5-26) is very similar to Eq. (5-41).

(3) Martins (46), and "turbulent" Eq. (5-36) are close in form if  $R$  is related to  $d$  and  $C_u$ .

(4) It is also noticed that for fully turbulent flow, if  $R=d/10$  which is recommended by Parkins (1991), "turbulent" Eq. (5-36) reduces to the Stephenson's formula Eq. (5-48 when  $K_t = 4$ ).

(5) Wilkins Eq. (5-45) is a typical case of "power law" (5-31), in which the kinematic viscosity  $\nu$  and gravity acceleration  $g$  are included in the coefficient 0.0465 with unit  $\frac{[\text{second}]^{1.85}}{[\text{meter}]^{0.825}}$  in Wilkins' formula Eq. (5-45)). It is important to note that Wilkins formula the coefficient will change with unit being used.

## 5.4 Computer simulation of $i \sim V$ relationships

To compare the characteristics of different formulae, it is assumed that the rockfill material is angular, uniform in size, and the hydraulic radius  $R$  equals  $d/10$ . Computer

simulations were done using a spreadsheet program. The range of porosity of rockfill material varies from 0.35 to 0.5, and the size of rock particles was varied from 1 cm to 200 cm to simulate field conditions. Numerous curves showing the relationships between  $i$  and  $V$  were plotted and analyzed. Only a sample of these simulations is shown in Figs. 5-4 to 5-10, and the results of comparisons are presented in Tables 5-2 to 5-5. These results show that:

- (1) For  $n=0.35-0.5$ , when the diameter  $d$  is small (about 0.01 m), "quadratic", "general", and "modified Stephenson" relationships are close. It is noted that these relationships are all in quadratic form.
- (2) For  $n=0.35-0.5$ , when  $d$  varies from 0.04 m to 2 m, "quadratic", "turbulent", "Wilkins", "general", and "modified Stephenson" relationships are very close.
- (3) For  $n=0.45-0.5$ , when  $d$  is between 0.04m and 0.10m, "McCorquodale", "quadratic", "turbulent", "Wilkins", "general", and "modified Stephenson" relationships are very close.
- (4) For  $n=0.35 -0.5$ , when  $d$  is larger than 0.04 m, "Gent", "Martins", and "Ergun" expressions underestimate  $i$  from that obtained from "quadratic", "turbulent", "Wilkins", "general", and "modified Stephenson" expressions. This becomes more evident with increase of  $n$ .

## **5.5 Computer Simulation of the relationship between $Re$ and $f$**

The parameters  $f$  and  $Re$  are defined by Eqs. (5-17) and (5-18) respectively. The basic formulations between  $f$  and  $Re$  are given by Eq. (5-23) and Eq. (5-29). It is of practical interest to compare the relationships between  $Re$  and  $f$  as obtained from various proposed relationships between  $i$  and  $V$ . The values of  $a$  and  $b$ , or  $C$  and  $N$  are summarized in Table 5-6. Figs. 5-10 to 5-17 show some results of this computer simulation. It may be observed that:

(1) If  $Re < 20$ , the "Ergun", "quadratic", and "general" expressions are almost identical, while the "modified Stephenson" expression is a little lower than the above three formulations. The "Gent" and "McCorquodale" expressions are much higher than others. It is noticed that all these curves are linear in this region.

(2) All curves except "McCorquodale" expression tend to approach constant  $f$  for turbulent flow ( $Re > 200$ ). For  $R = 0.015\text{m}$  to  $0.45\text{m}$  and  $r_E = 0.6$ , the  $f$  values are very close.

(3) For fully turbulent flow, and  $r_E$  lying between  $0.8$  to  $1.0$ , the "Martins", "Ergun", and "Gent" expressions give lower values of  $f$  than other expressions.

(4) "Wilkins" shows higher value of  $f$  if  $R > 0.045\text{m}$ , and lower values of  $f$  if  $R < 0.015\text{m}$  especially when  $Re > 400$ . This suggests that "Wilkins" expression may apply to a limited range of hydraulic radius, and for turbulent flow only.

(5) When  $R/d = 0.1$ , "turbulent" and "Stephenson" expressions are essentially identical.

## 5.6 Parameters of rockfill material

When a relationship for seepage flow is chosen, the most important parameters for the estimation of seepage through rockfill are porosity and the hydraulic mean radius. The porosity may be reasonably estimated from field experience relating the placement procedure, rockfill gradation, and type of rock particles. However the determination of the hydraulic mean radius is difficult.

Theoretically, the hydraulics mean radius should represent the true shape and size of the pore structures in rockfill material, and not the rock particle itself. The hydraulic mean radius should relate to the size and the shape of the particles and the porosity of the rockfill material. It is a statistical parameter.

The shape factor, which also indicates relative surface area efficiency,  $r_E$ , is stated as Eq. (5-10) by Hansen (1992):

$$r_E = \frac{J_{ROCK}}{J_{SPHERE}} = \frac{J_{ROCK}}{6} \quad (5-10)$$

To use it in the design, some basic experiments should be done in the field to obtain  $A_{VS}$ , i.e., the surface area per unit volume of rockfill. Eq. (5-12) is applicable when the relative surface area efficiency  $r_E$  can be obtained by experiment:

$$R = \frac{e d}{6 r_E} \quad (5-12)$$

Isbash(1931), Ergun (1952), Dinoy (1971), Stephenson (1979), and Li and Hu (1988) used the average diameter to represent the size of rock particles. Wilkins(1956), Leps (1973), and Parkins (1991) recommended the use of the average diameter to represent the hydraulics mean radius. Garga, Townsend, and Hansen (1991) considered that the shape of a rock particle is ellipsoidal and presented a relationship between the hydraulics mean radius and the porosity and the b axis of ellipse.

Most experimental data available to date were obtained from the consideration that an average diameter of rock particles can be used to represent the rockfill material. In some studies (e.g., Stephenson (1979), Li and Hu (1988), and the present study the available data on similarly shaped (i.e., angular) rock particles has been analyzed to obtain the coefficients in the various formulae. However, the representation of the hydraulics mean radius in terms of the average diameter only (e.g., Wilkins(1956), Leps (1973), and Parkins (1991)) can apply to the cases where the rock particles have similar shape to the ones used in the experimental studies.

Parkins(1991) recommended that for Wilkins(1956) exponential formula, the mean hydraulics radius be approximated as one tenth of the diameter of rock particles:

$$R = 0.1d \quad (5-69)$$

A regression of combined data from both Leps(1973) and Hansen(1992) indicates:

$$R = 0.136d \quad (5-70)$$

Figure 5 -18 shows the data and the regression equation, which is recommended for small rockfill dams built with crushed rockfill material.

Garga, Townsend, and Hansen (1991) derived a relationship between the mean hydraulics radius and the b axis of the ellipse, for rockfill whose shape can be approximated to an ellipsoidal shape:

$$R = (0.71 n^2 - 0.201 n + 0.052) e^{0.195B} \text{ (cm)} \quad (5-71)$$

where B = length of intermediate axis of an ellipse, in cm. It should be noticed that this relationship may apply to the same kind of material as used in Garga, Townsend, and Hansen (1991)'s experiment. The limitation of Eq. (5-71) is that the influence of the length of longest axis and shortest axis of an ellipse are not accounted for in the equation, and that a rock particle may be highly irregular in shape.

It is noticed that most formulae are applicable to clean, monosized rock particles while in practice, rockfills are not monosized. Based upon examination of the grain size curves for ten rockfill dams, and taking into account the effects of segregation, Leps (1973) proposed that "the 50% size can reasonably be considered the dominant size for flow calculations, provided that the minus 1-in. material is less than 30%, and preferably less than 10%, by weight". Leps further stated that if there is more than 30% of minus 1-in. material, the fill should probably be treated as an earthfill and its permeability should be determined by conventional soil mechanics tests. In a compacted rockfill, the vertical permeability of the rockfill will be relatively low due to segregation of fines, while the horizontal permeability will be only slightly affected and will be reasonable predictable. Leps (1973) stated that a correction to account for the

layering may be of academic interest only, since it would be small in comparison to the probable error in estimating the void velocity for the cleaner part of each layer.

Hence the average size of rockfill can be used to predict the seepage velocity in low-head flowthrough and overtopping rockfill dams.

## 5.7 Comparison between power law and quadratic law

Theoretically both the power law and the quadratic law can represent the seepage law for non-Darcy flow. However in their application in engineering practice, there are some important differences to be considered.

### (1) Power law

When a power law is used to represent the law of seepage flow in rockfill material, the formula is:

$$i = c_0 V^{c_1} \quad (5-2)$$

From Eq. (5-31), it is easily obtained:

$$c_0 = \frac{C}{8gR^{1+N}n^{2+N}v^N} \quad (5-72)$$

and

$$c_1 = 2 + N \quad (5-73)$$

The values of C and N are obtained from the relationship between the Reynolds number and friction coefficient:

$$f = C Re^N \quad (5-29)$$

in which, the value of N depends on the value of the Reynolds number. For very low Reynolds number,  $N=-1$ , Eqs. (5-2) and (5-72) show that Darcy law applies. For high Reynolds number ( $Re > 200$ ),  $N=0$ , and the seepage flow is fully turbulent. For Reynolds number in the transition zone between Darcy flow and fully turbulent seepage flow, the value of N increases from -1 to 0. Hence, the values of  $c_0$  and  $c_1$  also depend on the value of Reynolds number. In engineering design, the following approach is suggested for use with a power law:

(a) assume the range of Reynolds number.

(b) choose the values of C and N from the available literature or from site specific tests. Li and Hu (1988) derived the following relationships for the coefficients in Eq. (5-2):

$$c_0 = \frac{a v^{-b}}{d^{1+b} g n^{2+b}} \quad (5-74)$$

and

$$c_1 = 2+b \quad (5-75)$$

where a, and b are coefficients depending on the range of Reynolds number which are given in Table 5-7.

(c) undertake simulation with the selected C and N.

(d) calculate the Reynolds number to check if it is in the range of the assumed value. If yes, the calculation is finished; otherwise, go to step (a).

In Wilkins' formula,

$$c_0 = \frac{0.0465}{R^{0.925} n^{1.85}} \quad (5-76)$$

and

$$c_1 = 1.85 \quad (5-77)$$

Fortunately in the prototype, the seepage flow in a rockfill dam is often fully turbulent ( $Re > 200$ ). In this case,  $N$  is zero in the power law. The recommended equation is:

$$i = \frac{0.4V^2}{gRn^2} \quad (5-78)$$

If the rockfill particle size  $d$  is used in the design, Li, Garga, and Davies give (1995):

$$i = \frac{3.837 V^2}{d g n^2} \quad (5-79)$$

Substituting Eq. (5-69) in Eq. (5-78):

$$i = \frac{4 V^2}{d g n^2} \quad (5-80)$$

This is the same equation given by Stephenson (1979).

The conclusion for power law is that:

(i) if detailed information is available for the determination of the constants  $C$  and  $N$  corresponding to each range of Reynolds number, then the power law can be applied to all ranges of Reynolds number, from Darcy flow to fully turbulent flow;

(ii) if seepage flow in the prototype is fully turbulent, the constant  $N=0$ , in which case Eq. (5-78) to Eq. (5-80) may be applied.

(iii) If the range of Reynolds number in the prototype is not known, then the power law is difficult to apply.

## (2) Quadratic law

The general relationship between Reynolds number and friction coefficient is:

$$f = \frac{a}{Re} + b \quad (5-23)$$

Previous analyses have shown that this function is suitable to describe the relationship between Reynolds number and friction coefficient from Darcy flow to fully turbulent flow with unique constants  $a$  and  $b$  (an important advantage over the power law). The formula to describe the relationship between velocity and hydraulic gradient derived from this relationship is in quadratic form (i.e., so called quadratic law). The following two equations were obtained (Li, Garga, and, Davies, 1995):

$$i = \frac{12 \nu}{R^2 g n} V + \frac{0.38}{R g n^2} V^2 \quad (5-26)$$

and

$$i = \frac{1300 \nu}{d^2 g n} V + \frac{3.84}{d g n^2} V^2 \quad (5-41)$$

When the Reynolds number is very small, the first term dominates, i.e., Darcy law applies. When Reynolds number is large ( $Re > 200$ ), the second term dominates

### (3) Conversion between quadratic law and power law

George and Hansen (1992) presented a method for the conversion between quadratic law and power law with the least square method. The range of the velocities lies from 0 to  $v_{max}$  (the maximum velocity) in the conversion. However as discussed, in the transition zone of seepage flow, the coefficients in the power law are to be obtained as a function of Reynolds number. Hence, if a quadratic law is converted to a power law, it is necessary that both the  $v_{max}$  and  $v_{min}$  are within a specific range of Reynolds number where the coefficients  $c_0$  and  $c_1$  change very slowly with Reynolds number.

## 5.8 Comparison with the prototype data

Extremely limited prototype data are available in the literature. In the present study, the two data points from Hell Hole Dam and Pit 7 Dam collected by Leps (1973) and one data point measured in Xibeikou Rockfill Dam (Hu, and etc., 1988), will be compared to the results of all the formulae previously presented.

(i) Hell Hole Dam (Leps, 1973)

The dam located in California was designed as an inclined-core rockfill, 410 ft high and 1570 ft long at the crest, with a volume of 8,800,000 yd<sup>3</sup>. Most of the rockfill was placed by dumping and sluicing in two high lifts. The first lift, about 220 ft high, was being constructed in 1964 and the closure of the rockfill dump had been made across the canyon. During the period December 21-24, 1964, an intensive rainstorm occurred and resulted in seepage flow through the unfinished rockfill dam. At 5:30 AM on December 23, the flowthrough discharge was about 19,000 cfs, and loss of rock from the downstream toe of the dam was observed and small slides were heard. The slides were progressively cutting back to the crest of the rockfill. By 9:10AM, all of the crest had slid downstream and loss of rock particles was rapidly progressing. At 9:30 AM on December 23, the dam was breached where overflow had begun in the opening created by the progressive slides. Leps (1973) assumed that the vertical cross section through which flow was occurring at failure was triangular and was about 420 ft long by 160 ft in maximum depth, and that the void ratio of the fill was about 0.75 (porosity  $n=0.43$ ), the average void velocity for the estimated 19,000 cfs throughflow at a position well back in the cross section of the embankment was 1.32 ft/sec (Leps, 1973). Leps estimated the hydraulic gradient  $i$  as 0.15, and concluded that the dominant rock size was close to 12 inches.

(ii) Xibeikou Concrete Faced Rockfill Dam (Hu, et al, 1988)

Xibeikou Concrete Faced Rockfill Dam is located in Yichang County in Hubei Province, China. The design height of the dam is 95 m. During the construction, the dam could not reach the required 300 m elevation to prevent overtopping. Hence a layer of large rockfill was built at the downstream slope with a flat slope 8.2:1 which protected the dam from flowthrough and overtopping flow in the flood period in 1987 when a discharge of 1460 m<sup>3</sup>/s occurred. The approximate height of the dam at this stage of construction was about 17 m. A team was organized by Gezhou Dam Engineering Board and Nanjing Hydraulic Research Institute to conduct the prototype observation.

The hydraulic gradient close to the downstream slope was found to be  $1/8.2=0.12$ . Two sets of seepage discharge were observed,  $49 \text{ m}^3/\text{s}$  and  $13 \text{ m}^3/\text{s}$  with the corresponding downstream seepage exit elevations 253.0 m and 251.3 m respectively (i.e., exit height 2.3 m and 0.6 m respectively). The bulk velocities were calculated as 0.22 m/s and 0.24 m/s for the two cases (Hu, et al, 1988). At the exit section, the dominant size of rockfill material is determined by the armour layer. Assuming a porosity of 0.45,  $d_{50}$  of the rockfill is 0.65 m. The bulk velocity corresponding to the hydraulic gradient 0.12 is taken as 0.229 m/s.

(iii) Pit 7 Afterbay Dam (Leps, 1973)

Pit 7 Afterbay Dam was designed in California in 1965 to be subjected continuously to throughflow and frequently to overtopping flow, with normal flows ranging from 2000 to 6650 cfs. The rockfill dam is 36 ft high, and 555 ft long with 20 ft in crest width, with downstream slope of 2.25:1, and upstream slope of 2:1.

The hydraulic gradient was observed to be nearly as steep as the downstream face of the rockfill dam. The dominant rock size is 2 in. Leps assumed that the cross section through which flow takes place is about 500 ft long by 15 ft deep, and the porosity of the rockfill material is 0.5. The computed flow through the rockfill is about 2200 cfs from Wilkins' relationship, and compares well with observations.

Table 5-8 shows the results of the simulations with different formulae and the relative errors. In the simulation, Eq. (5-5) is used to calculate the mean hydraulics radius. The relative error is defined as:

$$\text{Relative Error} = \frac{\text{Velocity}_{\text{simulated}} - \text{Velocity}_{\text{prototype}}}{\text{Velocity}_{\text{prototype}}} \quad (5-82)$$

The formulae used to calculate velocities from hydraulic gradients are listed as follows:

(1) "general"

$$V = \sqrt{\left(\frac{169.1 \nu n}{d}\right)^2 + 0.2606 d g n^2 i} - \frac{169.1 \nu n}{d} \quad (5-83)$$

(2) modified Stephenson

$$V = \sqrt{\left(\frac{100 \nu n}{d}\right)^2 + 0.25 d g n^2 i} - \frac{100 \nu n}{d} \quad (5-84)$$

(3) Ergun

$$V = \sqrt{\left(\frac{42.86 (1-n) \nu}{d}\right)^2 + 0.5714 \frac{d g n^3 i}{(1-n)}} - \frac{42.86 (1-n) \nu}{d} \quad (5-85)$$

(4) Gent

$$V = \sqrt{\left(\frac{499.4 (1-n) \nu}{d}\right)^2 + 0.8271 \frac{d g n^3 i}{(1-n)}} - \frac{499.4 (1-n) \nu}{d} \quad (5-86)$$

(5) McCorquodale

$$V = \sqrt{\left(\frac{43.21 \nu}{n^{1/2} R}\right)^2 + 1.235 g n^{1/2} R i} - \frac{43.21 \nu}{n^{1/2} R} \quad (5-87)$$

(6) Wilkins

$$V = 5.243 n R^{0.5} i^{0.54} \quad (5-88)$$

(7) Martins ( $C_u = 1$ )

$$V = 0.56 n \sqrt{2 g d i} \quad (5-89)$$

(8) Stephenson:

$$V = 0.5 n (d g i)^{0.5} \quad (5-90)$$

(9) "quadratic" law

$$V = \sqrt{\left(\frac{16.13 \nu n}{R}\right)^2 + 2.631 R g n^2 i} - \frac{16.13 \nu n}{R} \quad (5-91)$$

(10) "turbulent" law

$$V = \sqrt{2.5 g R n^2 i} = 1.58 n \sqrt{g R i} \quad (5-92)$$

From Table 5-8 it is observed that "turbulent", "quadratic", and Wilkins expressions give good predictions with maximum relative error 3%, 4%, and 5% respectively; "general", and "modified Stephenson" expressions provide values with maximum relative errors 15% and 17% respectively. However the Ergun, Gent, McCorquodale, and Martins expressions give results with maximum relative errors 32%, 55%, 28%, and 38% respectively.

## 5.9 Determination of the most appropriate formula in design

The selection of the most appropriate formula will depend on the objective of the analysis and the type of information available on the rockfill material.

### (1) The estimation of seepage discharge with known average $i$ :

When the average hydraulic gradient through a rockfill dam is known or estimated by some empirical relationships, e.g. Hansen (1992), the discharge through the dam can be estimated by the calculation of average velocity.

(i) If mean hydraulics radius and porosity for the rockfill are known, and

a), if the seepage flow can confidently be described as fully turbulent, then "turbulent" expression can be the used to calculate the seepage velocity;

b), if the flow pattern through the rockfill material is uncertain (e.g., complicated distribution of rockfill, or existence of small size rockfill), then "quadratic", or "general" expressions may be used;

(ii) If the porosity and the dominant rock size for the rockfill are known, but the mean hydraulics radius for the rockfill is unknown:

- a). for crushed rockfill material (angular), the mean hydraulic radius may be estimated by Eq. (5-5), the recommendations in (i) can be used here;
- b). for semi-rounded shape, e.g., gravel, no confident relationship is available between the dominant rock size and the mean hydraulics radius. Expression "modified Stephenson" formula can be used for the prediction of the seepage bulk velocity.

If the tail water level is below the point of emergence on the seepage face, it had no effect on the height of the point of emergence, which was determined using the following formula (Parkins, 1963):

$$h_c = \frac{q}{n} \left[ \frac{c_0}{\sin \theta} \right]^{(1/c_1)} \quad (5-93)$$

where  $\theta$  is the angle of downstream slope. Hansen (1992) argued that  $\sin \theta$  should be replaced by  $\tan \theta$  when the downstream slope is steep:

$$h_c = \frac{q}{n} \left[ \frac{c_0}{\tan \theta} \right]^{(1/c_1)} \quad (5-94)$$

For fully turbulent flow, Eq. (5-78) which was obtained by Li, Garga, and Davies (1995) is the best formula for application. From Eq.(5-78),  $c_1 = 2$ , and

$$c_0 = \frac{0.4}{g R n^2} \quad (5-95)$$

Hence for fully turbulent flow:

$$h_c = \frac{q}{n} \left[ \frac{0.4}{g R n^2 \tan \theta} \right]^{0.5} \quad (5-96)$$

(2) The estimation of seepage discharge with unknown average hydraulic gradient  $i_{ave}$ :

In a design, if the average hydraulic gradient is not known, the procedure to calculate the discharge flow through a rockfill dam is described as followings.

Step 1: Estimate the average hydraulic gradient by revised Hansen's formula (Hansen, 1992):

$$i_{ave} = 0.8 \left( \frac{h}{H} \right)^{1.4} \left( \frac{H}{B_u + B_c + 0.5B_d} \right)^{\frac{3}{2}} \quad (5-97)$$

where

H = the height of the dam;

h = the upstream water depth;

$B_u$  = the horizontal length of the upstream slope;

$B_c$  = the horizontal length of the crest;

$B_d$  = the horizontal length of the downstream slope.

For the description, please refer to Figure 2-1(a).

Step 2: Estimate the unit-width discharge by the following formula which is the multiplication of the upstream water depth h and the average velocity that is estimated by the new "turbulent" law Eq. (5-92):

$$q = 1.58 n h \sqrt{g R i_{ave}} \quad (5-98)$$

### **(3) Computer simulation of the seepage field (by FEM):**

Finite element analysis can be used to obtain detailed pore pressure distribution inside a rockfill dam in order to conduct slope stability analysis or unravelling slope failure analysis.

It is important to observe that in a rockfill dam, the hydraulic gradient may change from position to position, from very small values to very high values; the flow pattern of seepage flow may also vary from Darcy flow to fully turbulent flow within the simulation domain. The followings are some considerations:

(i) both the Darcy law and "turbulent" law may not be appropriate if either is applied to all the seepage regions;

(ii) the power law is difficult to apply, as the Reynolds number is unknown at each position inside the seepage field. Further, the exponential coefficient is a function of Reynolds number, and hence a trial and error procedure should be conducted for each element. Also there appears to be no acceptable relationship between the Reynolds number and the exponential coefficient in the power law.

(iii) the quadratic law is easy to apply, since it is valid for all ranges of Reynolds number with unique constants in the relationship which do not change with Reynolds number.

Hence, the quadratic law is recommended for FEM computer simulations.

If the porosity and the dominant rock size for the rockfill are known, but the mean hydraulics radius for the rockfill is unknown, then for crushed rockfill material (angular), the mean hydraulics radius may be estimated by Eq. (5-5).

**(4) Evaluation of the free surface curve in a rockfill dam by 1-D analysis**

With finite element method an accurate free surface can be obtained. But for most practical cases, a reasonable estimation of the free surface curve from 1-dimension analysis may suffice. While it is difficult to use a quadratic law in a general formula to describe the free surface curve, it is easy to use the power law. The followings are some analyses which may be useful for a designer.

Considering that the seepage flow is a steady, horizontal flow (Figure 5-19), the specific energy is defined as (Stephenson, 1979):

$$E = y + \frac{V^2}{2g} = y + \frac{q^2}{2gn^2y^2} \quad (5-99)$$

$$\frac{dE}{dx} = \frac{dy}{dx} \left(1 - \frac{q^2}{gn^2y^3}\right) \quad (5-100)$$

Eq. (5-100) may be written as:

$$-\frac{dE}{dx} = i = c_0 \left(\frac{q}{ny}\right)^{c_1} \quad (5-101)$$

Substituting Eq. (5-100) in (5-101) it is obtained:

$$-\int_{y_1}^y \left(y^{c_1} - \frac{q^2}{gn^2y^{3-c_1}}\right) dy = \int_{x_1}^x c_0 \left(\frac{q}{n}\right)^{c_1} dx \quad (5-102)$$

Case (a)  $c_1 \neq 2$ :

$$\frac{y_1^{1+c_1} - y^{1+c_1}}{1+c_1} + \frac{q^2}{gn^2(2-c_1)} \left(\frac{1}{y_1^{2-c_1}} - \frac{1}{y^{2-c_1}}\right) = c_0 \left(\frac{q}{n}\right)^{c_1} (x - x_1) \quad (5-103)$$

Case (b)  $c_1=2$  (fully turbulent flow)

$$\frac{y_1^3 - y^3}{3} + \frac{q^2}{gn^2} \ln \frac{y_1}{y} = c_0 \left(\frac{q}{n}\right)^2 (x - x_1) \quad (5-104)$$

where

$$c_0 = \frac{0.4}{gRn^2} \quad (5-95)$$

From Figure 5 -19 , it is noticed that:

$$y_1 = y_0 - \frac{q^2}{2gn^2 y_0^2} \quad (5-105)$$

If  $y_0$ ,  $q$ ,  $n$ ,  $c_0$ , and  $c_1$  are known, the free surface curve of the non-Darcy seepage flow can be obtained by assuming  $y$  to calculate  $x$ . For example, for  $y_1=20$  m,  $n=0.39$ ,  $q = 3.24 \text{ m}^3/\text{s/s}$ ,  $R=0.02$  m,  $c_1=2$ ,  $c_0=13.41$ , and at  $x_1=30$  m, the free surface curve may be represented by the following equation:

$$x = 30 + 174.8 \ln \frac{20}{y_2} + 8.282(20^3 - y_2^3) \quad (5-106)$$

As another example, all the parameters are the same as above except that  $c_1 = 1.85$  and  $c_0 = 9.90$  (from Wilkins' formula, i.e., Eq. (5-88)):

$$x = 33.66 - 0.00201 y^{2.85} - 0.943 y^{-0.15} \quad (5-107)$$

## 5.10 Conclusions

1. Based on pipe flow theory, new definitions of Reynolds number  $Re$  and friction coefficient  $f$  have been proposed (Eqs. (5-17), (5-18), (5-20), and (5-21)). With the new definition, seepage flow is fully turbulent when  $Re > 200$ . The relationships between  $i$  and  $v$  for both quadratic seepage law and power seepage law have been presented in Eqs. (5-26), (5-27), (5-33), (5-34), and (5-36).

2. Based on Stephenson's definitions for Reynolds number and friction coefficient, a new relationship between Reynolds number and friction coefficient Eq. (5-40) has been presented. According to this definition, when  $Re_{\text{stephenson}}$  is larger than 2000, the seepage flow in rockfill is fully turbulent. A new relationship between  $i$  and  $V$  has been presented in Eq. (5-41).

3. Computer simulations with wide range of porosity ( $n=0.35\sim 0.5$ ) and rockfill size ( $d=0.01\text{m} \sim 2.0\text{ m}$ ) indicate that in most conditions, the  $i$ - $V$  curves given by "general", Wilkins, "quadratic", "turbulent", and "modified Stephenson" expressions are very close.

4. A comparison of different expressions of  $i$  and  $V$  reported in the literature applicable for rockfill indicates that these are applicable only in a limited range of seepage flow. The experimentally derived expressions reported in the literature are special cases of the general expressions derived in this Chapter (Eqs. (5-24), (5-25), (5-31), or (5-32)).

5. Eq. (5-70) may be used to predict the mean hydraulics radius of rockfill.

6. From literature review and from the simulation of some available prototype data, it is concluded that the 50% size can reasonably be considered as the dominant size for flow calculations in flowthrough rockfill design.

7. The differences between the power law and the quadratic law are analyzed. For power law, the constants  $C$  and  $N$  are functions of Reynolds number.  $N=1$  for Darcy

flow and  $N=0$  for fully turbulent flow. For quadratic law, the constants  $a$  and  $b$  are unique for all ranges of Reynolds number (from Darcy flow to fully turbulent flow). Quadratic law is better than power law for the numerical modelling by finite element method.

8. Simulations for the prototype data shows that the "turbulent", Wilkins, and "quadratic" expressions give the closest results to the prototype data. If the seepage flow in prototype is fully turbulent, "turbulent" expression Eq. (5-36), is the best choice for design.

9. Methods to estimate the discharge through a rockfill dam have been proposed. When the average hydraulic gradient through the dam is unknown, Eq. (5-98) may be used to estimate the unit-width discharge through the dam.

10. Eqs. (5-103) and (5-104) may be used to estimate the free surface curve of seepage flow in a flowthrough rockfill dam.

Table 5-1 Relationship between hydraulic gradient  $i$  and velocity  $v$  from different authors

Name of Authors	Equation	Eq. No.	Comment
Ergun(1952)	$i = 150 \frac{(1-n)^2 v}{g n^3 d^2} V + 1.75 \frac{(1-n)}{d g n^3} V^2$	(43)	rearranged
McCorquodale et al (1978)	$i = \frac{70 v}{g n R^2} V + \frac{0.81}{g n^{1/2} R} V^2$	(44)	for crushed rockfill (Hansen, 1992)
Wilkins (1956)	$i = \frac{0.0465 V^{1.85}}{R^{0.925} n^{1.85}}$	(45)	$R = d/10$ (Parkin, 1991).
Martins (1990, 1991)	$i = \frac{V^2(1-n)}{0.56^2 n^3 2gd}$	(46)	rearranged for uniform rockfill material, $C_U = 1$
Gent (1991)	$i = 1207.06 \frac{(1-n)^2 v}{g n^3 d^2} V + 1.209 \frac{(1-n)}{d g n^3} V^2$	(47)	transformed for rockfill
Stephenson (1979)	$i = \frac{K_1 V^2}{g d n^2}$	(48)	$K_1 = 4$ , for rockfill; $K_1 = 2$ for semi- rounded stone; $K_1 = 1$ for smooth polished marbles.

Table 5-2 Simulation for n=0.35

d (m)	Figure	Curves close to "quadratic"	Other important characteristics
0.01	4	"general", "modified Stephenson"	"McCorquodale" and "Gent" are higher than others
0.04-0.1	5-6	"general", "Wilkins", "turbulent", and "modified Stephenson"	"Gent", "Martins", "Ergun", and "McCorquodale" are lower
0.4-2.0	7-9	the same as above	the same as above

Table 5-3 Simulation for n=0.40

d (m)	Curves close to "quadratic"	Other important characteristics
0.01	"general", "modified Stephenson", and "Gent",	"McCorquodale" is much higher than others
0.04	"general", "Wilkins", "turbulent", and "modified Stephenson"	"Gent", "Martins", "Ergun", and "McCorquodale" are close and lower than others
0.1	the same as above	the same as above
0.4-2.0	the same as above	the same as above

Table 5-4 Simulation for n=0.45

d (m)	Curves close to "quadratic"	Other important characteristics
0.01	"general", "modified Stephenson"	"McCorquodale" is much higher than others
0.04	"general", "Wilkins", "turbulent", and "modified Stephenson"	"Gent", "Martins", and "Ergun" are close and lower than others; "McCorquodale" is close to "quadratic" when l is not high
0.1	the same as above	"Gent", "Martins", and "Ergun" are close and lower than others
0.4-2.0	the same as above	"Gent", "Martins", "Ergun", "McCorquodale" are close and lower than others;

Table 5-5 Simulation for n=0.5

d (m)	Curves close to "quadratic"	Other important characteristics
0.01	"general", "modified Stephenson"	"McCorquodale" is much higher than others
0.04	"general", "Wilkins", "turbulent", "modified Stephenson", and "McCorquodale"	"Gent", "Martins", and "Ergun" are close and much lower than others
0.1	"general", "Wilkins", "turbulent", and "modified Stephenson"	"Gent", "Martins", and "Ergun" are close and much lower than others; "McCorquodale" is a little lower than "quadratic"
0.4-2.0	the same as above	"Gent", "Martins", and "Ergun" are close and much lower than others; "McCorquodale" is a lower than "quadratic" and higher than "Gent", "Martins", and "Ergun"

Table 5-6 The coefficients in the relationship between Re and f

Author	a or C	Equation number	b or N	Equation number
Ergun(1952)	$a = \frac{33.3}{r_E^2}$	(49)	$b = \frac{2.33}{r_E}$	(50)
McCorquodale (1978)	a=560	(51)	$b = 0.65 n^{1.5}$	(52)
Wilkins (1956)	$C = \frac{0.37 g R^{0.225}}{\nu^{0.15}}$	(53)	N=-0.15	(54)
Martins(1991)	$C = \frac{2.13}{r_E}$	(55)	N=0	(56)
Gent (1991)	$a = \frac{268}{r_E^2}$	(57)	$b = \frac{1.61}{r_E}$	(58)
Stephenson (1979)	C=3.2	(59)	N=0	(60)
general	$a=10380(R/d)^2$	(61)	$b = 30.7 \frac{R}{d}$	(62)
modified Stephenson	$a=6400(R/d)^2$	(63)	$b = 32 \frac{R}{d}$	(64)
turbulent	C=3.15	(65)	N=0	(66)
quadratic	a=98.8	(67)	b=3.04	(68)

Table 5-7 Coefficient in the power law (after Li and Hu, 1988)

$R_e$ Stephenson	0.01-10	10-100	100-420	420-3300	>3300
a	800	2.846	2.815	2.145	4.0
b	-1	-0.774	-0.776	-0.507	0

Table 5-8 Comparison between simulations and the prototype data

	Prototype general	modified Stephenson	Ergun	Gent	McCorquodale	Wilkins	Martins	quadratic	turbulent	Prototype Dam
Velocity (m/s)	0.134	0.118	0.177	0.208	0.153	0.141	0.185	0.139	0.137	Pit 7
Relative error	N/A	-12%	32%	55%	14%	6%	38%	4%	2%	
Velocity (m/s)	0.173	0.147	0.189	0.227	0.221	0.167	0.198	0.172	0.168	Hell Hole Dam
Relative error	N/A	-15%	9%	31%	27%	-4%	14%	-1%	-3%	
Velocity (m/s)	0.360	0.341	0.457	0.550	0.498	0.384	0.479	0.400	0.390	Xibeikou
Relative error	N/A	-5%	27%	53%	38%	7%	33%	11%	8%	

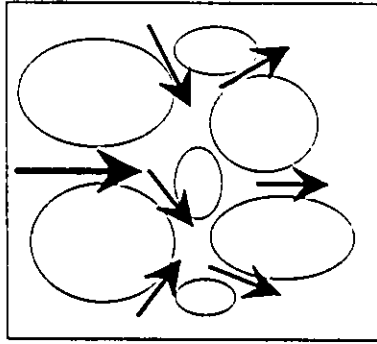


Figure 5 -1 Illustration of Flow Path in Rockfill

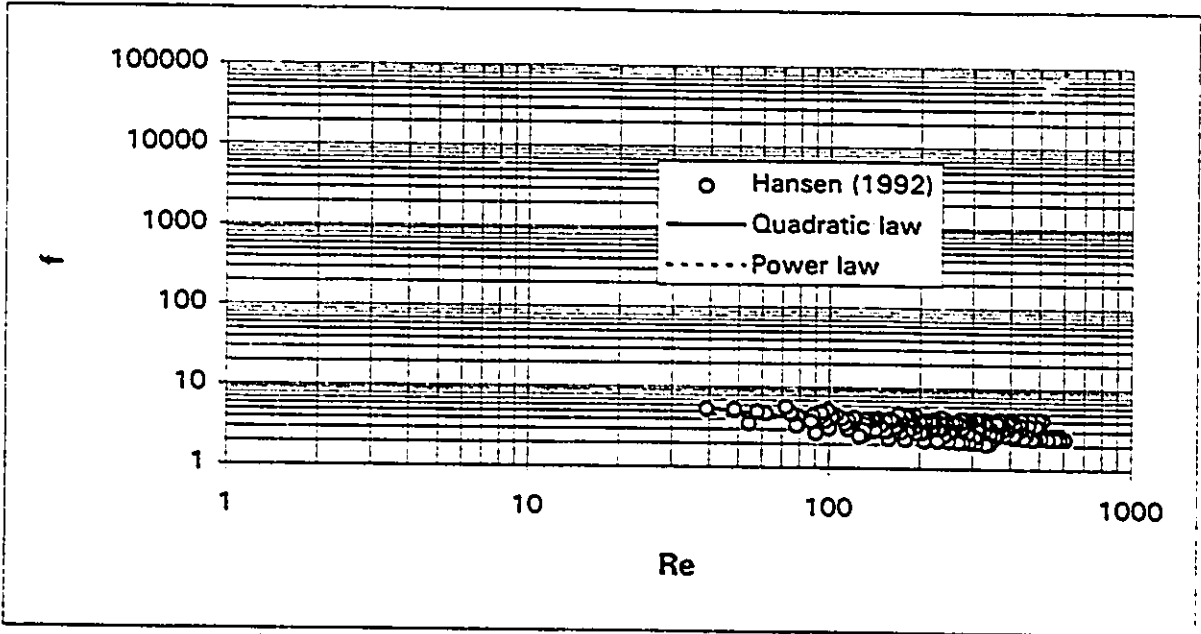


Figure 5-2 New Relationship between  $Re$  and  $f$  in terms of Hydraulic Mean Radius

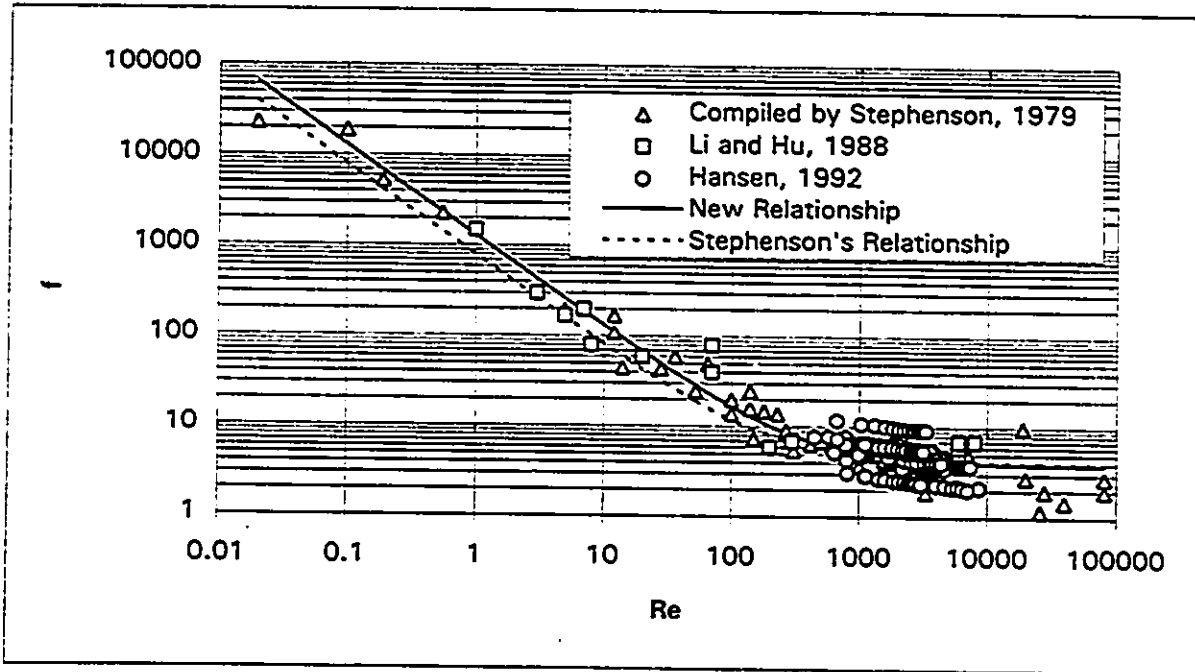


Figure 5-3 Relationship between  $f$  and  $Re$  in Terms of  $d_{50}$

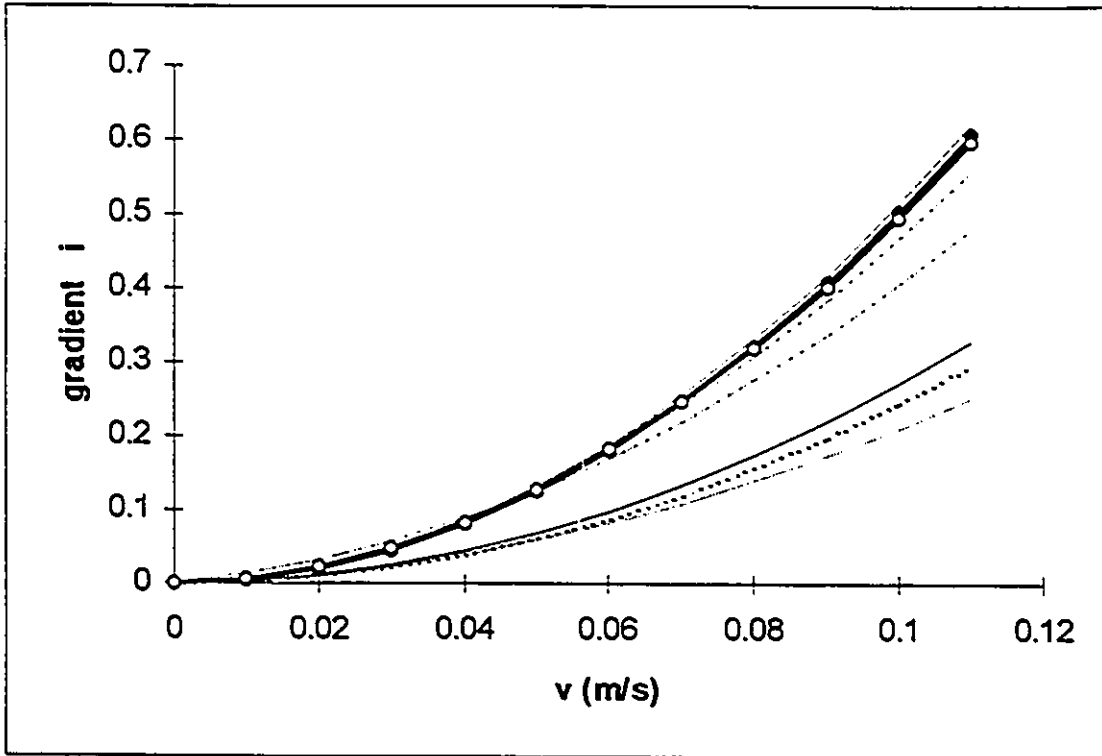


Figure 5-4 Relationship between  $i$  and  $v$  for rockfill with  $d_{50}=0.04\text{m}$ ,  $n=0.45$

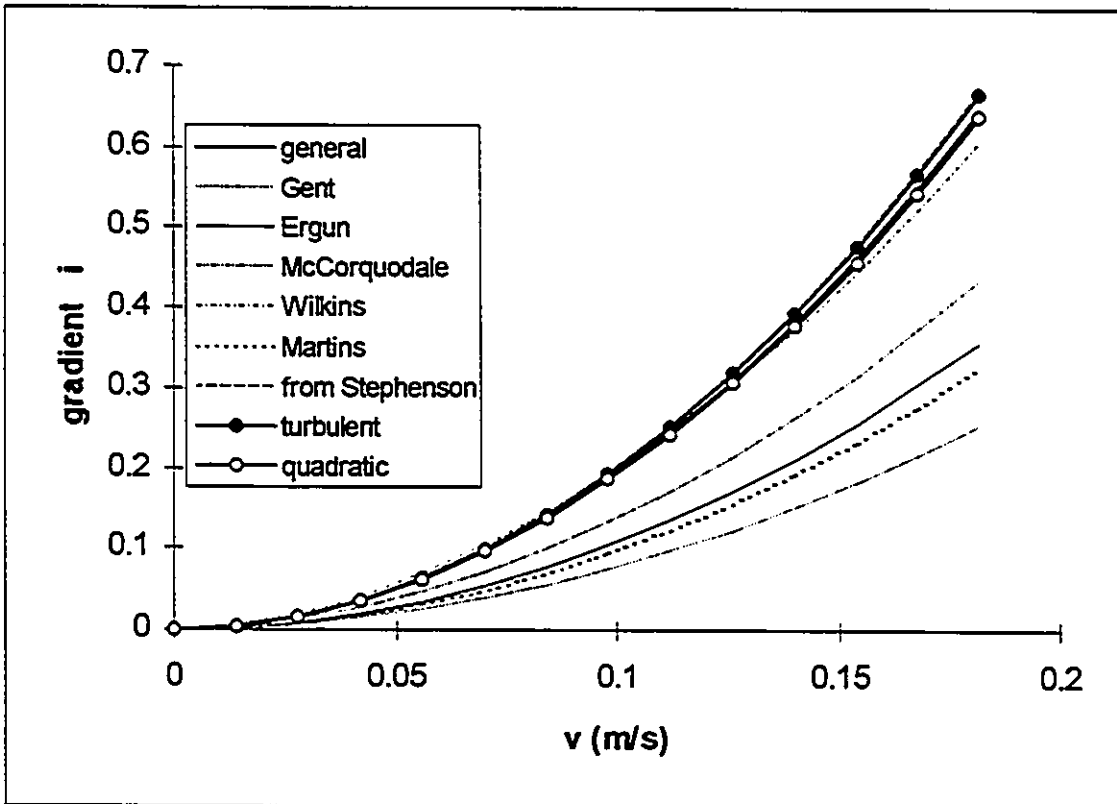


Figure 5-5 Relationship between  $i$  and  $v$  for rockfill with  $d_{50}=0.1\text{m}$ ,  $n=0.45$

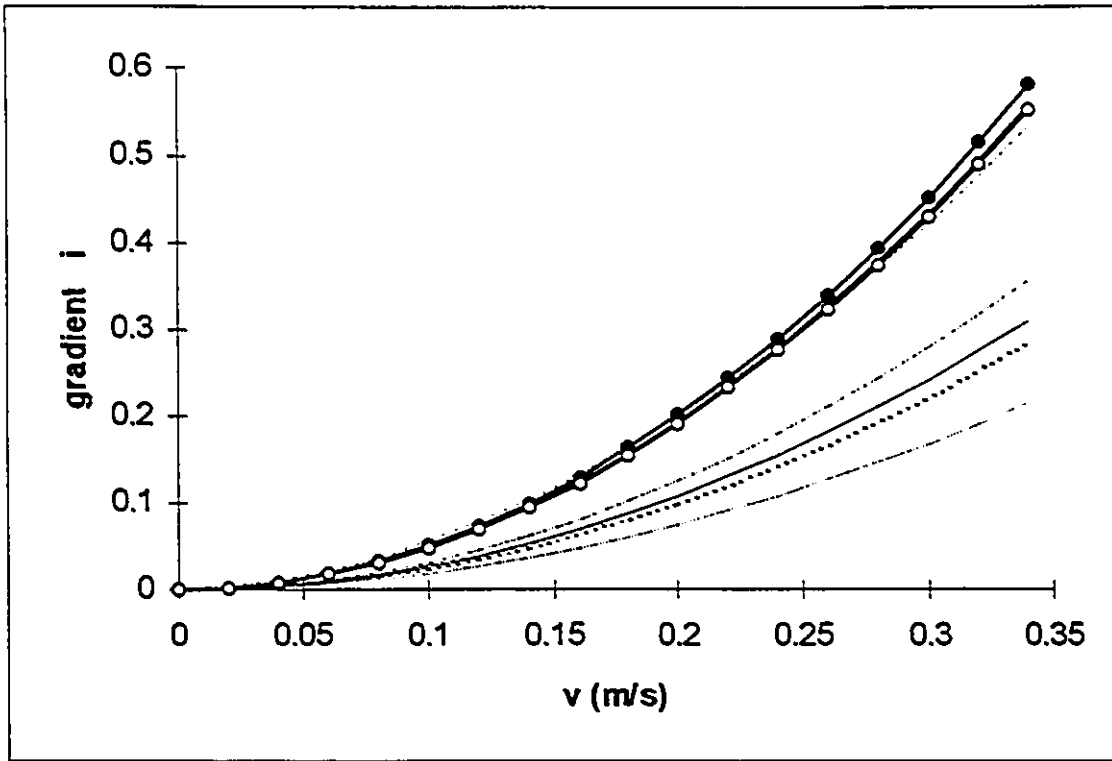


Figure 5-6 Relationship between  $i$  and  $v$  for rockfill with  $d_{50}=0.4m$ ,  $n=0.45$

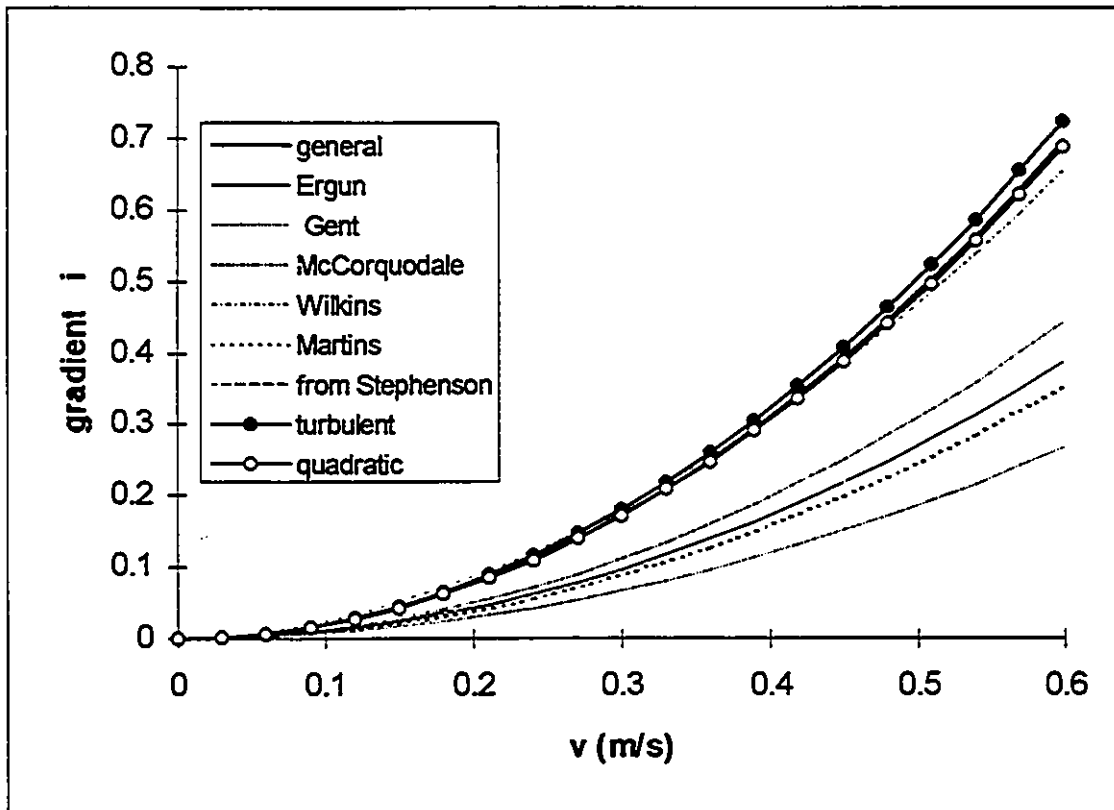


Figure 5-7 Relationship between  $i$  and  $v$  for rockfill with  $d_{50}=1m$ ,  $n=0.45$

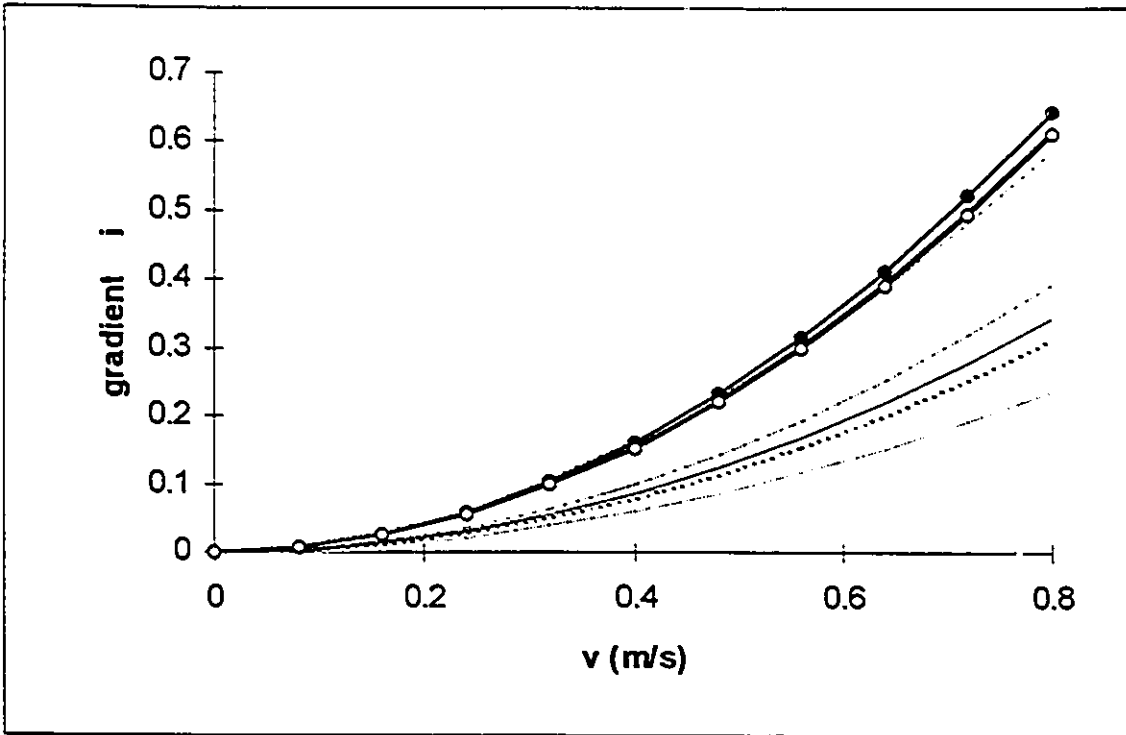


Figure 5-8 Relationship between  $i$  and  $v$  for rockfill with  $d_{50}=2\text{m}$ ,  $n=0.45$

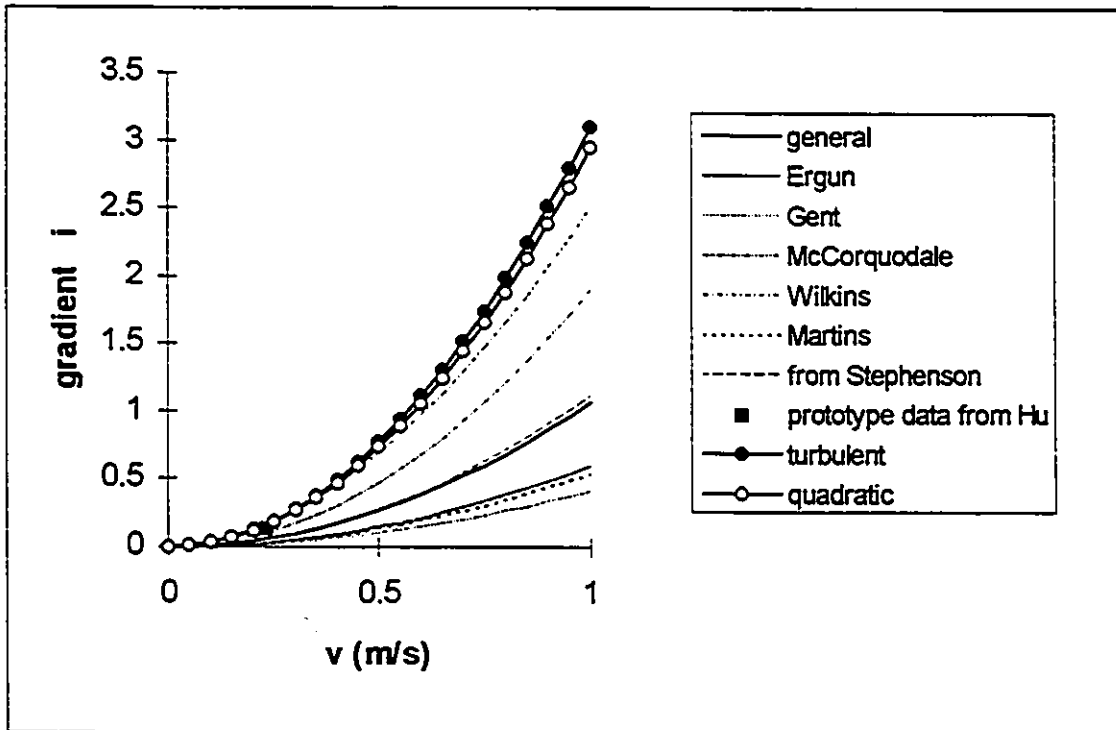


Figure 5-9 Relationship between  $i$  and  $v$  for rockfill with  $d_{50}=0.65\text{m}$ ,  $n=0.45$

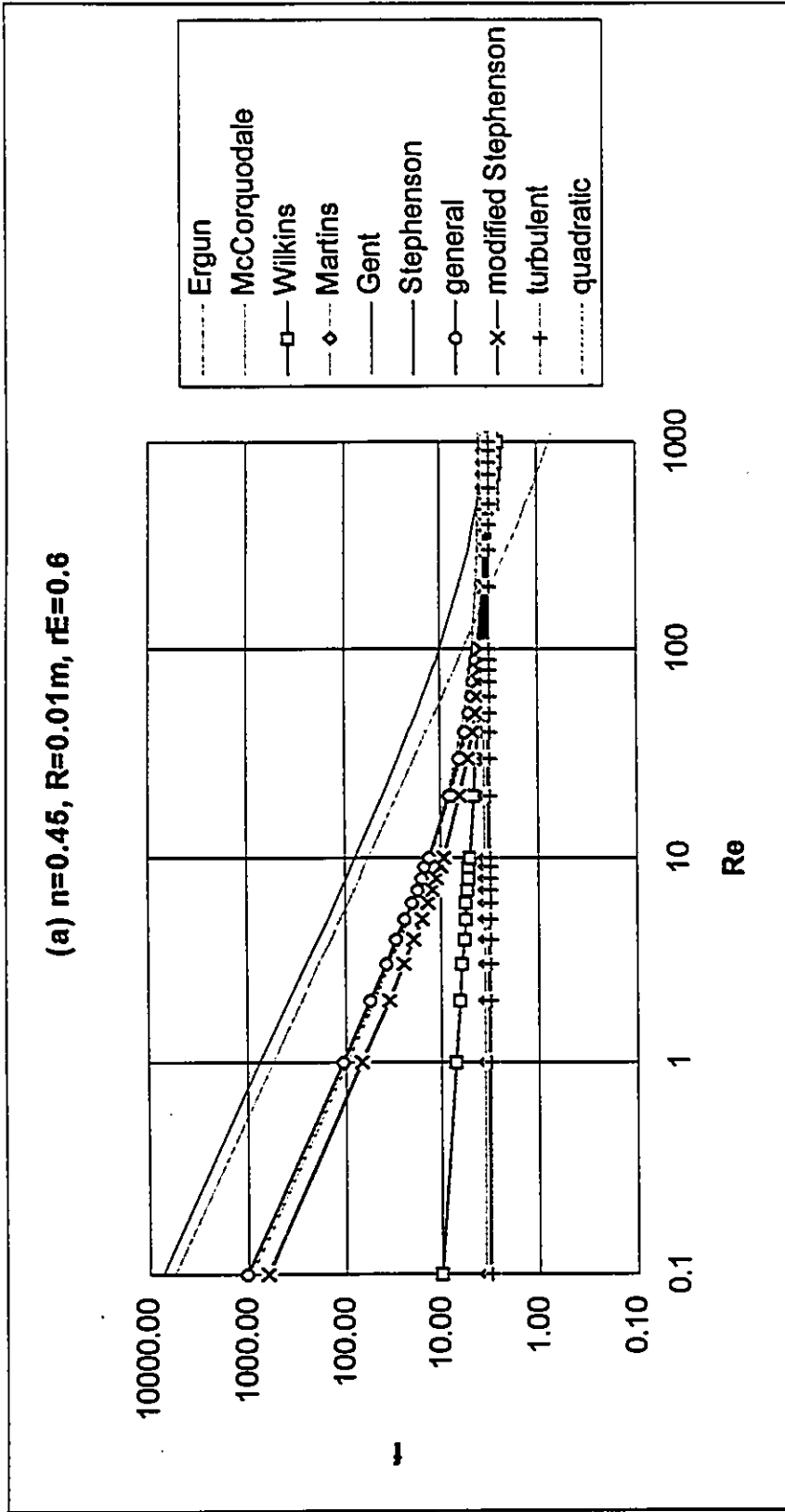


Figure 5 -10 Simulated Relationship between Re and f (a)

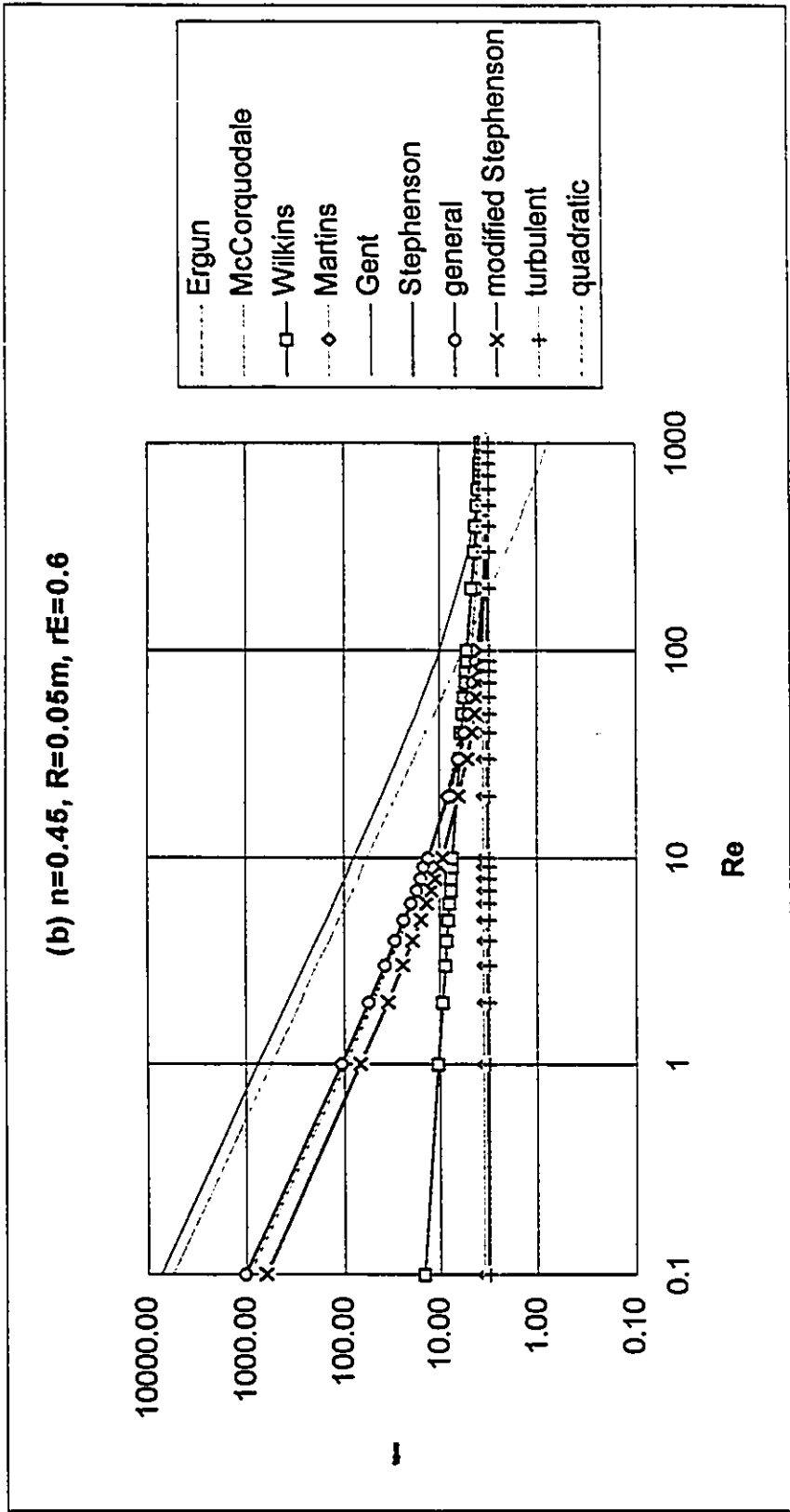


Figure 5 -11 Simulated Relationship between  $Re$  and  $f$  (b)

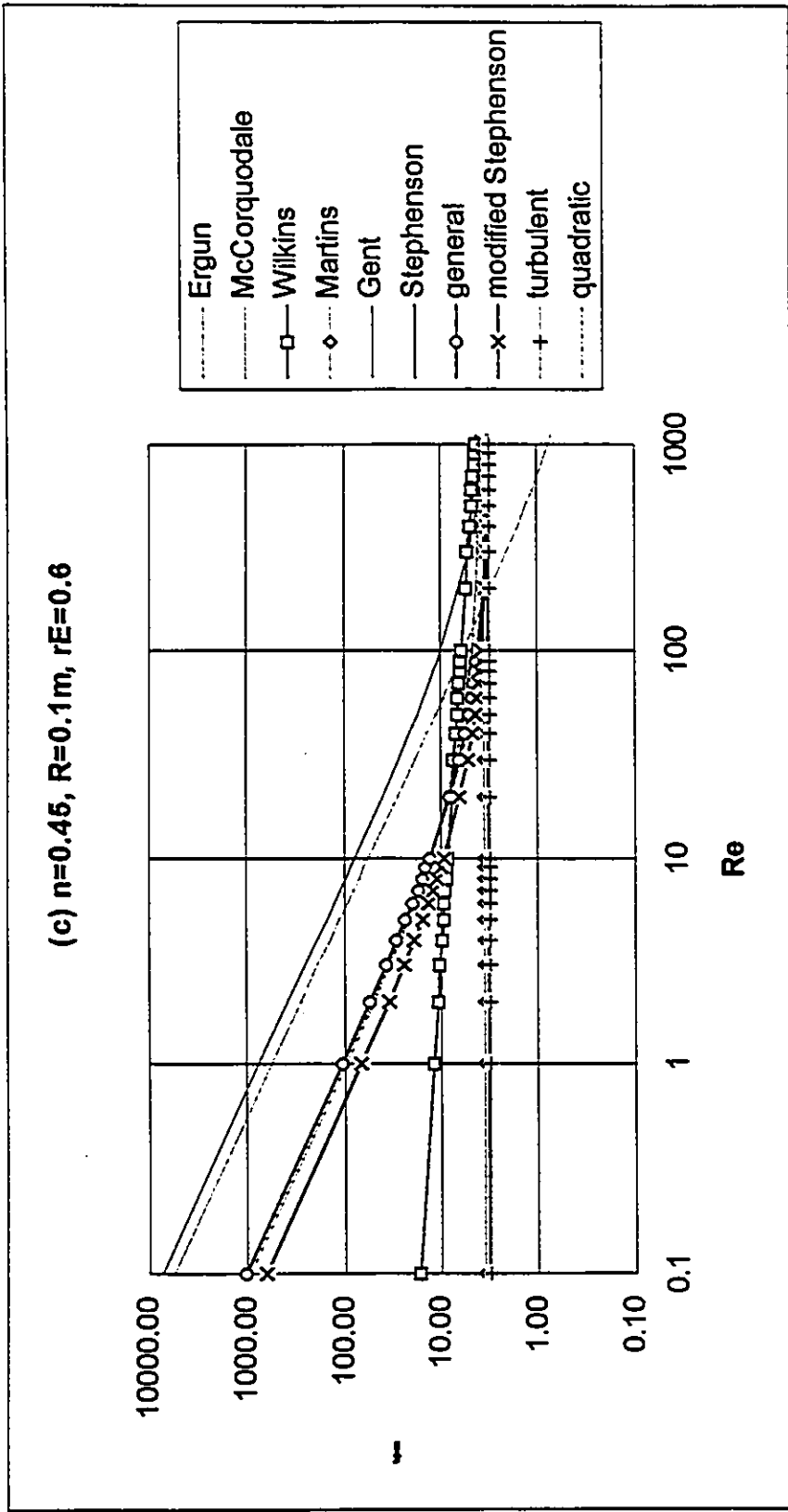


Figure 5 -12 Simulated Relationship between  $Re$  and  $f$  (c)

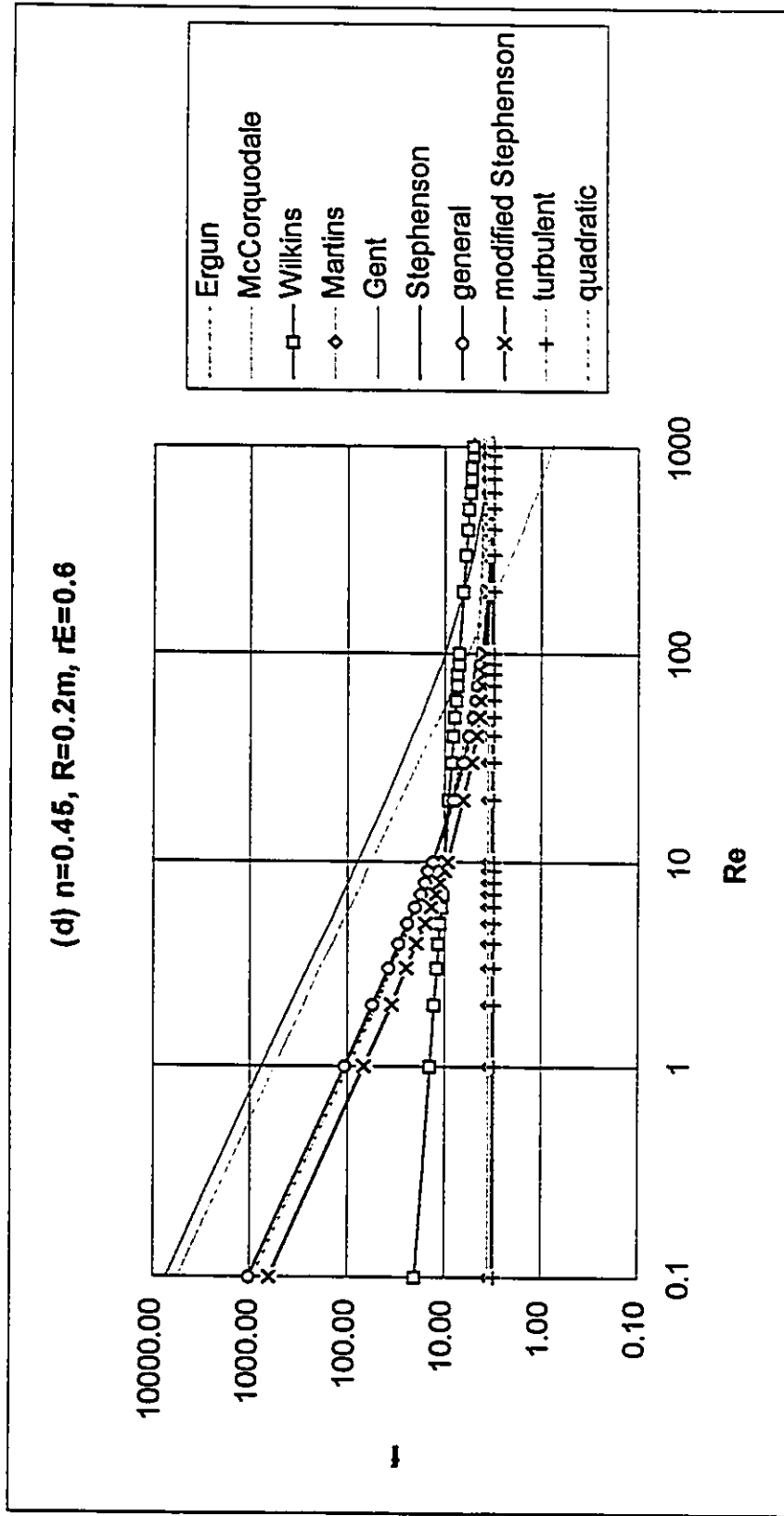


Figure 5 -13 Simulated Relationship between Re and f (d)

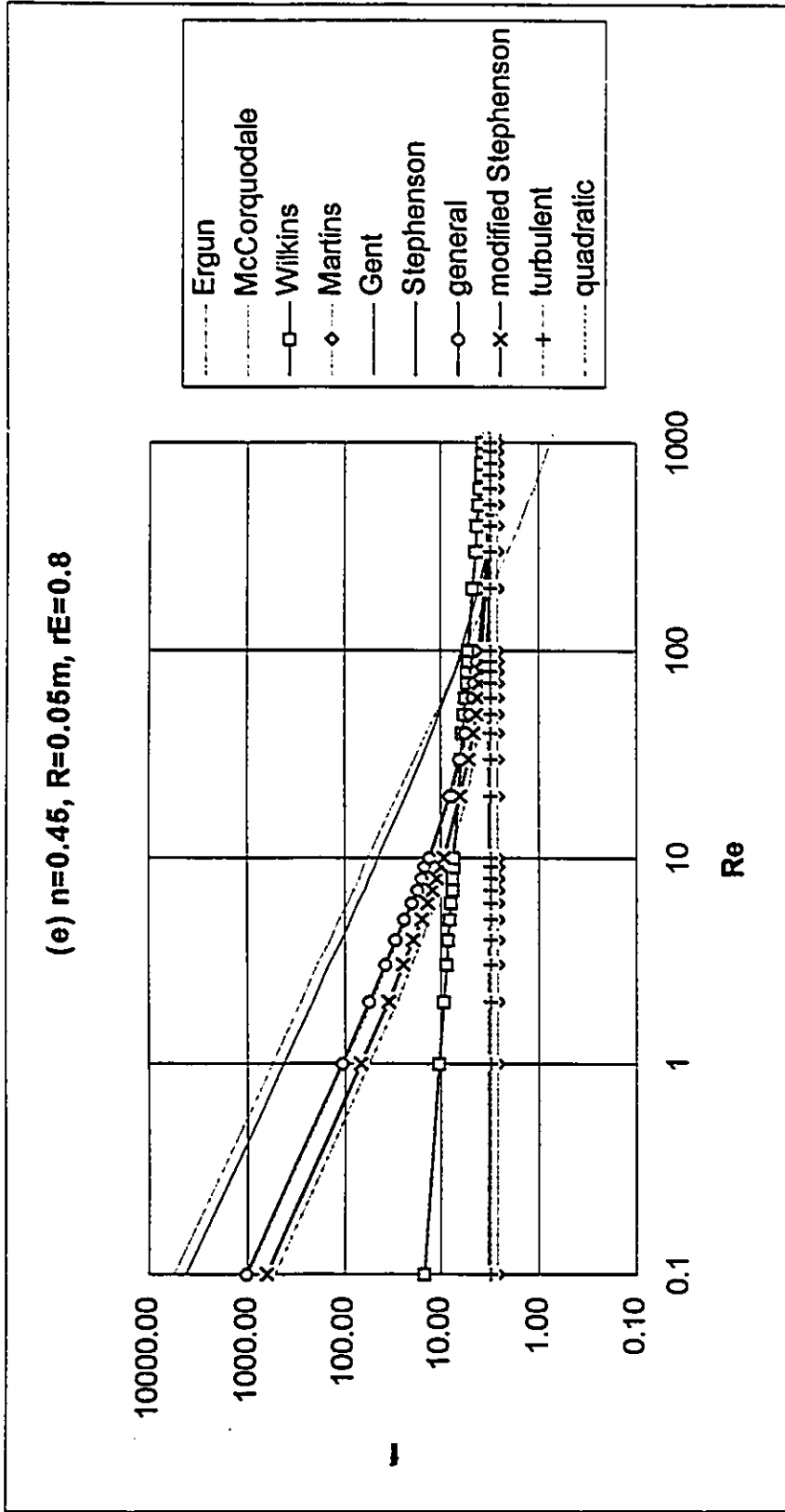


Figure 5 -14 Simulated Relationship between Re and f (e)

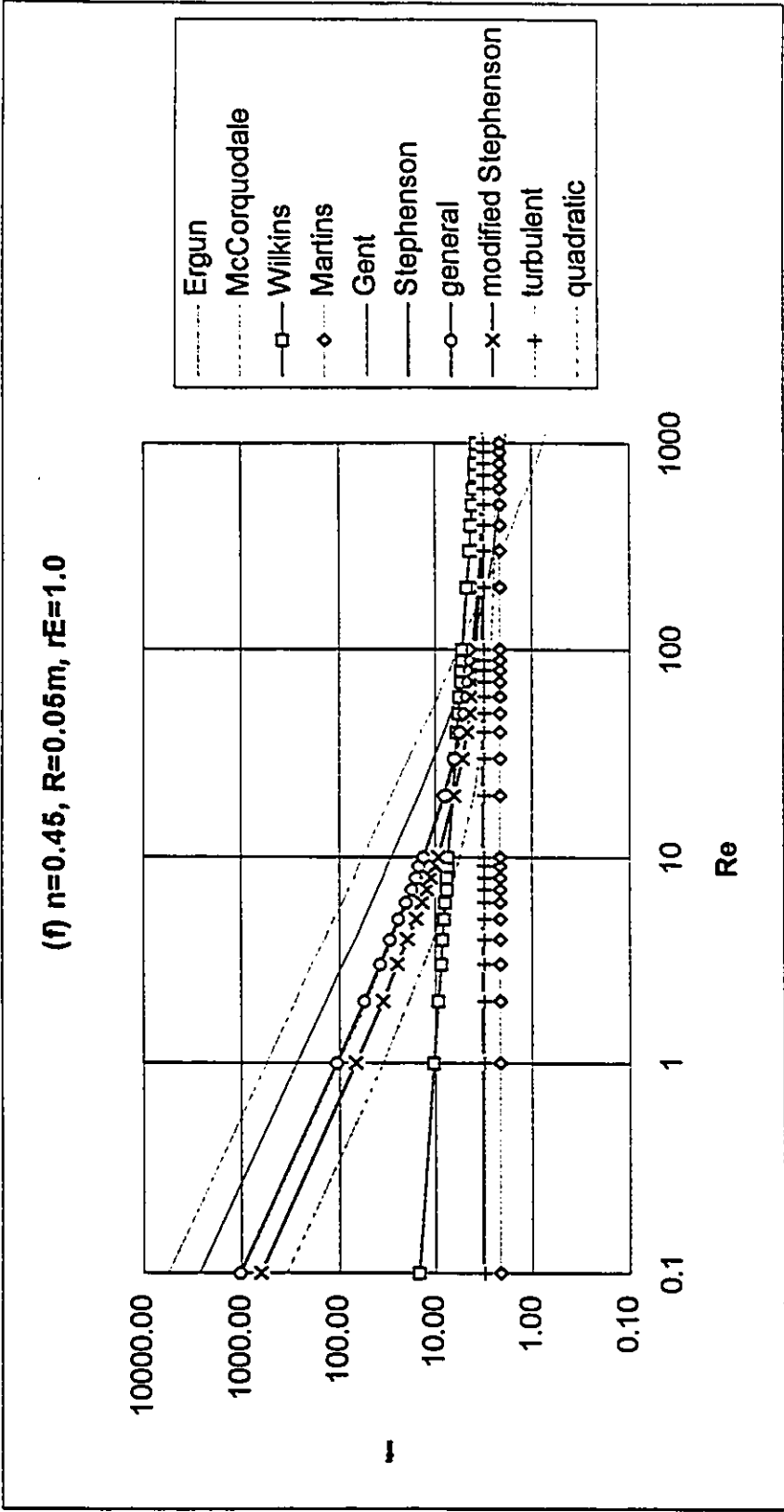


Figure 5 -15 Simulated Relationship between  $Re$  and  $f$  (f)

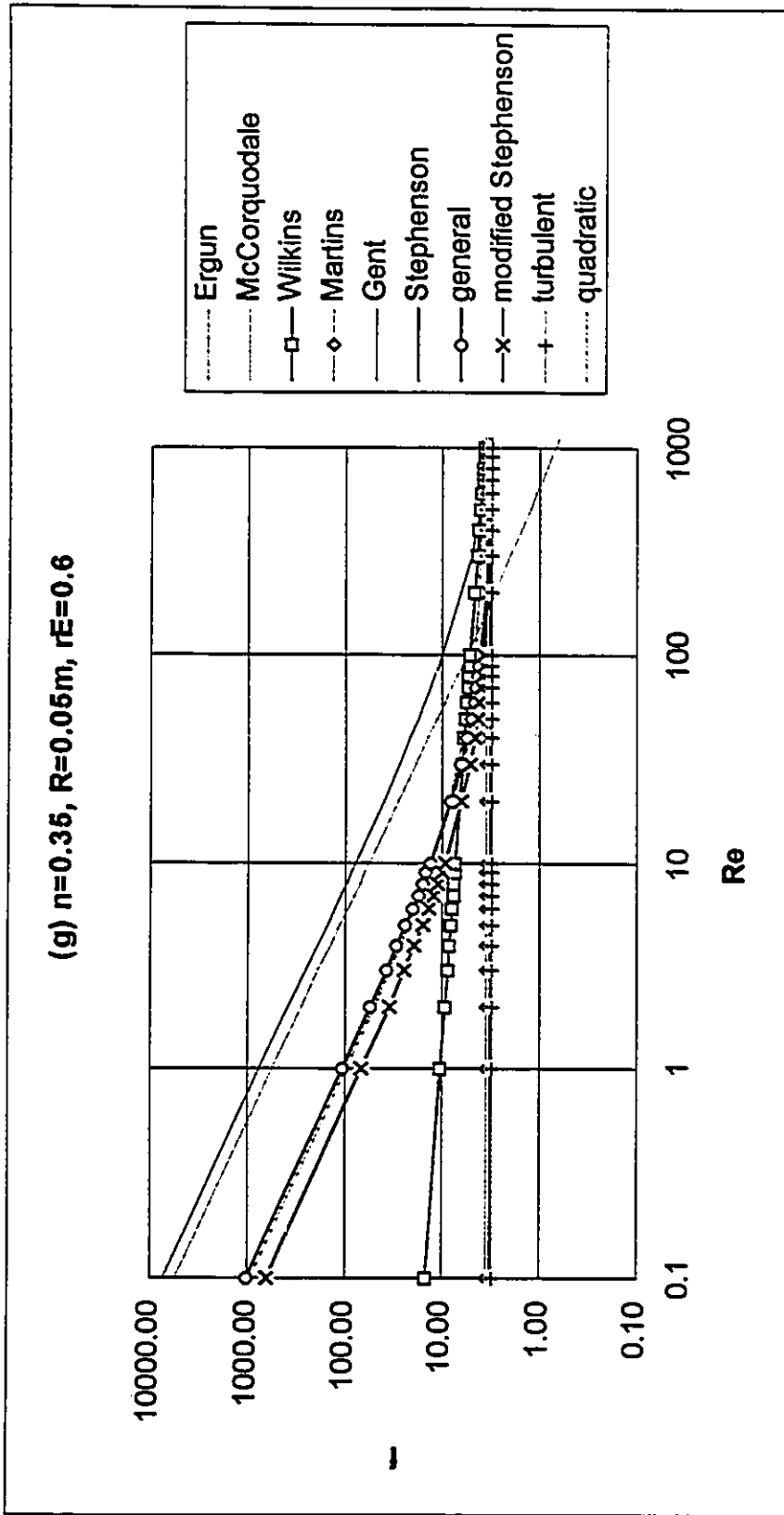


Figure 5 -16 Simulated Relationship between Re and f (g)

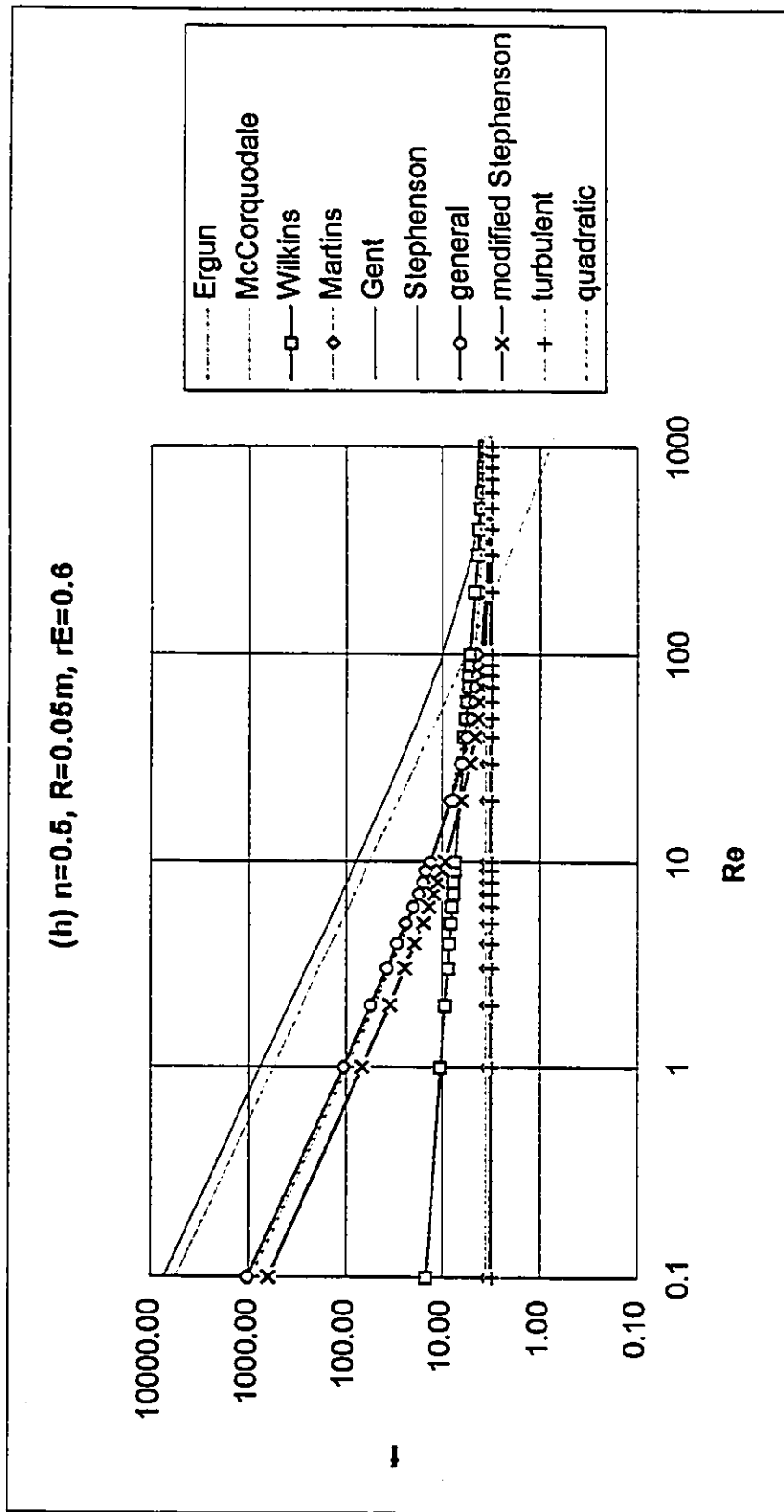
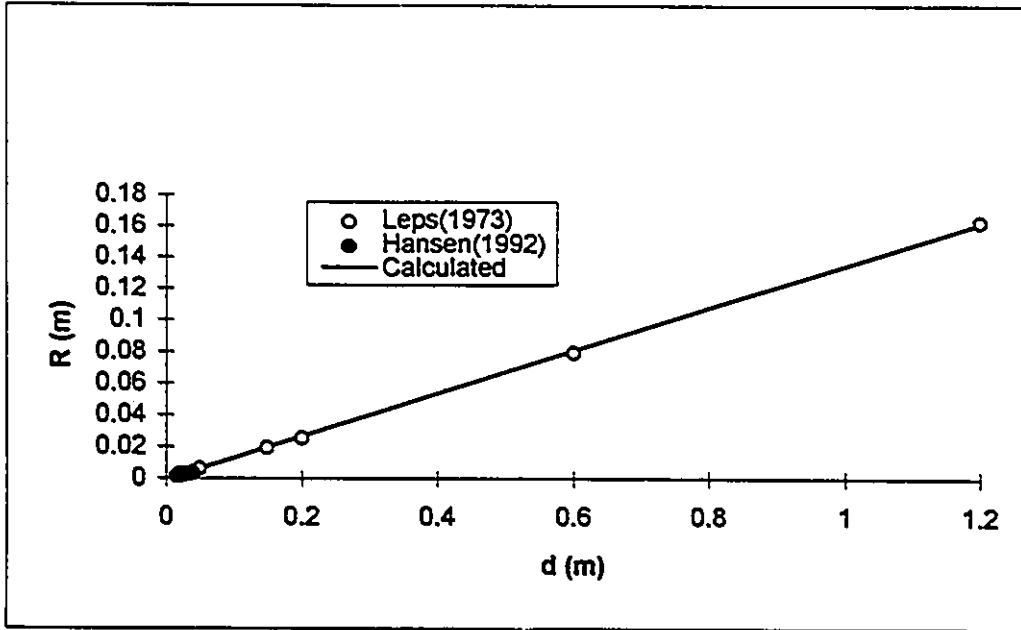
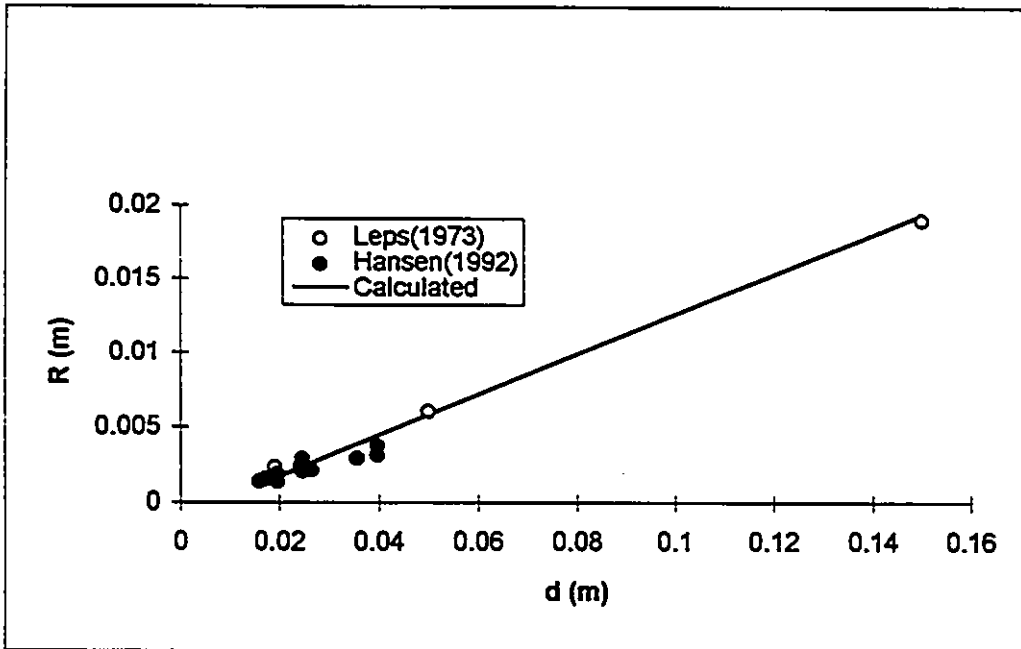


Figure 5 -17 Simulated Relationship between Re and f (h)



(a)  $d = 0 - 1.2$  m



(b)  $d = 0 - 0.16$  m

Figure 5-18 Relationship between Diameter and Hydraulic Mean Radius

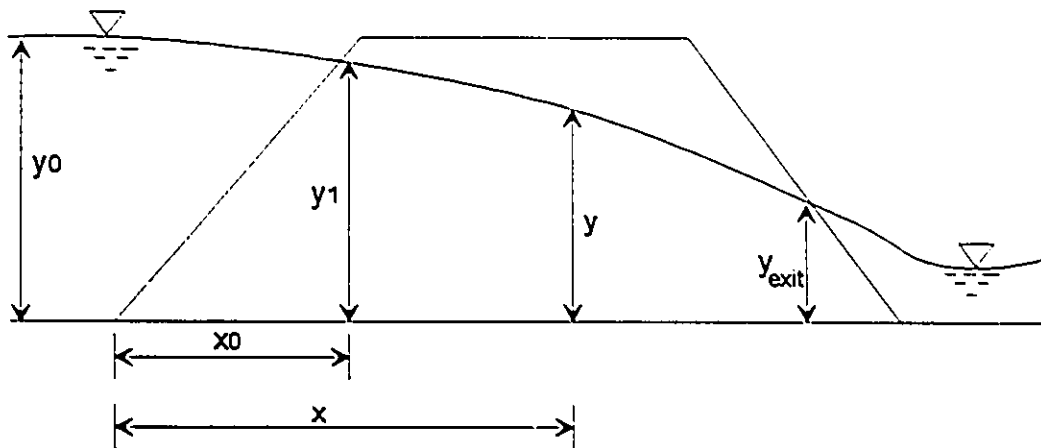


Figure 5-19 Definition of 1-D seepage flow in a dam

# Chapter 6 Finite Element Method for Non-Darcy Flow in Rockfill

## 6.1 Introduction

For non-Darcy flow in rockfill, the compressibility of rock particles and water are negligible.

Due to the difficulty in solving the 2-D non-Darcy seepage flow by hand sketching method, computer modelling is required to obtain an estimate of seepage force and pore pressure within rockfill dams. In order to solve the equation for the spatial varied flow at the downstream slope of a rockfill dam, the seepage velocity distribution near the downstream slope of a rockfill dam is needed. In order to study the unraveled failure condition and slope stability, the seepage forces and pore pressure distributions, the overtopping flow depth and velocity distributions, as well as the size of rock particles and the slope of the downstream slope are important input parameters. The complexity of the problem makes the design impossible without computer modelling.

It has been shown that the finite element method has the advantage in handling the problems with complicated boundary conditions. In this study, this method has been used to solve the non-linear equation for non-Darcy flow. As indicated by available publications on non-linear seepage flow simulations, the non-Darcy phreatic surface is much close to that for Darcy flow. This observation is very helpful in developing a finite element model with new linearization method.

Quadratic isoparametric quadrilateral element may be used in the model, as it has high accuracy and make it feasible to model the free water surface and complicated boundary conditions. For seepage flow with free surface, the free surface is unknown. An iteration technique is therefore required to obtain the solution. The numerical model

will provide discharge, and the hydraulic potential head at each node, and the hydraulic gradient and the velocity distribution at some nodes in the solution domain.

The assumption of the present study is that the rockfill material within a rockfill dam is a continuum media whose property is determined by the non-Darcy coefficients and the porosity. No deformation is considered in the model.

## 6.2 Governing Equations and Boundary Conditions

For non-Darcy flow in rockfill, the compressibility of rock particles and water are negligible. The continuity equation is

$$\frac{\partial u}{\partial x} + \frac{\partial v}{\partial y} = 0 \quad (6-1)$$

where  $u$  and  $v$  are the velocities in  $x$  and  $y$  directions respectively.

Using the continuity condition, Volker (1969) derived the 2-D governing equations for non-Darcy Flow. For quadratic law:

$$\begin{aligned} \frac{\partial}{\partial x} \left\{ \left[ -\frac{a}{2b} + \sqrt{\left(\frac{a}{2b}\right)^2 + \frac{|H_s|}{b}} \right] \frac{(-H_x)}{|H_s|} \right\} \\ + \frac{\partial}{\partial y} \left\{ \left[ -\frac{a}{2b} + \sqrt{\left(\frac{a}{2b}\right)^2 + \frac{|H_s|}{b}} \right] \frac{(-H_y)}{|H_s|} \right\} = 0 \end{aligned} \quad (6-2)$$

where  $a$  and  $b$  are the coefficients in the quadratic relationship between  $i$  and  $v$  defined in Chapter 5,  $H_x$  and  $H_y$  are the hydraulic gradients in  $x$  and  $y$  directions respectively,  $H_s$  is the total hydraulic gradient which is the vector sum of  $H_x$  and  $H_y$ .

For power law:

$$\frac{\partial}{\partial x} \left[ \left( \frac{|H_s|}{c_0} \right)^{1/c_1} \frac{(-H_x)}{|H_s|} \right] + \frac{\partial}{\partial y} \left[ \left( \frac{|H_s|}{c_0} \right)^{1/c_1} \frac{(-H_y)}{|H_s|} \right] = 0 \quad (6-3)$$

where  $c_0$  and  $c_1$  are the coefficients in the quadratic relationship between  $i$  and  $v$  defined in Chapter 5.

The above equations may be summarized as:

$$\frac{\partial}{\partial x} \left( k_x \frac{\partial H}{\partial x} \right) + \frac{\partial}{\partial y} \left( k_y \frac{\partial H}{\partial y} \right) = 0 \quad (6-4)$$

where  $k_x$  and  $k_y$  are the seepage coefficients in  $x$  and  $y$  directions respectively. They are defined as:

$$k = k_x = k_y = \frac{1}{\frac{a}{2} + \sqrt{\frac{a^2}{2} + b \frac{\partial H}{\partial s}}} \quad \text{for quadratic law,}$$

$$= \frac{1}{\frac{a}{2} + \sqrt{\frac{a^2}{2} + b \sqrt{\left( \frac{\partial H}{\partial x} \right)^2 + \left( \frac{\partial H}{\partial y} \right)^2}}} \quad (6-5)$$

$$k = k_x = k_y = c_0^{\frac{-1}{c_1}} \left( \frac{\partial H}{\partial s} \right)^{\frac{1-c_1}{c_1}}$$

$$= \frac{1}{c_0^{\frac{1}{c_1}}} \left[ \sqrt{\left( \frac{\partial H}{\partial x} \right)^2 + \left( \frac{\partial H}{\partial y} \right)^2} \right]^{\frac{1-c_1}{c_1}} \quad \text{for power law.}$$

(6-6)

Equations (6-4), (6-5), (6-6) are used in the computer modelling with finite element

method.

Two basic kinds of boundary appear in the problem.

(1) First or Dirichlet type boundary  $\Gamma_1$ :

$$H(x, y)|_{\Gamma_1} = H_0(x, y) \quad (6-7)$$

For the first type boundary, the value of the potential head  $H(x, y)$  is known along the boundary  $\Gamma_1$ .

(2) Second or Neumann boundary  $\Gamma_2$ :

$H(x, y)$  is unknown.

$$k_x \frac{\partial H}{\partial x} \cos(n, x) + k_y \frac{\partial H}{\partial y} \cos(n, y) = q \quad (6-8)$$

where  $q$  = unit discharge at the boundary  $\Gamma_2$ ;

$n$  = the direction normal to the boundary  $\Gamma_2$  acting outward from the solution domain (see Figure 6-1).

Hence, along the second boundary  $\Gamma_2$ , the discharge is known.

Figure 6-1 shows the problem domain and the boundary conditions. It is noticed that:

- Domain: OABCD;

-  $\Gamma_1$  boundary conditions:

$$OA: H = H_1 \quad (6-9)$$

$$BC: H = y(x) \quad (6-10)$$

$$CD: H = H_2 \quad (6-11)$$

-  $\Gamma_2$  boundary conditions:

$$OD: \text{Eq. (6-8) applies.}$$

- Free surface boundary:

Both (6-8) and (6-10) must be satisfied.

### 6.3 Quadratic Quadrilateral Element

One of the benefits of isoparametric elements is the accurate presentation of curved boundaries by using a quadratic polynomial for the interpolation function. There are eight nodes in the elements, i.e., four nodes at the four corners, and four nodes at the four mid-sides of the elements (Figure 6-2).

#### 6.3.1 Shape Function

The interpolation function in global coordinates is given by:

$$H(x,y)^c = \alpha_1 + \alpha_2 x + \alpha_3 y + \alpha_4 x^2 + \alpha_5 xy + \alpha_6 y^2 + \alpha_7 x^2 y + \alpha_8 xy^2 \quad (6-12)$$

where  $x$  and  $y$  denote the global coordinates of an element (see Figure 6-2).

The interpolation function in local coordinates is:

$$H(r,s)^c = \alpha_1 + \alpha_2 r + \alpha_3 s + \alpha_4 r^2 + \alpha_5 rs + \alpha_6 s^2 + \alpha_7 r^2 s + \alpha_8 rs^2 \quad (6-13)$$

where  $r$  and  $s$  are local coordinates of the element (see Figure 6-3).

Hence in local coordinates:

$$H(r,s)^{c(e)} = G_i H_i + G_j H_j + G_k H_k + G_l H_l + G_m H_m + G_n H_n + G_o H_o + G_p H_p \quad (6-14)$$

With shape functions:

$$G_i = \frac{1}{4} (1-r)(1-s)(-1-r-s) \quad (6-15)$$

$$G_j = \frac{1}{4} (1+r)(1-s)(-1+r-s) \quad (6-16)$$

$$G_k = \frac{1}{4} (1+r)(1+s)(-1+r+s) \quad (6-17)$$

$$G_l = \frac{1}{4} (1-r)(1+s)(-1-r+s) \quad (6-18)$$

$$G_m = \frac{1}{2} (1-r^2)(1-s) \quad (6-19)$$

$$G_n = \frac{1}{2} (1-s^2)(1+r) \quad (6-20)$$

$$G_o = \frac{1}{2} (1-r^2)(1+s) \quad (6-21)$$

$$G_p = \frac{1}{2} (1-s^2)(1-r) \quad (6-22)$$

### 6.3.2 Transformation from global coordinate to local coordinate

$$x = \{G\}_{1 \times 8} \{X\}_{8 \times 1} = \sum_{i=1}^8 G_i(r,s) X_i \quad (6-23)$$

$$y = \{G\}_{1 \times 8} \{Y\}_{8 \times 1} = \sum_{i=1}^8 G_i(r,s) Y_i \quad (6-24)$$

where

$X_i$  and  $Y_i$  denotes the global coordinates of the  $i$  th node (see Figure 6-2).

$$\{G\}_{1 \times 8} = \{G_i, G_j, G_k, G_l, G_m, G_n, G_o, G_p\} \quad (6-25)$$

$$\{X\}_{8 \times 1} = \{X_i, X_j, X_k, X_l, X_m, X_n, X_o, X_p\}^T \quad (6-26)$$

$$\{Y\}_{8 \times 1} = \{Y_i, Y_j, Y_k, Y_l, Y_m, Y_n, Y_o, Y_p\}^T \quad (6-27)$$

Define Jacobian matrix:

$$[J]_{2 \times 2} = \begin{bmatrix} \frac{\partial x}{\partial r} & \frac{\partial y}{\partial r} \\ \frac{\partial x}{\partial s} & \frac{\partial y}{\partial s} \end{bmatrix} = \begin{bmatrix} J_{11} & J_{12} \\ J_{21} & J_{22} \end{bmatrix} \quad (6-28)$$

The inverse of Jacobian matrix is:

$$[J]^{-1}_{2 \times 2} = \frac{1}{\det J} \begin{bmatrix} \frac{\partial y}{\partial s} & \frac{\partial y}{\partial r} \\ -\frac{\partial x}{\partial s} & \frac{\partial x}{\partial r} \end{bmatrix} = \frac{1}{\det J} \begin{bmatrix} J_{22} & -J_{12} \\ -J_{21} & J_{11} \end{bmatrix} \quad (6-29)$$

where

$$\det J = \begin{vmatrix} \frac{\partial x}{\partial r} & \frac{\partial y}{\partial r} \\ \frac{\partial x}{\partial s} & \frac{\partial y}{\partial s} \end{vmatrix} = \begin{vmatrix} J_{11} & J_{12} \\ J_{21} & J_{22} \end{vmatrix} \quad (6-30)$$

Hence:

$$\begin{Bmatrix} \frac{\partial}{\partial r} \\ \frac{\partial}{\partial s} \end{Bmatrix} = [J] \begin{Bmatrix} \frac{\partial}{\partial x} \\ \frac{\partial}{\partial y} \end{Bmatrix} \quad (6-31)$$

and

$$\begin{Bmatrix} \frac{\partial}{\partial x} \\ \frac{\partial}{\partial y} \end{Bmatrix} = [J]^{-1} \begin{Bmatrix} \frac{\partial}{\partial r} \\ \frac{\partial}{\partial s} \end{Bmatrix} \quad (6-32)$$

### 6.3.3 Gauss Quadrature Integration

Several schemes for numerical integration are available, but the Gauss quadrature approach is the most widely found (Allaire, 1985, pp. 471). Here we will use the Gauss quadrature integration approach.

The numerical integration of function  $g(x)$  may be expressed as:

$$\int_{-1}^1 g(x) dx = \sum_{i=1}^N w_i g(R_i) \quad (6-33)$$

where  $N$  is the number of nodes,  $w_i$  is weighting factor, and  $R_i$  the location of sampling point. 3x3-point Gauss quadrature integration method is used in the present finite element model for high accuracy ( $\Delta x^5$ , where  $\Delta x$  is the size of an element). Table 6-1 lists the values of  $w_i$  and  $R_i$  for the integration of 1-dimension function  $g(x)$ .

For a two dimensional function  $g(x,y)$ , the Gaussian numerical integration for  $N_G \times N_G$  integration nodes is:

$$\int_{-1}^1 \int_{-1}^1 g(x,y) dx dy = \sum_{i=1}^{N_G} \sum_{j=1}^{N_G} w_i w_j g(x_i, y_j) \quad (6-34)$$

Figure 6-4 shows the Gauss quadrature integration points in the 2-dimension global coordination.

By the shape functions given above, the potential head interpolation function in

element  $e_i$  is given by Eq. (6-14) which may be written as:

$$H_{e_i} = \sum_{j=1}^8 G(r,s) H_j \quad (6-35)$$

where  $H_j$ ,  $j=1, 2, \dots, 8$ , are the potential head values at each node (see Fig. 6-2). In element  $e_i$ ,  $H_{e_i}$  can replace the unknown potential head function  $H(x,y)$ .

## 6.4 Variational Method

Three methods, i.e., direct, variational, and residual, are available to formulate the finite element equations.

The direct method was originally used to develop the finite element method for aircraft structures in the early 1950s. Today direct methods are still employed in structural analysis. Physically all parameters employed in this method may be interpreted on physical grounds. But the method is difficult to apply to 2-D or 3-D problems. It does not apply to our problem.

The variational method involves a quantity called a function (variational function here). The finite element equations come by minimizing the derivatives of the variational function. The advantage of the variational method, which is the most popular of the three methods for solid mechanics problems, include the familiarity of energy techniques in solid mechanics and easy extension to 2-D and 3-D problems. The disadvantage of variational method is that for a lot of problems, the variational function is not found by mathematician. For the governing equations and boundary conditions of our problem, the variational function is available (Allarie, 1985, pp. 318). Here it is not necessary to list it. Variational method will be used in this study.

The residual method is the most general of the three techniques and, also, the most difficult to understand physically. In this method, it is assumed that the exact solution is unknown. Instead, some approximation of the exact solution is employed. Substitution

of the approximate solution into the differential equation results in an erroneous value  $r$ , rather than zero. The error  $r$  is then multiplied by a weighting function, and the product is integrated over the solution region. The result of the integration is called residual  $R$  and is set to zero. Actually, there is a weighting function and a residual  $R$  for each unknown nodal value, so that the result is a global set of algebraic equations which are the equations of the finite element method. Residual method is the popular method for problems where the variational function is not found. As for our problem, the variational function is known. Hence variational method is used.

With Eq. (6-35) the variational function in the whole solution domain may be expressed by:

$$E(H) = \sum_{i=1}^M E^e(H) = \sum_{i=1}^M E^e(H_{c_i}) = E(\bar{H}) \quad (6-36)$$

where  $\bar{H}$  is a function of  $H_j$ ,  $M$  is total number of elements,  $j=1, 2, \dots, n$ .  $n$  is the total number of nodes with unknown potential head.

By minimizing  $E(\bar{H})$ , the following expression should be satisfied:

$$\frac{\partial E(\bar{H})}{\partial H_i} = 0, \quad i = 1, 2, 3, \dots, n \quad (6-37)$$

Substituting Eq. (6-36) into Eq. (6-37), it may be obtained:

$$\frac{\partial E(\bar{H})}{\partial H_i} = \frac{\partial}{\partial H_i} \sum_{j=1}^M E^e(H_{c_j}) = \sum_{j=1}^M \frac{\partial}{\partial H_i} E^e(H_{c_j}) = 0 \quad (6-38)$$

Since the value of Eq. (6-38) is associated with the total number of elements around the node  $i$ , say  $M_i$ , and the property of shape function:

$$G_i(r_j, s_j) = \begin{cases} 1, & i = j; \\ 0, & i \neq j. \end{cases} \quad (6-39)$$

we have:

$$\frac{\partial E(\bar{H})}{\partial H_i} = \sum_{j=1}^M \frac{\partial}{\partial H_i} E^e(H_{e_j}) = 0 \quad (6-40)$$

Hence, for each node with unknown potential head, a numerical equation may be constructed. n equations can be built, which may be solved numerically to calculate the  $H_i$  term for all the n nodes.

## 6.5 Formation of Element Matrix

In each element e, by variation method:

$$\begin{aligned} \frac{\partial E^e(H)}{\partial H_i} = & \iint_e \left( k_x \frac{\partial H}{\partial x} \frac{\partial}{\partial H_i} \left( \frac{\partial H}{\partial x} \right) + k_y \frac{\partial H}{\partial y} \frac{\partial}{\partial H_i} \left( \frac{\partial H}{\partial y} \right) \right) \\ & - \int_{\Gamma_2 \cap e} q \frac{\partial H}{\partial H_i} d\Gamma_2 \end{aligned} \quad (6-41)$$

Assuming that  $k_x$  and  $k_y$  are constants within each element, one may obtain:

$$\left\{ \frac{\partial E^e(H)}{\partial H_i} \right\} = [h^e]_{8 \times 8} \{H\}_{8 \times 1} + \{f^e\} \quad (6-42)$$

where:

$$[h^e] = \begin{bmatrix} h_{11}^e & h_{12}^e & h_{13}^e & h_{14}^e & h_{15}^e & h_{16}^e & h_{17}^e & h_{18}^e \\ h_{21}^e & h_{22}^e & h_{23}^e & h_{24}^e & h_{25}^e & h_{26}^e & h_{27}^e & h_{28}^e \\ h_{31}^e & h_{32}^e & h_{33}^e & h_{34}^e & h_{35}^e & h_{36}^e & h_{37}^e & h_{38}^e \\ h_{41}^e & h_{42}^e & h_{43}^e & h_{44}^e & h_{45}^e & h_{46}^e & h_{47}^e & h_{48}^e \\ h_{51}^e & h_{52}^e & h_{53}^e & h_{54}^e & h_{55}^e & h_{56}^e & h_{57}^e & h_{58}^e \\ h_{61}^e & h_{62}^e & h_{63}^e & h_{64}^e & h_{65}^e & h_{66}^e & h_{67}^e & h_{68}^e \\ h_{71}^e & h_{72}^e & h_{73}^e & h_{74}^e & h_{75}^e & h_{76}^e & h_{77}^e & h_{78}^e \\ h_{81}^e & h_{82}^e & h_{83}^e & h_{84}^e & h_{85}^e & h_{86}^e & h_{87}^e & h_{88}^e \end{bmatrix} \quad (6-43)$$

$$f_i^e = - \int_{\Gamma_2 \cap e} q N_i ds \quad (6-44)$$

$$h_{ij}^e = \iint_e \{B_i\}^T [M] \{B_j\} dx dy \quad (6-45)$$

in which

$$\{B_i\} = \begin{bmatrix} \frac{\partial G_i}{\partial x} \\ \frac{\partial G_i}{\partial y} \end{bmatrix} \quad (6-46)$$

$$[M] = \begin{bmatrix} k_x & 0 \\ 0 & k_y \end{bmatrix} \quad (6-47)$$

It should be kept in mind that  $k_x$  and  $k_y$  are not constants but depend on the hydraulic gradients.

As

$$\begin{bmatrix} \frac{\partial G_i}{\partial x} \\ \frac{\partial G_i}{\partial y} \end{bmatrix} = [J^{-1}] \begin{bmatrix} \frac{\partial G_i}{\partial r} \\ \frac{\partial G_i}{\partial s} \end{bmatrix} \quad (6-48)$$

and

$$dx dy = |J| dr ds \quad (6-49)$$

Eq. (6-42) may become:

$$h_{ij}^e = \int_{-1}^1 \int_{-1}^1 \{B_i\}^T [J^{-1}]^T [M] [J^{-1}] \{B_j\} |J| dr ds \quad (6-50)$$

where

$$\{B_i\} = \begin{bmatrix} \frac{\partial G_i}{\partial r} \\ \frac{\partial r}{\partial G_i} \\ \frac{\partial G_i}{\partial s} \end{bmatrix} \quad (6-51)$$

Now let

$$h_{ij}^e = \{B_i\}^T [J^{-1}]^T [M] [J^{-1}] \{B_j\} |J| \quad (6-52)$$

we have

$$h_{ij}^e = \int_{-1}^1 \int_{-1}^1 h(r,s) dr ds = \sum_{i=1}^{N_G} \sum_{j=1}^{N_G} w_i w_j h(r_i, s_j) \quad (6-53)$$

where  $N_G$  = the number of total Gauss Integration Points. It is noticed that matrix  $[M]$  depends on the hydraulic gradients acting on the element and hence velocity of the flow within the element.

## 6.6 Formation of the Global Equations

In the previous section 6.5, only one element was considered. The objective is to for all the elements in the solution domain, build corresponding equation, then sum up with Eq. (6-40).

For readability, we rewrite Eq. (6-40):

$$\sum_{j=1}^M \frac{\partial}{\partial H_i} E^{c_j}(H_{c_j}) = 0, \quad i=1, 2, \dots, N. \quad (6-54)$$

Therefore for  $n$  unknown values of potential head  $H_i$ ,  $i=1, 2, \dots, n$ , there are  $n$  equations, which may be expressed in the form of matrix as:

$$[K']_{N \times N} \{H'\}_{1 \times N} + \{f\}_{1 \times N} = 0 \quad (6-65)$$

where

$$K'_{ij} = \sum_{j=1}^M h_{ij}^{c_j} \quad (6-66)$$

$$\{H'\} = \begin{Bmatrix} H_1 \\ H_2 \\ H_3 \\ \vdots \\ H_n \\ H_{n+1} \\ \vdots \\ H_N \end{Bmatrix} \quad (6-67)$$

$$\{f\} = \begin{Bmatrix} \sum_{j=1}^{M_1} f_1 c_j \\ \sum_{j=1}^{M_2} f_2 c_j \\ \vdots \\ \sum_{j=1}^{M_n} f_n c_j \\ \sum_{j=1}^{M_{n+1}} f_{n+1} c_j \\ \vdots \\ \sum_{j=1}^{M_N} f_N c_j \end{Bmatrix} \quad (6-68)$$

where N is the total number of nodes in the solution domain.

$H_i$  ( $j=1, 2, \dots, n$ ) is unknown, while  $H_i$  ( $j=n+1, n+2, \dots, N$ ) is known ( $\Gamma_1$  boundary). Inserting the (N-n) known potential values into Eq. (6-65), the final global equation may be obtained:

$$[K]_{n \times n} \{H\}_{1 \times n} = \{F\}_{1 \times n} \quad (6-69)$$

where

$$\{H\} = \begin{Bmatrix} H_1 \\ H_2 \\ \vdots \\ H_{n-1} \\ H_n \end{Bmatrix} \quad (6-70)$$

[K] is a diagonally symmetric and positively definite matrix in which most elements have zero value (sparse matrix). {F} is known. Hence, when [K] include only constants, Eq. (6-69) represents a system of linear equations ( n equations with n unknown variables, i.e.,  $H_i$ ,  $i=1, 2, \dots, n$ ). From the discussion at the end of the previous section, it is noticed that the matrix [K] depends on the hydraulic gradients at nodes which are not known. Hence, Eq. (6-69) is nonlinear. This is one of the main difficulties in the

solution. Another one is that for free surface problems, the location of the free surface is unknown.

## 6.7 FEM Solution for Non-Darcy Flow in Rockfill

The program developed in this paper is for general use in engineering design. It can be used for 2-D Darcy flow with free surface, 2-D confined Darcy flow, 2-D non-Darcy flow with free surface, and 2-D confined non-Darcy flow. In this section, solution for free surface Darcy seepage flow and non-Darcy seepage flow is described. For confined Darcy seepage flow and non-Darcy seepage flow, the only thing to do is to set the maximum iteration number for free surface as 1 in the input data. No change is necessary in the program.

The two difficulties mentioned at the end of the previous section make the direct solution of Eq. (6-69) impossible. The current method used to solve the system of equations is described in following steps:

6.7.1 Assuming the values of  $k_x$  and  $k_y$ , solve Eq. (6-69) for Darcy flow with free surface. The program allows anisotropy in permeability to be considered for Darcy flow.

(1) Value of  $k_x$  and  $k_y$  based on the least square method:

For Darcy flow:

$$i = \frac{v}{k} \quad (6-71)$$

For most rockfill dams,

$$k = k_x = k_y \quad (6-72)$$

Figure 6-5 shows the relationships between  $i$  and  $v$ . The curve for non-Darcy law is

known, while the curve for Darcy law is derived from the non-Darcy law by the least square method.

a. Power Law

From Chapter 5, the power relationship between  $i$  and  $v$  is:

$$i = c_0 v^{c_1} \quad (6-73)$$

Define

$$\text{Diff1} = \int_{v_1}^{v_2} (c_0 v^{c_1} - \frac{v}{k})^2 dv \quad (6-74)$$

As usually in the fluid field, the minimum velocity is zero,  $v_1$  may be set as zero. From Eq. (6-74), it is derived that:

$$\text{Diff1} = \frac{c_0}{2c_1 + 1} v_2^{2c_1 + 1} - \frac{2c_0}{k(2 + c_1)} v_2^{2+c_1} + \frac{v_2^3}{3k^2} \quad (6-75)$$

$$\frac{\partial \text{Diff1}}{\partial (\frac{1}{k})} = \frac{2c_0}{2 + c_1} v_2^{2+c_1} + \frac{2 v_2^3}{3k^2} \quad (6-76)$$

By setting:

$$\frac{\partial \text{Diff1}}{\partial (\frac{1}{k})} = 0 \quad (6-77)$$

the value for  $k$  is derived as:

$$k = \frac{2 + c_1}{3 c_0} v_2^{1-c_1} \quad (6-78)$$

b. Quadratic Law

From Chapter 5, the quadratic relationship between  $i$  and  $v$  is:

$$i = av + bv^2 \quad (6-79)$$

Define

$$\text{Diff2} = \int_{v_1}^{v_2} (av + bv^2 - \frac{v}{k})^2 dv \quad (6-80)$$

Let  $v_1$  be zero, one may obtain:

$$\text{Diff2} = \left(a - \frac{1}{k}\right)^2 \frac{v_2^3}{3} + \frac{b^2 v_2^5}{5} + \frac{b}{2} \left(a - \frac{1}{k}\right) v_2^4 \quad (6-81)$$

By:

$$\frac{\partial \text{Diff2}}{\partial \left(\frac{1}{k}\right)} = -2 \left(a - \frac{1}{k}\right) \frac{v_2^3}{3} - \frac{b}{2} v_2^4 = 0 \quad (6-82)$$

it is obtained:

$$k = \frac{1}{a + \frac{3}{4} b v_2} \quad (6-83)$$

(2) Assuming the free surface, solve for the Darcy flow. The flow chart is shown in Fig. 6-6.

(i) The program reads the read necessary data about the mesh size, coordinates of control points in the mesh, information about the condition of the flow (Darcy or non-

Darcy flow, free surface seepage flow or confined seepage flow, if non-Darcy flow either power law or quadratic law to be used), the seepage coefficients.

- (ii) Assume the free surface and generate mesh;
- (iii) For each element, build element matrix.
- (iv) Build the global equations.
- (v) Insert boundary conditions and solve the global equations.
- (vi) Check the values of head potential at the free surface to see if the difference between the calculated value and previous assumed value is less than the tolerance. If yes, go to step vii; otherwise go to step (ii).
- (vii) Calculate hydraulic gradient, velocity, and discharge.

In Figure 6-6, the DiffHSurf is defined as:

$$\text{DiffHSurf} = \begin{cases} \frac{|H_t^{\text{Free surface}} - H_{t-1}^{\text{Free surface}}|}{|H_t^{\text{Free surface}}|}, & \text{when } |H_t^{\text{Free surface}}| > 0.00001 \\ |H_t^{\text{Free surface}} - H_{t-1}^{\text{Free surface}}|, & \text{when } |H_t^{\text{Free surface}}| \leq 0.00001 \end{cases} \quad (6-84)$$

6.7.2 Using Eqs. (6-5) and (6-6), calculate the non-Darcy coefficient based on the hydraulic gradient calculated in the above calculations. Eq. (6-5) is valid for quadratic law, while Eq. (6-6) is used for power law (both options are provided in the program).

6.7.3 Solve the fluid field by the finite element model described in 6.7.1 with non-Darcy coefficient obtained in section 6.7.2.

6.7.4 Calculate the following expression for all nodes in the solution domain:

$$\text{DiffH} = \begin{cases} \frac{|H_t^{\text{Any node}} - H_{t-1}^{\text{Any node}}|}{|H_t^{\text{Any node}}|}, & \text{when } |H_t^{\text{Any node}}| > 0.00001 \\ |H_t^{\text{Any node}} - H_{t-1}^{\text{Any node}}|, & \text{when } |H_t^{\text{Any node}}| \leq 0.00001 \end{cases} \quad (6-85)$$

check if the DIFFH < Tolerance for all the nodes. If this not true for any node, go to 6.7.2, until for all the nodes, DIFFH < Tolerance.

6.7.5 Calculate the discharge, and print the output.

It is emphasized that the program developed above can equally be applied to Darcy unconfined flow, and Darcy and non-Darcy confined flow conditions. Several control switches are provided in the input data file to cater for the above conditions as desired.

## 6.8 Example Solution of the FEMND2D for Non-Darcy Flow in Rockfill

In order to verify if the developed FEMND2D program is reasonable, simulations were for comparison with the experimental results from McCorquodale (1970) and from Volker (1969). McCorquodale (1970) carried out experiments in a hydraulic flume using uniform sized particles with  $d_{50} = 1.6$  cm; while Volker (1969) used  $d$  size of 1.9 cm in similar experiments.

Figure 6-8 shows the simulation result of one set of data from McCorquodale (1970). The total number of elements is 30. It is noticed that

- (1) the free surface of Darcy law is lower than that of experiment with maximum error of 6%;
- (2) the free surface of non-Darcy flow are very close to that from experiment with

maximum relative error of 1%;

(3) the isopotential lines for non-Darcy flow are closer to that of the experiment than the Darcy flow lines.

The discharge obtained from experiment is  $454 \text{ cm}^3 / \text{s/cm}$ . The discharge from non-Darcy flow is  $482 \text{ cm}^3 / \text{s/cm}$ , with relative error of 6.2% which is acceptable. The discharge from Darcy flow is  $349 \text{ cm}^3 / \text{s/cm}$ , with relative error 23.1% which is much larger than that predicted by non-Darcy flow.

Figure 6-9 shows the simulation result of the dam model examined by Volker (1969). The total number of elements in the above simulation by FEMND2D was only 36. The simulation results are similar to that obtained by Volker (1969). The free surface of the experiment is between that of the non-Darcy flow and the Darcy flow. Here that of the non-Darcy flow is the highest. Both free surface curves of Darcy flow and non-Darcy flow are close to that of experiment with maximum relative error 2%. The measured discharge of experiment was  $0.114 \text{ ft}^3 / \text{s/ft}$ . The Darcy flow discharge is  $0.09 \text{ ft}^3 / \text{s/ft}$ , 21% less than that from the experiment. The non-Darcy flow discharge is  $0.122 \text{ ft}^3 / \text{s/ft}$ , 7% more than that measured in the experiment.

## 6.9 Conclusions

In this chapter, a finite element method for 2-dimension non-Darcy flow with 8 nodes quadratic isoparametric elements has been developed.

(1) According to the governing equation and boundary conditions, the mathematical aspects of quadratic quadrilateral element and the variational method were applied to develop the element matrix and global equations with unknown head potentials as variables;

(2) To solve the nonlinear problem, a linearization method was developed. The initial

Darcy coefficients were obtained based on the least squared method. Formulae were derived for both power law and quadratic law for non-Darcy flow. Iterations are performed for both the free surface of seepage flow and the non-Darcy coefficients in Eq. (6-4).

(3) Example simulations and comparisons with experimental results show that the model developed provides very reasonable results.

Table 6-1 Location of Sampling Points and Weighting Factors for Gauss Quadrature  
(after Allaire, 1985)

Number of Points N	Location of Sampling Points $R_i$	Weighting Factor ( $w_i$ /Area)
1	0.0	2.0
2	$\pm 0.5773502692$	1.0
3	0.0	0.8888888889
	$\pm 0.7745966692$	0.5555555556

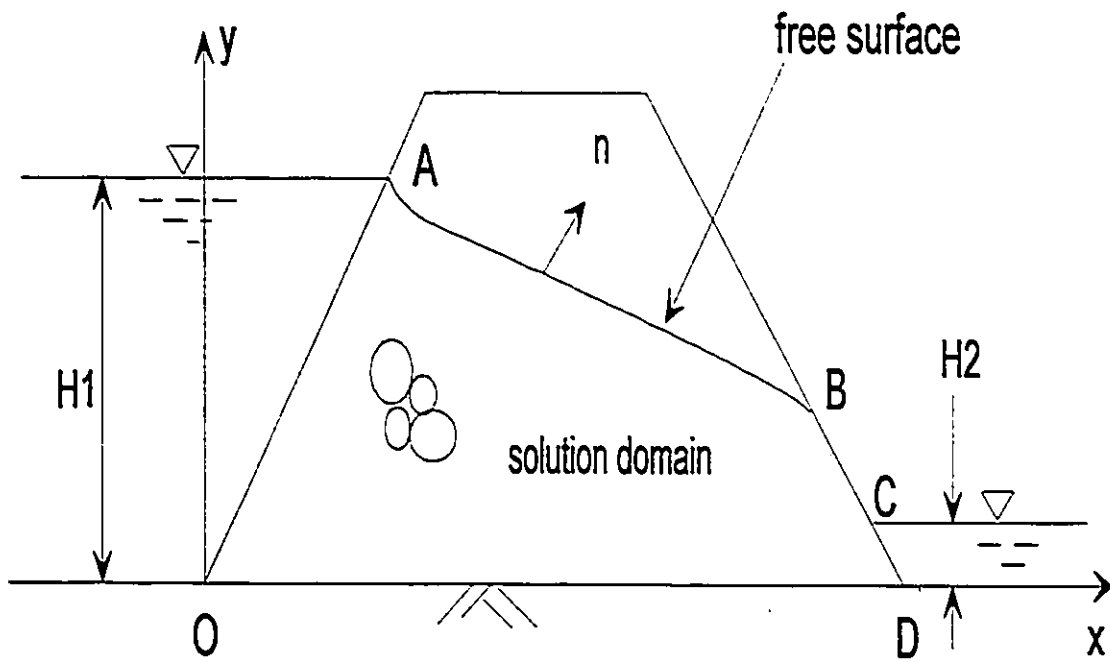


Figure 6-1 Boundary Condition

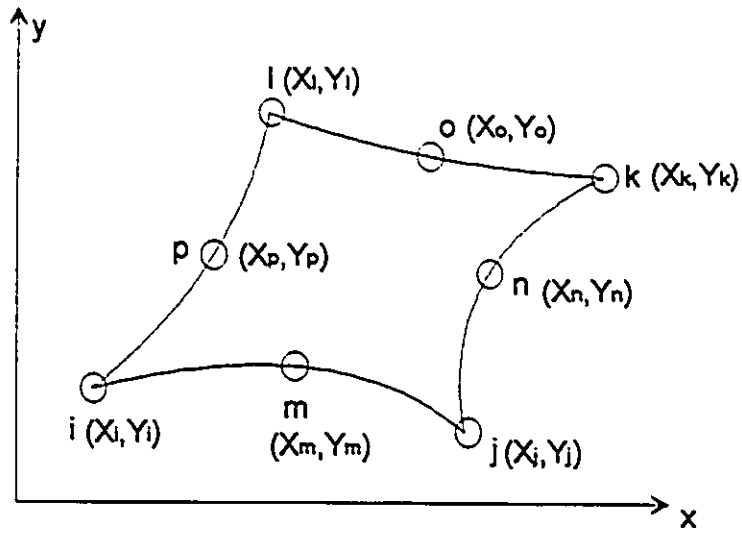


Figure 6-2 Element in global coordinates

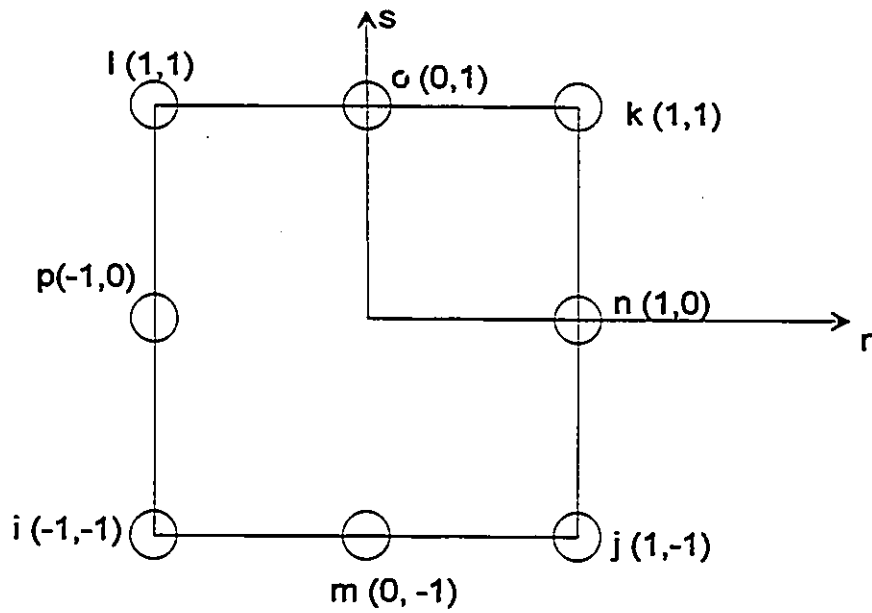


Figure 6-3 Element in local coordinates

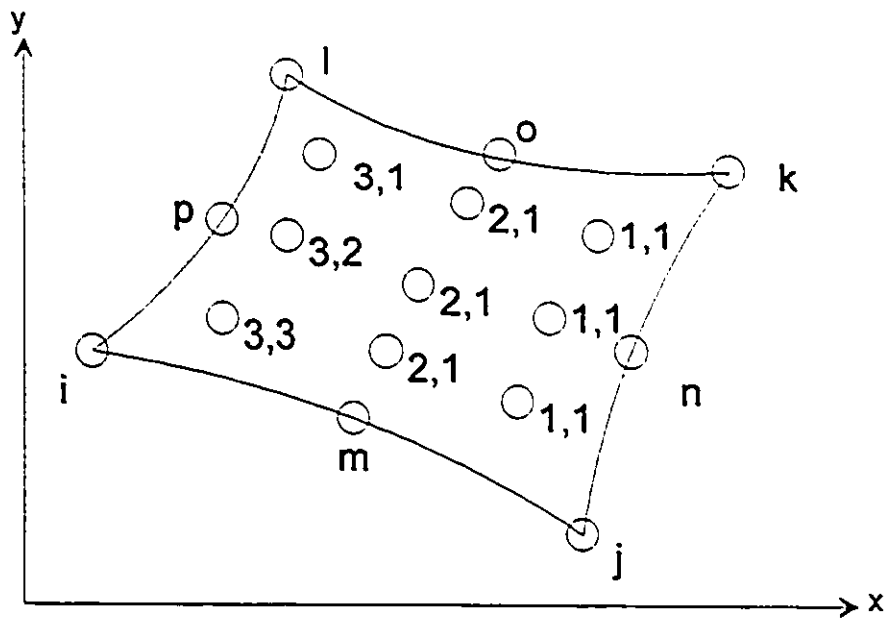


Figure 6-4 3x3-point Gauss quadrature integration

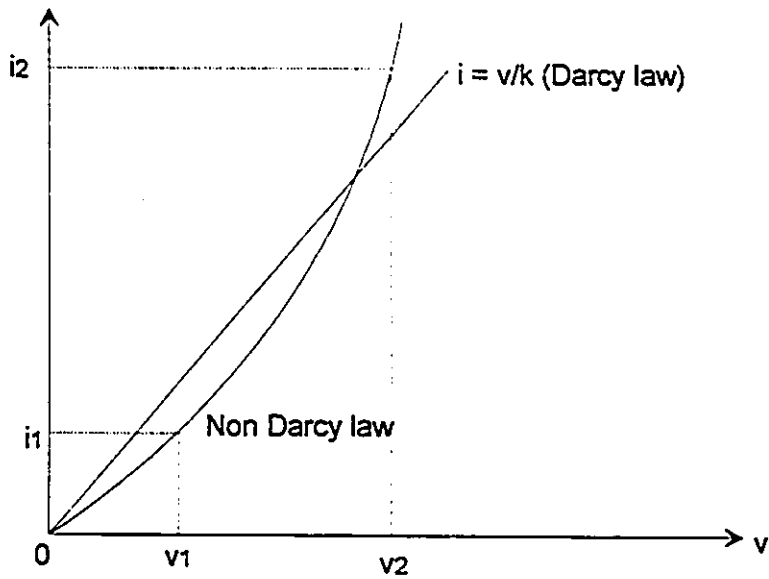


Figure 6-5 Selection of Darcy seepage coefficient for Non-Darcy Seepage Simulation

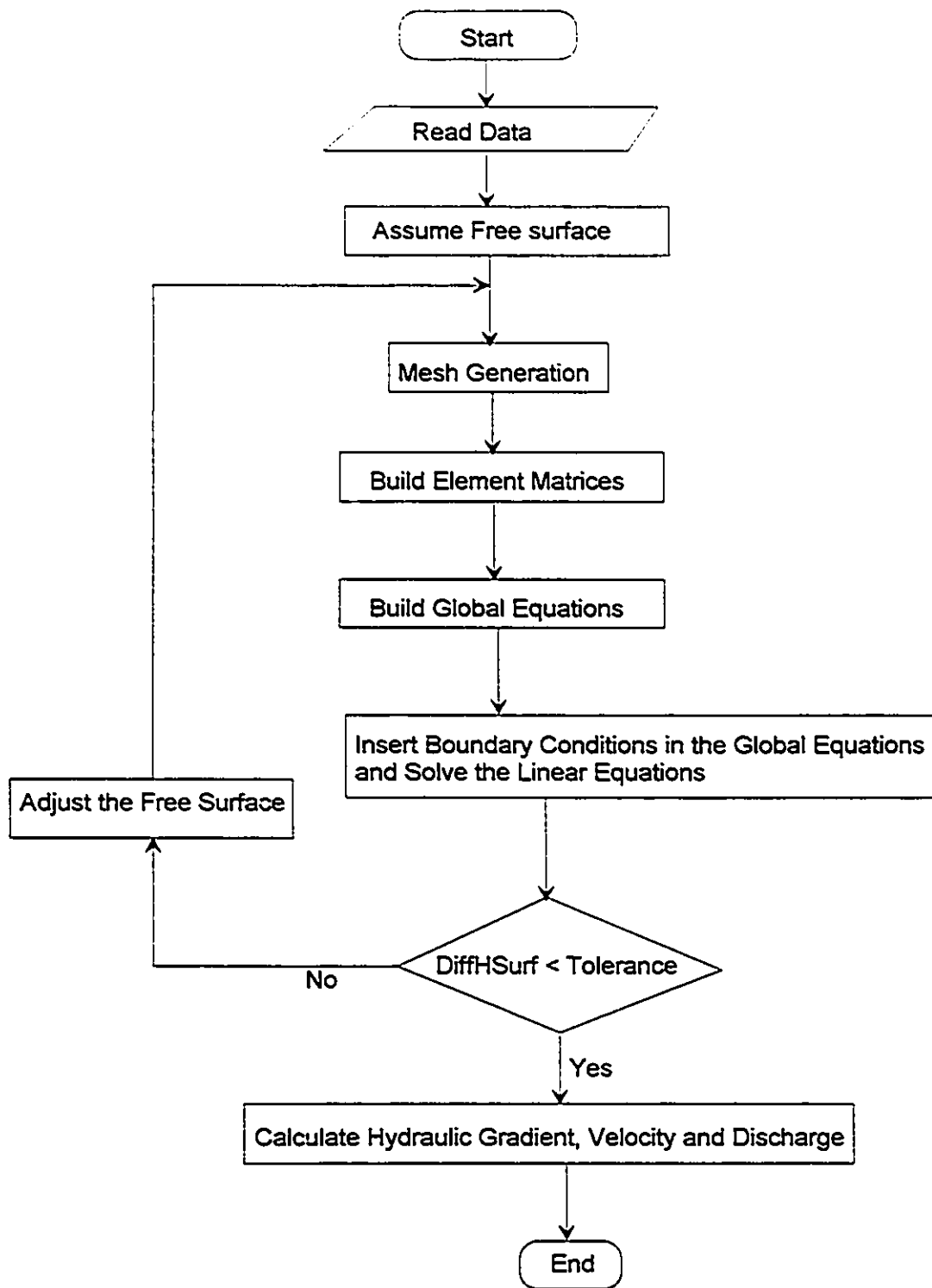


Figure 6-6 Flow Chart of Finite Element Method for Free Surface Darcy Flow

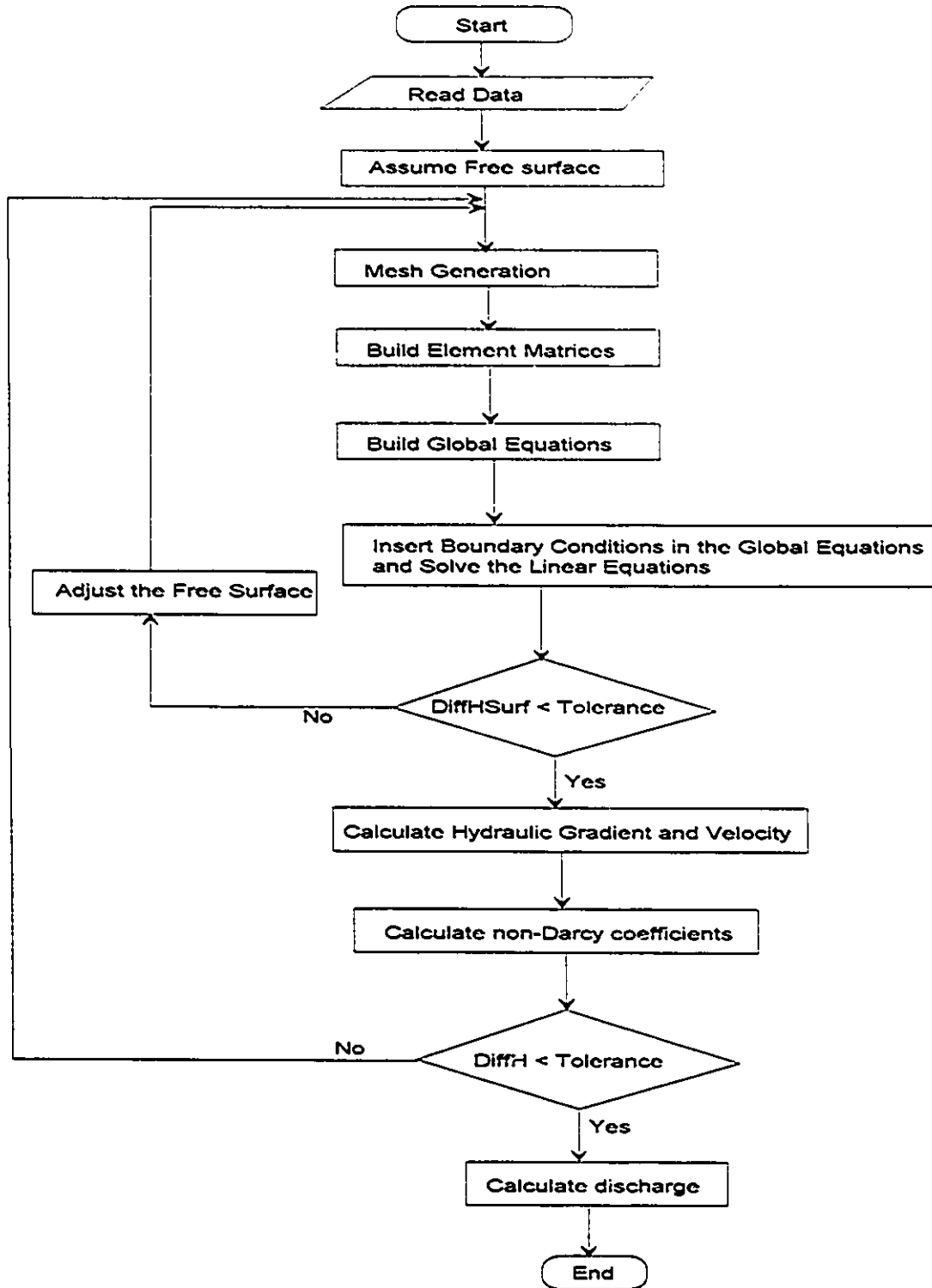


Figure 6-7 Flow Chart of Finite Element Method for Free Surface non-Darcy Flow

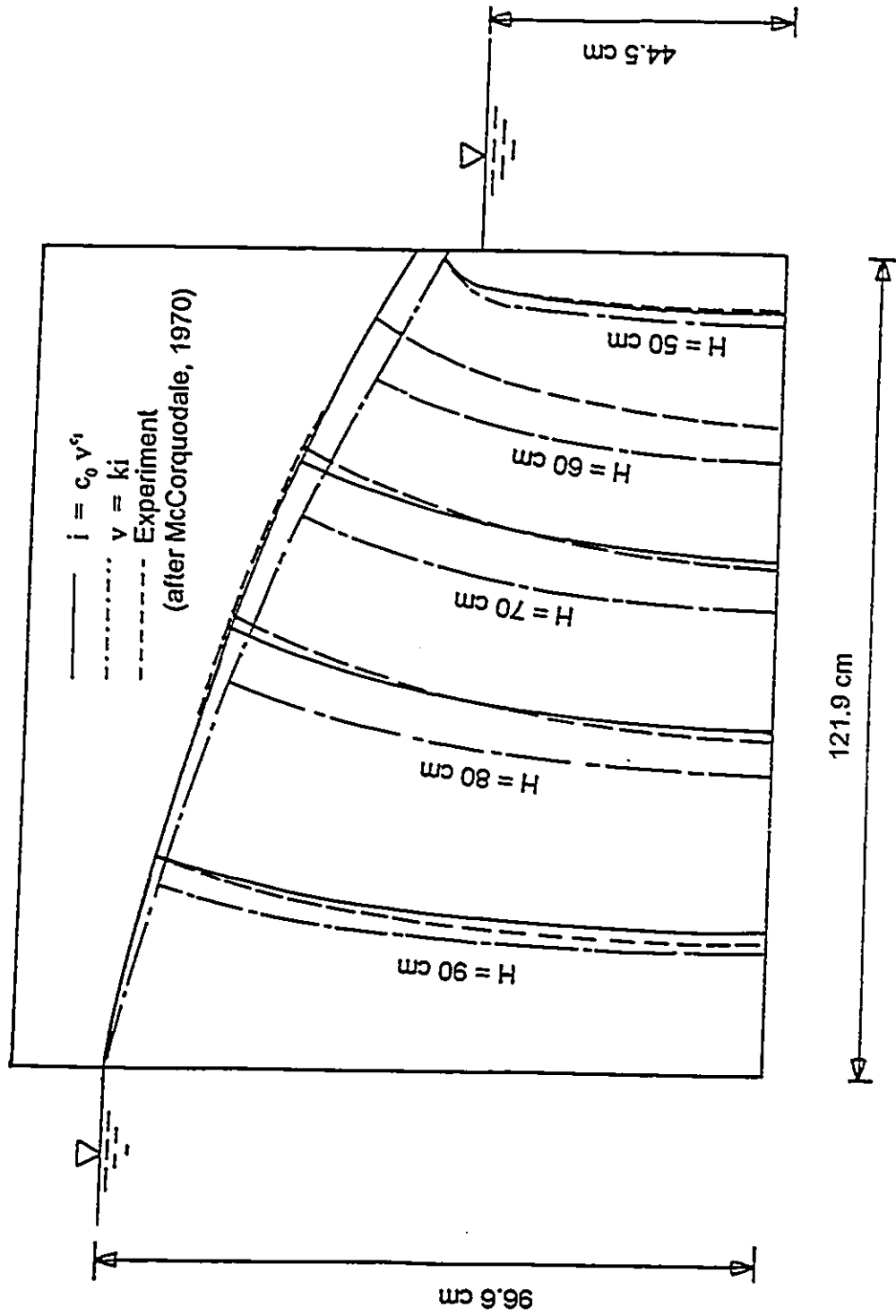


Figure 6-8 A simulation of finite element method

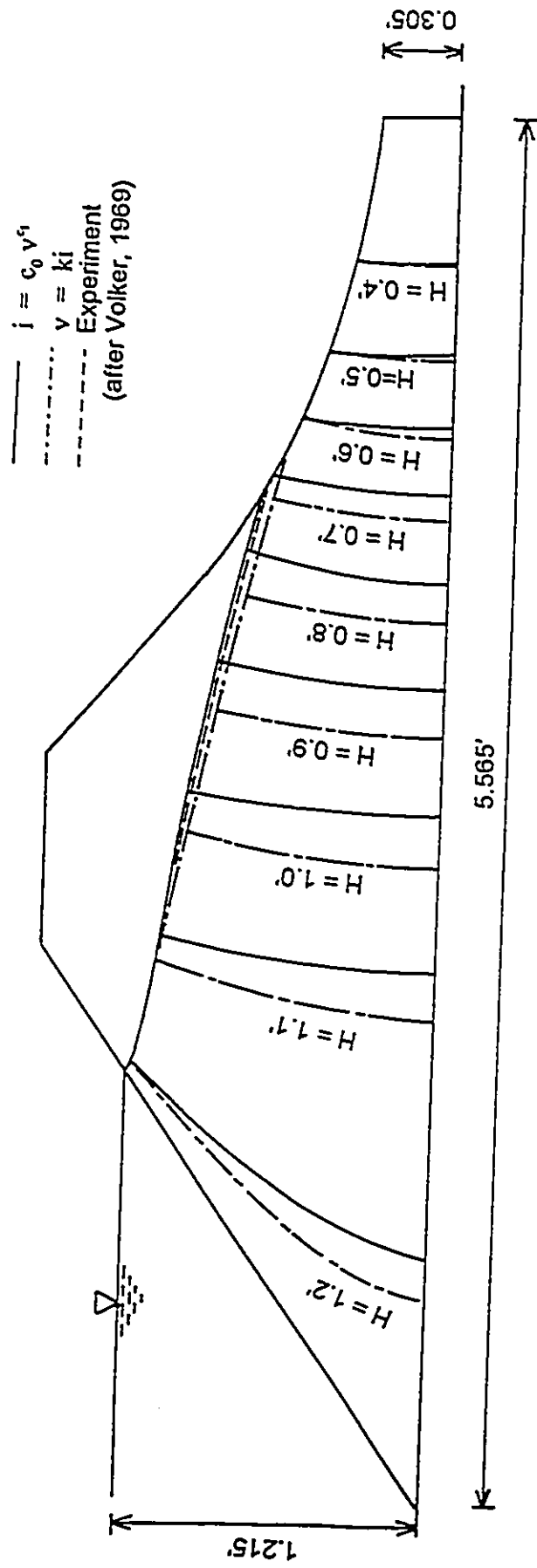


Figure 6-9 A simulation of flow through dam with no cut-off wall

# **Chapter 7      Derivation of New Formulae for Stability Analysis at the Downstream Slope of an Overtopped Rockfill Dam**

## **7.1 Introduction**

Stability analysis is one of the main tasks of the engineering design of an overtopped rockfill dam. Original contributions to the stability analysis have been made in this research, and are presented in this chapter. The design methods available in the literature were described in Chapter 2 and are not mentioned in this chapter. The use of all the methods including those described in Chapter 2 will be further discussed in Chapter 8.

Three aspects of stability analysis were conducted and are described in this chapter: the analysis of individual particle, the design of mesh protection along the downstream slope, and the design of steel bars in the rockfill dam to prevent sliding of the downstream slope of an overtopped rockfill dam. The stochastic behavior of the pore pressure will be considered in the analysis.

## **7.2 Individual Particle at the Downstream Slope**

Figure 7-1 shows the diagram of the forces acting on an individual particle, which is subjected to both flow-through (seepage flow) and overtopping flow conditions.

In Fig. 7-1,  $T$  is the drag force, or the shear force due to overtopping flow;  $F$  is seepage force;  $W$  is the gravitational force;  $R$  is the resultant resistant force acting on the particle by the surrounding rock particles; and  $P$  is the statistical value of pulsating force;  $v$  is the average velocity of open channel flow;  $h$  is the depth of overtopped flow. The following assumption is made based on the experimental observation that sliding

will be the basic failure mode. The use of pulsating force P has been undertaken for the first time. The force P is the pulsating force caused by a combination of mainly turbulent seepage flow and the influence of overtopping flow.

### 7.2.1 Calculation of the drag force T

T is the drag force (or shear force).

The shear stress  $\tau$  for open channel flow may be described as:

$$\tau = \gamma_w R J \quad (7-1)$$

where

$\tau$  = shear stress due to overflow;

$\gamma_w$  = unit weight of water;

R = hydraulic mean radius for overtopping flow;

J = the hydraulic gradient ( the value is close to the tangent of the downstream slope angle) for steep open channel flow.

In Eq. (7-1), R should not be confused with the hydraulic mean radius of the particles.

Considering wide channels:

$$R \approx h \quad (7-2)$$

where h = the height of the overtopping flow.

From open channel flow theory (in SI unit):

$$v = \frac{1}{n_d} R^{2/3} J^{1/2} \quad (7-3)$$

where

$n_d$  = Manning coefficient;  
 $v$  = velocity.

Substituting (7-2) in (7-3):

$$J = \frac{n_d^2 v^2}{h^{4/3}} \quad (7-4)$$

Substituting (7-4) and (7-2) in (7-1):

$$\tau = \frac{n_d^2 \gamma_w v^2}{h^{1/3}} \quad (7-5)$$

Assuming that the projected exposed surface area along the slope (in a direction perpendicular to the slope) of the particle at the downstream slope is  $A$ . Let:

$$A = \eta D^2 \quad (7-6)$$

where

$D$  = identical spherical diameter;

$\eta$  = coefficient determined by the shape of the particle;

$\eta = \frac{\pi}{4}$  for perfect spherical particles.  $\eta$  can be experimentally determined if required.

The drag force  $T$  acting on the particle is then calculated as :

$$T = \frac{\gamma_w n_d^2 v^2 A}{h^{1/3}}$$

Substituting (7-6) in the above equation:

$$T = \frac{\gamma_w n_d^2 v^2 \mu D^2}{h^{1/3}} \quad (7-7)$$

### 7.2.2 Seepage Force (F)

The force F is shown in Figure 7-1. By Terzaghi ( Taylor, 1948 ):

$$F = k_f \gamma_w J_0 D^3 \quad (7-8)$$

where

$J_0$  = local hydraulic gradient;

$k_f$  = coefficient depending on the flow pattern around the particle, for uniform particles,  $k_f = 1$ .

If  $V_{min}$  = the minimum bulk volume which could contain a particle of volume  $V_p$  in a porous media with void ratio  $e$ ;

and  $V_p$  = the representative particle volume, i.e.,  $V_p = \frac{\text{average rock mass}}{\text{rock density}}$ .

then:

$$V_{min} = (1 + e) V_p \quad (7-9)$$

Hence, the seepage force here is represented as

$$F = k_f \gamma_w J_0 (1 + e) V_p \quad (7-10)$$

### 7.2.3 Gravity Force (W)

W is shown in Figure 7-1. It is calculated by:

$$W = \gamma_b V_p \quad (7-11)$$

where

$\gamma_b$  = buoyant unit weight.

#### 7.2.4 Pulsating Force (P)

The pulsating force has been ignored in all previously available design methods. However from the experiment of NHRI (Appendix 1), it was found that the pulsating pressure can be high and may contribute to the failure of the downstream slope of a rockfill dam.

Considering that P, the statistical value of pulsating force, is caused due to the stochastic behavior of fluid flow, it is assumed that P is proportional to the hydraulic gradient  $J_0$ , and the minimum bulk volume  $V_{min}$ . One may define:

$$P = k_p \gamma_w J_0 (1 + e) V_p \quad (7-12)$$

where

$k_p$  = pulsating coefficient which depends on the turbulence of the fluid field.

#### 7.2.5 Resultant Thrust ( R )

As shown in Figure 7-1, R is the resultant resistant force acting on the particle by the surrounding rock particles. The angle between R and the y direction (normal to the slope) is  $\phi$ .

#### 7.2.6 Equilibrium Equation at Critical Condition

At the moment of incipient motion of the slope, the forces acting on the particle are at limit equilibrium. By summing force in x direction (along the downstream slope):

$$T + F \cos \psi + W \sin \alpha + P \cos \omega = R \sin \varphi \quad (7-13)$$

By summing force in y direction:

$$P \sin \omega + F \sin \psi + R \cos \varphi = W \cos \alpha \quad (7-14)$$

R may be obtained as:

$$R = \frac{W \cos \alpha - P \sin \omega - F \sin \psi}{\cos \varphi} \quad (7-15)$$

### 7.2.7 Safety Factor of a Particle

The safety factor may be defined as:

$$FS = \frac{R \sin \varphi}{T + F \cos \psi + W \sin \alpha + P \cos \omega} \quad (7-16)$$

Substituting Eqs. (7-7), (7-10), (7-11), (7-12), and (7-15) into Eq. (7-16):

$$FS = \frac{W \cos \alpha - F \sin \psi - P \sin \omega}{\cos \varphi [T + F \cos \psi + W \sin \alpha + P \cos \omega]} \quad (7-17)$$

Substituting Eqs. (7-7), (7-10), (7-11), (7-12) in Eq. (7-17), one may obtain:

$$FS = \frac{\frac{\gamma_b}{\gamma_w} \cos \alpha - (k_F \sin \psi + k_p \sin \omega) J_o (1+e)}{\cos \varphi \left[ \frac{n^2 v^2}{h^{1/3}} \frac{A}{V_p} + (k_F \cos \psi + k_p \cos \omega) J_o (1+e) + \frac{\gamma_b}{\gamma_w} \sin \alpha \right]} \quad (7-18)$$

Let

$$\frac{A}{V_p} = \frac{1}{d_p} \quad (7-19)$$

Eq. (7-18) is written as:

$$FS = \frac{\frac{\gamma_b}{\gamma_w} \cos \alpha - (k_F \sin \psi + k_p \sin \omega) J_o (1+e)}{\cos \varphi \left[ \frac{n_d^2 v^2}{h^{1/3} d_p} + (k_F \cos \psi + k_p \cos \omega) J_o (1+e) + \frac{\gamma_b}{\gamma_w} \sin \alpha \right]} \quad (7-20)$$

In Eq. (7-20),  $k_F$ ,  $d_p$ ,  $\gamma_b$ , and  $e$  are determined by the properties of rockfill material. The parameters  $h$ , and  $v$  are determined by the overflow. The hydraulic gradient  $J_o$  is determined by the seepage flow.

From Eq. (7-20), it is noticed that:

- (1) The larger the value of  $\alpha$ , the smaller the value of FS and vice-versa. This is why the downstream slope for overtopped rockfill dam without protection is usually very flat.
- (2) The higher the velocity of overflow  $v$ , the lower the FS. The lower the depth of overflow  $h$ , the lower the FS for the same value of overflow discharge  $q$ .

$$q = vh \quad (7-21)$$

where  $q$  is unit discharge. If  $q$  is known, the higher  $v$  corresponds to lower  $h$ . Hence the value of  $q$  itself can not be the only criteria for engineering design. From open channel flow theory, the larger the slope angle  $\alpha$ , the higher the velocity  $v$ . Hence  $q$  and  $\alpha$  together determine the stability and therefore the size of the particles located at the

downstream slope. The design criteria published by Abt and Johnson (1991) from experimental data was a proper one and corroborates this conclusion. They obtained the following expression:

$$D_{50} = 5.23i^{0.43}q_f^{0.56} \quad (\text{in.}) \quad (7-22a)$$

where

$q_f$  = the unit discharge at failure (cfs/ft);

$i$  = the gradient of the slope,  $i = \tan \alpha$ .

The above expression can be transformed to SI units as:

$$D_{50} = 0.503i^{0.43}q_f^{0.56} \quad (\text{m}) \quad (7-22b)$$

where  $q_f$  = the unit discharge at failure in  $\text{m}^3/\text{s}/\text{m}$ .

(3) The larger the value of  $d_p$ , as defined by Eq. (7-19), the higher the FS, and vice-versa.

When  $V_p$  is constant, the larger the value of  $A$  the lower is the value of  $d_p$ , and vice-versa. This is why thin slab-shaped rock particles fail more easily under the condition of overflow, if the largest surface is located along the downstream slope.

(4) The higher the value of  $J_0$ , the smaller the FS. This is because higher hydraulic gradient corresponds to higher seepage force.

The practical application of Eq. (7-20) will be discussed in Chapter 8. If detailed information of the seepage fluid field is not obtained by numerical modelling or physical modelling (as happens in most small dams' design), an approximate method to count the seepage flow is described here. Because it was concluded that the seepage direction near the downstream slope is almost horizontal when the flow over the slope is steep open channel flow, that is:

$$\psi = \omega = \alpha \quad (7-23)$$

By the experimental data measured from NHRI, the value of  $k_p$  may be obtained from the sum of pulsating force  $P$  and the seepage force  $F$ .

$$\begin{aligned}
 k_p + k_r &= \frac{F + P}{\gamma_w J_o (1 + e) \frac{\pi}{6} d_{50}^3} \\
 &= \frac{0.064 * \gamma_w * \frac{\pi}{4} (0.044)^2}{\gamma_w \left(\frac{1}{1.5}\right) (1 + 1.08) \frac{\pi}{6} (0.044)^3} \\
 &= 1.6
 \end{aligned}
 \tag{7-24}$$

Hence  $k_p = 0.6$  for the overtopped rockfill dam built of uniform size of particles.

Eq. (7-20) can be rewritten as the following easy-to-use formula:

$$FS = \frac{\frac{\gamma_b}{\gamma_w} \cos \alpha - (k_F + k_p) J_o (1 + e) \sin \alpha}{\cos \phi' \left[ \frac{n_d^2 v^2}{h^{1/3} d_p} + (k_F + k_p) J_o (1 + e) \cos \alpha + \frac{\gamma_b}{\gamma_w} \sin \alpha \right]}
 \tag{7-25}$$

where  $k_p$  may be taken as 0.6, and  $k_r$  is 1 for almost uniform rockfill material.

### 7.3 Design of the mesh at the Downstream Slope of an Overtopped Rockfill Dam

Figure 7-2 shows the diagram of the forces acting on an individual particle in a slope over which a reinforcing mesh is placed. The only difference between Figure 7-1 and Figure 7-2 is that in the latter there is one extra force  $S$  which represents the constraint provided by the mesh at the downstream slope. The force  $S$  can make a unstable

particle stable if the mesh is properly designed. This mesh may consist of welded rebars, steel chains or (in future) composite plastic material.

Force equilibrium in x direction:

$$S = T + F \cos \psi + W \sin \alpha + P \cos \omega - R \sin \phi \quad (7-26)$$

Force equilibrium in y direction:

$$P \sin \omega + F \sin \psi + R \cos \phi = W \cos \alpha \quad (7-27)$$

From Eq. (7-27):

$$R = \frac{W \cos \alpha - F \sin \psi - P \sin \omega}{\cos \phi} \quad (7-28)$$

Substituting Eq. (7-28) in Eq. (7-26):

$$S = T + \frac{F \cos (\psi - \phi) + W \sin (\alpha - \phi) + P \cos (\omega - \phi)}{\cos \phi} \quad (7-29)$$

Substituting Eqs. (7-7), (7-10), (7-11), (7-12) in the above equation, the force required for the mesh by the stability of one rock particle along the downstream slope:

$$S = \gamma_w V_p \left\{ \frac{n^2 V^2}{h^{1/3}} + \frac{[k_F \cos (\psi - \phi) + k_p \cos (\omega - \phi)] J_0 (1 + e) + \frac{\gamma_b}{\gamma_w} \sin (\alpha - \phi)}{\cos \phi} \right\} \quad (7-30)$$

If detailed information of the seepage fluid field is not obtained by numerical modelling or physical modelling (as happens in most small dams' design), an approximate method to estimate the seepage flow is described here. The seepage direction near the downstream slope is assumed horizontal when the flow over the slope is steep open channel flow.

$$\psi = \omega = \alpha \quad (7-23)$$

By the experimental data measured from NHRI, the value of  $k_p$  was obtained as 0.6, while  $k = 1$  for almost uniform rockfill material.

Eq. (7-27) is then simplified as:

$$S = \gamma_w V_p \left\{ \frac{n_d^2 v^2}{h^{1/3}} + \frac{[k_F + k_p] J_0(1+e) \cos(\alpha - \varphi) + \frac{\gamma_b}{\gamma_w} \sin(\alpha - \varphi)}{\cos \varphi} \right\}$$

$$(7-31)$$

The stress in the mesh can be obtained from:

$$\sigma_m = \frac{S}{a_m d_{50}}$$

where:

- $\sigma_m$  = the shear stress in the mesh, in the direction of the slope;
- $a_m$  = the area of the cross section of the mesh (see Fig. 7-3);
- $d_{50}$  = the average diameter of rock particles at the downstream slope.

For practical design:

$$a_m = F_m \frac{S}{\sigma_{all}} \frac{l_x}{d_{50}} \quad (7-32)$$

where:

$F_m$  = the factor of safety for the mesh;

$\sigma_{all}$  = the allowable tensile strength of the mesh.

## 7.4 Design of Steel Bars in Rockfill Dams

Figure 7-4 shows an arrangement of reinforcement by steel bars inside the downstream slope. The steel bars would invariably be connected to the mesh. In Fig. 7-4,

$\alpha$  = the angle of the downstream slope;

$H$  = the height of the downstream slope.

It is assumed that the distribution of the required stress inside the rockfill slope which has to be resisted by the anchors is triangular as shown in Fig. 7-4. An analogy may be made to the distribution of horizontal stress in horizontal ground.  $t$  denotes the maximum stress at the base of the dam. The downstream slope is divided into slices. For each slice, the forces are shown in Fig. 7-5.

In Fig. 7-5,

$W_{bi}$  = the buoyant weight of slice  $i$ ;

$T_i$  = the shear force acting on slice  $i$  due to the overtopping flow;

$N_i$  = the normal force at the base of the slice;

$N_{Ti}$  = the shear force along the base of the slice;

$J_i$  = the average hydraulic gradient of seepage flow in the slice,  $J_{xi}$  and  $J_{yi}$  are its components in  $x$  and  $y$  direction respectively;

$E_i, E_{i+1}$  = the horizontal inter-slice forces;

$Y_i, Y_{i+1}$  = the vertical inter-slice forces;

$\Delta x_i$  = the width of the slice.

$G_i$  = the total (resultant) force mobilized in the steel bars traversing the slice.

The method recommended by Lambe and Whitman (1979, pp.354) is used here to account for the forces of the seepage flow on the slope stability: to use the buoyant weight instead of the total weight for the slice and consider the seepage force acting on the rock particles within the  $i^{\text{th}}$  slice. Since for an earth dam, the hydraulic gradient inside the dam is small (Darcy law usually applies), the seepage force is often omitted. But for overtopped rockfill dams, the hydraulic gradient is usually quite high, and the particle size is large. Hence, the seepage force is an important force that influences the stability of the slope.

At the moment of incipient motion of the slice, the forces acting on the  $i^{\text{th}}$  slice are at limit equilibrium. By summing forces in the y direction (Fig. 7-5):

$$N_i \cos \beta_i + N_{Ti} \sin \beta_i - \gamma_w J_{y1} A_i - W_{bi} - T_i \sin \alpha_i - (Y_i - Y_{i+1}) = 0 \quad (7-33)$$

where

$$N_{Ti} = \frac{N_i \tan \varphi'}{F_s} \quad (7-34)$$

Similar to the Bishop method, let

$$Y_i = Y_{i+1} \quad (7-35)$$

then:

$$N_i = \frac{\gamma_w J_{y1} A_i + W_{bi} + T_i \sin \alpha_i}{\cos \beta_i + \frac{\tan \varphi'}{F_s} \sin \beta_i} \quad (7-36)$$

Now consider the forces in x direction:

The resisting force on slice  $i$  is:

$$\text{Resistance force} = N_{\tau} \cos \beta_i + S_i \quad (7-37)$$

The driving force on slice  $i$  is:

$$\text{Driving force} = T_i \cos \alpha + \gamma_w J_{x_i} A_i + N_i \sin \beta_i + (E_i - E_{i+1}) \quad (7-38)$$

If  $n$  is the total number of slices, the total resistance force is calculated as:

$$\text{Total Resistance force} = \sum_{i=1}^n (N_{\tau} \cos \beta + G_i) \quad (7-39)$$

The total driving force is given by:

$$\begin{aligned} \text{Total driving force} = & \sum_{i=1}^n T_i \cos \alpha + \sum_{i=1}^n \gamma_w J_{x_i} A_i + \sum_{i=1}^n N_i \sin \beta_i \\ & + \sum_{i=1}^n (E_i - E_{i+1}) \end{aligned} \quad (7-40)$$

$$\sum_{i=1}^n T_i \cos \alpha = \sum_{i=1}^n \tau_i \Delta x_i \quad (7-41)$$

where  $\tau_i$  was defined by Eq. (7-1).

Assume that:

$$\sum_{i=1}^n (E_i - E_{i+1}) = 0 \quad (7-42)$$

$$\sum_{i=1}^n N_i \sin \beta_i = \sum_{i=1}^n \left[ (\gamma_w J_{Y_i} A_i + W_{bi} + T_i \sin \alpha) \frac{\sin \beta_i}{\cos \beta_i + \frac{\tan \phi'}{F_s} \sin \beta_i} \right]$$

(7-43)

$$\sum_{i=1}^n N_{Ti} \cos \beta_i = \frac{\tan \phi'}{F_s} \sum_{i=1}^n N_i \cos \beta_i$$

$$= \frac{\tan \phi'}{F_s} \sum_{i=1}^n \left[ (\gamma_w J_{Y_i} A_i + W_{bi} + T_i \sin \alpha) \frac{\cos \beta_i}{\cos \beta_i + \frac{\tan \phi'}{F_s} \sin \beta_i} \right]$$

(7-44)

The buoyant weight:

$$W_{bi} = \gamma_b A_i$$

(7-45)

Defining the safety factor as:

$$F_s = \frac{\text{Total resistance force}}{\text{Total driving force}}$$

(7-46)

The factor of safety may be obtained from:

$$F_s = \frac{\sum_{i=1}^n (N_{Ti} \cos \beta_i + G_i)}{\sum_{i=1}^n T_i \cos \alpha + \sum_{i=1}^n \gamma_w J_{x_i} A_i + \sum_{i=1}^n N_i \sin \beta_i}$$

(7-47)

or

$$\sum_{i=1}^n G_i = F_s \left[ \sum_{i=1}^n \tau_i \Delta x_i + \gamma_w \sum_{i=1}^n J_{xi} A_i + \sum_{i=1}^n \frac{\sin \beta_i (\gamma_w J_{yi} A_i + \gamma_b A_i + \tau_i \Delta x_i \tan \alpha)}{\cos \beta_i + \frac{\tan \varphi'}{F_s} \sin \beta_i} \right]$$

$$- \frac{\tan \varphi'}{F_s} \sum_{i=1}^n \frac{\cos \beta_i (\gamma_w J_{yi} A_i + \gamma_b A_i + \tau_i \Delta x_i \tan \alpha)}{\cos \beta_i + \frac{\tan \varphi'}{F_s} \sin \beta_i}$$

(7-48)

Assuming linear distribution of stress (see Fig. 7-4), it is obtained that:

$$\frac{1}{2} tH = \sum_{i=1}^n G_i \quad (7-49)$$

hence

$$t = \frac{2 \sum_{i=1}^n G_i}{H} \quad (7-50)$$

Let

$$m_i = \cos \beta_i + \frac{\tan \varphi'}{F_s} \sin \beta_i \quad (7-51)$$

we have

$$t = \frac{2F_s}{H} \left[ \sum_{i=1}^n \tau_i \Delta x_i + \gamma_w \sum_{i=1}^n J_{x_i} A_i + \sum_{i=1}^n \frac{\sin \beta_i (\gamma_w J_{y_i} A_i + \gamma_b A_i + \tau_i \Delta x_i \tan \alpha)}{m_i} \right] - \frac{2 \tan \phi'}{H F_s} \sum_{i=1}^n \frac{\cos \beta_i (\gamma_w J_{y_i} A_i + \gamma_b A_i + \tau_i \Delta x_i \tan \alpha)}{m_i}$$

(7-52)

The above analysis should be repeated for several depths of slip surface in order to obtain the maximum value of  $t$  for design. The anchor force has to be mobilized by that length which lies outside the potential failure plane. This is illustrated in Fig. 7-6.

Anchor  $i$  will be required to mobilize the force shown in the hatched area in Fig. 7-6. Let

$$\tan \theta = \frac{t}{H} \quad (7-53)$$

Required anchor force for anchor  $i$  is:

$$B_i = (y_{\text{top}} - y_{\text{bottom}}) \left( H - \frac{y_{\text{top}} + y_{\text{bottom}}}{2} \right) \tan \theta \quad (7-54)$$

where  $y_{\text{top}}$ , and  $y_{\text{bottom}}$  are defined in Figure 7-6.

The free length of the anchor with diameter  $d$ ,  $l_i$  is then:

$$l_i \geq \frac{B_i}{\pi d \sigma'_n \tan \phi'} \quad (7-55)$$

where

$\phi'$  = the friction angle between steel bar and rockfill; and

$$\sigma_n' = \left( H - \frac{y_{\text{top}} + y_{\text{bottom}}}{2} \right) \gamma_b \quad (7-56)$$

In a design, the procedure is suggested as follows:

- (1) Select different slip surfaces (there is no limitation for the shape of slip surface, but for the time being circular shape is used);
- (2) For each slip surface, calculate  $t$  and then  $\tan\theta$  using Eq. (7-52) and (7-53) respectively;
- (3) Choose the maximum value of  $\tan\theta$  to calculate the required anchor forces for steel bars at each elevation using Eq. (7-54);
- (4) Calculate the length of anchor required at each locations using Eq. (7-55). If at some locations, one steel bar is not enough, more steel bars could be used at the same level in the horizontal direction. If this is still not feasible, reduce the vertical distance between close steel bars. If this is still not feasible, reduce the downstream slope and go back to step 1.

## 7.5 Concluding Remarks

Based on experimental observations and available experience of overtopped rockfill dams, the following original stability analyses have been provided:

- (1) the expression for the design of the downstream slope protected by large rock particles only (Eq. 7-20);
- (2) the expressions for the design of mesh along the downstream slope to protect the downstream slope (Eqs. (7-30) and (7-32)); and,

(3) the expressions for the design of steel bars in the rockfill dam to prevent the slide of the downstream slope of an overtopped rockfill dam (Eqs. (7-52), (7-53), (7-54), and (7-55)).

The use of these relationships in practical design will be discussed in Chapter 8.

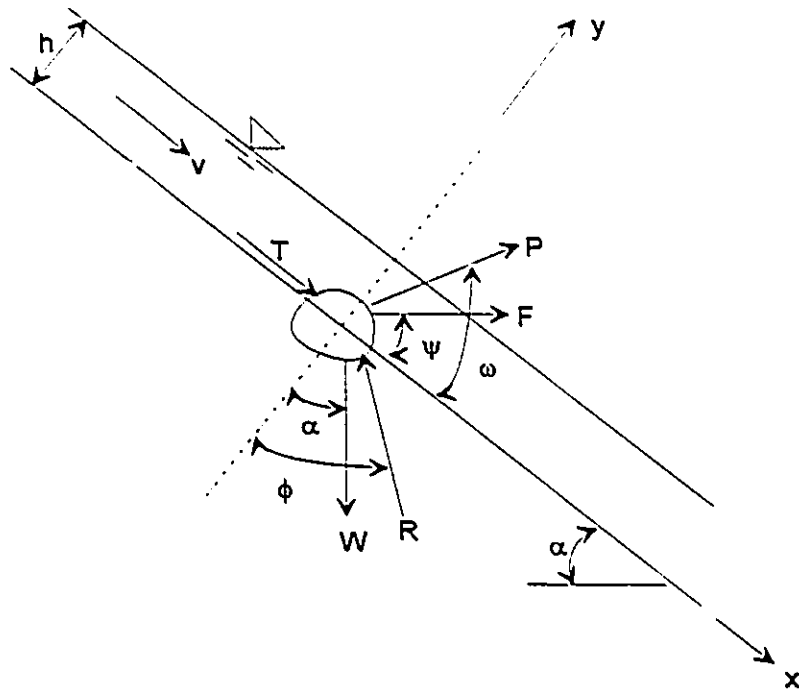


Figure 7-1 Forces acting on a particle at the downstream slope

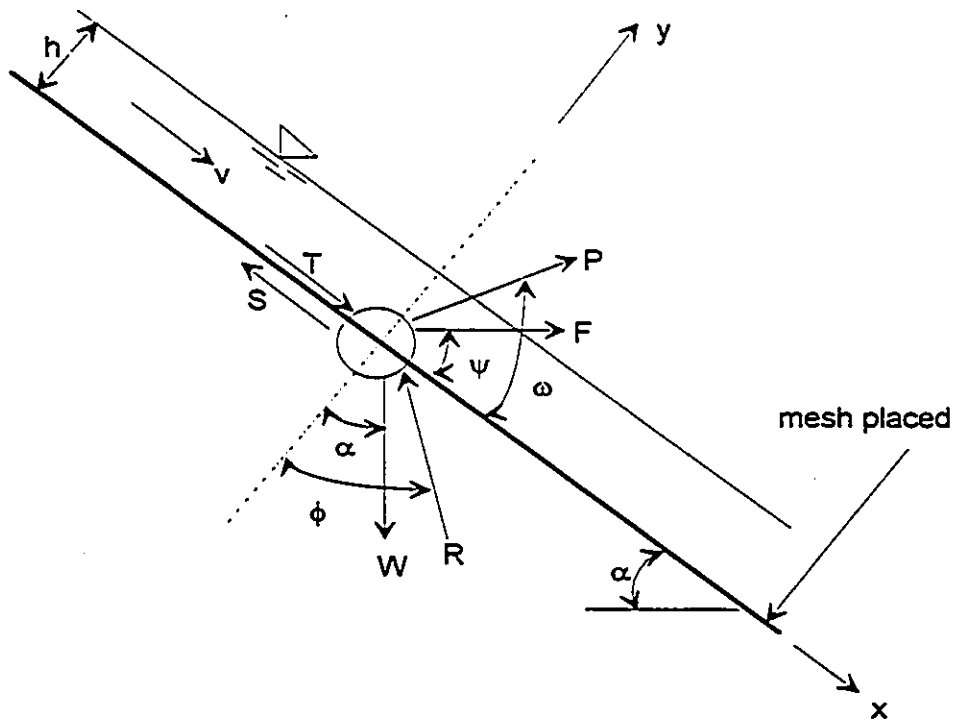


Figure 7-2 Forces acting on a particle at the downstream slope protected with mesh

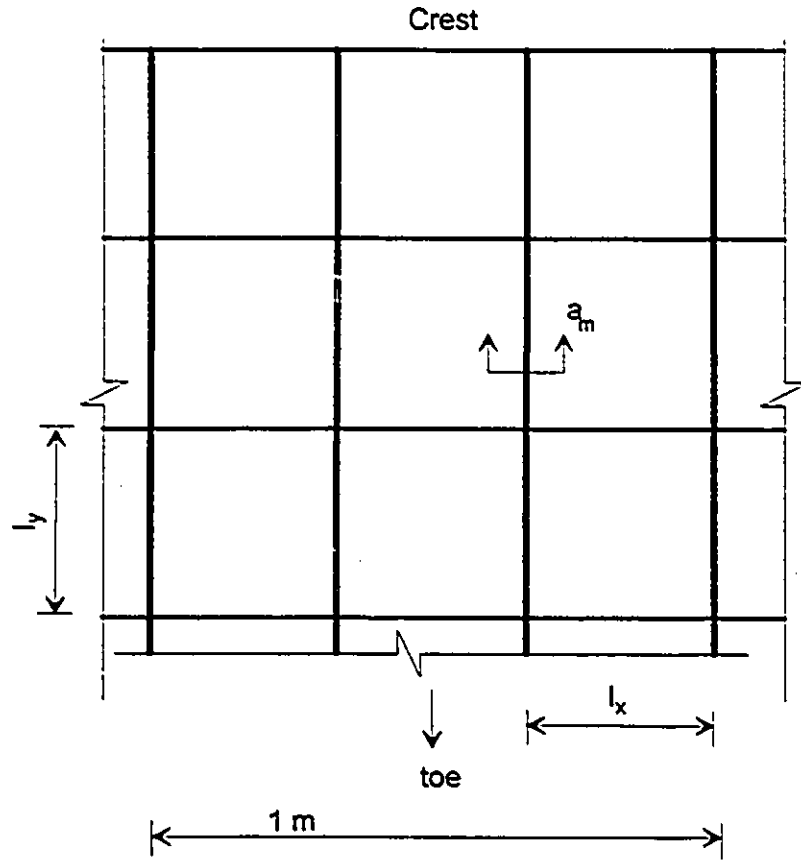


Figure 7-3 Description of mesh

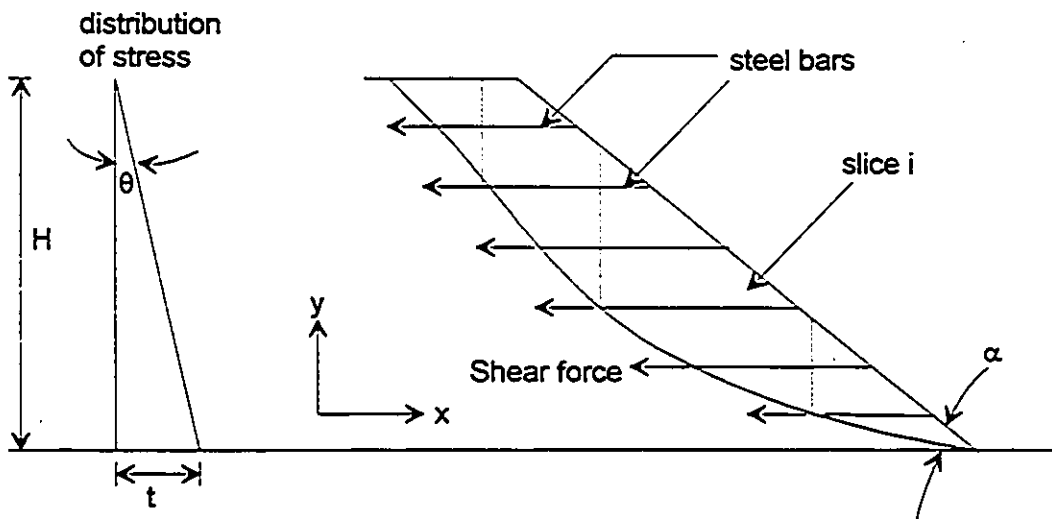


Figure 7-4 Diagram for the analysis of steel bars

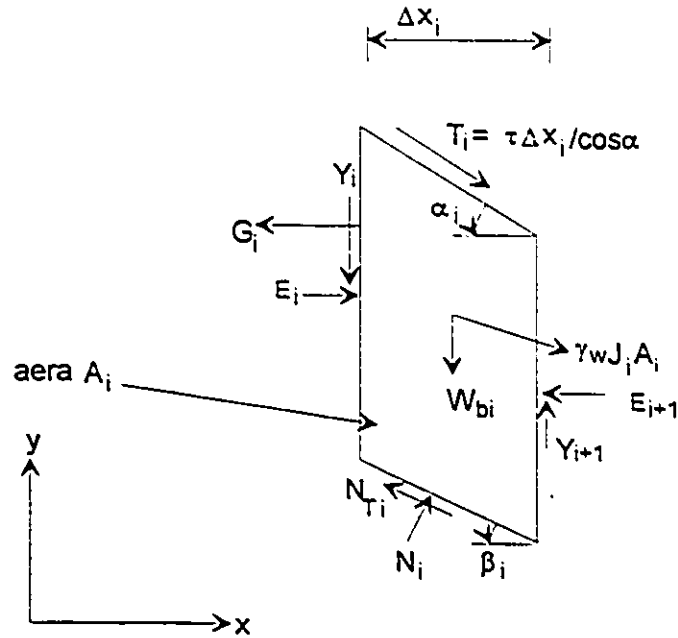


Figure 7-5 Force Diagram for the  $i^{\text{th}}$  slice

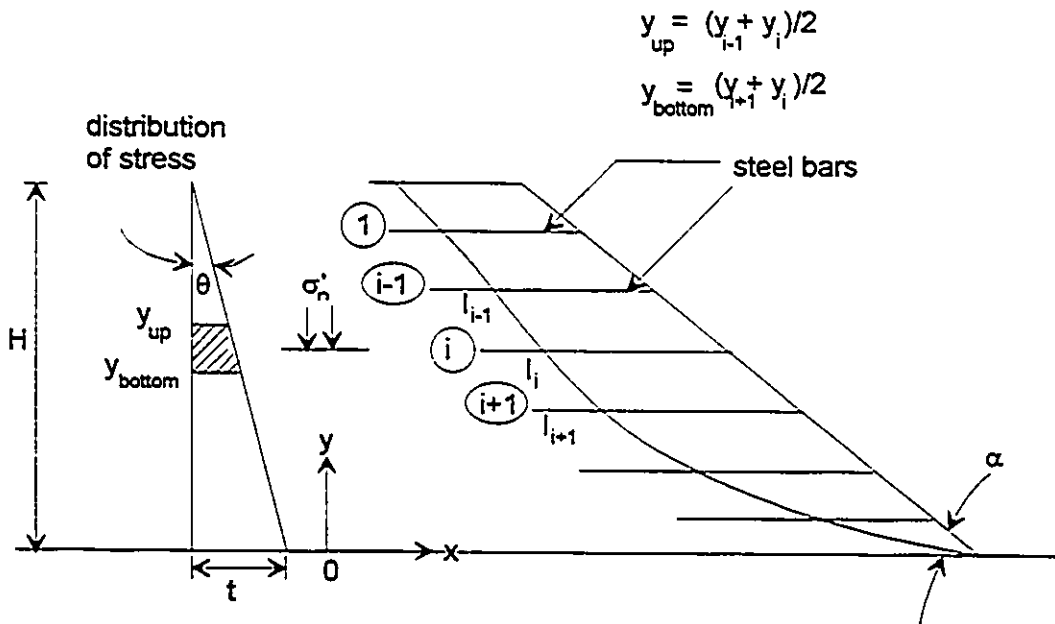


Figure 7-6 Design of steel bars

# **Chapter 8 A Proposed Design Methodology for Flowthrough and Overtopped Rockfill Dams**

## **8.1 Introduction**

Any engineering design requires a proper design methodology. At present, the most common design method is that proposed by Parkin (1963, 1991). Hansen (1992) carried out comprehensive studies on the design of flowthrough rockfill dams with emphasis on the slope stability, the finite difference method for seepage flow, the behavior in sub-zero temperatures, and the spatially varied flow. The comprehensive studies at the Nanjing Hydraulic Research Institute were concentrated on the design of overtopped rockfill dams, especially on the type of flow patterns, the determination of discharge, failure patterns of the downstream slope in an overtopped rockfill dam, and the non-Darcy theory which is the basis of the present study. In this chapter, a new design methodology is proposed. The following text describes the recommended design methodology, step by step.

## **8.2 Design Methodology for Flowthrough and Overtopped Rockfill Dams with or without Detailed Pore Pressure Distribution**

The formulae which are recommended for use in the design of flowthrough and overtopped rockfill dams are summarized below. Figure 8-1 shows the definition of the parameters in an overtopped rockfill dam. In a practical design example, the dam may be subjected to both flowthrough, and overtopping flow.

### 8.2.1 Seepage flow through the dam

Velocity of turbulent seepage flow in a dam can be evaluated by the newly derived expression given by Eq. (5-92):

$$v = \sqrt{2.5gRn^2i} = 1.58n\sqrt{gRi} \quad (8-1)$$

where

$n$  = porosity of the rockfill dam;

$g$  = gravity acceleration;

$i$  = hydraulic gradient of non-Darcy flow;

$R$  = mean hydraulic radius which may be defined by Eq. (5-70):

$$R = 0.136 d_{50} \quad (8-2)$$

The average hydraulic gradient through the dam for flowthrough conditions can be estimated by the following expression which was derived by Hansen (1992):

$$i_{ave} = 0.8 \left( \frac{H_0}{H} \right)^{1.4} \left( \frac{H}{B_u + B_c + 0.5B_d} \right)^{\frac{2}{3}} \quad (8-3)$$

where

$H_0$  = the upstream water depth;

$H$  = the height of the dam;

$B_u$  = the horizontal length of the upstream slope;

$B_c$  = the horizontal length of the crest;

$B_d$  = the horizontal length of the downstream slope.

The estimation of the unit-width discharge through the dam can be obtained from the following expression. It is the multiplication of the upstream water depth  $h$  and the average velocity as estimated by the new turbulent law Eq. (8-1):

$$q_s = 1.58 nh \sqrt{g R i_{ave}} \quad (8-4)$$

where

$q_s$  = unit-width flowthrough discharge [ $L^3/T/L$ ];

$h = \min\{H, H_0\}$ ;

$i_{ave}$  = average hydraulic gradient through the dam which is estimated by Eq. (8-3).

Total seepage discharge through the dam is:

$$Q_s = q_s L \quad (8-5)$$

where  $L$  = the average length of the dam in the valley where the flowthrough and overtopped rockfill dam section is located.

### 8.2.2 Overtopping flow

Two issues are involved in the design of overtopped rockfill dams. These are the determination of overtopping discharge, and the estimation of the water surface curve at the downstream slope.

#### (1) Discharge over the crest of a dam

The unit-width discharge over the crest,  $q_{crest}$ , of the dam may be calculated by (Hu, and Li, 1989):

$$q_{crest} = m\sigma (2g)^{0.5} H_{over}^{1.5} \quad (8-6)$$

where

$\sigma$  = coefficient of submergence. For free flow  $\sigma=1$ ;

$m$  = discharge coefficient;

$H_{over}$  = upstream water head (measured from the crest of the dam);

$g = 9.81 \text{ m/s}^2$ .

The value of  $m$  is generally taken as 0.44 for free flow. More detailed determination of  $m$  and  $\sigma$  are given in Figure 2 in Appendix 1, based on the NHRl experimental data.

The overtopping discharge (over the crest) is:

$$Q_{\text{crest}} = q_{\text{crest}} L_{\text{crest}} \quad (8-7)$$

where  $L_{\text{crest}}$  = the length of the crest.

If the required total discharge capacity from hydrological consideration is  $Q_{\text{total}}$  and the flowthrough seepage discharge is  $Q_s$ , then the design overtopping discharge (over the crest) is given by:

$$Q_{\text{over}} = Q_{\text{total}} - Q_s \quad (8-8)$$

(2) Estimation of the water surface curve for the spatially varied flow at the downstream slope

Hansen (1992) derived a modified expression based on Chow (1959) for the estimation of the free surface profile for spatially varied flow over the downstream slope (Fig. 8-2):

$$\Delta d' = \frac{1}{\cos \alpha} \left\{ \frac{Q_1(V_1 + V_2)}{g(Q_1 + Q_2)} \left( V_2 - V_1 + \frac{V_2}{Q_1} (Q_2 - Q_1) \right) - S_f \Delta x \right\} \quad (8-9)$$

where

$\Delta d'$  = the local drop in depth  $d$  relative to the bed;

$\alpha$  = angle of downstream slope;

$x$  = coordinate in the direction of the slope;

$\Delta x$  = the distance between section 1 and section 2 along the slope ( $=x_2 - x_1$ );

$S_f$  = friction slope;

- Q<sub>1</sub> = discharge of the flow at section 1;
- Q<sub>2</sub> = discharge of the flow at section 2;
- V<sub>1</sub> = velocity of the flow at section 1;
- V<sub>2</sub> = velocity of the flow at section 2.

The Manning equation for fully turbulent flow is widely used in open channel hydraulics. The value of the Manning coefficient  $n_d$  obtained by Maynord was given by Eq. (2-81):

$$n_d = 0.038D_{50}^{1/6} \quad (8-10)$$

The friction slope is then obtained by the Manning equation:

$$S_f = \left[ \frac{v n_d}{R_o^{2/3}} \right]^2 \quad (8-11)$$

where  $R_o$  = the hydraulic mean radius of the overtopped rockfill flow.

The shear force may now be determined from the known friction slope,  $S_f$ , by the following expression:

$$\tau_o = \gamma_w R_o S_f \quad (8-12)$$

where  $R_o$  = the hydraulic radius of the overtopping flow.

### 8.2.3 Design of the average rock size at the downstream slope

The design criteria (Eq. (2-90)) published by Abt and Johnson (1991) from experimental data can be used for an preliminary estimate of the  $d_{50}$  required to protect the downstream slope. However it should be noted that their experimental set up did not permit any seepage flow through the dam. Hence the average size estimated from Eq. (2-90) is likely to be in the unsafe side. After  $d_{50}$  is estimated by Eq. (2-90) or by

experience, the safety of a designed downstream slope of an overtopped rockfill dam is calculated by Eq. (7-20) in Chapter 7:

$$FS = \frac{\frac{\gamma_b}{\gamma_w} \cos \alpha - (k_F \sin \psi + k_p \sin \omega) J_0 (1 + e)}{\cos \phi \left[ \frac{n_d^2 v^2}{h^{1/3} d_p} + (k_F \cos \psi + k_p \cos \omega) J_0 (1 + e) + \frac{\gamma_b}{\gamma_w} \sin \alpha \right]}$$

(8-13)

It should be noted that if the result of a non-Darcy finite element flowthrough seepage analysis (Chapter 6) are available, then the parameters  $\psi$  and  $\omega$  are known. Eq. (8-13) can then be used directly. However in many cases and generally for the design of small dams, such results may not be available. In such case, a simplification can be made by assuming that  $\psi = \omega = \alpha$  in the case of a steep open channel flow. Clearly if the downstream pool elevation is very high, then the condition of a steep open channel flow is not satisfied. In such case, the use of this simplification will lead to an overly conservative design. The simplified expression for the factor of safety is given by:

$$FS = \frac{\frac{\gamma_b}{\gamma_w} \cos \alpha - (k_F + k_p) J_0 (1 + e) \sin \alpha}{\cos \phi \left[ \frac{n_d^2 v^2}{h^{1/3} d_p} + (k_F + k_p) J_0 (1 + e) \cos \alpha + \frac{\gamma_b}{\gamma_w} \sin \alpha \right]}$$

(8-14)

where  $k_p$  may be taken as 0.6, and  $k_f$  is 1 for almost uniform rockfill material (this is true for most flowthrough and overtopped rockfill dams).

The required depth  $t$ , of the protection layer may be estimated by Abt's expression (Abt, 1988):

$$t_r = \max\{1.5D_{50}, D_{100}\} \quad (8-15)$$

where  $D_{100}$  = the maximum diameter of the rockfill material.

#### 8.2.4 Design of mesh at the downstream slope

The required restraining force on a simple average sized particle from the mesh is given by Eq. (7-30):

$$S = \gamma_w V_p \left\{ \frac{n_s^2 v^2}{h^{1/3}} + \frac{[k_F \cos(\psi - \varphi) + k_P \cos(\omega - \varphi)] J_0(1+e) + \frac{\gamma_b}{\gamma_w} \sin(\alpha - \varphi)}{\cos \varphi} \right\}$$

(8-16)

Again if detailed information about  $\psi$  and  $\omega$  (for seepage flow) is not available, the following expression may be used by assuming that  $\psi = \omega = \alpha$  :

$$S = \gamma_w V_p \left\{ \frac{n_s^2 v^2}{h^{1/3}} + \frac{[k_F + k_P] J_0(1+e) \cos(\alpha - \varphi) + \frac{\gamma_b}{\gamma_w} \sin(\alpha - \varphi)}{\cos \varphi} \right\}$$

(8-17)

where  $k_p$  may be taken as 0.6, and  $k_r$  is 1 for almost uniform rockfill material.

If the mesh size is  $l_x \times l_y$  (see Fig. 7-3), then the cross section area of each strand is given by:

$$a_m = F_m \frac{S}{\sigma_{all} d_{50}} \quad (8-18)$$

where:

$F_m$  = the factor of safety for the mesh;

$\sigma_{all}$  = available tensile strength of the mesh;

$d_{50}$  = the average diameter of rock particles at the downstream slope.

### 8.2.5 Design of anchor bars in the downstream slope

The maximum lateral stress from anchor bars at the base of dam (Fig. 7-4) is given by:

$$t = \frac{2F_s}{H} \left[ \sum_{i=1}^n \tau_i \Delta x_i + \gamma_w \sum_{i=1}^n J_{xi} A_i + \sum_{i=1}^n \frac{\sin \beta_i (\gamma_w J_{yi} A_i + \gamma_b A_i + \tau_i \Delta x_i \tan \alpha)}{m_i} \right] - \frac{2 \tan \phi'}{HF_s} \sum_{i=1}^n \frac{\cos \beta_i (\gamma_w J_{yi} A_i + \gamma_b A_i + \tau_i \Delta x_i \tan \alpha)}{m_i} \quad (8-19)$$

where

$$m_i = \cos \beta_i + \frac{\tan \phi'}{F_s} \sin \beta_i \quad (8-20)$$

Different slip surface ( or failure planes) should be analyzed in order to obtain the maximum value of  $t$ .

The required anchor force,  $B_i$ , for anchor  $i$  is given by:

$$B_i = (y_{top} - y_{bottom}) \left( H - \frac{y_{top} + y_{bottom}}{2} \right) \tan \theta \quad (8-21)$$

where

$$\tan \theta = \frac{t}{H} \quad (8-22)$$

The free length of the anchor with diameter  $d$ ,  $l_i$  is then given by:

$$l_i \geq \frac{B_i}{\pi d \sigma_n \tan \phi'} \quad (8-23)$$

where

$\phi'$  = the friction angle between steel bar and rockfill; and

$$\sigma_n' = \left( H - \frac{y_{top} + y_{bottom}}{2} \right) \gamma_b \quad (8-24)$$

### 8.2.6 Summary of Design Methodology

The following design steps are recommended.

**Step 1:** Determine the geometry (location of the dam, height, length of crest, upstream slope, downstream slope), the importance of the dam, the geological consideration, and the political consideration.

**Step 2:** Determine the availability of the rockfill in the field, and economic benefits of an overtopped dam versus other dam designs.

**Step 3:** Determine discharge, upstream water depth, and downstream water depth by hydrograph analysis.

**Step 4:** Determine the discharge that can flow through the rockfill by non-Darcy finite element method developed in Chapter 6 if the flow condition is complex or the dam is very important, or by Eqs. (8-1) ~ (8-4) if the downstream water level is shallow and the dam is small. When the flow condition is complex or the dam is very important, the finite element method developed in Chapter 6 may also be used to estimate the pore pressure distribution in the rockfill dam.

Step 5: Protection of the downstream slope. Two kinds of protection are recommended here.

(1) Protection with large particles

There are situations, where adequate supply of large rockfill is economically available, e.g., in mining projects, and where the inclination of the downstream slope is not of concern. In such a case, a safe overtopped slope may be designed with the use of rockfill only. The design procedure is as follows:

(i) Firstly, estimate the average diameter of rock particles to be used to protect the slope or estimated by experience or by Eq. (2-90).

(ii) Calculate the safety factor of the slope  $FS$  by Eq. (8-13) if the detailed information about seepage flow has been obtained by the finite element method in Step 4, or by Eq. (8-14) if this information is not available.

(iii) If  $FS$  is larger than a certain value that depends on the importance of the dam (for most cases  $FS \geq 1.5$ ), the design is complete; else, increase the average diameter of the rock particles and go back to (ii).

(iv) The depth of the rock layer is estimated by Eq. (8-15).

(2) Protection with mesh and anchor bars

There are situations, where adequate supply of large rockfill is not economically available, or where the inclination of the downstream slope is of concern. In such a case, a steep downstream slope may be designed with the use of mesh along the slope and anchor bars within the slope.

The mesh along the slope can be designed by the following steps:

(i) Calculate the required restraining force on a single average sized particle by Eq. (8-16) if the detailed seepage information is obtained by the non-Darcy finite element method developed in Chapter 6, or by Eq. (8-17) if this information is not available.

(ii) Determine the size of the mesh opening according the size of rockfill material. The size of mesh opening should be smaller than the size of external layer of rockfill at the downstream slope.

(iii) Estimate the required cross section area of each strand of the mesh by Eq. (8-18). If it is compatible to the available material, it is determined; else, adjust the size of the mesh, until this is true.

Anchor bars are required to keep the mesh fixed along the slope. The design procedure is as follows:

(iv) Select different slip surface (there is no limitation for the shape of slip surface in the theoretical derivation, but for the time being circular shape is used);

(v) For each slip surface, calculate  $t$  and then  $\tan\theta$  with Eq. (8-19) and (8-22) respectively;

(vi) Choose the maximum value of  $\tan\theta$  to calculate the required anchor forces for steel bars at each level using Eq. (8-21);

(vii) Calculate the length of anchor required at each locations with Eq. (8-23). If at some locations, one steel bar is not enough, more steel bars could be used at the same level in the horizontal direction. If this is still not feasible, reduce the vertical distance between close steel bars. If this is still not feasible, reduce the downstream slope and go back to step iv.

### **8.3 Summary**

A concrete design methodology for flowthrough and overtopped rockfill dams with or without detailed pore pressure distribution has been fully described in Section 8.2. It should be noticed that in this method, the hydraulic gradient of the seepage flow at the downstream slope is conservatively assumed to be equal to the tangent of the downstream slope angle and flows out horizontally. This phenomena was observed at NHRI for steep open channel flow. This treatment may be too conservative for other flow conditions when the downstream water level is high enough to influence the flow pattern at and near the toe. Two examples are given in Appendix 3 to show the design of a rockfill dam protected with large particles and that protected with a steel mesh and steel bars.

For complicated flow conditions or medium-height dam, it is advisable to conduct the finite element analysis of the non-Darcy flow within the rockfill dam by the method developed in Chapter 6. In this case the value of the hydraulic gradient of the seepage flow within the dam should be obtained from the results of the finite element analysis.

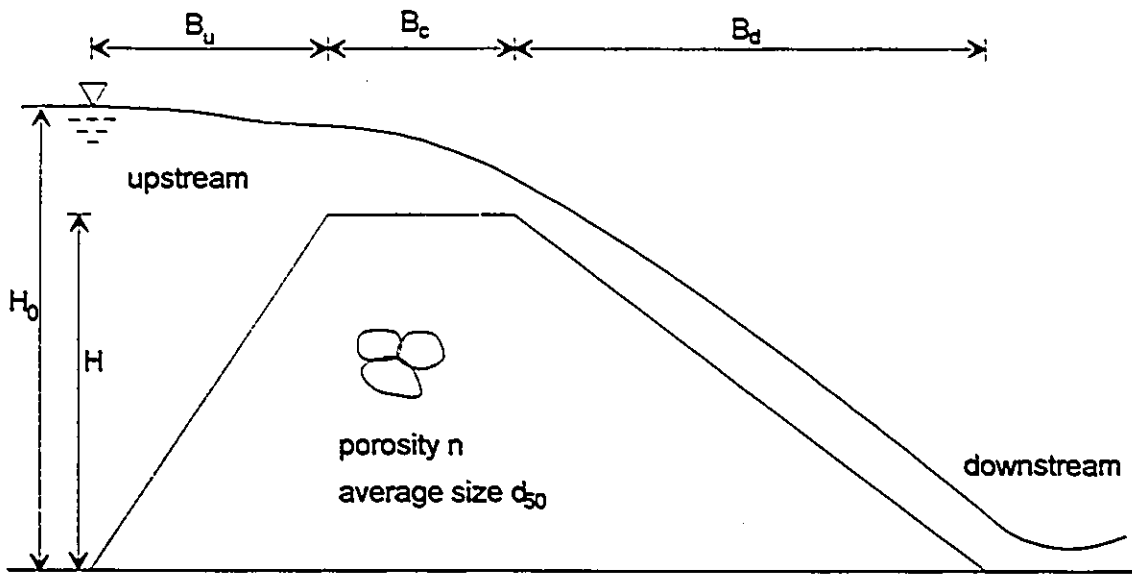


Figure 8-1 Definition of an overtopped rockfill dam

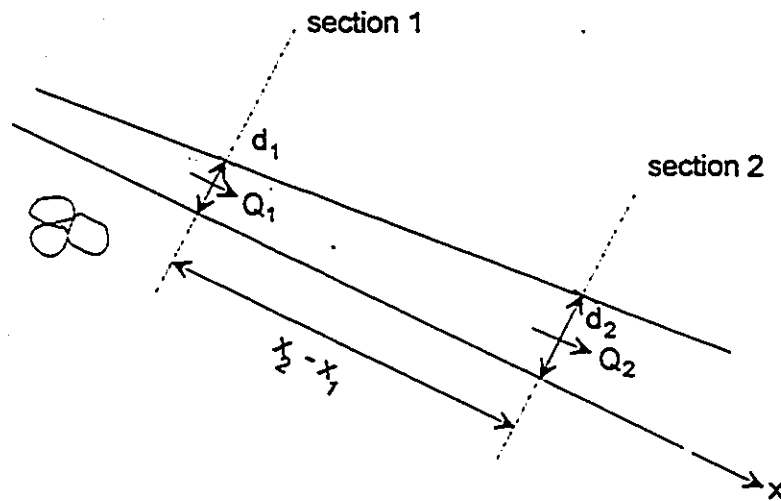


Figure 8-2 Spatially varied flow at the downstream slope

## Chapter 9 Summary of Conclusions and Suggestions for Future Research

### 9.1 Conclusions

1. Based on pipe flow theory, new definitions of Reynolds number  $Re$  and friction coefficient  $f$  have been proposed in Chapter 5. With the new definition, seepage flow is fully turbulent when  $Re > 200$ . The general relationships between  $Re$  and  $f$  for both quadratic seepage law and power seepage law have been presented for the first time. New relationships between hydraulic gradient  $i$  and velocity  $v$  of the non-Darcy flow in rockfill have been derived in Chapter 5 for practical engineering design. The derived relationships are found to be close to the available prototype data.

2. Computer simulations with wide range of porosity ( $n=0.35\sim 0.5$ ) and rockfill size ( $d=0.01\text{m} \sim 2.0\text{m}$ ) indicate that in most conditions, the  $i\sim V$  curves given by "general", Wilkins, "quadratic", "turbulent", and "modified Stephenson" expressions are very close. A comparison of different expressions of  $i$  and  $V$  reported in the literature applicable for rockfill indicates that these are applicable only in a limited range of seepage flow. The experimentally derived expressions reported in the literature are special cases of the general expressions derived in Chapter 5.

3. The mean hydraulic radius of rockfill may be predicted by the empirical relationship derived in Chapter 5. From the literature review and from the simulation of some available prototype data, it is concluded that the 50% size can reasonably be considered as the dominant size for flow calculations in flowthrough rockfill design.

4. The differences between the power law and the quadratic law are analyzed. The constants in the power law are functions of Reynolds number. The constants in quadratic law are unique for all ranges of Reynolds number (from Darcy flow to fully turbulent flow). The quadratic law is better than the power law for numerical modelling of pore pressure distribution in a rockfill dam.

5. Methods to estimate the discharge through a rockfill dam have been proposed. When the average hydraulic gradient through the dam is unknown, Eq. (5-98) may be used to estimate the unit-width discharge through the dam.
6. Eqs. (5-103) and (5-104) are derived for the estimation of the free surface curve of seepage flow in a flowthrough rockfill dam.
7. A finite element method for 2-dimension non-Darcy flow with 8 nodes quadratic isoparametric elements has been developed. Example simulations show that the model developed provided very reasonable results .
8. An expression (Eq. 7-20) for the design of the downstream slope protected by large rock particles has been derived. The pulsating force is considered in this derivation.
9. The expressions for the design of mesh along the downstream slope to protect the downstream slope (Eqs. (7-30) and (7-32)) are derived.
10. The expressions for the design of steel bars in the rockfill dam to prevent the slide of the downstream slope of an overtopped rockfill dam (Eqs. (7-52), (7-53), (7-54), and (7-55)) are derived.
11. A practical design methodology for flowthrough and overtopped rockfill dams has been fully described in Chapter 8. Two examples are given to show the design of a rockfill dam protected with large particles and one protected with steel mesh and steel bars.
12. For the first time, stochastic behavior of the forces acting on force panels is studied. It is found that the probability distribution is very close to Gauss distribution, and most energy is within the range between 0 and 10 Hz.
13. Model tests show that the failure of a uniform overtopped rockfill dam unprotected

or protected with large rock particles, the initial failure is local and shallow. The position depends on the downstream water level, the placement, and the type of protection. For the first time, two basic possible failure patterns are found to depend on the velocity of the increase of the upstream water level.

14. By combining the Prandtl mixing-length turbulent model with the non-linear seepage equation, two analytical solutions are derived for 1-dimension non-Darcy seepage flow in rockfill channel. In comparison to the other models, the solutions presented are simpler in form, and with a relative error of 12%.

## **9.2 Suggestions for Future Research**

1. It is suggested that computer simulation of the seepage fluid field of the non-Darcy flow of a flowthrough and overtopped rockfill dam with an upstream impervious facing be carried out. The finite element program developed in Chapter 6 can be used for this study. This analysis should be conducted with the dam profile of the experiment conducted by Wilkins (1956) to compare with the experimental results. A user-friendly interface to the finite element program should be developed.

2. Large-scale (prototype-like) physical modelling for non-Darcy seepage flow in a flowthrough and overtopped rockfill dam, and the failure condition should be undertaken. The boundary condition of the upstream impervious facing should be simulated in the prototype-like model. The finite element program developed in Chapter 6 should be used to compare the experimental results.

3. A probabilistic analysis of the stability of the downstream slope of an flowthrough and overtopped rockfill dam should be carried out in the light of the conclusion obtained in Chapter 4 that the total force acting on the slope has a Gauss distribution. Further assumption(s) may be needed to conduct the study successfully.

## Chapter 10    References

Abt, S. R., and Johnson, T. L., 1991. Riprap design for overtopping flow. ASCE Journal of Hydraulic Engineering, Vol. 117, No. 8, August, p. 959-972.

Abt, S. R., et al., 1987. Development of Riprap Design Criteria by Riprap Testing in Flumes: Phase I, USNRC Report NUREG/CR-4651, prepared for NRC by Colorado State University and Oak Ridge National Laboratory, May.

Abt, S. R., et al., 1988. Development of Riprap Design Criteria by Riprap Testing in Flumes: Phase II, NUREG/CR-4651, U.S. Nuclear Regulatory Commission, Washington, D.C., May, 113.

Ahmed N and Sunada D.K., 1969. Nonlinear flow in porous media. ASCE Journal of the Hydraulics Divisions, Vol. 95, Hy6, Nov., p.1947-1857.

Allaire, Paul E., 1985. Basics of the finite element method, Wm. C. Brown Publishers, USA. pp. 455-479.

Basak P., 1976. Steady non-Darcian seepage through embankments. Journal of the Irrigation and Drainage Division, ASCE, Vol. 103, IR4, Dec., p.459-473.

Becker, E., Chan, C. K., and Seed, H. B., "Strength and deformation Characteristics of Rockfill Materials in Plane Strain and Triaxial Compression Tests", University of California, Berkaley, 1972

Berube Y., Gilbert R., Frenette M., LaRochelle P., and Pantu I., 1972. Mine waste containment and water quality in a northern environment. Department of Indian and Northern Affairs, ALUR 1-72-31. 184 pp.

Brownell L.E., and Katz D.L., 1947. Flow of fluids through porous media. ASCE Chemical Engineering Progress, Vol. 43, Oct., p.537-548.

Campbell D.B., 1989. Some observations relative to the performance of flow-through rock drains. 13th Annual BC Mine Reclamation Symposium, June 7-9, p.119-128.

Chen, M. Z., Jin. L. J., Design of Rockfill Dam, pp.478-503, Hydraulic Publisher, Beijing, 1981

Chow V.T., 1959. Open Channel Hydraulics. McGraw-Hill, NY, 680 pp.

Combelles, J., Mackenzie, P., and McDinald, L. A., 1993. Reinforced Rockfill and Reinforced Fill for Dams: State of the art. GIGB/ ICOLD Bulletin 89, International Commission on Large Dams.

Cornett, Andrew M., 1995. A study of wave - induced forcing and damage of rock armour on rubble-mound breakwaters, University of British Columbia.

Curtis R.P., and Lawson J.D., 1967. Flow over and through rockfill banks. ASCE Journal of the Hydraulics Division, Sept., Vol. 93, Hy5, p.1-21.

Curtis R.P., and Lawson J.D., 1969. Closure to "Flow over and through rockfill banks". ASCE Journal of the Hydraulics Division, Jan., Vol. 95, Hy1, p.452-453.

Davies, Michael H., 1992. Wave - Soil - Structure Interaction in Coastal Engineering, Coastal Engineering, M-32, National Research Council Canada, Ph.D. thesis.

Dinoy A.A., 1971. Friction factor and Reynolds number relationship in flow through porous media. M. Eng. thesis, Asian Institute of Technology, Bangkok, Thailand.

Dudgeon C. R., 1964. Flow of water through coarse granular materials. M.Eng. thesis, University of New South Wales, Manly Vale, Australia.

Dudgeon, C.R., 1966. An experimental study of the flow of water through coarse porous media. *Houille Blanche*, 7: 785-801.

Elorza, F.J., and Ferragut, L., (1986). A Unified Algorithm to solve Nonlinear Groundwater Flow. VI International Conference on Finite Elements in Water Resources, Lisboa, Portugal, June 1986.

Ergun S., 1952. Fluid flow through packed columns. *Chemical Engineering Progress*, Vol.48 No.2, p.89.

Escande, (1953), Experiments Concerning the Filtration of Water Through Rock Mass, Reprint from Proc. Minnesota International Hydraulics Convention.

Forchheimer, P.H. (1901), *Wasserbewegung Durch Boden*. *Zeitschrift des Vereines Deutscher Ingenieure*. No. 49, pp. 1736-1749, No. 50, pp.1781-1788.

Forchheimer, P., *Hydraulik*, Teubner, Leipzig (1930)

Garga V.K., Smith H.R., and Scharer J., 1983. Abandonment of acid-generated mine tailings. VII Pan-American Conference on Soil Mechanics and Foundation Engineering, Vancouver, BC, Vol.2, p.613-626.

Garga, V. K., Townsend, R., and Hansen, D., (1991). A Method for Determining the Surface Area of Quarried Rocks. *Geotechnical Testing Journal*, GTJODJ, Vol. 14, No.1, March 1991, pp.35-45.

Gent, M.R.A. van (1991), Formulae to describe porous flow. *Communications on Hydraulic and Geotechnical Engineering*, ISSN 0169-6548 No. 92-2, Delft University of Technology and MAST-G6S report, project 1.

George, G. H., and Hansen D., (1992). Conversion between Quadratic and Power Law for non-Darcy Flow, *Journal of Hydraulic Engineering*, ASCE, Vol. 118, No. 5, May, pp. 792-797.

Gupta, A. D., and Paudyal, G. N., (1985). Characteristics of Free Surface Flow over Gravel Bed, J. of Irrigation & Drainage Engineering, ASCE, Vol. 111, No. 4, pp. 299-319.

Hansen, D., (1992). The behaviour of flowthrough rockfill dams. Ph.D. thesis. Department of Civil Engineering, University of Ottawa.

Hartung, F., and Scheuerlein, H. (1970). Design of overflow rockfill dams. Proc. Tenth Int. Congress of Large Dams, 1, 587-598.

Henderson, F.M., (1966). Open Channel Flow. Macmillan Publishing Co., Inc. and Collier Macmillan Publishers. pp. 211, pp. 88-162.

Hinton, E., and Owen, D.R.J., (1977). Finite element programming, Academic Press, London.

Huang, Wanxi, 1985, Characteristics of Soils, Hydraulic Publisher, Beijing

Hu, Qulie, (1986). Problems in overtopped rockfill dams. Nanjing Hydraulic Research Institute, Report Hydro8630, pp. 4-9.

Hu, Q. and etc. (1991). The Prototype Observation of the Overtopping Of Xibeikou Concrete-Faced Rockfill Dam in Flood Period. Gezhou Dam Engineering Board, and Nanjing Hydraulic Research Institute, March, Report #hydro8810.

Hu, Qulie, and Li, Bingjun, (1988). Experimental Study on the Overtopped Concrete Faced Rockfill Dam of the Tianshengqiao Hydroelectric Power Project in the Construction Period, Nanjing Hydraulic Research, Hydro 8856, pp. 24-31.

Hu, Qulie, and Li, Bingjun, (1989). Research on the Flowthrough and Overtopped Rockfill Dams: Initial Flow Patterns and Failure Conditions. Nanjing Hydraulic Research Institute, Hydro 8946. pp.19-22.

Hu, Qulie, and Li, Bingjun, (1989). Research on the Flowthrough and Overtopped Rockfill Dams: Overtopping Flow, Seepage Flow, and Protection. Nanjing Hydraulic Research Institute, Hydro 8947. pp.19-22.

Hu, Qulie, and Li, Bingjun, (1991). Overtopping Flow, Seepage Flow, and Protection of Flowthrough and Overtopped Rockfill Dams, (prepared for a training course), Nanjing Hydraulic Research Institute, pp.2-20.

Hu, Qulie and Li, Bingjun, (1991). Research on Concrete-Faced Rockfill Dam Overtopping Protection for the Upper Tian Sheng Qiao Hydroelectric Project. Journal of Nanjing Hydraulic Research Institute, NO. 4 (in Chinese).

Hu, Qulie, and Li, Bingjun, (1992). Analysis and Correction of Simulation for Seepage of Internal Rockfill Dam. International Symposium on Hydraulic Research in Nature and Laboratory, Nov. 17-20, Wuhan, China.

Isbash, S. V., 1931, O Filtracii V Krupnozernistom Materiale. Izv. Nauchno-issled, qust. Gidro-tekhniki (NIIG), Leningrad.

Jaeger, C., Engineering Fluid Mechanics, Blackie, London, England, 1956, pp. 1-404.

Jin, Zhongqing, (1989). Numerical Solution to the Navier-Stokes Equations and Turbulence Models, Hohai University Publishing Company (in Chinese), Nanjing, P. R. China.

Johnson H.A., 1971. Flow through rockfill dam. Journal of Soil Mechanics & Foundations Div., Vol.97, SM2, Feb., p.329-340.

Kells J.A., 1994. Energy dissipation at a gabion weir with through and overflow. Proceeding of Annual CSCE Conf., Winnipeg, June 1-4, Vol. 1, pp.26-35.

Kells J.A., 1993. Analysis of flow through a gabion dam. Proc. of 11th CSCE Canadian Hydrotechnical Conference, Fredericton, NB, June 8-11, Vol. I, pp. 51-60.

Kells J.A., 1991. Spatially varied flow over rockfill embankments. 10th Annual CSCE Conference, Vancouver, May 29-31, p.155-165.

Kells J.A., 1990. Flow through rockfill: an application to gabion dams. 10th Annual CSCE Conference, Vancouver, May 29-31, p.155-165.

Kirkham, C.E., 1967. Turbulent flow in porous media. Report DR11, University of Melbourne, Dept. of Civil Engineering, Feb., 146 pp.

Knauss, J. (1979). Computation of maximum discharge at overflow rockfill dams. Proc. 13th Congress of Int. Commission of Large Dams, p. 143-159.

Lambe, T. W., and Whitman, R. V., 1979. Soil Mechanics, SI Version. John Wiley & Sons, pp. 353-354.

Lane D., Berdusco R., and Jones R., 1986. Five years experience with the swift Creek rock drain at Fording Coal Limited. Proceeding of the International Symposium on Flowthrough Rock Drains, Cranrook, British Columbia, September 8-11, p.7-11.

Lawson, J. D., trollope, D. H., and Parkin, A. K. (1962). Some hydraulic aspects of unconventional rockfill dams. Proceedings, 1st Australia Conf. on Hydraulics and Fluid Mechanics, Perth, W. Aust., pp.159-172, (Pergamon - Ed. R. Silverster)

Leps T.M., 1973. Flow through rockfill, in "Embankment Dam Engineering", R.C. Hirschfeld, Ed., John Wiley and Sons, p.87-107.

Li, Bingjun, and Hu, Qulie, 1988. Simulation theory for overtopped rockfill dams in a hydraulic flume, Nanjing Hydraulic Research Institute, May.

Li, Bingjun, (1989). Research on the Characteristics of Hydraulics in Rough Gravel

Channels, Scientific Report Hydro 8956 (in Chinese), Nanjing Hydraulic Research Institute, December, pp. 1-30.

Li, Bingjun, (1990). Characteristics of Flow in Rough Channels with Permeable Bed, 7th Congress APD-IAHR, Beijing, November, pp. 1-7.

Li, Bingjun, and Hu, Qulie, (1990). Experimental Simulation of Rockfill Dam Overtopping, 7th Congress APD-IAHR, Beijing, November, pp. 1-7.

Li, Bingjun, (1991). Modelling technique and theoretical analysis of rockfill dam overtopping, Journal of Nanjing Hydraulic Research Institute, Sept., No. 3. pp. 283-289.

Li, Bingjun, (1992). Velocity profile and friction coefficient in rough permeable channels, Journal of Nanjing Hydraulic Research Institute, Sept., No. 3. pp. 283-289.

Li, Baojian, 1960. Seepage through rockfill dam, Institute of Hydraulic and Hydroelectric Engineering, Beijing, January

Marachi, D. N., Chan, C. K., Seed, H. B., and Duncan, J. M., Strength and Deformation Characteristics of Rockfill Materials, Report No. TE 69-5 to State of California Department of Water Resources, 1969

Martins, R., 1990. Turbulent seepage flow through rockfill structures. Water Power and Dam Construction, March, p.41-45.

Martins, R., 1991. Chapter 17 Principles of rockfill hydraulics. Advances in rockfill structures, Kluwer Academic Publishers, PP. 523-570.

Maynard, S. T., 1990. Flow resistance of riprap. ASCE, Journal of Hydraulic Engineering, Vol. 117, No.6, June, 1991.

McCorquodale, J. A., 1970. Finite element analysis of non-Darcy flow in porous media. PhD thesis, University of Windsor, Windsor, Ontario.

McCorquodale, J.A., Hannoura, A.A., and Nasser, M.S., 1978. Hydraulic conductivity of rockfill. *Journal of Hydraulic Research*, Vol.16, No. 2, pp.123-137.

Mustafa, S., and Rafindadi, N.A., 1989. Nonlinear steady state seepage into drains. *ASCE Journal of Irrigation and Drainage Engineering*, Vol. 115, No. 3, June, pp.358-376.

Nirandra, H.S., 1973. Non-Darcy flow through porous media. M. Tech. thesis, Dept. of Civil Engineering, I.I.T. Kanpur, India, July.

Olivier, H., 1967. Through and overflow rockfill dams - new design techniques. *Proceedings of the Institute of Civil Engineers*, paper No. 7012, vol. 36, pp.433-471.

Parkin, A.K., 1963a. Rockfill dams with inbuilt spillways. Part I, hydraulic characteristics. Bull. 6, University of Melbourne and Water Res. Found. of Australia, March, 88p.

Parkin, A.K., 1963b. Rockfill dams with inbuilt spillways. Part II, stability characteristics. Bull. 7, University of Melbourne and Water Res. Found. of Australia. December.

Parkin, A. K., 1971. Field Solutions for Turbulent Seepage Flow. *Journal of the Soil Mechanics and Foundations Division, Proceeding of ASME*, Vol. 97, No. SM1, January, pp. 209-218.

Parkins, A.K., 1991. Through and Overflow Rockfill Dams. *Advances in Rockfill Structures*, pp. 571-592. Kluwer Academic Publishers.

Powledge, G. R., and Dodge, R. A. (1985). Overtopping of small dams - an alternative for dam safety. Proc. Hydr. and Hydro. in Small Computer Age, ASCE, 2. Aug., 1071-1076.

Reese, A., 1984. Riprap sizing - four methods. Proceedings of the ASCE Specialty Conference on Water Resources for Development, Coeur d'Alene, Idaho, pp.397-401.

Sarkaria, G.S., and Dworsky, B.H., 1968. Model studies of an armored rockfill overflow dam. Water Power, November, pp.455-462.

Shand, N., and Pells, P.J.N., 1970. Experience in the design and construction of reinforced rockfill dams. Tenth International Congress on Large Dams, Montreal, Quebec, June 1-5, pp.291-319.

Sharp, B.B., and James, J.P., 1963. Spatially varied flow at the toe of a rockfill slope. Proceedings of the first Australian Conference on Hydraulics and Fluid Mechanics, Perth, Australia.

Slepicka, F., 1961. The law of filtration and limits of their Validity. IAHR 9th Congress, Dulrovník, pp. 383-394.

Smith, K.V.H., 1986. Probabilistic approach on the stability analysis of rock protection for earth weirs. Proc. Inst. of Civil Engineers, June, pp.243-253.

Smith, I.M., and Griffiths, D.V., 1988. Programming the finite element method. 2nd. John Wiley & Sons, pp.47-50.

Sparks, A.D., 1967. The sloughing, overtopping, and reinforcement of rockfill and earth dams. 9th International Congress on Large Dams, Istanbul, Turkey, Sept. 4-8, Vol. 4, pp.327-349.

Stephenson, D., 1978. Hydraulics of gabions and rockfill. XVI Convegno di Idraulica e Costruzioni Idrauliche, Torino, Italy, Sept., B-31-1 to B-31-11.

Stephenson, D., 1979. Rockfill in Hydraulic engineering. Elsevier Scientific, Amsterdam, 215 p.

Sunada, D.K., 1964. Laminar and turbulent flow through porous media. PhD thesis, University of California at Berkeley.

Taylor, D. W., (1948). Fundamentals of Soil Mechanics. John Wiley and Sons, New York.

Ulrich, T., 1987. Stability of rock protection on slopes. ASCE, Journal of Hydraulics, Vol. 113, No.7, July, pp.879-891.

Veiga Pinto, A., 1979. Caracteristicas de resistencia e deformabilidade dos materiais de enrocamento (in Portuguese), Revista da Sociedade Portuguesa de Geotecnia no. 27, November.

Volker, R.E., 1969. Nonlinear flow in porous media by finite elements. ASCE Journal of Hydraulics Division, Vol.95, HY6, November, pp.2093-2114.

Volker, R.E., 1975. Solutions for unconfined non-Darcy seepage. ASCE Journal of the Irrigation and Drainage Division, Vol.101, IR4, March, pp.53-65.

Ward, J.C., 1964. Turbulent flow in porous media. Journal of the Hydraulics Division, ASCE, Vol.92, HY4, September, pp.1-12.

Wilkins, J.K., (1956). Flow of water through rockfill and its application to the design of dams. Proceedings, 2nd Australia-New Zealand Conf. on Soil Mechanics and Foundation Engineering, Canterbury, N.Z. pp.141-149.

Wilkins, J.K. (1963). The stability of overtopped rockfill dams, Proceedings, 4th Australia-New Zealand Conf. on Soil Mech. and Found. Eng., Adelaide, Australia, pp.1-7.

Wright, D.E., 1968. Non-linear flow through granular materials. Journal of the Hydraulics Division, Vol.94, HY4, paper 6018, July, pp.851-872.

Wurbs, R.A., 1987. Dam-breach flood wave models. ASCE, Journal of Hydraulic Engineering, Vol. 113, No.1, January. pp.29-46.

Zagni, A. F. E., and Smith, K. V. H., (1976). Channel Flow over Permeable Beds of Graded Spheres, J. of the Hydr. Div., ASCE, Vol. 102, No. 2, pp. 207-222.

# **Appendix I: Summary of Useful Results from Nanjing Hydraulic Research Institute (NHRI)**

## **1.1 Introduction**

Research activities in flowthrough and overtopping rockfill dams have been conducted at the Nanjing Hydraulic Research Institute (NHRI) from 1985 to 1990. The major areas include physical modelling for the Tianshengqiao rockfill dam under construction, and its upper cofferdam, and comprehensive studies including characteristics of overtopping flow, seepage flow, protection method and failure pattern, analysis of stability, simulation theory, and prototype observation. The research is conducted by a group of scientists lead by Hu, Qulie, and Li, Bingjun, and the work has been presented in Hu and Li (1988, 89, 91, 92). It appears important to include applicable results in the present research. The following text presents a summary of these results.

## **1.2 Simulation Theory and Physical Model Design**

**1.2.1** Due to the fact that no model simulation theory was available for physical modelling of an overtopped rockfill dam, theoretical studies were conducted by Li and Hu (1990). These results were used for physical model design of an overtopped rockfill dam protected by steel mesh. The following guidelines were followed in the design of a physical model:

1. The physical model of rockfill dam overtopping should be undistorted and comply with the laws of similitude of gravity and flow resistance (Nanjing Hydraulic Research Institute, 1988).
2. For flow over a gentle slope, overflow plays an important role in controlling the fluid pattern. When  $R/d_{50} > 15$  (where  $R$  = hydraulic mean radius,  $d_{50}$  = the average diameter of rockfill particles), the hydraulic characteristics in prototype could be reflected in the physical model.

3. For flow over a steep slope, the effect of seepage flow on the overflow depends on the porosity and the size and shape of rockfill. If the permeability of the model is very high, the flow pattern in the model may be different from that in the prototype.
4. The initial condition of overtopping flow over a rockfill dam with the increase of upstream water level may not be simulated in a physical model if the permeability of rockfill is not low. The simulation of flow between the flowthrough stage and fully overtopping stage is difficult to model in the laboratory.
5. Since the model is designed according to gravity law, the permeability of rockfill in the model is not similar to that in the prototype. However, some important characteristics of the seepage field in prototype could be evaluated from the results in the physical model studies. The seepage rate in the model can be extended to the prototype by the following equation (not the gravity law!):

$$\lambda_v = \lambda_k i_M^{\frac{1}{N_M} - \frac{1}{N_P}} \quad (1-1)$$

where

$\lambda_v$  = the modelling scale for seepage velocity;

$\lambda_k$  = the modelling scale for the permeability of rockfill material;

$i_M$  = the hydraulic gradient measured in the model;

$N_M$  = the power order for power law measured in the model;

$N_P$  = the power order for power law in prototype, usually  $N_P = 2$ .

If  $N_P = N_M$ , Equation (1-1) becomes

$$\lambda_v = \lambda_k \quad (1-2)$$

This is the same as the simulation law of Darcy flow in physical modelling (Nanjing Hydraulic Research Institute, 1988). Eq. (1-2) provides a general modelling theory if  $N_P$

=  $N_M$ . In this case, the flow pattern of seepage flow in the physical model and that in the prototype are the same, i.e., it could be Darcy flow, fully turbulent flow, or at some intermediate stage. This also provides a method for the design of the scale of the physical model. Since in flowthrough and overtopped rockfill dams, seepage flow is usually fully turbulent in the prototype, it is necessary that the scale of the physical model be large enough to develop fully turbulent flow.

6. The size of the steel mesh used to protect the downstream slope should be designed according to the gravity similitude law. The diameter of the modelled mesh may be determined according to:

$$\lambda_\phi = (\lambda_l^3 / \lambda_{RR})^{1/2} \quad (1-3)$$

in which  $\lambda_\phi$  is the scale-factor of the diameter of reinforcing mesh,  $\lambda_{RR}$  the scale-factor of tensile strength of the mesh material,  $\lambda_l$  is the scale-factor of the dimension of the model. If the same type of material has been used in the model as that in the prototype, then  $\lambda_{RR} = 1$ . In this case, Eq. (1-3) becomes:

$$\lambda_\phi = \lambda_l^{3/2} \quad (1-4)$$

For example, in the modelling of the Tianshengqiao rockfill dam, a scale of  $\lambda_l = 36$  was used. The diameter of steel mesh in the field was  $\phi_P = 40\text{mm}$ . from Eq. (1-4) indicated that the diameter that should be used in the physical model was  $\phi_M = 0.18\text{ mm}$ , which was too small to be modelled. In the simulation of Tianshengqiao rockfill dam, a plastic mesh was therefore used in the physical modelling (Hu, and Li, 1989).

1.2.2 Experimental studies of the Tianshengqiao rockfill dam and the upper cofferdam under construction in flood period were also conducted at the Hydraulic Laboratory of Nanjing Hydraulic Research Institute (Hu, and Li, 1989). The scales of the models were 1/36 and 1/25.

Experiments were conducted in a flume 0.8 m wide, 3 m in height, and 35 m in length. Figure I - 1 shows the profiles of some physical models (Hu, and Li, 1989). The height of the upstream cofferdam was approximately 21.1 m, the upstream slope was 1:3.5, and downstream slope was 1:1.5. Concrete blocks, steel mesh, and steel bars were used to protect the downstream slope of the upstream cofferdam. The upstream slope of the unfinished rockfill dam (under construction) was 1.4:1, and the downstream slope 1.29:1. The surface of the unfinished dam was protected with large-size rock particles, while its downstream slope is protected by the concrete blocks, steel mesh, and steel bars. Reinforcing cages were used at the toe of the downstream slopes of the upstream cofferdam and the unfinished rockfill dam.

### **I.3 Summary of Experimental Results from NHRI**

#### **I.3.1 Characteristics of Overtopping Flow**

Photographs I-1 and I-2 show the flow pattern of steep open channel flow with shallow downstream water depth.

##### **I.3.1.1 Estimation of Discharge**

Unit width discharge over a rockfill dam may be calculated by:

$$q = m\sigma (2g)^{0.5} H_o^{1.5} \quad (I-5)$$

where

$\sigma$  = coefficient of submergence, for free flow  $\sigma=1$ ;

$m$  = discharge coefficient;

$H_o$  = upstream water head (over the crest of the dam);

$g = 9.81 \text{ m/s}^2$ .

The value of  $m$  and  $\sigma$  are given in Figure I-2, based on the NHRI experimental data.

### 1.3.1.2 Hydraulic Jump at the Downstream Slope

Due to the seepage flow within the rockfill dam, the open channel flow appears to be pushed up by the downstream seepage flow. The pressure measurement show that there is no negative pressure at the base of the hydraulic jump. Experiments also show that there is no undercurrent in the reverse direction under all flow conditions. The hydraulic jump at the downstream slope is found to be located at the surface of overtopping flow. The conjugate depth (Fig. 1-3) is derived as (Hu and Li, 1989):

$$\frac{h_2}{h_1} = \frac{1}{2} \left[ \frac{K_0 \sin \theta}{2 Fr_1 + \cos \theta} \frac{L}{h_1} + \sqrt{\left( \frac{K_0 \sin \theta}{2 Fr_1 + \cos \theta} \frac{L}{h_1} \right)^2 + 4 \frac{2 Fr_1 + \cos \theta + K_0 \sin \theta}{2 Fr_1 + \cos \theta} \frac{L}{h_1}} \right] \quad (1-6)$$

where  $K_0 = \text{constant}$ , usually  $K_0 = 1$ .

$$Fr_1 = \frac{V_1}{\sqrt{g h_1}} \quad (1-7)$$

$$Fr_1 = \frac{V_1}{\sqrt{g h_1}} \quad (1-8)$$

Studies show that with the increase of  $h_1$  and decrease of  $Fr_1$ , it is possible for incomplete jump (actually wave at the free surface) to take place at the downstream slope. This was observed in the experiments.

### 1.3.1.3 The Influence of Seepage Flow on Total Discharge

It was observed from the experiments that when the size of the rockfill material is small, the seepage discharge is very small compared with the overtopping flow. With the increase of the size of rockfill material, the percent of seepage discharge over the total discharge would increase (maximum 24% found in the experiments).

#### 1.3.1.4 Selection of the Profile of An Unfinished Rockfill Dam during Flood Period

A large rockfill dam usually takes several years for its construction. The flood discharge through the dam site in the flood period each year during construction is a very important design consideration. In conventional construction design, an upstream cofferdam (which in many cases resembles a medium size dam ) and a diversion tunnel with high discharge capacity are usually provided and which are generally very expensive. Considerable economy can be realized if large flows are allowed to flow over the unfinished dam section (or part of it). In this case, some protection for the downstream slope and the crest may be necessary. The provision for overtopping flow in the design implies that a lower upstream cofferdam, and small sized diversion tunnels will be required.

The profile of an unfinished rockfill dam is usually very long compared to its height. Experiments at the Nanjing Hydraulic Research Institute show that open channel flow theories can be applied. The key considerations in the design are to make the flow pattern stable, the average velocity uniform along the flow direction, and to ensure that the damage due to erosion at the downstream exit is prevented. The hydraulic gradient within the dam is close to the gradient of the free water surface of overtopped flow, except at the upstream and downstream regions of the dam. Some theoretical and computational models to estimate the seepage flow were proposed by Li (1990).

#### 1.3.2 Summary of Results on Seepage Flow

Power law was used in the studies. The relationship between velocity and hydraulic gradient is derived as:

$$v = \left( \frac{d e^{1-b} g n^{2+b}}{a v^{-b}} \right)^{1/(1+b)} i^{1/(2+b)} \quad (1-9)$$

where

$n$  = the porosity of a rockfill dam;

$g$  = the gravitational acceleration;

$d$  = average diameter;

$a$  = coefficient which depends on the Reynolds number and can be determined from Table I-1;

$b$  = coefficient which depends on the Reynolds number and can be determined from Table I-1;

$e$  = the void ratio;

$\nu$  = the kinetic viscosity.

The disadvantage of the above approach is that the range of Reynolds number in a rockfill dam should be known before the determination of  $a$  and  $b$ . For prototype rockfill dams, the seepage flow within rockfill is usually fully turbulent. Hence,  $a$  is 4, and  $b$  is 0 for prototype dams.

Detailed pressure distributions and seepage paths have been measured in physical models. It was found that for unfinished rockfill dam, when the "crest" is very long compared with the height of the dam, the average seepage gradient is approximately that of the surface of the overtopping flow. This means that the seepage flow in the unfinished rockfill dam can be estimated by 1-dimension empirical relationships. This finding makes the design much easier.

Pulsating pressures were measured at the downstream slope of an overtopped rockfill dam. Figure I-4 shows a set of results. It was found for the first time that:

(1) Pulsating energy is distributed in the frequency range: 0 ~ 10 Hz. The probability density curve is close to the normal distribution.

(2) The pulsating pressure normal to the downstream slope may reach a maximum value of about half of the upstream water head over the crest. The reason of this phenomenon may be that the seepage flow is fully turbulent and that the interaction of turbulent overtopping flow and turbulent seepage flow can have strong influence on the

instability of the particle. For a safe design, the pulsating force should be included. Unfortunately this force was not accounted for in previous design methods.

## **1.4 Prototype Observation**

Prototype observation is an important method to check the design criteria obtained from theory or/and from experiment. Experience was obtained from the prototype observation of the unfinished Xibeikou Concrete Faced Rockfill Dam overtopping in the flood period of 1987 (Hu, et. al, 1988).

Xibeikou Concrete Faced Rockfill Dam is located in Yichang County in Hubei Province, China. The design height of the dam is 95 m. During the construction, the dam could not reach the required elevation to prevent overtopping. Hence a layer of large rockfill was built at the downstream slope with a flat slope 8.2:1 to protect the flowthrough and overtopping flow in the flood period in 1987 for a discharge of 1460 m<sup>3</sup>/s. The approximate height of the dam under construction was about 17 m. A team was organized by Gezhou Dam Engineering Board and Nanjing Hydraulic Research Institute to conduct the prototype observation. The velocity, discharge, water level, free surface curve, the deformation of the dam, seepage pressure, flow pattern, and stability of rock particles at the downstream slope were measured.

On August 28, 1987, at 18:45, the upstream water level reached 265 m. At 20:10, water started to flow through the dam. At 23:00, the surface of the unfinished rockfill dam was almost all covered by water, and the upstream water level at the upstream shoulder of the dam was 266.7 m, while the water depth above the crest was 2.67 m. On August 29, 1987, at 2:00AM, the water surface level at the upstream shoulder of the dam was 266.4 m. At 6:00AM, the water level dropped to 264 m, and there was no flow over and through the dam. The observation of flow through and over the dam lasted all evening.

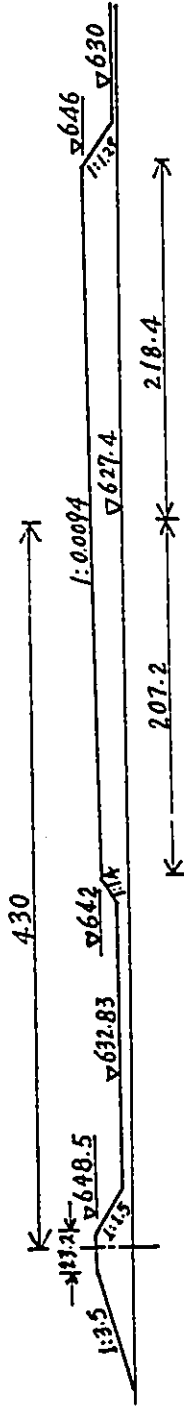
The maximum discharge through and over the dam was  $62.3 \text{ m}^3/\text{s}$ . The deformation settlement of the surface of the unfinished was found to be small. The water through the dam was very clear, no rockfill material in the dam was found to be lost due to the flow through and over the dam. No large rock particles at the downstream slope were found to have been moved by the flow. The use of a very flat downstream slope and large rock particles as a protection method was found to be successful. However from economical point of view, the protection method was too conservative.

## **1.5 Conclusion**

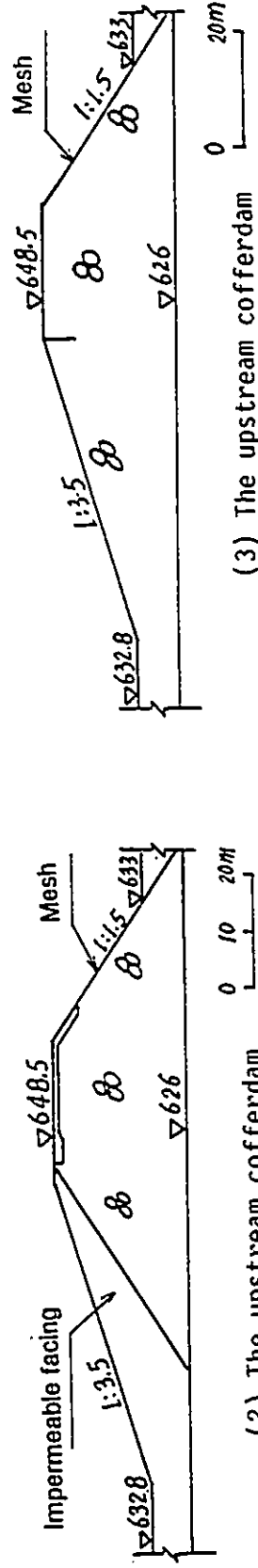
The research activities from 1986 to 1990 were concentrated on the characteristics and physical modelling of flow through and over rockfill dams. The results were used in unfinished rockfill dams, e.g., the Tianshengqiao Concrete Faced Rockfill Dam, and the Xibeikou Concrete Faced Rockfill Dam in China. Most of the results which are useful in small complete flowthrough and overtopped rockfill dam are presented in this Chapter and also became an important background for this study at the University of Ottawa.

Table I -1 Determination of Coefficients a and b

Re	<10	10 ~100	100~420	420~3300	>3300
a	800	2.846	2.815	2.145	4
b	-1	-0.774	-0.776	-0.507	0



(1) The longitudinal profile of the dam 0 36m



(2) The upstream cofferdam

(3) The upstream cofferdam

Figure I-1 The configuration of physical models

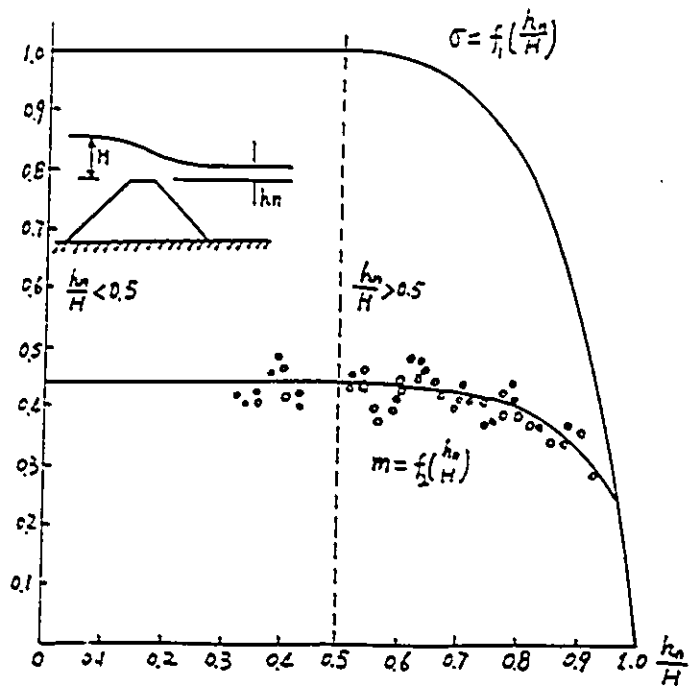


Figure I-2 Value of  $m$  and  $\sigma$

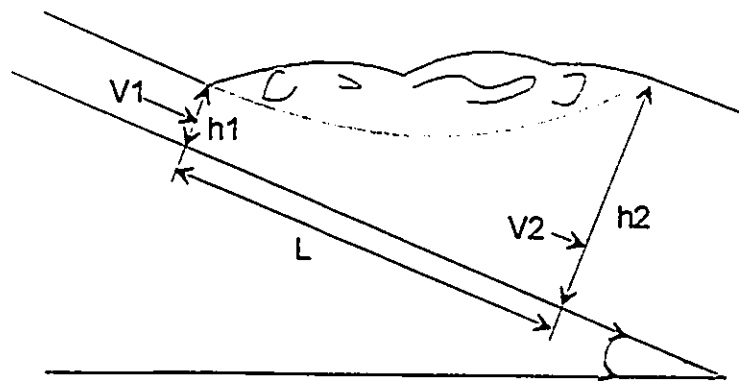
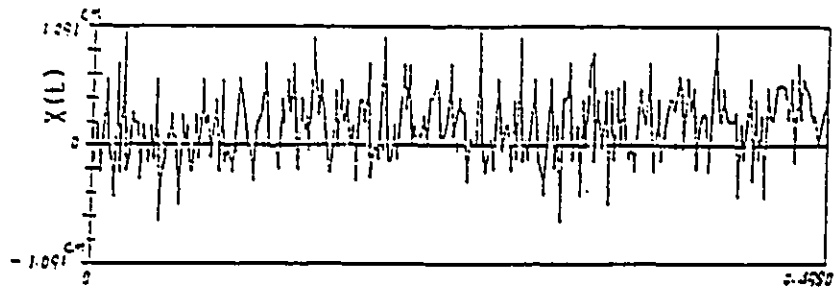
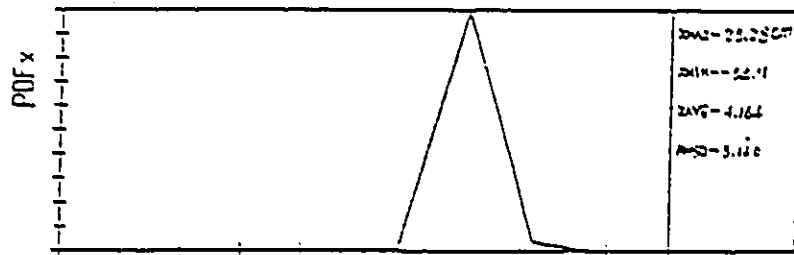


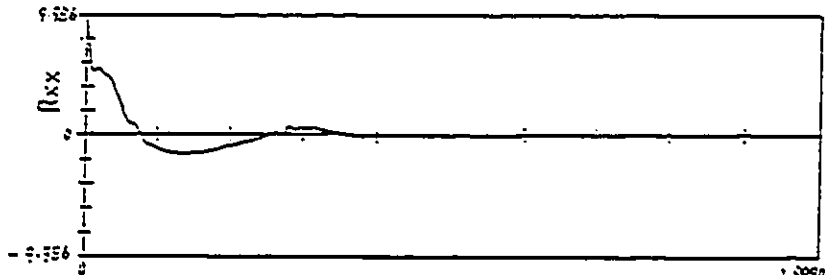
Figure I-3 Definition of Parameters in Hydraulic Jump



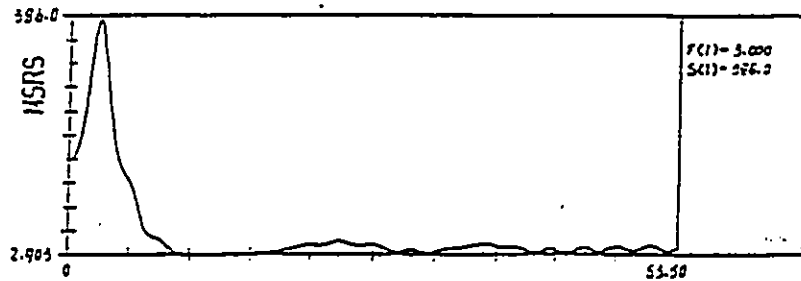
Original Data



Probability density distribution

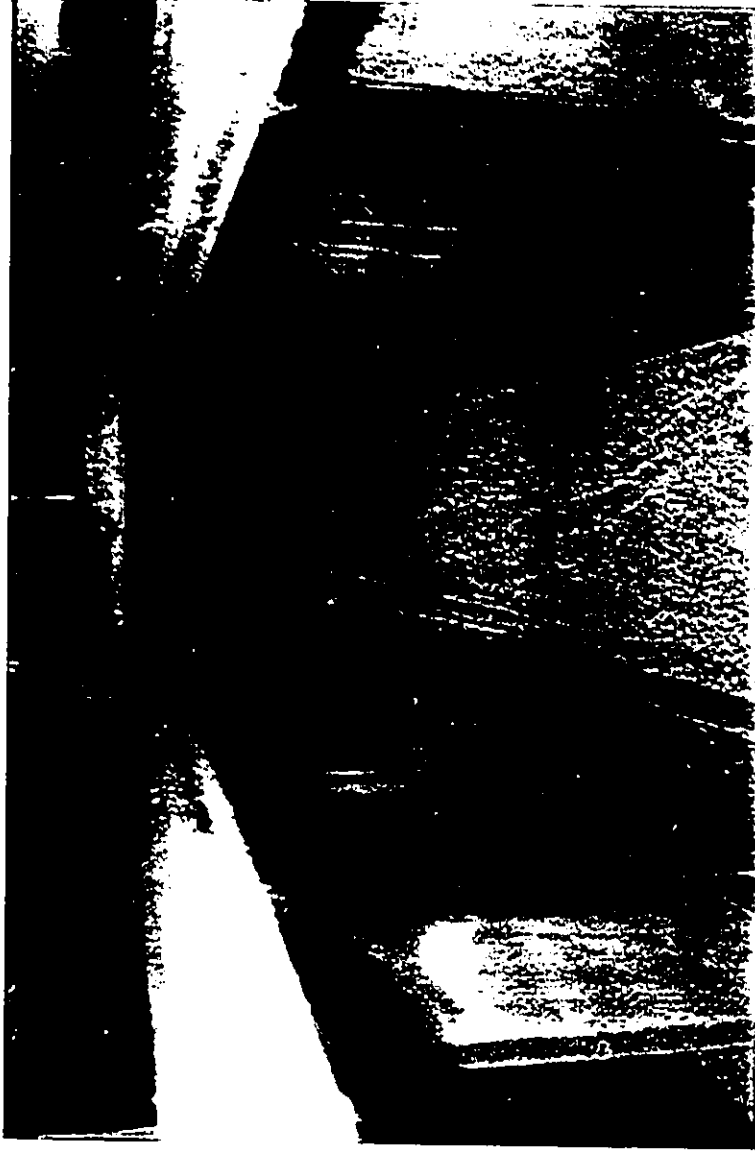


Autocorrelation function



Power density distribution

Figure I-4 A sample of pulsating pressure results



Photograph I-1 A downstream view of steep open channel flow



Photograph I-2 A side view of steep open channel flow

## **Appendix II Examples for the Design of Flowthrough and Overtopped Rockfill Dams**

This appendix presents detailed design and calculations for a realistic situation using the methodology proposed in Chapter 8. It is assumed that the dam is small, and detailed pore pressure distribution in the dam is not available.

### **II.1 Geometry of the dam**

The site selected is located approximately 1 km from Highway 210 in the Paradise River basin in Newfoundland. The foundation comprises of hard rock with negligible soil cover. Ample supply of rockfill required for the construction of the dam can be readily available by opening a small rock quarry in the site. The average width of the valley where the dam is located is 87.3 m. The width at the crest is also taken as 87.3m to simplify the example. Hence, the design given here is for a two-dimension problem. For 3-dimension design, the length of the dam changes along the downstream slope. In this case, more calculations may be needed to calculate the distribution of unit-weight discharge along the downstream slope. Two designs are given in this appendix.

In the first case, it is assumed that the downstream slope is protected by large size of particles only. The height of the dam is 5.5m; the upstream slope 1.4:1, the downstream slope is 3:1; the width of crest is 4m. Fig. II-1 shows the configuration of the dam.

The apron at the downstream has a slope of 9.8:1. Details of the apron are shown in Figure II-2.

For the second case, it is assumed that the dam is protected by steel mesh and steel bars at the downstream slope. The height of the dam is again 5.5 m with both the upstream and the downstream slopes inclined at 1.4:1. The crest width is 4 m (Fig. II-3).

## II.2 Rockfill

For the main part of the dam, the size of rock particles is between 15 cm and 30 cm. The average size is 22.5 cm.

The mean hydraulic radius is determined by Eq. (8-2):

$$R = 0.136 * 0.225 = 0.0306 \text{ m}$$

## II.3 Case 1: Design of the rockfill dam protected by large particles only (Figs. II-1 and II-2)

From hydrological analysis, the maximum stream discharge was estimated at 110 m<sup>3</sup>/s. The seepage flow through the dam may be calculated by the following steps:

(1) Average hydraulic gradient

By Eq. (8-3):

$$i_{ave} = 0.8 * (1)^{1.4} \left( \frac{5.5}{7.7 + 4 + 0.5 * 16.5} \right)^{\frac{3}{2}} = 0.116$$

(2) Seepage discharge

The unit width discharge is calculated by Eq. (8-4):

$$\begin{aligned} q_s &= 1.58 * 0.4 * \sqrt{9.8 * 0.0306 * 0.116} * 5.5 \\ &= 0.648 \text{ m}^3 / \text{s} / \text{m} \end{aligned}$$

Hence the total seepage discharge through the dam is determined by Eq. (8-5):

$$Q_s = q_s L = 0.648 \text{ (m}^2/\text{s)} * 87.3 \text{ m} = 56.6 \text{ m}^3/\text{s}$$

### (3) Overtopping discharge

The discharge over the crest of the dam is given by Eq. (8-8):

$$Q_{\text{crest}} = Q_{\text{total}} - Q_s = 110 \text{ m}^3/\text{s} - 56.6 \text{ m}^3/\text{s} = 53.4 \text{ m}^3/\text{s}$$

The unit-width discharge over the crest of the dam is given by Eq. (8-7):

$$q_{\text{crest}} = \frac{Q_{\text{crest}}}{L_{\text{crest}}} = \frac{53.4 \text{ m}^3/\text{s}}{87.3 \text{ m}} = 0.612 \text{ m}^3/\text{s}/\text{m}$$

The upstream water head over the dam is calculated by Eq. (8-6):

$$H_0 = \left( \frac{q_{\text{crest}}}{m \sigma \sqrt{2g}} \right)^{\frac{2}{3}} = \left( \frac{0.612}{0.44 * 1 * \sqrt{2 * 9.8}} \right)^{\frac{2}{3}} = 0.462 \text{ m}$$

The length of the downstream slope (without apron):

$$l_{ds} = \frac{H}{\sin \alpha} = \frac{5.5}{\sin 18.4} = 17.4 \text{ m}$$

Assuming linear distribution of the seepage velocity out of the downstream slope,

$$v_{s,av} = \frac{q_s}{l_{\text{dslope}}} = \frac{0.648}{17.4} = 0.0372 \text{ m/s}$$

The overtopping discharge along the downstream slope is

$$Q = Q_{\text{crest}} + v_{s,av} * x_s * L(x_s)$$

where  $x_s$  = the distance long the downstream slope from the intersection of crest and downstream slope.

The unit width discharge over the slope is given by:

$$\begin{aligned} q &= q_{\text{crest}} + v_{s,\text{av}} * x_s \\ &= 0.621 + 0.0372 x_s \text{ (m}^2 \text{/s)} \end{aligned}$$

It is noticed that the discharge increases along the slope. As expected, the critical section for the design is at the toe of the downstream slope.

#### (4) Design downstream slope protection by rock layer

With the design of the apron, there are two critical sections to be considered in the design. One is at the toe (the slope is very flat as shown Fig.II-2). The other is at the height of 1.47 m (see Figs. II-1 and II-2).

In the design procedure described in Chapter 8, firstly estimate the average diameter or rock particles by experience or Eq. (2-94) (here the latter is used). Then calculate the safety factor of the slope FS by Eq. (8-14). If the FS is smaller than 1.5, increase the average diameter and re-calculate FS until  $FS \geq 1.5$ . The depth of the rock layer is determined by Eq. (8-15).

For the section at the toe, the total discharge is exactly  $110 \text{ m}^3 \text{/s}$ , unit-width discharge  $q = 110/87.3 = 1.26 \text{ m}^2 \text{/s}$ . Assuming that the probability of a concentrated flow is high (as the quality of the construction may not be very high), the concentration coefficient is selected as 2.0 by Eq. (2-92). The unit discharge at failure by Eq. (2-91):

$$\begin{aligned} q_f &= c_f q \\ &= 2 * 1.26 = 2.52 \text{ m}^3 \text{/s / m} \end{aligned}$$

The average diameter for the protection by Eq. (2-90):

$$D_{50} = 0.503 * 0.102^{0.43} 2.52^{0.56}$$

$$= 0.316 \text{ m}$$

At the height of 1.47m, that is, the intersection of the downstream slope with slope 3:1 and the apron with slope 9.8:1, the value of  $x_g = 17.4 - 1.47 / \sin 18.4 = 12.8$  m. The discharge is then calculated by:

$$q = 0.621 + 0.0372 * 12.8$$

$$= 1.10 \text{ m}^3 / \text{s} / \text{m}$$

The unit discharge at failure by Eq. (2-91):

$$q_f = c_f q$$

$$= 2 * 1.10 = 2.20 \text{ m}^3 / \text{s} / \text{m}$$

The average diameter of the rock particles in the protection layer is given by:

$$D_{50} = 0.503 * 0.102^{0.43} 2.20^{0.56}$$

$$= 0.293 \text{ m}$$

The average size of protected rock particles should be larger than the above  $D_{50}$  size. For the Paradise river, the available  $D_{50}$  rockfill size is 0.32 m, which is adequate.

To check the safety factor against unravelling failure of the particles along the downstream slope, Eq. (8-14) may be used. The following parameters are obtained for use in Eq. (8-14).

$$\frac{\gamma_b}{\gamma_w} = \frac{G-1}{1+e} = \frac{2.7-1}{1+0.667} = 1.02.$$

$$k_p = 1.34, \text{ and } k_f = 1 .$$

$J_0 = 0.102$  at the toe of the apron, and  $J_0 = 0.333$  at the intersection of the 3:1 slope and the apron.

$\alpha = 5.2$  at the toe of the apron, and  $J_0 = 18.4$  at the intersection of the 3:1

slope and the apron.

$$d_p = D_{50}/2 = 0.16 \text{ m.}$$

$$\phi' = 45^\circ.$$

By Eq. (8-10), Manning coefficient

$$\begin{aligned} n_d &= 0.0380 D_{50}^{1/6} \\ &= 0.0380 * 0.32^{1/6} = 0.022 \end{aligned}$$

By Manning Equation for wide open channel:

$$v = \frac{1}{n_d} h_o^{2/3} J_o^{1/2}$$

it is obtained that

$$q = v h_o = \frac{1}{n_d} h_o^{5/3} J_o^{1/2}$$

Hence

$$h_o = \left( \frac{q n_d}{J_o^{1/2}} \right)^{3/5}$$

$$\begin{aligned} \text{At the toe, } J_o = 0.102, \quad h_o &= \left( \frac{q n_d}{J_o^{1/2}} \right)^{3/5} = \left( \frac{1.26 * 0.022}{0.102^{1/2}} \right)^{3/5} = 0.231 \text{ m. Velocity } v = q/h \\ &= 1.26/0.231 = 5.45 \text{ m/s.} \end{aligned}$$

At the intersection of 3:1 slope and the apron,  $J_o = 0.333$ ,

$$\begin{aligned} h_o &= \left( \frac{q n_d}{J_o^{1/2}} \right)^{3/5} \\ &= \left( \frac{1.10 * 0.022}{0.333^{1/2}} \right)^{3/5} = 0.149 \text{ m} \end{aligned}$$

$$\text{Velocity } v = q/h = 1.1/0.149 = 7.38 \text{ m/s.}$$

The safety of the rock particles along the slope is given by Eq. (8-14). At the toe:

$$\begin{aligned}
 FS &= \frac{\frac{\gamma_b}{\gamma_w} \cos \alpha - (k_F + k_p) J_0 (1+e) \sin \alpha}{\cos \varphi \left[ \frac{n_d^2 v^2}{h^{1/3} d_p} + (k_F + k_p) J_0 (1+e) \cos \alpha + \frac{\gamma_b}{\gamma_w} \sin \alpha \right]} \\
 &= \frac{1.02 * \cos 5.8 - (0.6+1) * 0.102 * (1+0.667) \sin 5.8}{\cos 45 \left[ \frac{0.022^2 * 5.45^2}{0.231^{1/3} * 0.16} + (0.6+1) * 0.102 * (1+0.667) \cos 5.8 + 1.02 * \sin 5.8 \right]} \\
 &= \frac{1.01 - 0.027}{0.707 * (0.146 + 0.271 + 0.103)} = 2.7
 \end{aligned}$$

The above factor of safety indicates that with the use of the apron, the toe of the dam has adequate stability.

At the intersection between the 3:1 slope and the apron:

$$\begin{aligned}
 FS &= \frac{\frac{\gamma_b}{\gamma_w} \cos \alpha - (k_F + k_p) J_0 (1+e) \sin \alpha}{\cos \varphi \left[ \frac{n_d^2 v^2}{h^{1/3} d_p} + (k_F + k_p) J_0 (1+e) \cos \alpha + \frac{\gamma_b}{\gamma_w} \sin \alpha \right]} \\
 &= \frac{1.02 * \cos 18.4 - (0.6+1) * 0.333 * (1+0.667) \sin 18.4}{\cos 45 \left[ \frac{0.022^2 * 7.36^2}{0.149^{1/3} * 0.16} + (0.6+1) * 0.333 * (1+0.667) \cos 18.4 + 1.02 * \sin 18.4 \right]} \\
 &= \frac{0.968 - 0.280}{0.707 * (0.309 + 0.843 + 0.032)} = 0.82
 \end{aligned}$$

The above factor of safety indicates that the downstream slope from the crest to its intersection with the apron is unsafe for overtopping flow. This slope has to be flatter than 3:1. An alternative design may be to use a uniform flatter downstream slope, say

5.5:1 ( $\alpha=10.3^\circ$ ) with the same apron. The calculation can now be repeated, as shown below.

Assuming linear distribution of the seepage velocity out of the downstream slope,

$$v_{s,av} = \frac{q_s}{l_{dslope}} = \frac{0.648}{5.5/\sin 10.3} = 0.0211 \text{ m/s}$$

$$\begin{aligned} q &= q_{crest} + v_{s,av} * x_s \\ &= 0.621 + 0.0211 * (5.5 - 1.47) / \sin 10.3 \\ &= 1.10 \text{ m}^3/\text{s/m} \end{aligned}$$

At the intersection of 5.5:1 slope and the apron,  $J_0 = 1/5.5 = 0.182$ ,

$$\begin{aligned} h_0 &= \left( \frac{q n_d}{J_0^{1/2}} \right)^{3/5} \\ &= \left( \frac{1.10 * 0.022}{0.182^{1/2}} \right)^{3/5} = 0.179 \text{ m} \end{aligned}$$

Velocity  $v=q/h = 1.1/0.179 = 6.15 \text{ m/s}$ .

$$\begin{aligned} FS &= \frac{\frac{\gamma_b}{\gamma_w} \cos \alpha - (k_F + k_p) J_0 (1+e) \sin \alpha}{\cos \phi' \left[ \frac{n_d^2 v^2}{h^{1/3} d_p} + (k_F + k_p) J_0 (1+e) \cos \alpha + \frac{\gamma_b}{\gamma_w} \sin \alpha \right]} \\ &= \frac{102 * \cos 10.3 - (0.6+1) * 0.182 * (1+0.667) \sin 10.3}{\cos 45 \left[ \frac{0.022^2 * 6.15^2}{0.179^{1/3} * 0.16} + (0.6+1) * 0.182 * (1+0.667) \cos 10.3 + 102 * \sin 10.3 \right]} \\ &= \frac{1.0 - 0.0868}{0.707(0.203 + 0.478 + 0.182)} = 1.5 \end{aligned}$$

If the required safety factor is 1.5, then the downstream slope is now safe.

The maximum size of the available rock particles for the protection layer  $D_{100}$  is 0.60 m.

Now the depth of the protection layer is determined by Eq. (8-15):

$$\begin{aligned}t_r &= \max\{1.5D_{50}, D_{100}\} \\ &= \max\{1.5 * 32, 60\} = 60 \text{ cm}\end{aligned}$$

Now the design is complete.

It is easily to check from Olivier's formula Eq. (2-83) that the downstream slope is 5.2:1 when the discharge over and through the dam makes the slope critical as noted below:

$$\begin{aligned}\tan \alpha &= \left( \frac{0.423 D_{50}^{3/2} (G-1)^{5/3}}{q_{cr}} \right)^{6/7} \\ &= \left( \frac{0.423 * 0.32^{3/2} * (2.7-1)^{5/3}}{1.26} \right)^{6/7} = 0.194\end{aligned}$$

$\alpha = 10.99^\circ$ . The slope is  $\frac{1}{0.194} : 1 = 5.2 : 1$ . Hence, the Oliver criteria is close to the new design criteria presented in the report (in the unsafe side) for this design example. It is also of interest to compare the results with Stephenson's criteria Eq. (2-88):

$$D_{50} = \left[ \frac{q_s (\tan \alpha)^{7/6} n^{1/6}}{0.22 g^{1/2} [(1-n)(G-1) \cos \alpha (\tan \phi - \tan \alpha)]^{5/3}} \right]^{2/3}$$

$$= \left[ \frac{1.26(0.182)^{7/6} 0.4^{1/6}}{0.22 * 9.8^{1/2} [(1-0.4)(2.7-1) \cos 10.3 (\tan 45 - 0.182)]^{5/3}} \right]^{2/3}$$

$$= \left( \frac{0.148}{0.496} \right)^{2/3} = 0.446 \text{ m}$$

It is noticed that Stephenson's expression give the highest requirement for the size of the rock particles for this example. It should be kept in mind that only in our criteria and Stephenson's criteria, the seepage force is considered. The pulsating force included in the present criteria is the first time that the stochastic behaviour of the fluid field has been considered.

#### II.4 Case 2: Design of steel mesh protection along the downstream slope (Fig. II-3)

From the hydrological analysis, the maximum discharge was 110 m<sup>3</sup>/s. The seepage flow through the dam may be calculated by the following steps:

(1) Average hydraulic gradient

By Eq. (8-3):

$$i_{ave} = 0.8 * (1)^{1.4} \left( \frac{5.5}{7.7 + 4 + 0.5 * 7.7} \right)^{3/2} = 0.168$$

(2) Seepage discharge

The unit width discharge is calculated by Eq. (8-4):

$$\begin{aligned} q_s &= 1.58 * 0.4 * \sqrt{9.8 * 0.0306 * 0.168} * 5.5 \\ &= 0.780 \text{ m}^3 / \text{s} / \text{m} \end{aligned}$$

Hence the total seepage discharge through the dam is determined by Eq. (8-5):

$$Q_s = q_s L = 0.78 (\text{m}^2 / \text{s}) * 87.3 \text{ m} = 68.1 \text{ m}^3 / \text{s}$$

(3) Overtopping discharge

Hence the discharge over the crest of the dam is given by Eq. (8-8):

$$Q_{\text{crest}} = Q_{\text{total}} - Q_s = 110 \text{ m}^3 / \text{s} - 68.1 \text{ m}^3 / \text{s} = 41.9 \text{ m}^3 / \text{s}$$

The unit-width discharge over the crest of the dam is given by Eq. (8-7):

$$q_{\text{crest}} = \frac{Q_{\text{crest}}}{L_{\text{crest}}} = \frac{41.9 \text{ m}^3 / \text{s}}{87.3 \text{ m}} = 0.480 \text{ m}^3 / \text{s} / \text{m}$$

The upstream water head over the dam is calculated by Eq. (8-6):

$$H_0 = \left( \frac{q_{\text{crest}}}{m \sigma \sqrt{2g}} \right)^{\frac{2}{3}} = \left( \frac{0.480}{0.44 * 1 * \sqrt{2} * 9.8} \right)^{\frac{2}{3}} = 0.393 \text{ m}$$

The length of the downstream slope:

$$l_{ds} = \frac{H}{\sin \alpha} = \frac{5.5}{\sin 35.5} = 9.46 \text{ m}$$

Assuming linear distribution of the seepage velocity out of the downstream slope,

$$v_{s,av} = \frac{q_s}{l_{dslope}} = \frac{0.780}{9.46} = 0.082 \text{ m/s}$$

The unit width discharge over the downstream slope is given by:

$$\begin{aligned} q &= q_{crest} + v_{s,av} * x_s \\ &= 0.480 + 0.082 x_s \text{ (m}^2 \text{/s)} \end{aligned}$$

As  $q$  increases along the slope, the critical section for the design is located at the toe of the downstream slope. At the toe, the unit-width discharge:

$$q = \frac{110 \text{ m}^3/\text{s}}{87.3 \text{ m}} = 1.26 \text{ m}^3/\text{s} / \text{m}$$

$$J_0 = 1/1.4 = 0.714, h_0 = \left( \frac{q n_d}{J_0^{1/2}} \right)^{3/5} = \left( \frac{1.26 * 0.022}{0.714^{1/2}} \right)^{3/5} = 0.129 \text{ m.}$$

Velocity  $v = q/h = 1.26/0.129 = 9.79 \text{ m/s}$ .

The volume of an average rock particle is given by is:

$$V_p = \frac{1}{6} \pi D_{50}^3 = \frac{1}{6} * 3.14 * 0.225^3 = 0.00596 \text{ m}^3$$

The required shear force on one particle is calculated by Eq. (8-17):

$$\begin{aligned}
S &= \gamma_w V_p \left\{ \frac{n_s^2 v^2}{h^{1/3}} + \frac{[k_F + k_P] J_o (1+e) \cos(\alpha - \varphi) + \frac{\gamma_b}{\gamma_w} \sin(\alpha - \varphi)}{\cos \varphi} \right\} \\
&= 9800 \text{ (kN / m}^3\text{)} * 0.00596 \text{ (m}^3\text{)} * \\
&\quad \left\{ \frac{0.022^2 9.79^2}{0.129^{1/3}} + \frac{(1+0.6) * 0.714 * (1+0.667) \cos(35.54 - 45) + 1.02 \sin(35.54 - 45)}{\cos 45} \right\} \\
&= 58.41 \left\{ 0.0917 + \frac{1.878 - 0.168}{0.707} \right\} = 58.41 * 2.51 = 146.6 \text{ kN}
\end{aligned}$$

The size of the steel mesh should be larger than the size of the smallest rock size in the protected layer. Here the mesh size is selected as 20 \* 30 cm<sup>2</sup> (l<sub>x</sub> = 20 cm, l<sub>y</sub> = 30 cm). The area of the steel in the mesh along the slope per unit width, a<sub>m</sub>, is determined by Eq. (8-18):

$$\begin{aligned}
a_m &= F_m \frac{S}{\sigma_{all} D_{50}} \\
&= 1.5 * \frac{146.6}{137.2 * 1000 * 0.32} \\
&= 0.005009 \text{ m}^2 = 5009 \text{ mm}^2
\end{aligned}$$

The number of vertical strands of the mesh per meter length of the slope is 1/0.2=5.

The diameter of the mesh is  $\left(\frac{3.14}{4} * 5009 / 5\right)^{1/2} = 28.0 \text{ mm}$ . If the mesh size is 15\*20

cm (l<sub>x</sub> = 15 cm, l<sub>y</sub> = 20 cm). The diameter of the mesh is now

$$\left(\frac{3.14}{4} * \frac{5009}{1/0.15}\right)^{1/2} = 24.3 \text{ mm}.$$

To conduct the slope stability analysis, the detailed distribution of shear stress along the downstream slope and hence the surface curve of the spatially varied overtopping flow are required. Here the method provided by James and Sharp (1963) and demonstrated by Hansen (1992) are used.

The unit-width discharge at the intersection between the crest and the downstream slope was calculated in the previous section (II.4) as  $q_{\text{crest}} = 0.48 \text{ m}^2/\text{s}$ . The related critical depth is calculated as:

$$h_c = \sqrt[3]{\frac{q^2}{g}} = \sqrt[3]{\frac{0.48^2}{9.8}} = 0.286 \text{ m} \quad (q: \text{unit width discharge, here } q = q_{\text{crest}})$$

The water depth at the intersection between the crest and the downstream slope is calculated by the "brink depth" defined by Henderson (1963) as:

$$h_b = 0.715 h_c = 0.715 * 0.286 = 0.204 \text{ m}$$

The calculation procedure in Hansen (1992) is used (which is essentially from Chow, 1959). In the latter, very detailed standardized steps were listed. The result is shown in Table II-1. Eqs. (8-10), (8-11), and (8-12) are used in Table II-1. Since the flow at the crest is not turbulent, a value of Manning coefficient  $n_d$  smaller than that (0.022 in this example) in fully turbulent flow should be used in the design. Similar to Hansen (1991), this value of the Manning coefficient is used as 0.015 in this example. From a value of 0.015 at the crest,  $n_d$  increases along the slope until it reaches the value of 0.022 at the toe.

The downstream slope is then divided into 11 slices (Fig. II-4). Detailed information and calculation are listed in Table II-2. Eqs. (8-19), and (8-20) are used in the calculation. The maximum stress of the stress distribution of anchoring bars at the base of the dam is calculated in Table II-2 as:  $t=97934 \text{ N/m}$ . Hence by Eq. (8-22),

$$\tan \theta = \frac{t}{H} = \frac{97934}{5.5} = 17806 \text{ N/m}^2$$

Assuming that the heights of the locations of steel bars in the slope are 0, 1.0 m, 2.0 m, 3.0m, 4.0 m, 5.0 m.

At the bottom,  $y = 0$ ,

By Eq. (8-21), the required anchor force for anchor 1 is:

$$\begin{aligned} B_1 &= (y_{\text{top}} - y_{\text{bottom}}) \left( H - \frac{y_{\text{top}} + y_{\text{bottom}}}{2} \right) \tan \theta = \\ &= (0.5 - 0) \left( 5.5 - \frac{0.5 + 0}{2} \right) * 17806 = 46740 \text{ N} \end{aligned}$$

Assume that the friction angle between steel bar and rockfill is also  $45^\circ$ . The effective shear stress is determined by Eq. (8-24):

$$\sigma_n' = \left( H - \frac{y_{\text{top}} + y_{\text{bottom}}}{2} \right) \gamma_b = \left( 5.5 - \frac{0.5 + 0}{2} \right) * 10000 = 52500 \text{ N / m}^2$$

The free length of the anchor with diameter  $d = 0.04\text{m}$  is given by Eq. (8-23):

$$l_1 \geq \frac{B_1}{\pi d \sigma_n \tan \varphi'} = \frac{46740}{3.1416 * 0.04 * 52500 * 1} = 7.08\text{m}$$

A similar calculation can be conducted to estimate the length of anchor at each locations.

## II.5 Discussion

Two detailed design examples have been presented for a real situation using the methodology proposed in Chapter 8. It is assumed that the dam is small, detailed pore

pressure distribution in the dam is not available, and the downstream water level is low. For medium-height and high dam, it is advisable to conduct the finite element analysis of the non-Darcy flow within the rockfill dam by the method developed in Chapter 6 to obtain the detailed value of the hydraulic gradient of the seepage flow for the design.

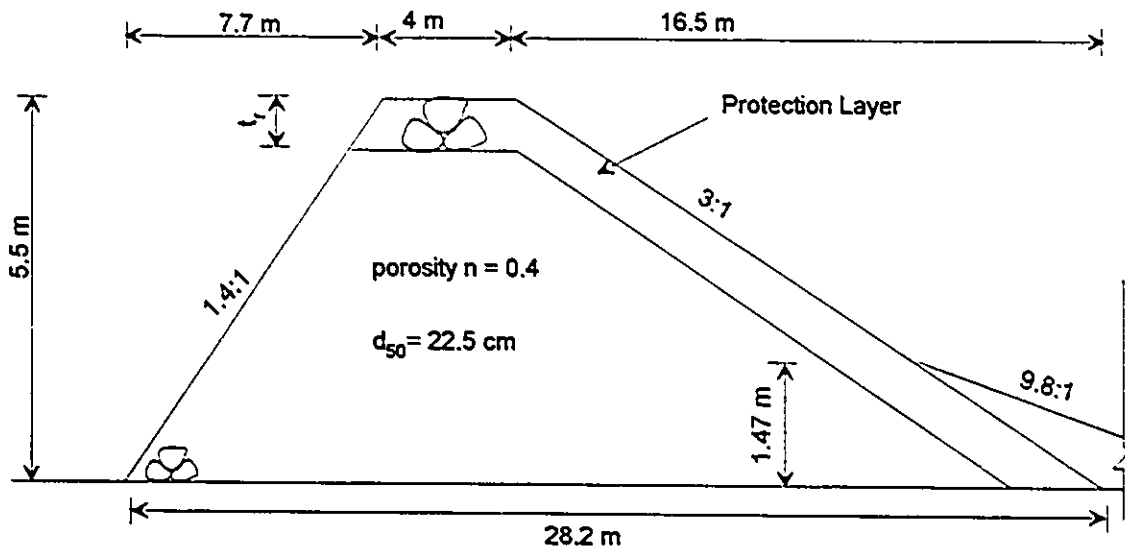


Figure II-1 An overtopped rockfill dam protected by large particles

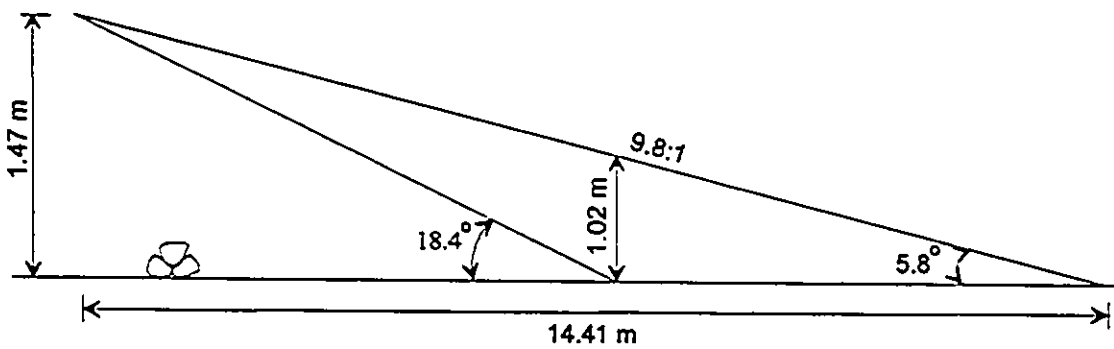


Figure II-2 Apron of the overtopped rockfill dam protected by large particles

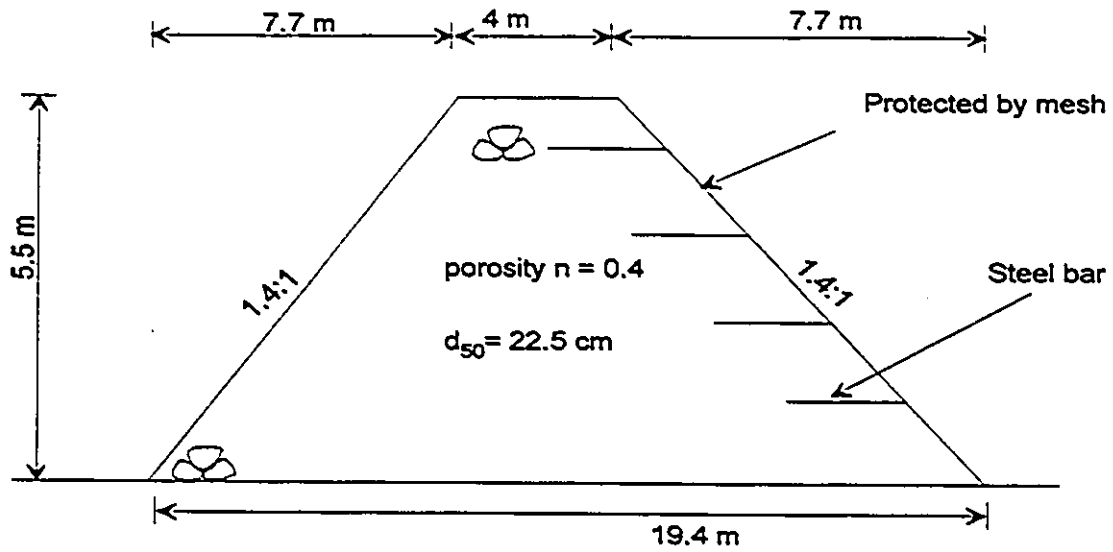


Figure II-3 An overtopped rockfill dam protected by steel mesh and steel bars

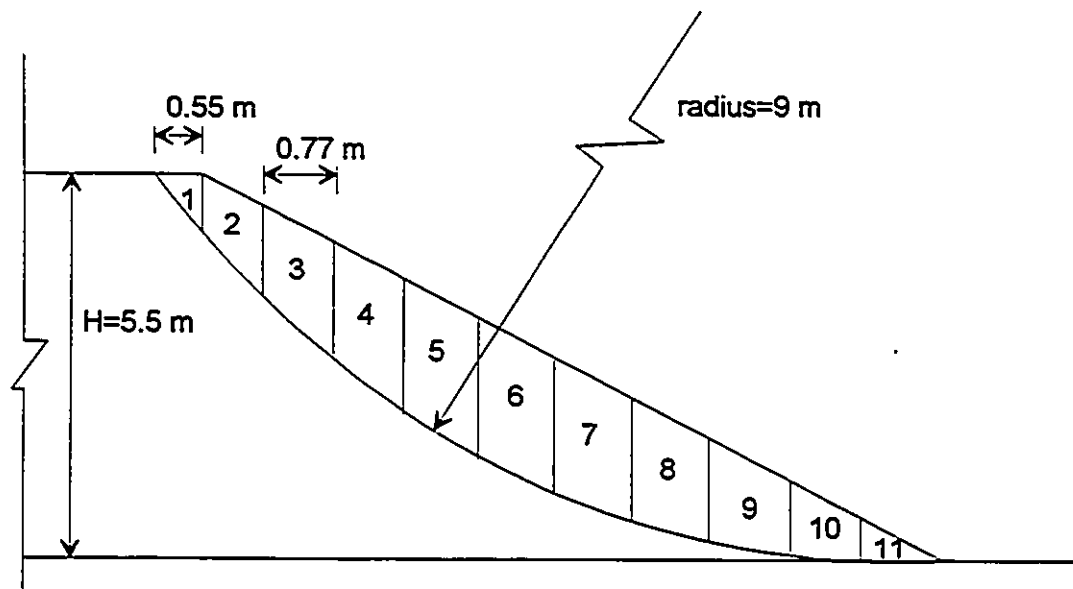


Figure II-4 Description of dividing the slices at the downstream slope

Table II-1 Water surface of overtopping of an overtopped rockfill dam

1	2	3	4	5	6	7	8	10	12	9	
distance from crest along downstream slope (m)	$\Delta X$ (m)	Zo Local Bed elevation (m)	$\Delta d$ Assumed Drop in water level (m)	Z elevation at water level (m)	d local depth (m)	A area (m <sup>2</sup> )	Q (m <sup>3</sup> /s)	Q1+Q2 (m <sup>3</sup> /s)	$\Delta Q$ (m <sup>3</sup> /s)	v (m/s)	Froude Number
#											
1	0	5.5		5.704	0.204	17.81	41.9			2.35	1.00
2	0.946	4.95	0.579	5.125	0.175	15.26	48.71	90.61	6.81	3.19	1.43
3	1.892	4.40	0.547	4.578	0.178	15.51	55.52	104.23	6.81	3.58	1.71
4	2.838	3.85	0.541	4.037	0.186	16.28	62.33	117.85	6.81	3.83	1.95
5	3.784	3.30	0.540	3.497	0.196	17.13	69.14	131.47	6.81	4.04	2.22
6	4.73	2.75	0.539	2.958	0.207	18.08	75.95	145.09	6.81	4.20	2.53
7	5.676	2.20	0.539	2.419	0.218	19.02	82.76	158.71	6.81	4.35	2.93
8	6.622	1.65	0.539	1.88	0.229	19.97	89.57	172.33	6.81	4.49	3.49
9	7.568	1.10	0.539	1.3411	0.240	20.92	96.38	185.95	6.81	4.61	4.39
10	8.514	0.55	0.539	0.8022	0.251	21.87	103.19	199.57	6.81	4.72	6.35
11	9.46	0.00	0.539	0.2633	0.261	22.82	110.00	213.19	6.81	4.82	112.11

Table II-1 Water surface of overtopping of an overtopped rockfill dam (continued)

	11	13	14	15		16	17	$\tau$
						head loss	$\Delta d$	Mean
						due to	computed	Shear
			$\Delta d$	Hydraulic	$n_d$	friction	DROP	stress
	$v1+v2$	$\Delta v$	due to	radius	Manning's	slope	In water	
			impact loss	R	coefficient		level	(N/m <sup>2</sup> )
	(m/s)	(m/s)	(m)	(m)			(m)	
#								
1								
2	5.54	0.839	0.436	0.189	0.015	0.147	0.583	234
3	6.77	0.389	0.353	0.176	0.016	0.198	0.550	294
4	7.41	0.249	0.315	0.182	0.017	0.222	0.537	341
5	7.86	0.206	0.302	0.191	0.017	0.239	0.541	385
6	8.24	0.166	0.285	0.202	0.018	0.252	0.537	429
7	8.55	0.149	0.277	0.212	0.019	0.264	0.541	473
8	8.84	0.135	0.268	0.223	0.020	0.275	0.543	517
9	9.09	0.121	0.259	0.234	0.020	0.285	0.543	562
10	9.33	0.111	0.251	0.245	0.021	0.294	0.545	607
11	9.54	0.101	0.243	0.256	0.022	0.303	0.545	653

Table II-2 Stability analysis of the steel bars in the downstream slope

	1	2	3	4	5	6	7	8
	$\Delta x$	$\tau$	$\tau \Delta x$	$A_i$				
	Width of slice	Mean Shear stress (unit width)		Area of the slice	$\gamma_w J_d A_i$	$\gamma_b A_i$	$\tau \Delta x \tan \alpha$	
Slice #	$\beta_i$ $\alpha$	(N/m <sup>2</sup> )	(N/m)	(m <sup>2</sup> )	(N/m)	(N/m)	(N/m)	(N/m)
1	63.0 0	200.00	110.00	0.358	2505	3580	79	3659
2	54.0 35.54	234.03	180.21	1.182	8271	11820	129	11949
3	52.0 35.54	293.57	228.05	1.451	10153	14510	161	14671
4	38.5 35.54	340.76	262.38	1.578	11042	15780	187	15967
5	32.0 35.54	385.07	296.51	1.617	11314	16170	212	16382
6	27.2 35.54	428.86	330.22	1.559	10909	15590	236	15826
7	22.0 35.54	472.61	363.91	1.368	9572	13680	260	13940
8	16.0 35.54	516.99	398.08	1.155	8082	11550	284	11834
9	13.0 35.54	561.91	432.67	0.905	6332	9050	309	9359
10	8.5 35.54	607.36	467.67	0.597	4177	5970	334	6304
11	5.5 35.54	653.40	503.12	0.212	1483	2120	359	2479

Table II-2 Stability analysis of the steel bars in the downstream slope (continued)

	9	10	11	12	13	14	
							$\frac{2 \tan \varphi'}{HF}$ (col 14)
	$\cos \beta$	$\sin \beta$	$m_i$		$(2'Fs/H)^*$		
Slice				col8*col10	(col3+col5+col12)	col8*col9	
#				/col11	(N/m)	/col11	
1	0.4540	0.8910	1.05	3110	3123	1585	384
2	0.5878	0.8090	1.13	8576	9288	6231	1511
3	0.6157	0.7880	1.14	10133	11188	7916	1919
4	0.7826	0.6225	1.20	8300	10893	10434	2530
5	0.8480	0.5299	1.20	7226	10275	11584	2803
6	0.8894	0.4571	1.19	6058	9435	11787	2858
7	0.9272	0.3746	1.18	4437	7840	10982	2662
8	0.9613	0.2756	1.15	2849	6179	9935	2408
9	0.9744	0.2250	1.12	1872	4711	8111	1866
10	0.9890	0.1478	1.09	857	3001	5733	1390
11	0.9954	0.0958	1.06	224	1206	2330	585
					$\Sigma=76938$		$\Sigma=20996$
							$l = 97934(N/m)$

## Appendix III Case Studies

This appendix compares the factor of safety of the downstream slope as provided by equations derived in Chapter 7 to field experience.

### III.1 Xibeikou Concrete Faced Rockfill Dam (1987) (downstream slope protected by rock particles)

The profile of the downstream the Xibeikou dam is shown in Figure III-1 (Hu, 1988). The field observation is described in Chapter 5.

From the field measurement, the downstream seepage-exit depth is 2.3 m, and unit discharge  $q$  is  $0.51 \text{ m}^3/\text{s}/\text{m}$ . Hydraulic gradient  $i = 1/8.2 = 0.12$ .

From Eqs. (8-4) and (8-2):

$$h = \frac{0.51}{1.58 * 0.45 * (9.8 * (0.136 * 0.65) * 0.12)^{0.5}} = 2.22 \text{ m}$$

The water head at the upstream slope (measured from the bottom of the dam):

$$H = 2.3 + 2.22 = 4.5 \text{ m}$$

At the toe of the dam, from Hansen (1992, pp. 154 & pp.325):

$$Fr_0 = \frac{1}{4} \left[ 11 \log \left( \frac{h_c}{H} \right) + 12 \right] = \frac{1}{4} \left[ 11 \log \left( \frac{2.3}{4.5} \right) + 12 \right] = 2.2$$

$$y_0 = \left[ \frac{q^2}{Fr^2 g} \right]^{1/3} = \left[ \frac{0.51^2}{2.2^2 * 9.8} \right]^{1/3} = 0.18 \text{ m}$$

Then velocity at the toe can be calculated as:

$$v = \frac{q}{y_0} = \frac{0.51}{0.18} = 2.83 \text{ m/s}$$

By Eq. (8-10):

$$n_d = 0.038 d_{50}^{1/6} = 0.038 \times 0.65^{1/6} = 0.035$$

Void ratio of the slope (from Lamb and Whiteman, 1979):

$$e = \frac{n}{1-n} = \frac{0.45}{1-0.45} = 0.818$$

$$\frac{\gamma_b}{\gamma_w} = \frac{G-1}{1+e} = \frac{2.7-1}{1+0.818} = 0.94$$

From Eq. (8-14):

$$FS = \frac{0.94 \cos 7^\circ - (0.6+1) 0.12 (1+0.818) \sin 7^\circ}{\cos 45^\circ \left[ \frac{0.035^2 \times 2.83^2}{0.2^{1/3} \times 0.325} + (0.6+1) \times 0.12 \times (1+0.818) \cos 7^\circ + 0.94 \sin 7^\circ \right]}$$

$$= \frac{0.933 - 0.042}{0.707 [0.052 + 0.346 + 0.114]} = 2.46$$

Hence the safety factor  $FS = 2.46 \gg 1.5$ . The Xibeikou Dam is safe (this is also proved in the field observation). It is very conservative for the flowthrough condition.

### III.2 Hell Hole Dam (1964)

The profile of the downstream the Hell Hole Dam is shown in Figure III-2.

From the data provided by Leps (1971), seepage discharge is  $537.7 \text{ m}^3/\text{s}$ . The shape of the notch is shown in Fig. III-3.

Unit discharge at the top of the notch:

$$q_s = \frac{537.7}{128} = 4.2 \text{ m}^3/\text{s}/\text{m}$$

Considering the flow concentration (due to the shape of notch):

$$q_{\max} = 2 * q_s = 2 * 4.2 \text{ m}^3/\text{s}/\text{m} = 8.4 \text{ m}^3/\text{s}/\text{m}$$

From the field measurement, the downstream seepage-exit depth  $h_e$  is 17.7 m, and  $h_o = 47.2$  m. The hydraulic gradient  $i = 0.15$  (from field measurement). The water head at the upstream slope  $H = 73$  m. The void velocity is  $V_v = 0.403$  m/s.

At the toe of the dam,

$$Fr_0 = \frac{1}{4} \left[ 11 \log \left( \frac{h_e}{H} \right) + 12 \right] = \frac{1}{4} \left[ 11 \log \left( \frac{17.7}{47.2} \right) + 12 \right] = 1.83$$

$$y_0 = \left[ \frac{q^2}{Fr^2 g} \right]^{1/3} = \left[ \frac{8.4^2}{1.83^2 \cdot 9.8} \right]^{1/3} = 1.29 \text{ m}$$

The velocity at the toe:

$$v = \frac{q}{y_0} = \frac{8.4}{1.29} = 6.51 \text{ m/s}$$

By Eq. (8-10)

$$n_d = 0.038 d_{50}^{1/6} = 0.038 \times 0.3^{1/6} = 0.031$$

$$\frac{\gamma_b}{\gamma_w} = \frac{G - 1}{1 + e} = \frac{2.7 - 1}{1 + 0.75} = 0.971$$

From Eq. (8-14):

$$FS = \frac{0.971 \cos 26.6^\circ - (0.6 + 1) 0.15 (1 + 0.75) \sin 26.6^\circ}{\cos 45^\circ \left[ \frac{0.031^2 \times 6.51^2}{129^{1/3} \times 0.15} + (0.6 + 1) \times 0.15 \times (1 + 0.75) \cos 26.6^\circ + 0.971 \sin 26.6^\circ \right]}$$

$$= \frac{0.868 - 0.188}{0.707 [0.249 + 0.376 + 0.435]} = 0.91$$

Hence the safety factor  $FS = 0.91 \ll 1.5$ . The Hell Hole Dam is not safe (this is also proved in the field observation). The failure was observed from the toe and sliding and removal of rock had progressed from the toe up to the crest (Leps, 1973). This failure mechanism is the same as observed in our experimental studies at NRC Hydraulics Laboratory.

It is of interest to comment on the influence of the pulsating force. If the pulsating force is not considered in the calculation, the safety factor is calculated as (from Eq. (8-14)):

$$FS = \frac{0.971 \cos 26.6^\circ - 1 \times 0.15 (1 + 0.75) \sin 26.6^\circ}{\cos 45^\circ \left[ \frac{0.031^2 \times 6.51^2}{129^{1/3} \times 0.15} + 1 \times 0.15 \times (1 + 0.75) \cos 26.6^\circ + 0.971 \sin 26.6^\circ \right]}$$

$$= \frac{0.868 - 0.118}{0.707 [0.249 + 0.235 + 0.435]} = \frac{0.750}{0.650} = 1.2$$

This result shows that the failed Hell Hole Dam had the safety factor of 1.2 for the field condition. This data shows that without the consideration of the pulsating force in our design expression, a false prediction of the safety factor may be obtained for the stability of the downstream slope of a flowthrough and overtopped rockfill dam.

By Olivier's method (from Eq. (2-83)):

$$\tan \alpha = \left[ \frac{0.423 d_{50}^{3/2} (G-1)^{5/3}}{q} \right]^{2/7} = \left[ \frac{0.423 \times 0.3^{3/2} (2.7-1)^{5/3}}{8.4} \right]^{2/7} = 0.055$$

The required slope is 18:1, which is much flatter than 2:1. Not safe.

By Abt's method, the diameter of rock particles required to protect the downstream slope is (from Eq. (2-90)):

$$d_{50} = 0.503 i^{0.43} q_{\max}^{0.56} = 0.503 \left(\frac{1}{2}\right)^{0.43} 8.4^{0.56} = 1.23 \text{ m}$$

Hence the required diameter at the slope is much larger than the diameter in Hell Hole Dam. The dam is not safe.

### III.3 Pit 7 Afterbay Dam

The profile of the Pit 7 Afterbay Dam is described as in Figure III-4.

For the stability analysis purpose, the profile of the downstream can be simplified as in Figure III-5.

From the field observation, the hydraulic gradient was observed to be nearly as steep as the downstream face, i.e.,  $i_{\text{ave}} = 0.44$ .

Total discharge

$$Q_{\text{total}} = 5000 \text{ cfs} = 141.5 \text{ m}^3 / \text{s}$$

and the flowthrough discharge

$$Q_{\text{seep}} = 2200 \text{ cfs} = 62.3 \text{ m}^3 / \text{s}$$

The void ratio:

$$c = \frac{n}{1-n} = \frac{0.5}{1-0.5} = 1$$

Overtopping flow from the crest:

$$Q_{\text{over}} = Q_{\text{total}} - Q_{\text{seep}} = 141.5 - 62.3 = 79.2 \text{ m}^3/\text{s}$$

The length of the crest is 500 ft, i.e., 15.2 m. Hence, the unit overtopping discharge:

$$q_{\text{over}} = \frac{Q_{\text{over}}}{15.2 \text{ m}} = \frac{79.2 \text{ m}^3/\text{s}}{15.2 \text{ m}} = 5.21 \text{ m}^3/\text{s}/\text{m}$$

and the unit seepage discharge:

$$q_{\text{seep}} = \frac{Q_{\text{seep}}}{15.2 \text{ m}} = \frac{62.3 \text{ m}^3/\text{s}}{15.2 \text{ m}} = 4.10 \text{ m}^3/\text{s}/\text{m}$$

The length of the downstream slope is 16.94 m. The increasing rate of overtopping discharge along the downstream slope is:

$$\frac{dQ}{dx} = \frac{Q_{\text{seep}}}{16.94 \text{ m}} = \frac{62.3 \text{ m}^3/\text{s}}{16.94 \text{ m}} = 3.68 \text{ m}^3/\text{s}/\text{m}$$

$$\frac{\gamma_b}{\gamma_w} = \frac{G-1}{1+e} = \frac{2.7-1}{1+1} = 0.85$$

The critical water depth at the crest is (Henderson, 1966, pp. 36):

$$h_c = \sqrt[3]{\frac{q_{\text{over}}^2}{g}} = \sqrt[3]{\frac{5.21^2}{9.8}} = 1.4 \text{ m}$$

At the toe, the Manning coefficient (from Eq. (8-10)):

$$n_d = 0.038 d_{50}^{1/6} = 0.038 \times 0.0508^{1/6} = 0.023$$

The calculation procedure in Hansen (1991) is used (which is essentially from Chow, 1959). In the latter, very detailed standardized steps were listed. The result is shown in

Table III-1. Eqs. (8-10), (8-11), and (8-12) are used in Table III-1. Since the flow at the crest is not turbulent, a value of Manning coefficient  $n_d$  smaller than that (0.023 in this example) in fully turbulent flow should be used in the design. Similar to Hansen (1991), this value of the Manning coefficient is used as 0.015 in this example. From a value of 0.015 at the crest,  $n_d$  increases along the slope until it reaches the value of 0.023 at the toe.

The downstream slope is then divided into 11 slices (Fig. III-6). Detailed information and calculation are listed in Table III-2. Assuming that the safety factor of the slope is  $FS=1.5$ . The  $t$  required calculated from Table III-2 is 84824 N/m. Hence, the required horizontal resistance force is (from Eq. 7-49):

$$\sum B_i = \frac{1}{2} tH = \frac{1}{2} 84824 \times 6.88 = 291,794 \text{ N} = 291 \text{ KN}$$

The resistance force provided by each steel bar is calculated by the following formula which is alternative form of Eqs. (8-23):

$$B_i = \pi d_i \sigma_n \tan \phi' l_i$$

where

$d$  = the diameter of the anchor bar  $l$ ;

$l_i$  = the length of the anchor bar where resistance is provided;

$\phi'$  = the friction angle between steel bar and rockfill; and

$\sigma_n'$  = the vertical effective stress at the depth of anchor bar.

Calculations give the total resistance force provided by the anchors inside the slope as 301 KN which is larger than the required value of 291 KN. Hence the safety factor of the slope is approximately 1.5. It is noticed that the upper part of the dam was protected by the anchor bars connected together, the actual safety of factor of the dam should be higher than the value calculated here. Field observations show that the dam is safe.

### III.4 Conclusion

The case studies show that the design methodology developed in the thesis is appropriate and the results obtained by the methods correspond to the real situation in the field studies.

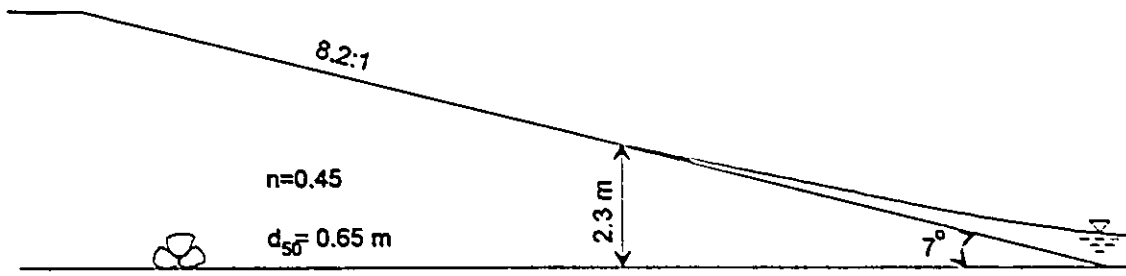


Figure III-1 The Downstream Slope of the Unfinished Xibeikou Concrete Faced Dam

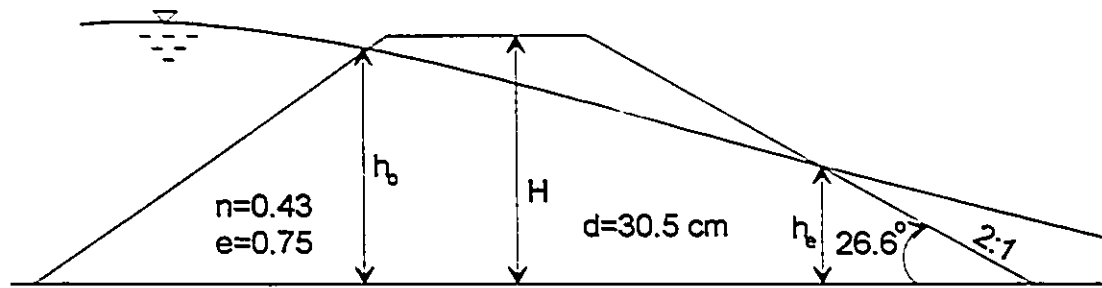


Figure III-2 Profile of Hell Hole Dam (1964)

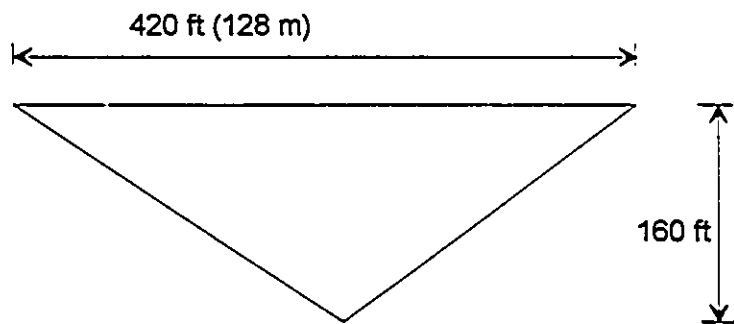


Figure III-3 Shape of the Notch at the Hell Hole Dam

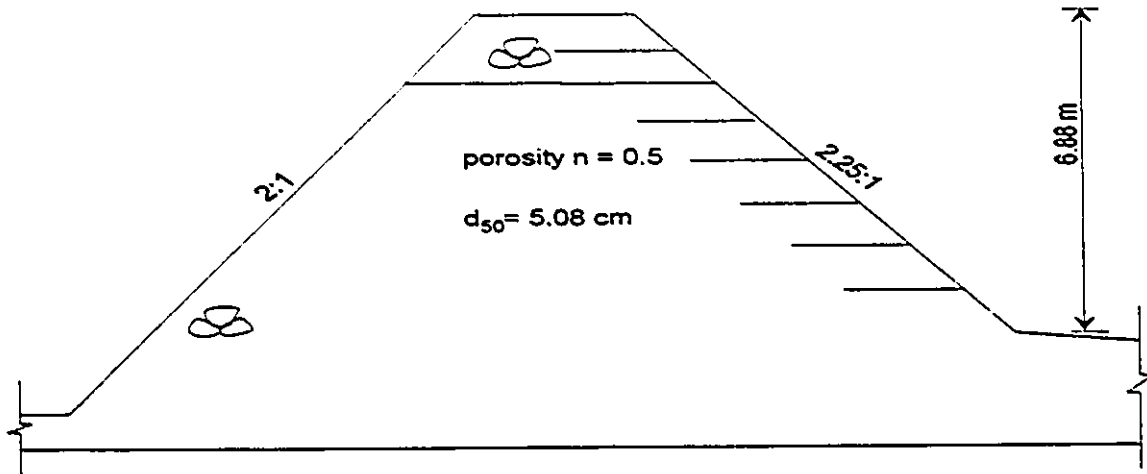


Figure III - 4 Profile of Pit 7 Afterbay Dam

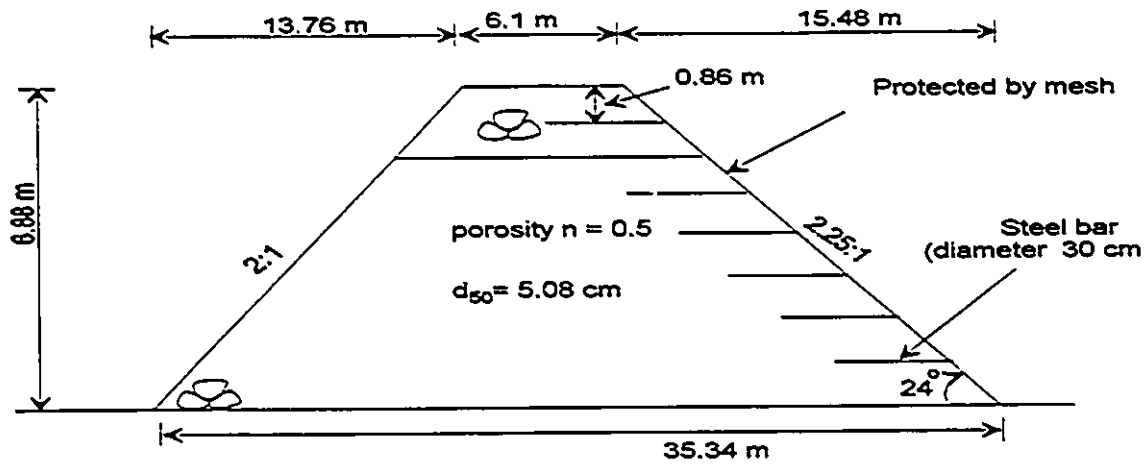


Figure III - 5 Simplified Profile of Pit 7 Afterbay Dam

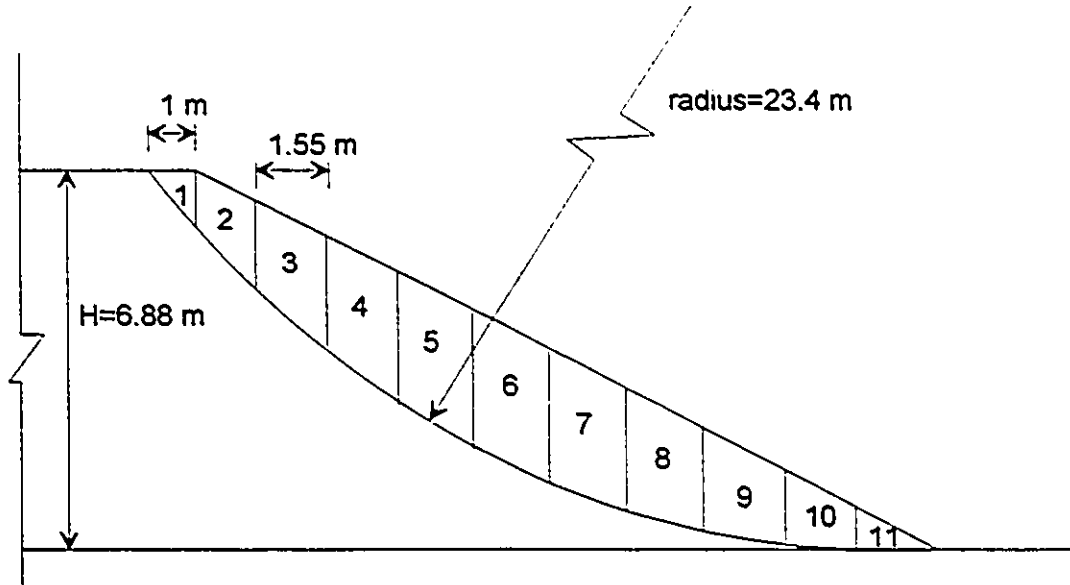


Figure III-6 Slices at the downstream slope

Table III-1 Water Surface of Overlapping Flow at the Downstream Slope

#	1	2	3	4	5	6	7	8	10	12	9	
	distance from crest along downstream slope (m)	$\Delta x$ (m)	$Z_0$ Local Bed elevation (m)	$\Delta d$ Assumed Drop in water level (m)	Z elevation at water level (m)	d local depth (m)	A area (m <sup>2</sup> )	Q (m <sup>3</sup> /s)	Q1+Q2 (m <sup>3</sup> /s)	$\Delta Q$ (m <sup>3</sup> /s)	v (m/s)	Froude Number
1	0	0	6.88		8.28	1.400	21.28	79.2			3.72	1.00
2	1.694	1.694	6.19	1.000	7.28	1.089	16.56	85.43	164.63	6.23	5.16	1.58
3	3.388	1.694	5.50	0.700	6.58	1.079	16.40	91.66	177.09	6.23	5.59	1.72
4	5.082	1.694	4.81	0.690	5.89	1.078	16.39	97.89	189.55	6.23	5.97	1.84
5	6.776	1.694	4.12	0.680	5.21	1.088	16.54	104.12	202.01	6.23	6.30	1.93
6	8.47	1.694	3.43	0.660	4.55	1.117	16.98	110.35	214.47	6.23	6.50	1.96
7	10.164	1.694	2.74	0.655	3.895	1.152	17.51	116.58	226.93	6.23	6.66	1.98
8	11.858	1.694	2.05	0.654	3.241	1.187	18.05	122.81	239.39	6.23	6.81	1.99
9	13.552	1.694	1.36	0.654	2.587	1.223	18.58	129.04	251.85	6.23	6.94	2.00
10	15.246	1.694	0.67	0.653	1.934	1.259	19.14	135.27	264.31	6.23	7.07	2.01
11	16.94	1.694	0.00	0.635	1.299	1.299	19.74	141.50	276.77	6.23	7.17	2.01

Table III.1 Water Surface of Overtopping Flow at the Downstream Slope (continued)

#	v1+v2 (m/s)	13 $\Delta v$ (m/s)	14 $\Delta d$ due to impact loss (m)	15 Hydraulic radius R (m)	$n_d$ Manning's coefficient	$S_f$	16 head loss due to friction slope	17 $\Delta d'$ computed DROP in water level (m)	$\Delta y$	$\tau$ Mean Shear stress (N/m <sup>2</sup> )
1										
2	8.88	1.437	0.987	1.245	0.010	0.038	0.080	1.067	0.814	468
3	10.75	0.430	0.545	1.084	0.011	0.058	0.121	0.666	0.570	619
4	11.56	0.383	0.553	1.079	0.013	0.071	0.147	0.700	0.561	748
5	12.27	0.325	0.541	1.083	0.014	0.083	0.173	0.714	0.553	884
6	12.79	0.201	0.459	1.103	0.016	0.094	0.197	0.656	0.537	1021
7	13.16	0.161	0.431	1.135	0.017	0.104	0.216	0.647	0.533	1157
8	13.46	0.146	0.419	1.169	0.019	0.113	0.235	0.655	0.532	1296
9	13.75	0.138	0.412	1.205	0.020	0.122	0.254	0.666	0.532	1440
10	14.01	0.124	0.399	1.241	0.022	0.131	0.272	0.671	0.531	1588
11	14.23	0.099	0.374	1.279	0.023	0.139	0.289	0.662	0.517	1738

Table III-2 Stability Analysis of the Downstream Slope Protected by Mesh and Rebars

			1	2	3	4	5	6	7	8	9
			$\Delta x$	$\tau$	$\tau \Delta x$	$A_i$	$\gamma_w J_d A_i$	$\gamma_b A_i$	$\tau \Delta x \tan \alpha$		
	$\alpha$	Width of slice	Mean Shear stress (unit width)	(N/m <sup>2</sup> )	(N/m)	Area of the slice (m <sup>2</sup> )	(N/m)	(N/m)	(N/m)	(N/m)	
Slice #	$\beta_i$	(m)	(N/m <sup>2</sup> )	(N/m <sup>2</sup> )	(N/m)	(m <sup>2</sup> )	(N/m)	(N/m)	(N/m)	(N/m)	$\cos \beta$
1	45.0	0	98.00	98.00	98.00	0.5	735	4165	70	4235	0.7071
2	39.0	24	468.10	725.55	725.55	2.02	2969	16826.6	518	17345	0.7771
3	34.1	24	618.95	959.37	959.37	2.71	3984	22574.3	685	23259	0.8281
4	30.5	24	748.30	1159.87	1159.87	3.1	4557	25823	828	26851	0.8616
5	23.9	24	884.11	1370.37	1370.37	3.26	4792	27155.8	978	28134	0.9143
6	22.5	24	1020.74	1582.15	1582.15	3.18	4675	26489.4	1130	27619	0.9239
7	17.2	24	1156.51	1792.60	1792.60	2.94	4322	24490.2	1280	25770	0.9553
8	13.0	24	1295.70	2008.34	2008.34	2.56	3763	21324.8	1434	22759	0.9744
9	8.0	24	1439.52	2231.26	2231.26	2.02	2969	16826.6	1593	18420	0.9903
10	6.0	24	1587.68	2460.90	2460.90	1.32	1940	10995.6	1757	12753	0.9945
11	4.0	24	1738.34	2694.43	2694.43	0.46	676	3831.8	1924	5756	0.9976

